REPORT DOCUMENTATION PAGE

1. Recipient's Reference	2. Originator's Reference	3. Further Reference	4. Security Classification of Document
	AGARD-AG-287 Volume 1	ISBN 92-835-1502-1	UNCLASSIFIED

5. Originator Advisory Group for Aerospace Research and Development
North Atlantic Treaty Organization
7 rue Ancelle, 92200 Neuilly sur Seine, France

6. Title TWO-DIMENSIONAL TURBULENT SEPARATED FLOW

7. Presented at

8. Author(s)/Editor(s)	9. Date
by Roger L.Simpson edited by A.D.Young	June 1985
10. Author's/Editor's Address	**11. Pages**
Various	104

12. Distribution Statement This document is distributed in accordance with AGARD policies and regulations, which are outlined on the Outside Back Covers of all AGARD publications.

13. Keywords/Descriptors

Turbulent flow	Velocity measurement
Two dimensional flow	Aerodynamics

14. Abstract

Many different flow cases with nominally two-dimensional turbulent separated flow regimes are discussed. Because of intermittent flow reversal and backflow near the wall, directionally sensitive measurement techniques such as hot-wire, pulsed-wire and laser anemometry are discussed. Experimentally-observed structure of detached flows on streamlined surfaces and around sharp-edged corners is discussed for steady and unsteady incompressible and compressible cases where large-scale structures dominate the flow behaviour. A number of differential and integral calculation methods are discussed. Traditional attached flow turbulence models do not describe detached flows well and methods which include experimentally-observed features of detached flow parameters seem to perform best.

This AGARDgraph was sponsored by the Fluid Dynamics Panel of AGARD. A second volume is in preparation.

AGARD-AG-287-Vol.I

AGARD-AG-287-Vol.I

AGARD

ADVISORY GROUP FOR AEROSPACE RESEARCH & DEVELOPMENT

7 RUE ANCELLE 92200 NEUILLY SUR SEINE FRANCE

AGARD AGARDOGRAPH No.287, Volume I

Two-Dimensional Turbulent Separated Flow

NORTH ATLANTIC TREATY ORGANIZATION

NORTH ATLANTIC TREATY ORGANIZATION

ADVISORY GROUP FOR AEROSPACE RESEARCH AND DEVELOPMENT

(ORGANISATION DU TRAITE DE L'ATLANTIQUE NORD)

AGARDograph No.287 Vol.1

TWO-DIMENSIONAL TURBULENT SEPARATED FLOW

by

Roger L.Simpson
Virginia Polytechnic Institute and State University
Blacksburg
Virginia 24016
USA

Edited by

A.D.Young
70 Gilbert Road
Cambridge, CB4 3PD
United Kingdom

This AGARDograph has been produced at the request of the Fluid Dynamics Panel of AGARD.

THE MISSION OF AGARD

The mission of AGARD is to bring together the leading personalities of the NATO nations in the fields of science and technology relating to aerospace for the following purposes:

— Exchanging of scientific and technical information;

— Continuously stimulating advances in the aerospace sciences relevant to strengthening the common defence posture;

— Improving the co-operation among member nations in aerospace research and development;

— Providing scientific and technical advice and assistance to the North Atlantic Military Committee in the field of aerospace research and development;

— Rendering scientific and technical assistance, as requested, to other NATO bodies and to member nations in connection with research and development problems in the aerospace field;

— Providing assistance to member nations for the purpose of increasing their scientific and technical potential;

— Recommending effective ways for the member nations to use their research and development capabilities for the common benefit of the NATO community.

The highest authority within AGARD is the National Delegates Board consisting of officially appointed senior representatives from each member nation. The mission of AGARD is carried out through the Panels which are composed of experts appointed by the National Delegates, the Consultant and Exchange Programme and the Aerospace Applications Studies Programme. The results of AGARD work are reported to the member nations and the NATO Authorities through the AGARD series of publications of which this is one.

Participation in AGARD activities is by invitation only and is normally limited to citizens of the NATO nations.

Published June 1985

ISBN 92-835-1502-1

Printed by Specialised Printing Services Limited
40 Chigwell Lane, Loughton, Essex IG10 3TZ

ACKNOWLEDGEMENTS

The author would like to thank the US Army Research Office, the US Office of Naval Research, the National Aeronautics and Space Administration, and the ' Air Force Office of Scientific Research for supporting his interests and research on separated turbulent flows during the ı ;t 14 years. During most of this time, the author was associated with Southern Methodist University, Dallas, Texas, wh re he received much encouragement and complete freedom to pursue his own research interests. Many former students and research associates were indispensible in this work.

The author would also like to thank all researchers who kindly supplied copies of papers and reports for this review. He regrets overlooking any work either because the scope of this review was too narrow or because he was was unaware of that work.

The author thanks the Fluid Dynamics Panel of NATO-AGARD for their support in the preparation of this work. Professors A.D.Young and K.Gersten were especially helpful. My family supported my efforts by allowing me uninterrupted time at home for this work. My friend and colleague, Dr Y.-T.Chew of the National University of Singapore, read this manuscript and offered many suggestions. Mrs Marge Teates of VPI & SU typed this manuscript.

CONTENTS

TWO-DIMENSIONAL TURBULENT SEPARATED FLOW

Roger L. Simpson
Virginia Polytechnic Institute and State University
Blacksburg, Virginia 24061 USA

SUMMARY

Many different flow cases with nominally two-dimensional turbulent separated flow regions are discussed. Because intermittent flow reversal and backflow occur in the near wall region, directionally-sensitive measurement techniques must be used to examine the flow structure. These techniques, which include hot-wire, pulsed-wire, and laser anemometry, are discussed here. The various states of the separation process can be located specifically by the amount of flow reversal near the wall. A terminology for these states is given here.

The experimentally-observed structure of detached flows on streamlined surfaces and around sharp-edged corners is discussed in detail for steady and unsteady incompressible and compressible cases. In all cases large-scale structures dominate the flow behavior, producing large shearing stresses in the middle of the detached shear flow and strongly influencing the local intermittent backflow. The turbulence structure strongly lags the mean flow behavior in the detachment and reattachment processes. For unsteady periodic separation there is considerable hysteresis of the flow during a cycle.

A number of differential and integral calculation methods are discussed. Traditional attached flow turbulence models and correlations do not describe detached flows well. Methods which include experimentally-observed features and/or correlations of detached flow parameters seem to perform best, although further improvements are still needed.

NOMENCLATURE

C, c	chord length
C_f, C_f'	$\tau_w/1/2\rho U_e^2$, $\tau_w'/1/2\rho U_e^2$, skin friction and fluctuation skin friction coefficients
C_p	$(p-p_o)/1/2\rho U_o^2$, pressure coefficient
F	defined by equation (IV.21)
F_u, F_v	$\overline{u^4}/(\overline{u^2})^2$, $\overline{v^4}/(\overline{v^2})^2$, flatness factors
f	frequency, Hz
H	δ^*/θ, shape factor; step height
h	$1-1/H$
L	length
l	$(-\rho uv/\lvert\partial U/\partial y\rvert(\partial U/\partial Y))^{1/2}$, Prandtl's mixing length
N	length of diffuser; distance from wall to maximum backflow position
n, s	normal and parallel to surface coordinates
M	distance from wall to y position where $\gamma_{pu} = 0.99$; Mach number
P, p'	mean and rms pressures
$\overline{q^2}$, q'	$\overline{u^2} + \overline{v^2} + \overline{w^2}$; $(\overline{q^2})^{1/2}$, respectively
R	streamwise radius of curvature of test wall
Re	Reynolds number based on subscripted length
S_u, S_v	$\overline{u^3}/\overline{u'^3}$, $\overline{v^3}/\overline{v'^3}$, skewness factors
T, t	time
U, V, W	instantaneous velocity components in x, y, z directions
U, V, W	time-mean velocity components in x, y, z directions
u, v, w	fluctuation velocities, e.g., $u = U-U$
u',v',w'	$(\overline{u^2})^{1/2}$, $(\overline{v^2})^{1/2}$, $(\overline{w^2})^{1/2}$
$-\overline{uv}$	kinematic Reynolds shearing stress
U_τ	$(\tau_w/\rho)^{1/2}$, shear velocity
U^+, y^+	U/U_τ, yU_τ/ν, law-of-the-wall coordinates
W	width
x, y, z	Cartesian coordinates
X_R	reattachment length
γ_{pu}	fraction of time flow moves downstream
γ_{pv}	fraction of time flow moves away from wall
δ	shear layer thickness, y where $U/U_e = 0.99$
δ^*	$\int_0^\infty \left(1-\frac{\rho U}{\rho_e U_e}\right)dy$, displacement thickness
ϵ_M	kinematic eddy viscosity, $-\overline{uv}/(\partial U/\partial y)$
θ	$\int_0^\infty \frac{\rho U}{\rho_e U_e}\left(1-\frac{U}{U_e}\right)dy$, momentum thickness; also angle
θ^*	$\int_0^\infty \frac{\rho U}{\rho_e U_e}\left(1-\left(\frac{U}{U_e}\right)^2\right)dy$, energy thickness
ν	kinematic viscosity
ρ	density
τ	time-averaged shearing stress; also dimensionless time
τ'	rms shearing-stress fluctuation

subscripts

e	condition immediately outside boundary layer
M	maximum value
o	reference condition
w	wall condition
∞	freestream condition

I. INTRODUCTION

Turbulent flow separation continues to be a nuisance to fluid dynamicists because it may be present in many practical machines and devices, thus reducing their performance, and because there is no adequate method to calculate such flows. In general, the maximum performance of such machines occurs at conditions close to the onset of separation. In order of increasing difficulty, designers of streamlined surfaces need to know

(a) whether or not a boundary layer separates for prescribed conditions,
(b) how the pressure distribution and flowfield are affected by boundary layer development with small regions of separated flow, and
(c) how the overall performance is affected when large regions of separation are present.

Some of the situations of interest occur in diffusers, engine inlets, fans and compressors, and on aircraft. The mean separated flow is nominally two-dimensional in many cases, but is three-dimensional in many more configurations (Peake and Tobak, 1980). Separation from bluff bodies is just as important as for streamlined shapes, e.g., boat-tailed bodies, flame stabilizers in gas turbines, large buildings subjected to wind loadings, etc. From a structural viewpoint, the aeroelastic response of the surface to strong pressure fluctuations produced by separation is an important consideration.

The purpose of this article on two-dimensional turbulent separated flows is to review our understanding of the physical behavior of such flows. The physical behavior of turbulence is flow dependent, so detailed experimental information is needed for understanding such flows and modelling the physics for calculation methods. The fact that there is flow reversal in mean two-dimensional separated flows requires that directionally-sensitive measurement techniques be used to obtain valid data. The degree of flow reversal is an indicator of the detached flow state. Different investigators have used different terminologies to describe their experiments.

In Chapter II below, the terminology to be used in the remainder of this article will be discussed. Chapter III deals with valid experimental techniques for separated flows. Chapter IV deals with the experimentally observed features of incompressible and compressible detached flows over streamlined and bluff bodies, with and without organized or self-induced unsteadiness. Calculation methods are not generally discussed in this chapter in order to clearly distinguish between the experimental facts and the results of modelling. Chapter V deals with efforts to calculate these flows. Chapter VI represents general conclusions and recommendations.

II. TERMINOLOGY

The term "separation" must mean the entire process of "departure" or "breakaway" or the breakdown of boundary-layer flow. An abrupt thickening of the rotational flow region next to a wall and significant values of the normal-to-wall velocity component must accompany breakaway, else this region will not have any significant interaction with the freestream flow. This unwanted interaction causes a reduction in the performance of the flow device of interest, e.g., loss of lift on an airfoil or loss of pressure rise in a diffuser.

It is too narrow a view to use vanishing surface shearing stress or flow reversal as the criterion for separation. Only in steady two-dimensional flow do these conditions usually accompany separation. In unsteady two-dimensional flow the surface shear stress can change sign with flow reversal, but without "breakaway". Conversely the breakdown of the boundary layer concept can occur before any flow reversal is encountered (Sears and Telionis, 1975; Shen, 1978). In three-dimensional flow the rotational layer can depart without the surface shear stress necessarily falling to zero; the wall shear is zero only at the singular points (Peake and Tobak, 1980).

For steady-freestream two-dimensional flows on streamlined surfaces, separation begins intermittently at a given location; that is, the flow reversal at that location occurs only a fraction of the total time. At progressively further downstream locations, the fraction of time that the flow moves downstream is progressively less. Figure 1 shows the streamwise distribution of the fraction of time that the flow moves downstream γ_{pu} near the wall for the Simpson et al. (1980) mean two-dimensional separated turbulent boundary layer. Sandborn and Kline (1961) were the first to point out this intermittent separation behavior. (Surprisingly, many separating flow analysts seem unaware of this feature.) The beginning of intermittent separation appears to mark the beginning of mean streamwise pressure gradient relief. Simpson (1976a) has shown that intermittent separation begins when the local turbulence intensity u'/U is greater than one-third.

Until recent years little new information about mean two-dimensional steady freestream turbulent separation has been available because of the lack of valid experimental techniques. With measurements having been made and being made with different types of instrumentation in different apparati, it is important to have a terminology that will allow quantitative comparisons and make the most of data that are difficult to obtain. Participants of the Colloquium on Turbulent Flow Separation (Simpson, 1979, 1981) proposed the following general terms for two-dimensional steady freestream separation:

A. Detachment - the location where the boundary layer flow leaves the wall; the locus of points where the limiting streamline of the flow leaves the surface.
B. Reattachment - locus of points where the limiting streamline of the time-averaged flow rejoins the surface.
C. Separation - the total process consisting of detachment, recirculation, flow free-shear layer, and in cases not involving a free wake, reattachment.
D. Stall - zone of recirculating fluid created by pressure forces.
E. Stalled Fluid - fluid with reverse or low velocity within a recirculating zone.

In contrast to these definitions, Newman pointed out that in normal usage in the past that "detachment" would be the same as "separation"; that the definition C would usually be called the "separation region and wake"; that "stall" would be defined as the condition of maximum lift; and that definition D would be called "backflow".

Figure 2 shows other proposed definitions of flow characteristics nearest the surface on which the separation process occurs. Except in singular cases such as a backward facing step, turbulent detachment is a zone. Sandborn and Liu (1968) and Simpson et al. (1977) have noted that the fraction of time that the flow moves downstream, γ_{pu} varies gradually from unity toward zero along this detachment zone. As discussed in

section II. B.3b, γ_{pu} reaches its minimum value at a given streamwise location outside of the near wall viscous layer. A spanwise line of detachment does not move up-and downstream as a unit in turbulent separation. Small three-dimensional elements of flow move upstream for a distance and are later carried downstream, as observed in the visualization studies of Schraub and Kline (1965). These reverse flows occur in regions of low kinetic energy and are caused by forces arising from the large-scaled structures and the adverse pressure gradient.

"Incipient detachment" has been observed in old experiments when flow markers such as a dye filament injected into liquids at the wall or a tuft mounted on the surface would move upstream occasionally. In the past this location has been loosely called incipient separation. (Here we will not use this latter term since it appears to have been used loosely to mean a flow near conditions required for the separation process to occur. In some cases such as in supersonic flow, the separation process occurred but was not documented; it was often called incipient separation.) The zone just downstream of incipient detachment is important since the displacement thickness of the boundary layer begins to increase rapidly.

"Intermittent transitory detachment" was observed in old experiments when tufts or dye filaments moved upstream a noticeably greater fraction of time than "occasionally". Sandborn and Kline indicated at the Colloquium that this location corresponds to where they previously called the location of "turbulent separation" or "intermittent separation" (1961). Currently Sandborn (1970) labels the velocity profile at this position as "unrelaxed". "Transitory detachment" and "detachment" correspond to the same location, if the streamwise velocity probability distribution at that location is symmetric. "Detachment" was called the location of "steady" separation by Sandborn and Kline while Sandborn (1970) notes that the velocity profile at this location is "relaxed". Until recently most calculators were concerned only with calculating the location of D, ignoring the fact that the turbulent separation process starts upstream of this location in all but singular cases where ID and D are at the same location.

The length of the region between the ID, ITD, TD and D points will depend on the geometry and the flow, but the definitions of these points are the same. γ_{pu} is not a sufficient variable to describe the flow behavior since it only represents the fraction of a streamwise velocity probability distribution that is positive. However, it is important that such an important feature be documented in all future work.

III. EXPERIMENTAL TECHNIQUES FOR SEPARATED FLOW

III. A. Introduction

The title of this chapter reflects the fact that the behavior of separated flows is sufficiently different from unseparated flows to warrant special attention to experimental techniques. The purpose here is to review some recent advances in these methods for measuring surface pressure and shear conditions, the velocity, pressure, and density fields and the onset of the separation process. Some discussion of the interpretation of data from these techniques is also given.

If we have two-dimensional mean flow separation either in a laminar or turbulent flow, it is well known that there is a region of backflow in the separation zone. For a steady laminar flow separation bubble, which may occur in ideal cases, interpretation of constant temperature hot-wire anemometer signals may be easy and backflow velocities can be accurately measured. Sandborn (1972) and Comte-Bellot (1976) summarize the general knowledge of the physical behavior of hot-wire and hot-film transducers. However, for most practical cases that involve turbulence, this technique and associated data interpretation procedures are not so simple to use. A hot-wire anemometer is not directionally-sensitive to the cooling velocity so one cannot deduce the flow direction from one sensor. Since relatively high turbulence intensities are encountered in separated flows and calibration results are free convection dependent near zero velocity, the hot-wire sensor fixed relative to the test surface is not an acceptable velocity measuring transducer for separated turbulent flows. Furthermore, it is likely that such a probe disturbs the flow to some degree. Even so, several recent modified hot-wire techniques have been developed and are discussed below. Surface hot-film elements do not disturb the flow but suffer from the same directional-insensitivity problem as hot-wires in regions of flow reversal. Recent advances in interpretation of signals near separation and in element manufacturing techniques are noted below.

The pitot-static tube is another classical velocity and static pressure measuring device that is commonly used for unseparated flows but should not be used in flows with flow reversal. It not only disturbs a separated flowfield but is sensitive to many factors that prevent reliable interpretation of the data: pressure measuring system response, yaw and pitch, turbulence, low Reynolds number effects, and flow reversal.

Surface liquid film flow visualization techniques can be used to guide measurements when there are strong changes in the mean flow direction. These techniques can also locate the vicinity of two-dimensional detachment. A brief discussion of these techniques is given below.

Surface pressure measurements can be used to determine the distribution of pressure gradient relief upon flow separation. A flow-field static-pressure probe has been developed that accounts for velocity fluctuation effects. Recent advances in solid-state electronics have produced inexpensive, sensitive, and somewhat more rugged pressure transducers. Surface membrane interferometry has been developed as a research tool for pressure measurements. These advances are briefly discussed below.

Since the introduction of the laser in the early 1960's, holography and laser anemometry (LDA) or velocimetry (LDV) have been developed as nonintrusive quantitative methods for flow measurements. Here we will discuss application of these modern techniques to separated flows, particularly those with flow reversal.

Pulsed-wire anemometry permits the magnitude and direction of the flow to be determined. A pulse of current through a heater wire warms the gas flowing by. Resistance thermometers located a distance up and downstream of the heater detect the passage of this heated fluid. The speed and direction of this fluid is determined through the use of an electronic circuit. With a continuous current passing through the heater of this probe, the instantaneous flow direction can be determined with this "thermal tuft". The use of these devices is discussed below.

Finally, even though we have sophisticated and expensive instrumentation, we must use modern data analysis techniques to deduce information. A brief outline of recent advances in signal processing of turbulent flow signals is given.

III. B. Surface Shear Stress Visualization Techniques

One of the easiest to use and least expensive separation diagnostic methods is the surface oil flow technique. It is intended to enable the nature of the flow over the surface of a model to be investigated quickly. The surface is coated with a specially-prepared paint consisting of a finely powdered pigment, a suitable oil medium and occasionally a dispersing agent. Air flowing over the surface carries the oil and a streaky powder deposit remains to mark the flow direction. The patterns made by the streaks indicate directly the local directions of the surface shearing stress and in the case of separating flows with local stagnation regions, indicate the general location of detachment.

Questions of the validity of this technique are raised that the liquid film interferes with the air boundary layer flow and that the streaks do not necessarily lay in the local surface shearing stress direction due to gravitational and pressure gradient effects. Squire (1960) analysed the motion of such a thin oil film and found that the boundary layer surface shear stress lines are followed by the film except near two-dimensional detachment. In this case Squire indicated that there is an oil deposit envelope upstream of the true detachment location for both incompressible and compressible flows. This early indication of detachment is less pronounced for turbulent than laminar flows. The distance that the detachment location is in error depends on the oil thickness and the model size but is independent of the oil viscosity. As long as the oil viscosity is sufficiently high to prevent significant film flow velocities, the film effect on the boundary layer motion is small.

Since mean two-dimensional turbulent separation begins with incipient detachment with occasional backflow, the oil film is actually subjected to strong unsteady shearing stresses and pressure gradients not considered in Squire's analysis. The time-averaged effect of these forces on the film as well as the film thickness determine the oil deposit envelope at detachment. One would need to accurately know the unsteady behavior of these air boundary layer parameters near the surface to properly interpret the exact location of two-dimensional detachment. In other words, to obtain anything more than an approximate idea of the two-dimensional detachment location with an oil flow technique would require considerable knowledge of the instantaneous boundary layer behavior. If we knew that, we would not need to use the oil flow technique!

Maltby (1962) compiled practical information on the preparation of oils for films. There seems to have been few advances in this technique over the last few years judging from the more recent separation studies (AGARD 1975). Two apparent improvements are worth noting. Settles, Bogdonoff, and Vas (1976) used a method for compressible flows that quickly produces a dry deposit that can be easily removed intact for storage. A mixture of kerosene and graphite was distributed well upstream of detachment. The mixture streamed along the test wall, coating the surface. The tiny graphite particles collected in a liquid line in the vicinity of separation. The kerosene quickly evaporated during a test, leaving a very tiny graphite pattern resembling pencil marks. The graphite patterns were preserved by lifting them off the model with transparent tape and pressing them onto white paper. The graphite accumulation line would seem to be close to the true zero-mean-shearing-stress line since the evaporation of the kerosene during a test eliminated the liquid ridge.

Langston and Boyle (1982) developed a surface skin friction line visualization technique for horizontal surfaces that is suitable for low speed flows up to a few hundred meters per second. A matrix of water insoluble ink dots was placed on an impervious test surface. A thin layer of oil of wintergreen (synthetic methyl salicylate) was sprayed on this surface, dissolving the ink dots. When the test flow was turned on, the ink flowed with the liquid film until the oil of wintergreen had evaporated, leaving permanent ink traces on the surface.

The meaning of oil-streak flow-visualization surface shear stress patterns for three-dimensional flows can be obtained from established topological rules. Peake and Tobak (1980) present a comprehensive review of the topography of skin-friction lines, along with selected examples for slender wings, symmetric separated flow about slender bodies, asymmetric separated flow about slender bodies, and separation around surface-mounted obstacles.

III. C. Hot-wire and Hot-film Techniques

As mentioned in the Introduction a hot-wire or hot-film velocity probe is insensitive to the flow direction and thus a single sensor fixed relative to the test surface is almost useless when the instantaneous flow direction is changing, as in a turbulent separated flow. For locations with backflow, rectified signal voltage probability diagrams are produced. As pointed out by Simpson (1976a), there is no unique way to relate the output of a hot-wire anemometer to the time flow behavior obtained by a directionally-sensitive laser anemometer when substantial backflow is present.

A rectified hot-wire anemometer signal will produce too large mean velocities and too small mean square fluctuations, as shown in Figure 3. When backflow occurs less than 10% of the time, mean velocities can be inferred from the signal. Good mean square fluctuations can be obtained with backflow less than 5% of the time (Simpson, 1976). If one knows the shape of the actual velocity probability distribution, then corrections can be made to hot-wire signals as long as there is a very small amount of flow reversal (Simpson, 1976a; Dengel and Vagt, 1982). Figure 3 shows that when negative samples of a pulsed-wire anemometer are deleted, the results agree with the erroneous hot-wire results. The correction procedures of Bradbury (1976) and Tutu and Chevray (1975) also resolve the large difference between hot-wire and pulsed-wire results when local turbulence intensities are below about 0.5.

Several attempts to alleviate this directional insensitivity difficulty have been made. Coles, Cantwell, and Wadcock have used a "flying hot-wire" (Coles and Wadcock, 1979), in which a hot-wire is swung in a circle through the flow at a known velocity and position as a function of time. Basically this introduces a sufficiently high bias velocity to the hot-wire so that the flow with respect to the wire is in an approximately known direction. Subtracting the bias velocity from the signal velocity determines the unknown fluid velocity contribution. Standard commercially-available X-array probes were used to determine U, V, u, and v velocities.

This technique has several special features. One good feature is that data are obtained along a line rather than at a point. A negative feature is that the wake of the whirling arm is a substantial moving disturbance in the flow. Another good feature is that the hot-wire probes are inherently self-calibrating in pitch. The hot-wire signals must be transmitted through slip rings from the whirling arm. One must make many passes through the separated flow with the "flying hot wire" in order to have enough data samples at each physical location so time-averaged turbulence quantities and mean velocities can be obtained. Thus the reproducibility of the swung apparatus position is important and a sophisticated data acquisition, retrieval, and processing computer system must be used. A linear version of the flying hot wire has been used by Perry and Watmuff (1979).

Recently, Thompson and Whitelaw (1983) presented a flying-hot-wire anemometer design in which the hot-wire probe is moved in a known non-circular path by a crank and slider mechanism. No slip rings are required. The path and speed of the hot-wire can be adjusted for the region containing flow reversal by the mechanism.

The relatively small split-film hot-film probe (TSI Model 1287) has two equal and constant temperature sensors on one quartz substrate, each covering 170° of the periphery. Because the local convective heat transfer coefficient around a circular cylinder varies with angle, the heat transfer to the fluid from each sensor is dependent on the incident flow direction. Thus, in principle, both the magnitude and direction of the flow perpendicular to the substrate axis can be determined, providing one knows whether the flow comes from downstream or upstream. Several investigations have attempted to use this probe with varying degrees of ease and success for unseparated flows (Spencer and Jones, 1971; Martin, 1975; Blinco and Sandborn, 1973; Fuller, 1974; Simpson and Shackleton, 1977). Young (1976) indicates that hot-film probes should be used with caution, since measured fluctuation quantities that are 30% too low can be obtained.

The most critical factor in using the split-film probe is obtaining a thermal balance between the two sensors. If the two sensors are not closely at the same temperature, thermal interference of one sensor with the second will occur. Individual constant temperature anemometer sets are used to power each sensor and the balancing resistance in the opposing bridge leg of each anemometer must be adjustable within 0.01 ohms for a 15 ohms operating resistance. Anemometer electronic drift must be minimized and circuit resistance values must be stable.

To use this split-film sensor in a separated flow with changing direction, which has not yet been done, would require keeping track of the instantaneous flow direction since there are two flow directions that would produce the same signal. One could locate downstream a single hot-wire perpendicular to the plane of the split as a thermal detector. Thus when the flow was in a downstream direction, it would cut the thermal wakes of the split-film sensors and determine uniquely the instantaneous incident flow direction in the U-V plane.

One can determine whether there is forward flow or backflow near the wall with a split-film. If the split between the films is perpendicular to the test wall, then the difference between the two output voltage signals would indicate whether the flow is moving downstream or upstream, even though there would still be the ambiguity of whether the flow was moving away from or toward the wall. A three sensor split-film (DISA Model 55R92) with each film having 120° of the perimeter can be used to eliminate the directional ambiguity of the instantaneous velocity in the U-V plane (Jorgensen, 1982).

The future of the split-film for separated flow is questionable. If a styrene substrate can be used, as noted in the discussion on surface hot-films below, then the thermal conductivity of the substrate would be 1/7th that of the current split-film probes. Thermal interference of the two or three sensors could be minimized with less sensitivity to small operating temperature differences. If a thermal-wake-detecting hot-wire must be used to determine flow direction, then one may as well use pulsed-wire anemometry, described in section III.F below, and avoid the quantitative uncertainties associated with the split-film probe.

Ligrani et al. (1983) review work on multiple hot-wire velocity and direction probes. In some designs, one constant-temperature wire detects the velocity and acts as a heater for one or more wires operated as resistance thermometers to sense the thermal wake and, therefore, determine the flow direction. In others, two or more constant-temperature wires are operated at different overheat ratios; the ratio of the effective velocities from these wires can indicate when the flow moves in the nominal downstream direction.

III. D. Surface Heat Transfer Techniques

The surface skin friction heat transfer gage, originally due to Ludwieg (1950), has been recently improved to reduce uncertainty in the interpretation of the results. This gage has much appeal since we are concerned with the wall region flow behavior during separation and this gage is non-intrusive and relatively simple to use in real applications, although a single wire gage is insensitive to the flow direction. As pointed out by Rubesin et al. (1975) this gage can be designed now to overcome some objections to the performance of previous designs. A properly designed gage can yield relatively less uncertain mean skin friction results near separation as compared to floating surface element results and results from mean velocity profiles. In addition, the signals of the dynamic flow behavior can be obtained.

The principle on which this gage is based requires that the surface-heated element have a dimension in the streamwise direction Δx that is small compared to the boundary layer thickness. The heat transferred from the heated element, which should be insulated from the surface substrate material, forms a thermal boundary layer within the viscous sublayer of the flow immediately adjacent to the surface. Based on these assumptions the analysis of Bellhouse and Schultz (1966) yielded the following relation between the heat flux Q_w from the constant temperature sensor to the fluid, the wall shear stress τ_w and pressure gradient dP/dx.

$$\tau_w = \frac{\mu^2 L}{a\rho Pr}\left(\frac{Q_w}{k\Delta T_w}\right)^3 - \frac{1}{2}\frac{b}{a}\left(\frac{k\Delta T_w}{Q_w}\right)\frac{dP}{dx} \qquad \text{(III.1)}$$

The constants a and b are given as 0.226 and 0.1046, respectively. ΔT_w is the difference between the wall temperature and the temperature of the edge of the thermal boundary layer, L is the effective streamwise sensor length, Pr is the Prandtl number, and ρ, μ, and k are the density, viscosity, and the thermal

conductivity, respectively. If a standard constant-temperature hot-wire anemometer set is used as a power source and the pressure gradient effect is negligible, the above equation can be written in terms of the measured voltage across the sensor.

$$\frac{E^2}{R\Delta T_w} = A\,(\rho\mu\tau)_w^{1/3} + B \qquad \text{(III.2)}$$

where A and B are strong functions of a gage design. B is a measure of the heat transfer rate conducted into the substrate while A varies with the effective streamwise length of the gage as $L^{2/3}$.

To maximize the element sensitivity to τ_w, a very low thermal conductivity substrate must be used. Rubesin et al. used low impact grade polystyrene ($k = 15$ W/m^2) whereas Bellhouse and Schultz used quartz ($k = 110$ W/m^2) and Liepmann and Skinner (1954) used ebonite ($k = 78$ W/m^2). High impact grade polystyrene has a much larger thermal conductivity. Not only is B smaller for the Rubesin et al. gage, but the ratio of the effective streamwise length to the actual gage length is much smaller, 2.5 as compared to 390 for the Liepmann and Skinner gage. The effective length needs to be as small as possible if pressure gradient and turbulent transport effects on the calibration can be neglected to make equation (III.2) universally valid. A smaller effective length reduces A, making the measured shear stress more sensitive to measured voltage changes. Rubesin et al., Murthy and Rose (1978), and Higuchi and Peake (1978) have shown that a polystyrene substrate gage has closely the same calibration in both laminar and turbulent flow that is nearly independent of the pressure gradients.

A gage was constructed by the author with the essential features of the Rubesin et al. gage. A 25 μm diameter platinum-10% rhodium wire was mounted between 1.32 mm diameter nickel electrodes located 1 cm apart whose ends were flush with the flat polystyrene surface. Conduction losses to the electrodes are small since the wire length-to-diameter ratio of 400 is large. Several drops of ethyl acetate were used to dissolve the polystyrene in the vicinity of the wire and imbed it in the surface. The ends of the wire were then soldered to the electrodes. A 0.00038 cm diameter wire was tried but was too fragile for use with simple construction techniques. Except at low velocities where free convection effects are important, calibrations of this gage in a laminar flow produced by a plate and cone viscometer fit equation (III.2). Skin friction results in good agreement with other techniques have been reported for the attached portion of the Simpson et al. (1981a) separating flow. Results for the attached portions of unsteady separating flows have been reported by Simpson et al. (1983).

Ajagu et al. (1982) presented a new design that also overcomes the substrate conduction problem. A 3.8×10^{-3} mm TSI tungsten wire was mounted about 2.5×10^{-2} mm above a surface on which was mounted a standard DISA nickel hot-film sensor on a quartz substrate. The hot-film sensor serves as a guard heater to prevent losses from the hot-wire to the wall. Ajagu et al. show that calibrations in laminar flow apply to turbulent flow.

If surface hot-wire sensors are about 1 cm apart there is no thermal wake interference between sensors. If sensors are placed closer than this together, the interference can be used for detection of flow reversal. The thermal wake from a higher temperature sensor would heat a low overheated downstream sensor for unseparated flow or a low overheated upstream sensor for a separated condition with backflow. The sensor wire located in the wake of the hottest wire requires less power for a specified overheat temperature. Rubesin et al. used three parallel wires 6.4 mm long and spaced 4.8 mm apart with middle wire being overheated higher than the other two.

Many people have used $\tau_w'/|\tau_w|$ values from a single sensor as an indicator of detachment and reattachment. This quantity increases from near zero for attached flows to a value of about 0.4 in the region where backflow is present, $0 < \gamma_{pu} < 1.0$ (Simpson et al., 1973, 1977). Unfortunately, theoretical considerations and laser anemometer measurements (Simpson, 1976) show that there is no unique relationship between these quantities, so the location of detachment features cannot be inferred. Owen and Johnson (1980) also point out that near detachment, unsteady and turbulent effects can dominate gage outputs and lead to erroneous results.

Arrays of these buried-wire sensors can be designed to determine the magnitude and direction of τ_w for three-dimensional boundary layers. For example, a bi-directional buried-wire gage, consisting of two high overheated sensors each mounted at 45° to the freestream velocity vector and 90° to each other, will determine the instantaneous shearing stress magnitude and the line of action for mean two-dimensional flows. To determine the unique direction, that is, whether the flow moves upstream or downstream, low overheated wires can be mounted upstream and downstream of these sensors to detect the thermal wakes as described in section III.E below.

Higuchi and Peake (1978) report satisfactory results with a 3 mm diameter bi-directional gage with two buried wires at 90° to one another and 45° to the freestream for a three-dimensional separated turbulent flow over a cone at high incidence angle. The surface shear stress angle is in qualitative agreement with the surface oil streak results, although there is some discrepancy in its magnitude. The magnitude of the mean shear stress was estimated to be about ±15% uncertain when calibrated with a Preston tube at one location on the surface. This gage could be used to determine the instantaneous flow direction of mean two-dimensional flows if flow reversals were accounted for.

III. E. Flow Direction Detector or "Thermal Tuft"

Although τ_w has been used as a parameter for location of detachment, its measurement in the near detachment region is relatively uncertain because τ_w approaches zero. A better, more sensitive, parameter is the fraction of the time that the flow moves downstream γ_{pu}. Although the L.D.V. is a versatile technique for detailed separated flow measurements, a simpler and less expensive technique using hot-wire sensors can be used to measure γ_{pu}. As mentioned above in section III.D, Rubesin et al. (1975) demonstrated the capability of a two sensor surface hot-wire gage with a central heater wire in the determination of the flow direction. Ligrani et al. (1983) reviewed other thermal wake flow direction detectors.

Eaton et al. (1979) further developed the "thermal tuft", which was also used by Ashjaee and Johnson (1980). The principle of operation is that the wake from a heater will heat either an upstream or downstream temperature sensor, depending on the flow direction. The probe shown in Figure 7 can be used as a thermal tuft. The simple electronic circuitry developed by Eaton et al. continuously compares the resistance of the two wires, producing a high or low output voltage depending on whether the flow is moving downstream or upstream, respectively.

Figure 4 shows a schematic plan view of the thermal tuft unit developed by Shivaprasad and Simpson (1982). Sensor 1 detects the downstream flow while sensor 2 detects flow moving upstream. If only the central heater wire is used, as in Eaton's original design, any crossflow reaching the central heater wire at an angle less than 22.6° to its axis will result in its wake missing the sensor wires. This design uses an additional heater wire on each side to eliminate this insensitivity.

For good sensitivity the heater wires of a thermal tuft must be sufficiently far from the sensor wires so that thermal conduction within the fluid is small compared to convection at low velocities. Bradbury and Castro (1971) found that the Peclet number based on the lowest fluid velocity to be detected and the distance between heater and sensor wires should be greater than 50 for good sensitivity to the velocity. In the Shivaprasad and Simpson design and that of Eaton et al., the closest spacing between heater and sensor wires is 2.5 mm. Thus for a Peclet number of 50, these designs have good sensitivity of the direction of fluid motions greater than 1/2 $msec^{-1}$. With less sensitivity, the thermal tuft can also detect the direction of smaller flow velocities, since it only needs some difference between sensor wire temperatures for proper operation.

Figure 5 shows that γ_{pu} values from the thermal tuft are consistently 0.05 to 0.1 higher than the LDA data for values not near zero or unity. This difference can be explained qualitatively. The portions of the flow that move in the downstream direction have a higher velocity on the average than the portions of the flow that move in the upstream direction (Simpson et al., 1981). This means that flow in the downstream direction moves more quickly over the probe and can change the sensed flow direction quicker than the reversed flow. In other words, during the times which the flow changes direction the signal tends to be biased in favor of the downstream flow direction. For γ_{pu} values near zero or unity, there are less frequent changes in the flow direction and the LDV and thermal tuft values are in better agreement. Nevertheless, there is agreement within the estimated uncertainty limits between directly measured L.D.V. data ($\pm$0.07) and thermal tuft data ($\pm$0.06). Since the thermal tuft provides continuous signals rather than discrete signals as provided by the L.D.V., it is more suited for measurements in unsteady flow where signal averaging is required for each phase of a flow cycle (Simpson et al., 1983).

III. F. Pulsed-wire Anemometry

The pulsed-wire anemometer (Bradbury and Castro, 1971) is capable of determining the flow velocity and direction within certain limitations. Their probe, shown schematically in Figure 6, has three fine wires. The central wire is pulsed with a short duration voltage pulse that in turn heats the fluid that is passing over that wire at that time. This heated fluid is convected away with the local instantaneous velocity of the flow. The other two wires on the probe are operated as resistance thermometers. They are used to measure the time for the heated fluid tracer to travel from the pulsed wire to one of the other wires. The component of velocity that is perpendicular to all three wires is measured, being the distance S between each wire divided by the pulse travel time. The flow direction is determined by which wire detects the thermal pulse. This probe has a blind spot for instantaneous flow directions where the heated wake does not pass over a detector wire.

There are several advantages to this instrument in addition to being directionally sensitive: there is no upper restriction on measurable turbulence level, it is usable in variable density flows, the calibration is probe geometry dependent only, and wire fouling is no significant problem. Castro (1971) measured u', v', and w' turbulence quantities as well as the mean velocity for a recirculating separated flow. To make such measurements, mean square fluctuation data from three probe orientations must be made and these quantities deduced from algebraic equations. It is not possible to measure u, v, and w fluctuations simultaneously.

Disadvantages to this commercially available probe include the limited usable velocity range (0.25 - 15 m/sec), limited mean velocity accuracy (1 to 5%), non-continuous signal, and large size (1 cm long wires). Measurements of low turbulence intensities are relatively uncertain. However, Castro and Cheun (1982) conclude that, in flows of such high intensity that hot wires would be useless, measurements of all the Reynolds stresses can be made with an accuracy probably better than 30% (for v') or even 15% (u' and uv). In the medium-intensity range (10-30%, say) it has been shown that, provided the yaw response extends to large enough angles, pulsed-wire measurements can be as accurate as hot-wire measurements. However, in this case the errors in uv and v' are rather greater than at higher intensities and depend critically on the extent of the yaw response. Eaton and Johnston (1980) also used the Bradbury and Castro probe with little calibration drift and about the same level of measurement uncertainty as reported above. Skinner et al. (1982) developed a low-speed probe design (0.12 - 2 m/sec). Only one detector wire was used, so backflows cannot be detected. Tomback (1973) discussed application of this instrument to inhomogeneous flows.

Westphal et al. (1981) and Eaton et al. (1982) also used a modified thermal tuft probe that had a 12.5 μm diameter nickel central heater wire. A probe (Figure 7) with traversable wires was developed and used to make velocity profile measurements within 0.2 mm of the wall. Mean skin friction values inferred from these measurements were within 2% of independently determined skin friction values. Ginder and Bradbury (1973) and Ruderich and Fernholz (1983) used a pulsed-wire probe to measure the skin friction. Castro and Dianat (1982, 1983) also report a similar skin friction probe that measures velocities 0.08 mm above the surface. Good skin friction probability diagrams can be obtained with these probes. Even though time-resolved skin friction values can be measured using this probe. measurable spectral frequencies are less than half of the reciprocal of the time of flight of a thermal pulse.

J. Kielbasa (1975) reported a system in which the heated wire is periodically pulsed and the frequency of thermal pulses received is directly proportional to the velocity perpendicular to the wires. The usable velocity range is between 10 cm/sec and 20 m/sec and the claimed accuracy is 1.5%. Only two wires are used and an electronic relay and a flip-flop circuit are used to decide in which direction there is flow.

III. G. Pressure Measurement Techniques

It is always useful to measure the mean pressure gradient relief associated with separation. Since there are strong pressure fluctuations associated with turbulent separation, we could expect these to play a strong role in the separation behavior. A great deal of experimental information has yet to be gathered on the fundamental relationship between turbulent pressure and velocity fluctuations in a separating flow. It would be very difficult to add much to Willmarth's (1975) review of pressure fluctuations beneath boundary layers and review of new experimental techniques (Willmarth, 1971). Most of this technology is applicable to separated flows.

Siddon (1969) has developed a small (1/8 inches diameter) fluctuating-static-pressure probe that removes errors caused by interaction of the probe body with streamwise and cross flow velocity fluctuations. These velocity fluctuations are measured by a two component force transducer and used with the pressure transducer signal in a signal processor to deduce the corrected static pressure. This development allows the measurement of true static pressure fluctuations in the flow within about 20% error. Of course, if the flow direction is changing such that the wake of the probe support washes the sensing elements, erroneous readings will be obtained. In this case this probe cannot be used.

In order to observe the instantaneous static pressure distribution over a large surface with separation, Emmerling's (1973) surface membrane interferometry could be used. The optical apparatus consists basically of a Michelson-Interferometer. One mirror of the interferometer is replaced by a reflecting membrane wall, which is part of the test wall. The turbulent wall pressure fluctuations cause the flexible wall to be displaced by several light wavelengths. The instantaneously occurring fringe patterns can then be recorded with a high-speed camera. This technique is sensitive to pressure fluctuations of the order of 1 microbar. Of course, this is mainly a laboratory research technique rather than for actual equipment or models. Analysis of the time variation of the number of fringes on each small membrane is tedious to perform by hand and can be automated.

In the last several years sensitive solid state integrated circuit pressure transducers have become commercially available at low prices. They are a pressure-sensing diaphragm and force-sensitive solid-state materials, with all temperature compensation, signal conditioning, and amplification included in one package. A temperature sensing circuit is often included.

Of course, the size and design of the measuring port for all surface static pressure measurements strongly influence the measurements, so one should consult Willmarth (1975) for the details of this effect.

III. H. Laser Anemometry

Laser anemometry is one of the valid experimental velocity measurement techniques that can be used for separated flow studies. In essence the principle of this experimental method is the scattering of closely monochromatic laser light by moving particles in the flow. Since the Doppler-shifted frequency of the scattered light is velocity dependent, fluid velocities can be deduced if the scattering particles follow the flow. Naturally there is no disturbance to the flow except the particle seeding, if any, so there is an obvious advantage to using this method in separated flows. Mazumder et al. (pp. 234-269, Thompson and Stevenson, 1974) note that one can easily supply small enough particles that follow the flow to most flowfields of interest. Several general references on laser anemometry with many other cited references include: Stevenson and Thompson (1972), Thompson and Stevenson (1974, 1979), Durst, Melling, and Whitelaw (1976), Durão et al. (1983) and the publications of the equipment manufacturers DISA and TSI. Here we will not review the many contributions made to laser anemometry in the last 20 years since its introduction, but will discuss the practical application of this technique to turbulent separated flows with flow reversal.

It is generally accepted that if one wishes to map a moderately-sized flowfield, the LDA focusing and receiving optics must be on one side of the flow for stable alignment. Otherwise, the repetitive realignment of the optics at each new spatial focusing position becomes tedious and very time consuming. Unfortunately, for Mie scattering of light (particle size $\gtrsim$ wavelength of light, the intensity of light backscattered toward the focusing optics is about 1/100th of the intensity of forward scattered light (Van de Hulst, 1964). Thus, having decided on a backscattering arrangement one must use large receiving lens and a high-powered laser in order to obtain an adequate signal.

If one simply collects the backscattered light from one focused incident beam and beats it with a reference frequency beam of unscattered light, he will find that his signal frequency is dependent on the angle of backscattering. In other words there is aperture broadening and the solid angle of the receiving optics must be decreased to eliminate this ambiguity. Since this step will unacceptably reduce the received signal power, one must abandon this approach and use a dual-scattering fringe system (Durst et al., 1976).

In this arrangement two equally intense beams of wavelength λ are focused at an angle Θ to one another with each beam waist in the focus volume of interest. Fringes of spacing $\lambda_f = \lambda/2\sin(\Theta/2)$ are formed because of interference of the light wavefronts. Now if a particle crosses these fringes with a component of velocity U perpendicular to the plane of a fringe, light is scattered in all directions with its intensity varying with frequency U/λ_f. Aside from the fact that the signal-to-noise ratio (SNR) is much greater in this arrangement (Mazumder, 1970), one can use a very large receiving lens with no additional aperature broadening. Only one component of velocity can be measured, so two other beams of different colors or wavelengths must be used to form another set of fringes which is perpendicular to the velocity component V.

If we wish to determine the flow direction with LDA, we must shift the frequency of one beam of a pair so that fringes in the focal volume are moving with time as the waves in the two beams beat together. Otherwise, a given speed particle moving upstream or downstream produces the same signal. As long as the shift frequency is more than twice the frequency change produced by the scattering particles, signals from particles moving in all directions will be obtained (Durst et al., 1976). There are several ways of frequency shifting light, but the most straightforward method uses an acoustic-optical Bragg cell (Buchhave, 1975). Basically, a Bragg cell uses an ultrasonic driver of frequency f_o in a medium to diffract incident light of frequency f in a single order with the resulting frequency $f + f_o$ (Williard, 1949). Not only is the laser output beam efficiently split by a Bragg cell, but equal beam intensities and path lengths and like polarization can be easily achieved. In the two-component backscattering fringe-type anemometer used

by this writer (Simpson and Chew, 1979), a dual Bragg cell shifts the horizontal first-order diffracted beam by 25 MHz and the vertical beam by 15 MHz. Signals of $(U-V)$ as well as U and V are available.

To measure W one can use a single incident beam with a third wavelength λ along the lens axis which measures only the velocity component parallel to that beam (Munoz et al., 1974). Basically, the back-scattered light is received back through the focusing lens and is beat with a reference beam to produce the doppler signal. Kreid and Gram (1976) appear to have increased the SNR ratio for this arrangement and use a Bragg cell to make the arrangement directionally sensitive. However, they require an etalon to increase the coherence length of the laser and a good optical table for precise alignment of the received signal and the reference beam. Shiloh and Simpson (1980) used a separate fringe-type anemometer to measure W whose beams entered the tunnel 90° to the U and V measuring beams. This arrangement has all of the advantages of a fringe system over a reference beam system, but with the disadvantage of a separate access window. By using three laser beams with different frequencies in a plane, a set of moving on-axis fringes can be formed to measure the on-axis velocity component, as well as the other velocity component in the plane (TSI, 1981). This arrangement produces high SNR signals for this on-axis component and eliminates the need for a separate access window.

A rapidly scanning one-velocity-component directionally-sensitive laser anemometer has been used to relate the structure of the backflow to the outer region flow (Chehroudi and Simpson, 1983). An oscillating mirror scanner is used to deflect the pair of collimated beams. A series of mirrors position the measurement volume along a vertical line perpendicular to the wind tunnel floor. In this case the maximum scanning length was 15 inches and the measured velocity component was perpendicular to the bisector of the two incident beams. By using two-cylindrical lenses, a single photodetector can be used with a short narrow slit to obtain signals from any measurement volume position. Since the oscillating mirror is the only moving part, forward-scattered signals can be obtained without movement or adjustment of the receiving optics.

Signal processing and interpretation of LDA signals is still in a state of refinement (Thompson and Stevenson, 1979; Buchhave et al., 1979; Durão et al., 1983). Without going into great detail, the several types of available signal processing techniques will be outlined. The frequency tracker has been used when so much seeding from natural impurities is present that a nearly continuous signal can be obtained. Unfortunately when the signal is not continuous, as for nearly all gas flows, the tracker can lock onto noise or become unlocked altogether. The validity of the output signal becomes dependent on signal dropout levels and the special circuits that are used to keep the tracker locked onto the frequency of one signal burst to the next (Buchhave et al., 1979). In high turbulence intensity flows such as in separated flows, the tracker can more easily lose the signal due to dropout (p. 184, Thompson and Stevenson, 1974). With a relatively noisy high-powered argon-ion laser, it is very difficult for a tracker to remain locked on the signal even for a continuous signal.

The frequency counter basically filters, amplifies, validates, and counts each burst of LDA signal (Durst et al., 1976). Unfortunately the SNR ratio must also be large (45 dB) to obtain unambiguous results since the electronics must pick a single frequency from each signal burst. If one can see the signal distinctly on an oscilloscope then there is some hope of using a frequency counter for processing.

The photon correlation technique (pp. 142-169, pp. 271-289, Vol. 1, Thompson and Stevenson, 1974) uses the auto-correlation of the received signal to determine the frequency. The latest correlators can produce a correlation function in 32 μsec. A number of workers are using it because virtually no seeding particles are required - natural particles are sufficient for light scattering, although relatively long record and correlation times are required for good results (Cummins and Pike, 1977; Mayo and Smart, 1980).

Fast spectrum analysis (Simpson and Barr, 1975) uses a swept-filter spectrum analyzer and pulse-shaping and sample-and-hold circuits. Sampling frequencies up to 8kHz can be obtained, making possible measurement of turbulence frequencies up to 4kHz. Very noisy signals (15 dB SNR) with a high level of signal dropout and high frequency signals normally associated with Bragg cell frequency shifted systems can be processed. In practice the broadband noise must be only low enough that the signal frequency can be discriminated. The faster the sweep rate the greater SNR required. For example a 25 dB SNR continuous signal can be discriminated at a 1800 Hz sweep rate.

This latter technique was used by Simpson et al. (1977, 1980) in their separated turbulent boundary layer measurements. This technique was chosen for economy, simplicity, and ease of validating data. Simpson (1976a) reported on the interpretation of LDA signals near separation and compared these results with hot-film anemometer results. Quantities such as mean velocities, turbulence intensities, Reynolds shearing stresses, third and fourth power values of turbulent fluctuations (skewness and flatness), and the fraction of time that the flow is in one direction can be obtained. Figure 8 is a typical histogram of particle velocities in the separated flow region. For frequencies greater than 25 MHz, the horizontal flow was downstream while lower frequencies corresponded to backflow upstream.

The seeding of separating flows determines the signal quality and data rate to a large extent. For liquid flows, an average concentration of a narrow diameter distribution of particles can be maintained to provide at most one particle in the measurement volume at any given time. By filtering the liquid, sub-micron particles that reduce the SNR can be eliminated, thus permitting a high enough SNR to permit counter or tracker signal processing.

For gaseous flows, the particle seeding situation is worse. Sub-micron-sized particles scatter background light and reduce the SNR. When using a frequency counter processor one must eliminate all sources of noise, so efforts have been made to eliminate sub-micron particles. Bachalo et al. (1977), Seegmiller et al. (1978), and Driver et al. (1983) used 0.5 μm polylatex sphere solid particles that were carried by an alcohol solvent into the test plenum where the alcohol evaporated. Driver et al. obtained about 50 signals/sec. in the backflow and 2000 signals/sec in the outer region. Johnson (1981) and Delery (1983) report that good seeding particles ($d < 1$ μm) can be produced by the natural condensation of oil vapor in transonic tunnels.

When a poly-disperse aerosol is used, many sub-micron particles are generated, leading to an unacceptably low SNR for using a frequency counter processor. In the Simpson et al. experiments, the sub-micron particles actually produced a white spectrum background noise that permitted more sensitive signal discrimination in fast spectrum analysis processing. About 400 signals/sec were obtained throughout the detached flow, except nearest the wall where a lower rate was achieved. Crabb et al. (1981) report 20 dB SNR signals produced by the condensation of kerosene vapors into particles less than 5 μm in diameter.

Spectrum analysis of these signals was used.

III. I. Holography Techniques

Holography makes possible the retrieval of all the information of the density field of a flow (Havener and Radley, 1972, 1974). The reconstructed image can be analyzed using conventional processes. Shadowgraphs can be obtained by focusing on different planes within the image of the density field, numerous schlieren photographs can be made by varying the knife edge orientation in the reconstructed image of the light source, and interferometric measurements can be obtained by combining the reconstructed light waves describing the flowfield with waves from a reference light that are independent of the flowfield (Vest, 1979; Trolinger, 1974). Havener and Radley (1974) used a Toepler schlieren and a pulsed ruby laser of 20 μsec width to record instantaneously the turbulent flow conditions of a Mach 3 two-dimensional meanflow separating boundary layer. High-frequency transient density fluctuations were recorded by double-pulsing the laser for a double exposure with an accurately controlled interval between pulses as short as 15 μsec.

For interferometric purposes dual holograms can be made at different times, one at a no flow condition and one with flow. Images are interfered upon reconstruction and the fringe configuration is controlled by precisely varying the orientation of the two holograms with respect to each other. The dual hologram plate holder must precisely align and hold the two holograms during image reconstruction (Radley and Havener, 1973). Because two-dimensional mean flows were examined, the resulting fringe pattern due to an instantaneous spatial average of the density across the flowfield produced a density approximately equivalent to a time-averaged value at a single spatial location. Havener and Radley (1974) interpreted mean velocity and temperature profiles from their density profiles using the perfect gas law, assumptions on the static pressure distribution, and Crocco's velocity-temperature relationship. The validity of these latter two relationships in the separation region is questionable, but reasonable results were obtained. Sirieix et al. (1981) and Delery (1981) used holographic interferometry to study the features of the shock-boundary-layer interaction shown in Figure 63. Johnson et al. (1980) and Lee et al. (1984) also have used holographic interferometry.

III. J. Signal Processing and Pattern Recognition Techniques

Today every well-equipped experimental fluid mechanics laboratory has programmable digital data processing Gibson (1973) outlines the fundamentals of digital techniques for turbulence research. Several recent approaches to signal analysis are worth discussing: short-time correlations, conditional averaging, and pattern recognition. These approaches do not assume that shear flow turbulence is random. On the contrary, recent turbulence research indicates that there is some coherence of the large-scaled structures (Davies and Yule, 1975; Hussain, 1983) present in turbulent shear flows. Much of the work discussed in Chapter IV indicates that these large-scaled structures are present in separating turbulent boundary layers.

If one observes transducer signals from a turbulent shear flow, repetitive sequences of signal behavior emerge. For example Nychas et al. (1973) note that there are ejections, sweeps, and interactions between fluid elements near the wall in an attached shear flow in a more or less regular sequence. Unfortunately the frequency of occurrence of these flow structures is not so regular that ordinary long-record-time correlations (Lumley and Tennekes, 1972) are useful. Long-record-time correlations tend to average time variations of periodicity that results in the familiar decaying harmonic correlation function.

For this reason short-averaging-time correlations can be used to examine the temporal similarity of turbulence signals from probes some distance from one another. Basically, a short record time is selected. One signal is time-delay correlated with another signal of equal record length until a high normalized correlation (0.9 or so) is obtained. This indicates that over the short record time the signals at the two locations and/or different times looked closely the same. This technique has much use for separated flows. For example, Figure 9 shows signals from two surface hot-films spaced in the streamwise flow direction in the detached region of the Simpson et al. (1977) flow. On the left the lower signal clearly leads the upper signal and there is distinct similarity of the signals. On the right the upper signal leads the lower in just as distinct similarity. By short-averaging-time time-delay correlations, one can determine the frequency of reversal of the leading and lagging signals and infer information on the upstream-downstream movement of coherent structures.

Conditional-averaging and pattern recognition techniques both use a pre-selected start condition (Van Atta, 1974), which when satisfied tells the signal processor to analyse the data in some specified way. Wallace et al. (1977), Blackwelder and Kaplan (1976) and many others have used pattern recognition methods to analyse unseparated turbulent flow coherent structures. Basically a flow sequence model is developed from conditional averaging of data, which in turn can be used to study the statistical variation of the properties of coherent structures. In other words, a basic pattern is compared with data to see when, how, and how often given flow structures occur. Clearly, such signal analysis techniques are useful for separated flows and can be used with multiple probes and scanning laser anemometer data (Chehroudi and Simpson, 1983).

IV. EXPERIMENTALLY-OBSERVED FEATURES OF SEPARATING AND REATTACHING TURBULENT SHEAR FLOWS

IV. A. Introduction

In this chapter, experimentally observed features of incompressible and compressible detached mean two-dimensional flows over streamlined and bluff bodies will be discussed. Sirieix (1975) surveyed earlier experimental results for these flows. The goal of this chapter is to survey the physical behavior of these flows as recently detected by valid experimental techniques discussed in Chapter III. No detached flow data obtained by invalid techniques will be discussed. The literature that is discussed does not include all experiments in which flow detachment or reattachment has been observed. Experiments which reveal insights on the flow structure are emphasized. Calculation methods are not generally discussed in this chapter so that the results from turbulence modelling, which are discussed in Chapter V, are clearly distinguished from experimentally observed facts.

In section IV.B , the behavior of adverse-pressure-gradient induced separation from streamlined surfaces for steady freestream flows is discussed. Brief observations about separating airfoil and two-dimensional diffuser flows are given before the structural details are discussed. Section IV.C deals with the behavior of detaching and reattaching flows around sharp-edged bluff bodies. Section IV.D discusses compressibility effects, especially the behavior of shock-wave induced detachment. Flow unsteadiness,

which often accompanies the separation process in nominally two-dimensional flows, is discussed in section IV. E.

IV. B. Adverse-Pressure-Gradient Induced Separation on Streamlined Surfaces

For streamlined surfaces, there is no sudden change in wall curvature, so no intuitive location of detachment can be determined. When a turbulent boundary layer on such a streamlined surface encounters a sufficiently strong adverse pressure gradient, the shear layer decelerates, grows in thickness, and has some intermittent backflow as detachment is approached. Two common cases, airfoil and diffuser flows, are briefly discussed before going into detailed flow features.

IV. B.1 Observations of the Inviscid Flow Behavior in Steady Freestream Two-Dimensional Airfoil Flow with Separation

Figure 10 shows experimental chordwise distributions of the suction side velocity just outside the boundary layer U_e for an airfoil at several angles of attack α. Downstream of the zone of detachment the velocity and pressure appear to remain nearly constant until the trailing edge of the airfoil. In general, one will observe this same behavior for a variety of bodies, including a circular cylinder and many different airfoil designs, several examples of which are presented by Cebeci et al. (1972). For these cases, one must conclude from these observations that in the separated flow zone the velocity and pressure just outside the shear layer approach the free-streamline condition - constant pressure and velocity.

Downstream of the trailing edge, U_e must eventually return to U_∞ in both magnitude and direction, since this irrotational flow outside the shear layer obeys Bernoulli's equation. In cases where detachment occurs close to the trailing edge, no constant pressure region is observed and the freestream velocity continues to decrease, sometimes to below the U_∞ value. In these cases the velocity downstream of the trailing edge must increase to U_∞. We will label these two types of flow as free-streamline separation and near trailing edge separation. The data of McDevitt et al. (1976) for transonic flow over an airfoil also show these two classes of separated flow behavior for shock-induced separation at high Reynolds numbers (Figure 11).

In the case of near trailing edge separation, there is apparent strong interaction between the wakes of the suction and pressure sides, since the thickness and velocity scales are not extremely different. Thus, the velocity U_e distribution in the detached flow and near wake regions is controlled by both shear layers. We might say that free-streamline separation occurs when the velocity and length scales of the suction side shear layer are much larger than those found on the pressure side. In other words, when the suction side detachment occurs sufficiently far upstream of the trailing edge so that the pressure side shear flow only very weakly interacts with the suction side shear flow, then a free-streamline separation region is possible.

The near wake region is a critical part of a detached flow since it is characterized by strong interaction of both separated shear layers with the inviscid flow and controls the downstream distance to where the pressure is uniform. It is clear from the inviscid simulation work of Jacob (1975) that an accurate description of this region is very important to the overall drag calculation. Coles and Wadcock (1979) show detailed flow structure data for the near wake shear flow of a lifting airfoil with turbulent separation (Figure 12). Adair et al. (1983) and Thompson and Whitelaw (1983) present near wake data for their test flow. To further emphasize the applicability of free-streamline separation and to examine the important details, airfoil flow inviscid "simulation" efforts will be briefly reviewed.

Bhateley and Bradley (1972) used an equivalent airfoil system consisting of a linearly varying vorticity distribution over the surface of each airfoil element to simulate the separated wake. The computed boundary-layer displacement thickness was superimposed on the airfoil contour to form an equivalent airfoil surface for each element. This procedure was iterated until convergence occurred. The flow downstream of detachment was allowed to develop as a free-streamline flow with no surface boundary conditions. There was tangential flow on only that part of the equivalent airfoil having attached flow. The pressure distribution downstream of detachment was assumed constant and equal to that value of pressure obtained by linear extrapolation of the equivalent body boundary point pressures to the detachment point. They used the experimentally obtained detachment location.

Very good calculations of lift and pressure coefficient were made with this method as long as the free-streamline model satisfied the data. For low angles of attack, trailing edge separation was present for their test cases and pressure coefficient predictions in this region were not good. When there was a long pressure gradient relaxation zone between attached and detached states, their estimate of the free-streamline pressure was also in error. They point out the deficiency of not having a wake model. In summary, their method did not include any pressure gradient relaxation model, no wake model, and used experimental data to locate detachment. It still did a good job in many cases of calculating the pressure coefficient, which basically supports the free-streamline idea.

Jacob presented a similar type method for single airfoils (1969) and for multiple-element airfoils with the capability of inclusion of ground effects (Jacob and Steinbach, 1974). Vortex and source distributions on the contour were used and a boundary layer thickness effect was described as an outflow from the airfoil. The "dead air" or separated zone above the body was simulated as shown in Figure 13 with a separation streamline AO. This separating streamline was required to be tangent to the surface at A. The pressure was required to be equal at three special points of the separating streamlines, at the beginning locations A and U and at point O above the trailing edge. In addition, the pressure was allowed to vary "very little" between points A and O. Thus, the separation streamline AO is not exactly a free-streamline, but in practice is close to being one. A source distribution along the body in the dead air region provided the outflow in this region. The circulation-contributing part of the potential flow and the outflow were adjusted to obtain the equal pressures at the three points. Geller's (1976) method for cascade flow is basically very similar to Jacob's (1969) procedure. The boundary layer displacement effect was assumed small and the simulated wake was assumed to have an infinite length.

Jacob (1976) modified his method to simulate the effect of the wake on the drag and lift, as shown in Figure 13. From the symmetric flow over various shaped ellipses, he determined that $a_s \approx S^*$ for body thickness to length ratios less than 1/2, where a_s is the x-coordinate location of a sink S downstream of

the body and S* is the length along the body surface between the two separation points. The strength of the sink S equals the strength of the source along the separated flow surface AU. Since Y_s was zero for these symmetric cases, he could only empirically determine the sink location that produced the best drag result. The Y_s for cases with non-zero angles of attack was assumed to be given by

$$Y_s = Y_M + (1 - X_M + a_s) \tan (\varepsilon\alpha) \qquad \text{(IV.1)}$$

where $\varepsilon = 0.5$ and X_M and Y_M are the coordinates of the midpoint of a straight line connecting the separation points. This reduces to zero for symmetric flow over a symmetric body.

There was considerable improvement over the low drag calculations of the 1974 version. For the cases presented, the lift-drag polar plots were in very good agreement with measurements even though in some cases the predicted lift coefficients were considerably different from the measurements. The effect of varying ε from 0.3 to 0.7 was said to be small on the drag prediction while the selection of laminar-turbulent transition "point" was found to be important. A very important conclusion from this work is that the wake flow behavior strongly influences the drag. This model has been extended to multiple airfoil systems with flow separation on one or more elements, including compressibility effects (Jacob, 1981).

Maskew and Dvorak (1978), Maskew et al. (1980) and Dvorak (pp. 1346-1352 in Kline et al., 1982) used a vortex wake model for the detached flow instead of the source distribution used by Jacob. The wake is represented by sheets of vorticity shed at the detachment location. Fairly good surface pressure calculations were obtained for the Wadcock NACA 4412 airfoil shown in Figure 12. Ribaut (1983) showed that the vorticity diffusion and dissipation was important in calculating the near wake behavior and drag. This result agrees with Jacob's in that the near wake behavior strongly influences the drag.

IV. B.2 Observations of the Flow Behavior in Two-Dimensional Diffusers

The flow behavior is primarily dependent on the diffuser geometry in two-dimensional diffusers (Fox and Kline, 1962). A typical curve of static pressure recovery, C_p, for the four flow regimes is shown as a function of the divergence angle 2θ in Figure 14. Line a - a represents the approximate dividing line between the unstalled and transitory stall regimes. The separation process does not occur in the unstalled regime. Line b - b divides the transitory stall regime from the fully-stalled regime. Complete pressure gradient relief occurs in the latter regime, similar to free-streamline separation for external flow. Figure 15 is a flow regime map in terms of the divergence angle 2θ and the diffuser length to inlet width ratio N/W.

Transitory stalls are large, pulsating detached flow regions which occur primarily in relatively narrow passages of very symmetric shape. A positive pressure gradient exists all along the surfaces in all known data. The peak pressure recovery is achieved at the lowest 2θ angles in this regime. At peak pressure recovery, both side walls have a non-zero fraction of time with flow reversal, but with $\gamma_{pu} > 1/2$ and no detachment. The overall pressure recovery starts to fall off with an increase of 2θ as soon as a zone of strong reversed flow is found solely on one side wall (Ashjaee et al., 1980). Even for $2\theta > 24°$, $\gamma_{pu} > 0.1$ on the stalled wall in the transitory stall regime, which indicates intermittent backflow.

The flow first detaches near the end of the diffuser, forming a stall. The stalled region grows toward the diffuser throat with fluid from the diffuser exit. After sufficient growth the stall becomes unstable, is entrained by the mainstream flow and is washed out of the diffuser. The sequence repeats itself. Kline and Johnston (Simpson, 1979) suggest that the positive dP/dx is essential in sustaining the transitory stall fluctuating flow pattern, since Smith and Kline (1974) have shown that the maximum unsteadiness occurs just before some fixed stall zone is observed. Of the four flow regimes it is the most complex and the least predictable. The unsteadiness of this flow regime is discussed further in section IV.E.3 below. Lyrio et al. (1981) briefly reviewed the literature on two-dimensional diffusers. Cutler and Johnston (1981) reviewed the effects of inlet conditions on diffuser performance; non-uniformities lead to lower pressure recovery while core turbulence leads to a better performance.

IV. B.3 Structure of an Adverse-Pressure-Gradient-Induced Separating Turbulent Shear Flow

A common thread that runs through both the separating airfoil and diffuser flows is that we would like to know and be able to predict when a small amount of detached flow occurs, i.e., when we have near trailing edge separation or the beginning of transitory stall. The best performance of these devices occurs near these conditions. Research over the last few years has revealed much about the structure of a steady freestream two-dimensional separating turbulent shear flow with some pressure recovery.

Here we will discuss the mean flow and Reynolds stresses behavior, both upstream and downstream of detachment. Experimental observations on the location of detachment are reviewed. The higher order turbulence correlations and the momentum and turbulence energy balances are considered. Wall curvature effects are briefly reviewed. Finally, we will discuss the large eddy structure for such a flow and the role of the large eddies in the backflow.

IV. B.3.a Mean Velocity Distribution

Figure 16 is a side view schematic of the 25 feet long, 3 feet wide test section of the wind tunnel used by Simpson, et al. (1981a). Figure 17 shows the free-stream velocity and non-dimensional pressure gradient dC_p/dx distributions obtained along the tunnel centerline of the bottom test wall. Active suction and wall jet boundary layer control prevented separation on the non-test walls. The separating turbulent boundary layer flow of Thompson and Whitelaw (1982) on a curved surface also had a surface dC_p/dx distribution upstream and downstream of detachment closely similar to Figure 17.

Figure 18 shows the mean streamline pattern for the flow in the vicinity of detachment. Note that in the backflow region the turbulence level is very high compared to the mean flow, so these mean streamlines do not represent the average pathlines for elements of fluid. As discussed below, it appears that the fluid in the backflow does not come from far downstream as the streamlines may suggest, but is supplied fairly locally.

Figure 24 in Simpson et al. (1980) shows that the U^+ vs, y^+ law-of-the-wall velocity profile holds all along the flow channel when the Ludwieg-Tillmann skin friction values are used. Although the Ludwieg-

Tillmann equation is good for H < 2 and

$$C_f = 0.246 \times 10^{-0.678H} Re_\theta^{-0.268} \qquad (IV.2)$$

$Re_\theta > 10^3$, it appears to produce values that agree within measurement uncertainties with Clauser plot estimates when H < 2.5. The modified Ludwieg-Tillmann equations given by Felsch et al. (Kline et al., 1969, p. 170) and given by Fernholz (1964) and used by Dengel et al. (1981) appear to slightly underestimate C_f near intermittent transitory detachment. Upstream of the intermittent backflow, the usual logarithmic form for $y^+ > 30$ holds

$$U^+ = \frac{1}{0.41} \ln |y^+| + 5.0 \qquad (IV.3)$$

when surface heat transfer gage and Preston tube measurements are used to obtain C_f.

Perry and Schofield (1973) proposed universal empirical correlations for the inner and outer regions of adverse pressure gradient boundary layers near separation. Their correlations apply to all types of adverse pressure gradient boundary layers on low curvature surfaces irrespective of whether they are in equilibrium or not, but with the restriction that the ratio $(-\overline{uv})_{max}/U_\tau^2$ must exceed 1.5. The maximum shearing stress at a given location occurs well away from the wall in these flows. Flow structures which produce this maximum shearing stress dominate the outer 90 - 95% of a layer. Since the wall shearing stress approaches zero at detachment, it is a poor parameter to use in describing mean velocity profile behavior away from the near wall region. Although Perry and Schofield examined other velocity and length scales, the ones related to the maximum shearing stress and its location from the wall proved best.

They proposed the defect law for the outer flow as

$$\frac{U_\infty - U}{U_s} = f_2(\eta_2) = 1 - 0.4\eta_2^{1/2} - 0.6 \sin(\pi\eta_2/2) \qquad (IV.4)$$

where $\eta_2 = y/\Delta$

and

$$\Delta = \frac{U_\infty}{U_s} \frac{\delta^*}{C} \qquad (IV.5)$$

U_s is determined by fitting data to equation (IV.4). C is a universal constant given by $C = \int_0^\infty f_2(\eta_2)(d\eta_2)$ and found empirically to be equal to 0.350. The inner law was defined as

$$\frac{U}{U_\tau} - h = f_1(\eta_1), \quad \eta_1 = \frac{y}{e}, \quad e = \frac{Lu_\tau^2}{U_{MP}^2} \qquad (IV.6)$$

where h is a constant and U_{MP}^2 and L are described later.

The conditions for the overlap between the inner and the outer region leads to the following relations:

$$\frac{U}{U_\infty} = 0.47 \left(\frac{U_s}{U_\infty}\right)^{3/2} \left(\frac{y}{\delta_1}\right)^{1/2} - \left(\frac{U_s}{U_\infty}\right) + 1 \qquad (IV.7)$$

$$f_1(\eta_1) = 6.4\,\eta_1^{1/2} \qquad (IV.8)$$

and

$$\frac{U_s}{U_{MP}} = 8\left(\frac{\Delta}{L}\right)^{1/2} \qquad (IV.9)$$

The condition $(-\overline{uv})_{max}/U_\tau^2 > 1.5$ was satisfied by the data for the region downstream of x = 105 inches. Hence, Perry and Schofield's correlations were tried for the locations downstream of 105 inches in the Simpson et al. (1981a) flow where the profiles of mean velocity as well as those of normal and shear stresses were available. The data for the normal stresses are also required since Perry and Schofield neglected the normal stresses term in the momentum equation while computing the shear stress profiles from the mean velocity profiles. It was shown later by Simpson et al. (1974) that the normal stresses terms play significant parts in both the momentum and the turbulence energy equations for flows approaching separation. The normal stresses effects have been considered in a way as discussed by Simpson et al. (1977) and in accordance the maximum pseudo-shear stress U_{MP}^2 is defined as

$$U_{MP}^2 = \left[-\overline{uv} + \int_{y=L}^{\infty} \frac{\partial(\overline{u^2} - \overline{v^2})dy}{\partial x}\right]_{max} \qquad (IV.10)$$

L is defined as the distance from the wall to the maximum in the pseudoshear stress profile.

Figures 19 and 20 show the velocity profiles plotted in the inner and outer layer co-ordinates. The

inner law correlation given by equations (IV.6) and (IV.8) seem to be satisfied reasonably well, although the higher slope of 8.05 satisfies the upstreammost profiles better (Simpson et al., 1977). In the region near the wall, equation (IV.6) takes the usual logarithmic form of equation (IV.3). By matching the logarithmic and the half power regions, Perry and Schofield obtained the expression for the point of tangency as $y_c = 0.58e$. The predicted point of tangency moves toward the wall as one proceeds downstream, indicating that the extent of the logarithmic region gradually decreases, which can also be seen from the mean velocity profiles in Figure 21. The Simpson et al. data satisfy the other matching condition given by equation (IV.9) to be a reasonable extent. The data upstream of intermittent backflow lie within the band represented by the scatter in the data plotted by Perry and Schofield.

When intermittent backflow is present, the profile lies above the Perry and Schofield profile in Figure 20 and dips below the half-power tangent line in Figure 19. Although clearly not as good a correlation as upstream, it appears to hold for $\gamma_{pumin} \geq 0.8$. For $1 \geq \gamma_{pumin} \geq 0.8$, U_s/U_e linearly increases from 0.9 to 1.1 according to the data of Simpson et al. (1977, 1981a, 1983).

Kader and Yaglom (1978) used dimensional analysis and the scaling parameters $\frac{1}{\rho} dP/dx$ and δ to obtain velocity profile correlations for adverse pressure gradient flows with a slowly changing U_e and pressure gradient, i.e., moving-equilibrium cases. Their outer region velocity profile correlation is more scattered than that of Perry and Schofield. Schofield (1980) pointed out that if Kader and Yaglom had used the maximum turbulent shearing stress instead of $(\delta/\rho)\, dP/dx$ in their dimensional analysis, they would have derived the Perry and Schofield results.

As one can see in Figures 21 and 22, there is some profile shape similarity for the backflow mean velocity downstream of 138 inches. Figure 23 shows a good correlation when normalized on the maximum negative mean velocity U_N and its distance from the wall N. A slightly poorer correlation results when δ is used instead of N. The U^+ vs. y^+ law-of-the-wall velocity profile is not consistent with this correlation since both U_N and N increase with streamwise distance, while the law-of-the-wall length scale ν/U_τ varies inversely with its velocity scale U_τ.

Simpson (1983) presented the equation

$$\frac{U}{|U_N|} = 0.3\left(\frac{y}{N} - \ln\left|\frac{y}{N}\right| - 1\right) - 1 \qquad \text{(IV.11)}$$

that describes the velocity profile of the middle region of the mean backflow, $0.02 < y/N < 1.0$, downstream of detachment ($\gamma_{pu} < 1/2$ near the wall). Farther away from the wall, $y/N > 1.0$, this equation does not describe the mean velocity profile well since this outer backflow region is influenced strongly by the large-scaled outer region flow. Nearer the wall than $y/N < 0.02$, the viscous layer can be described by

$$\frac{U}{|U_N|} = -C\left(\frac{y}{N}\right) + \frac{P_1}{2}\left(\frac{y}{N}\right)^2 \qquad \text{where } P_1 = \frac{N^2}{\rho\nu|U_N|}\frac{dP}{dx} \qquad \text{(IV.12)}$$

and C is a constant. For this flow $P_1 < 125$ and the pressure gradient term contributes little. Figure 24 shows a linear $|U_N|/U_e$ vs 1/H relationship for this flow (Simpson and Shivaprasad, 1983), as well as data to be discussed later.

An attempt (Simpson et al., 1980) was made to see if the mean velocity profiles downstream of separation could be composed of the "law-of-the-wake" (Coles and Hirst, 1969) $\omega(y/\delta)$ and a similarity distribution for the remaining wall flow. There is no significant profile similarity of the remaining wall flow.

Hastings and Moreton (1982) obtained a near-equilibrium detached flow. The test flow on a flat wall was accelerated from 23.5 mps over a 1 m distance and then decelerated over a distance of more than 1 m to detachment in a test section similar to that of Figure 16. Downstream of detachment the pressure gradient was adjusted ($U_e \sim (x - x_0)^{-0.12}$) to obtain self-similar mean velocity profiles (U/U_e vs. y/δ) over a length of 0.5 m. This profile is shown on Figure 22 to be almost exactly the same velocity profile ($H = 5.38$) as the Simpson et al. (1981a) data at 144 7/8" ($H = 5.40$), even though $32000 < Re_\Theta < 45000$ while $Re_\Theta = 16300$ for the Simpson flow. The non-dimensional pressure gradient $(-\delta^*/U_e)dU_e/dx$ is 0.0127 and 0.0120 for these profiles, respectively. The mean backflow fits the profile suggested by Simpson (1983) and agrees with the steady flow data shown in Figure 23. The fact that the non-equilibrium flow of Simpson et al. produces almost exactly the same mean velocity profile as the equilibrium flow of Hastings and Moreton for the same non-dimensional pressure gradient leads one to surmise that detached flows react rapidly to local conditions and are almost independent of the Reynolds number. The Gersten et al. (1983) straight-walled diffuser flow ($N/W = 3$, $2\Theta = 21°$, $Re = 6 \times 10^6$) contains a region of detached flow, whose outer region mean velocity profiles appear to agree with those in Figure 22.

Both the Simpson et al. and Hastings and Moreton flows show that the normal to wall mean velocity component is not small in the separated zone but is about 0.2 U_e or greater at the outer shear layer edge.

Buckles et al. (1983) used a laser-Doppler velocimeter to measure the streamwise velocity of turbulent water flow over a two-dimensional solid sinusoidal wave surface. The opposite wall was smooth and flat. A fully-developed channel flow entered the wavy-wall section. Figure 25 shows mean velocity profiles over the eighth of ten waves. A long stalled flow zone extended from detachment at $x/\lambda = 0.4$ to reattachment at $x/\lambda = 0.69$. Detachment occurs where there is an unfavorable pressure gradient and reattachment occurs just upstream of the maximum in pressure. The near wall backflow velocity profiles agree with the correlation of Simpson (1983).

IV. B.3.b Flow Detachment and Upstream-Downstream Intermittency

It is well established that the process of separation of a turbulent boundary layer due to an adverse pressure gradient does not occur at a single streamwise location but is spread over a streamwise region and

involves a spectrum of states. Sandborn and Kline (1961) and Sandborn and Liu (1968) defined the limiting points of the region as the "intermittent" and the "fully-developed" separation points. The former indicates the onset of the separation process by the appearance of intermittent backflow (intermittent transitory detachment) and the latter signifies the vanishing of the mean wall shear stress (detachment). Here we will use the terminology given in Figure 2.

Sandborn and Kline observed that a family of power-law type mean velocity profiles seemed to fit data near where appreciable intermittent backflow was observed. This family of profiles yielded the relation

$$h = \frac{H - 1}{H} = \left(2 - \frac{\delta^*}{\delta_{0.995}}\right)^{-1} \qquad \text{(IV.13)}$$

which is shown on Figure 26. The mean wall shearing stress is greater than zero at this condition. Another family of power-law mean velocity profiles that had zero shearing stress at the wall were used to describe conditions at detachment (eqn. 6 of Sandborn and Kline). Figure 26 shows this h vs. δ^*/δ relation at turbulent detachment, which also correlates laminar detachment data. The shaded regions on this figure show the data used by Sandborn and Kline and Kline et al. (1983) that support these relationships.

Figure 26 also shows h vs. δ^*/δ paths taken by several backward facing step reattaching and adverse-pressure-gradient-induced detaching flows. Using a modified Coles law-of-the-wall and law-of-the-wake mean velocity profile model, Kline et al. showed that the h vs. δ^*/δ path is only weakly Reynolds number dependent even for low δ^*/δ and is nearly the same for flows on flat or low curvature surfaces. The Perry and Schofield correlation produces a path among these data, as do the experiments of Chu and Young (1975). This path can be approximated by

$$h = 1.5(\delta^*/\delta) \qquad \text{(IV.14)}$$

for high Reynolds numbers. Note that it crosses the h vs. δ^*/δ relationships for intermittent backflow and detachment in the shaded regions. For near-equilibrium flows satisfying the Coles velocity profile model, intermittent transitory detachment occurs at $\delta^*/\delta = 0.42$, and $H = 2.70$.

The data of Simpson et al. (1977, 1981a), the data of Eaton and Johnston (1980), Driver et al.(1983) and Ruderich and Fernholz (1983) for reattaching flows, and the data of Buckles (1983) indicate that the locations where $\gamma_{pu} = 1/2$ and $\tau_w = 0$ are the same location. The data of Simpson et al. (1977, 1981a) indicate that $\gamma_{pu} \equiv 0.80$ at intermittent transitory detachment which agrees with equation (IV.13).

Kline et al. (1983) presented a proposed correlation for steady freestream flow that relates γ_{pumin} near the wall to h. The data of Simpson et al. (1977, 1981a), the data of Ashjaee and Johnston (1980) for a diffuser, and the Pronchick (1983) backward-facing step data fall along the path shown in Figure 27.

The apparent reason that this correlation is fairly good for flows with some backflow is that the shape of the mean velocity profiles is related to the turbulence structure of the entire shear layer. In other words, similar u', v' and -uv structures which produce u' near the wall also determine similar U profiles. Thus $\overline{u^2}$ and U near the wall strongly determine γ_{pu} (Simpson, 1976), while the mean-velocity profile determines Θ, δ^* and H.

Most of the LDV data on Figure 27 are closely fitted by

$$\gamma_{pu} = \frac{1}{2}\,\mathrm{erfc}\left(\frac{h - h_o}{\sqrt{2}\,\sigma}\right). \qquad \text{(IV.15)}$$

with $h_o = 0.73$ and $\sigma = 0.1$. As shown in Figure 27, $\sigma = 0.12$ is a poorer fit, especially for γ_{pu} near unity and near zero. With $\sigma = 0.1$, $h = 0.63$ is one standard deviation away from $\gamma_{pu} = 0.5$, transitory detachment. When $h = 0.63$, γ_{pu} is 0.84, which is close to the value of 0.80 that Simpson et al. (1981a) use as a definition of intermittent transitory detachment.

Simpson et al. (1977, 1981a) point out that the attached boundary-layer structure for steady free-stream flows, as described by Perry and Schofield (1973), ceases at intermittent transitory detachment. Collins and Simpson (1978) and Kline et al. (1981) note that boundary-layer calculation methods fail in the vicinity of intermittent transitory detachment. As noted by Collins and Simpson, such upstream calculation methods should be terminated at this location and downstream detached flow methods begun there.

All of the above-mentioned data have been for flows on flat or low-curvature surfaces. The data of Sandborn and Liu (1968) for $\delta/R \equiv 0.13$ and Chou and Sandborn (1973) for $\delta/R \equiv 0.1$ are shown on Figure 26. Here R is the streamwise radius of curvature of the test wall. The h vs. δ^*/δ paths for these flows are distinctly different from the low curvature flows. The Sandborn and Liu data indicate that $\gamma_{pu} \equiv 0.7$ at the location where equation (IV.13) is satisfied. Although there are no other pertinent data available on the effects of curvature at this time, it would appear that equation (IV.13) is not very good for calculating the location of intermittent transitory detachment for these flows.

Figure 16 shows the locations of incipient detachment, intermittent transitory detachment, and transitory detachment obtained from Figure 2. Data from LDV, thermal tuft, and from turbulence measurements with the gaussian velocity probability distribution result (Simpson, 1976).

$$\gamma_{pu} = \frac{1}{2}\left[1 + \mathrm{erf}\left(\frac{U}{2\,u_T}\right)\right] \qquad \text{(IV.16)}$$

are in good agreement in this figure. Figure 28 shows γ_{pu} profiles through the separation region.

Downstream of intermittent transitory detachment, Simpson et al. (1977) showed the existence of similarity in γ_{pu} distributions by normalizing and plotting $\left(\frac{\gamma_{pu} - \gamma_{pumin}}{1 - \gamma_{pumin}}\right)$ vs. y/M where γ_{pumin} was taken as the minimum value near the wall as obtained from a figure similar to Figure 28 and M was the distance of the peak in the u' distribution from the wall. The Simpson et al. (1981a) data also exhibit similarity,

particularly in the region $0.1 \leq y/M \leq 1.0$, with it improving as one moves downstream. Similarity profiles also exist for γ_{pv} or the fraction of time that the flow is away from the wall.

Figure 29 shows the distance M from the wall to where γ_{pu} is 0.99 vs. γ_{pumin} for the two steady flows of Simpson et al. and an unsteady flow. For $\gamma_{pumin} < 1/2$, M/δ^* is nearly constant at unity.

As with the data of Simpson et al. (1981a), the $\gamma_{pu} = 1/2$ line for the Buckles et al. (1983) flow begins at detachment, is well correlated with the occurrence of the zero mean streamwise velocity, and ends at reattachment. Like the near wall γ_{pu} data shown in Figure 28, Buckles et al. found regions of increased forward flow as the wall was approached. Simpson et al. (1981a) attribute this feature to wallward moving fluid spreading outwards as it impacts the wall, thus partially cancelling the reversed flow motion part of the time. At each streamwise location of the detached flow, γ_{pu} approaches unity near the maximum u' location, which agrees with the Simpson flows. Several velocity-time histories of the intermittent backflow region of the Buckles et al. flow are discussed with the flatness and shewness in section (IV. B.3c) below.

IV. B.3.c Reynolds Stresses

Figures 30 and 31 give a comparison of the distributions of $\overline{u^2}/U_e^2$, $\overline{v^2}/U_e^2$, and $\overline{w^2}/U_e^2$ at several streamwise locations of the Simpson et al. (1981a) flow. One can notice that $\overline{v^2}$ and $\overline{w^2}$ are approximately equal to the outer 90% of the boundary layer at most locations. Near the wall, $\overline{w^2}$ is greater than $\overline{v^2}$ at all locations. This feature is consistent with the measurements of Sandborn and Slogar (1955) in an adverse pressure gradient boundary layer approaching detachment. The shear stress correlation coefficient $-\overline{uv}/u'v'$ distributions upstream of detachment agree with those for the Schubauer and Klebanoff (1951) strong adverse pressure gradient boundary layer.

Figure 32 shows $-\overline{uv}/U_e^2$ profiles downstream of detachment while $-\overline{uv}/u'v'$ distributions are shown in Figure 33. As one moves downstream, the peaks for the distributions gradually move towards the outer edge of the boundary layer. Similar features such as correlation coefficients as low as 0.3 with the peaks occurring near the outer edge of the boundary layer were observed by Spangenberg et al. (1967) in their experiments on an adverse pressure gradient flow approaching separation. Nakayama (1985) observed values of $-\overline{uv}/u'v'$ as low as 0.1 near the wall near the trailing edge of a supercritical airfoil, with higher values near the outer boundary layer edge. Figure 33 indicates that the profiles for the separated region seem to exhibit some similarity.

Figure 34 gives the distributions of $-\overline{uv}/\overline{q^2}$ across the boundary layer (Shiloh et al. 1981) for several streamwise stations. The peaks in $\overline{q^2} = (\overline{u^2} + \overline{v^2} + \overline{w^2})$ profiles closely coincide with the peaks in the $-\overline{uv}$ profiles shown in Figure 32 since $-\overline{uv}/\overline{q^2}$ remains flat in the middle part of the boundary layer. The distribution given by Bradshaw (1967) for a zero pressure gradient boundary layer is also plotted as a solid line in the figure. One can notice good agreement between Bradshaw's distribution and the data far upstream of the regions of strong adverse pressure gradients and detachment. $-\overline{uv}/\overline{q^2}$ in the vicinity of detachment and downstream is smaller than upstream and has no universal distribution. This reduction in $-\overline{uv}/\overline{q^2}$ can be accounted for by the fact that normal stresses turbulence energy production as well as shear stress turbulence energy production are responsible for the magnitude of $\overline{q^2}$. Shiloh et al. (1981) present such a relationship, which is supported by the data of Nakayama (1985) for strong adverse-pressure-gradient flow on a supercritical airfoil.

Another important result shown in Figures 30 and 31 is the inflexional shapes of the u'^2/U_e^2 distributions near the wall. The slope of u'^2/U_e^2 increases for a short distance and then remains constant from inflexion point C until it is almost equal to v'^2/U_e^2 at inflexion point D. Point C coincides with the local near wall maximum in w'/u'. Point D occurs at a y/δ of almost 0.1.

Points C and D also have special significance in regard to profiles of U related data from Simpson et al. (1981a, b). Downstream of detachment point C corresponds closely to the position of minimum mean velocity U. Point D occurs at a slightly higher velocity. Figure 28 shows that point C closely corresponds to the minima in the upstream-downstream intermittency γ_{pu} and the intermittency of the flow away from the wall γ_{pv}. Figure 35 shows that points C and D lie on opposite sides of the hump in the flatness factor $F_u = (\overline{u^4})/(\overline{u^2})^2$. The hump itself shows that relatively large u fluctuations occur infrequently in this region, indicating the intermittent passage of very high and very low velocity fluid with respect to the mean velocity.

Figure 33 shows no special significance for points C and D, except that they lie in the region of increasing correlation of Reynolds shear stress-producing u' and v' motions. Point A seems to be near where $-\overline{uv}$ is first significantly greater than zero.

Eddy viscosity and mixing length values decrease as detachment is approached (Simpson et al., 1981a) This is due to normal stresses transport as discussed below. Downstream of detachment the mixing length l is imaginary and the eddy viscosity is negative in the backflow. As shown later the backflow is governed by turbulent diffusion and fluctuations, not the mean shearing stresses, so the eddy viscosity and mixing length models fail for the backflow region.

IV. B.3.d Turbulent Momentum and Energy Balances

In order to further understand the effect of detachment on the transport of momentum and turbulence kinetic energy, terms of the governing equations were obtained (Simpson et al., 1981b) using the measured quantities described above. The x-direction and y-direction momentum equations are, respectively

$$U\frac{\partial U}{\partial x} + V\frac{\partial U}{\partial y} = \frac{1}{\rho}\frac{\partial P}{\partial x} + \frac{\partial(-\overline{uv})}{\partial y} - \frac{\partial \overline{u^2}}{\partial x} \qquad \text{(IV.17)}$$

$$U\frac{\partial V}{\partial x} + V\frac{\partial V}{\partial y} = \frac{1}{\rho}\frac{\partial P}{\partial y} + \frac{\partial(-\overline{uv})}{\partial x} - \frac{\partial \overline{v^2}}{\partial y} \qquad \text{(IV.18)}$$

For each equation the terms on the left side are inertia or convective terms while the terms on the right side describe the pressure gradient, the shearing stress gradient, and the normal stress gradient, respectively. The turbulence energy equation is

$$\frac{U}{2}\frac{\partial \overline{q^2}}{\partial x} + \frac{V}{2}\frac{\partial \overline{q^2}}{\partial y} = -\frac{\partial}{\partial y}\overline{\left(v\left(\frac{p}{\rho} + \frac{q^2}{2}\right)\right)} - \overline{uv}\frac{\partial U}{\partial y} - (\overline{u^2} - \overline{v^2})\frac{\partial U}{\partial x} + \varepsilon \qquad \text{(IV.19)}$$

The terms on the left side are advection terms while the terms on the right side describe turbulent diffusion, turbulent shear stress production, normal stresses production, and dissipation, respectively. Dissipation was not measured, but was estimated near the wall in the detached region. In all three equations the viscous terms have been neglected since they are much smaller than the other terms.

The only important terms in the equation for momentum transport in the y-direction are the pressure gradient and the normal stress terms. This is true both upstream and downstream of detachment and leads to the following simplification of equation (IV.18).

$$-\frac{1}{\rho}\frac{\partial P}{\partial y} = \frac{\partial \overline{v^2}}{\partial y}$$

Upon integration it becomes $P(x,y) = P_\infty - \rho\overline{v^2}$. Differentiating this equation with respect to x produces

$$-\frac{1}{\rho}\frac{\partial P}{\partial x} = -\frac{1}{\rho}\frac{dP_\infty}{dx} + \frac{\partial \overline{v^2}}{\partial x} \qquad \text{(IV.20)}$$

which can be substituted into eqn. (IV.17).

In the detached flow region the convection terms in eqn. (IV.17) become unimportant in the inner layer. The momentum transfer due to shear mainly balances the x-direction pressure gradient. In the outer region in addition to the important convective terms, the normal stresses term becomes important as detachment is approached, as shown by Simpson et al. (1977). Hastings and Moreton (1982) also found this to be the case. The normal stresses play an important role in the vicinity of the maximum shear stress. Their importance increases progressively downstream and contributes up to half of the momentum transport in the outer region. Thus the inner layer in the separated region could be modeled by neglecting the convective terms while in the outer layer the additional effect of the normal stresses must be included.

As noted in the earlier work of Simpson et al. (1977), the normal stresses turbulence energy production terms are important in separating flows. Simpson et al. defined a nondimensional factor F as the ratio of total turbulence energy production to the shear-stress-related turbulence energy production

$$F = 1 - \frac{(u'^2 - v'^2)\,\partial U/\partial x}{-\overline{uv}\,\partial U/\partial y} \qquad \text{(IV.21)}$$

Figure 36 shows F-1 for the several locations just upstream of detachment. As indicated by these data and the data of Simpson et al. (1977) and Schubauer and Klebanoff (1950), the normal stresses effect becomes increasingly important as detachment is approached. In fact both Simpson et al. sets of data show good agreement in the corresponding regions of development, with a near doubling of the ratio between intermittent detachment and detachment. The present data in that region indicate the presence of a hump in the distributions near y/δ of 0.05 to 0.1, which becomes more significant as detachment is approached. This is a result of the mean velocity profiles becoming inflexional in nature, which produces a reduced $\partial U/\partial y$ in that region. In fact these humps increase rapidly along the flow until $\partial U/\partial y$ attains a zero value for each profile in the backflow region where the velocity reaches a minimum value. The earlier data of Simpson et al. (1977) at 124.3 inches also suggest the presence of a hump. In the mean backflow region the two types of production oppose each other, but they aid one another in the forward flow outer region. The distributions in the outer layer tend toward similarity and the ratio F-1 seems to be almost a constant of 0.6 for $0.2 \leq y/\delta \leq 0.7$. Simpson et al. (1981a) related the reduction in mixing length and eddy viscosity values in their detaching flow to F.

The results for the Bradshaw (1967) adverse-pressure gradient flow are in qualitative agreement with these data upstream of detachment. As far as shear production alone is concerned, the Simpson et al. (1981b) data in the region just upstream of detachment are in agreement with those of Spangenberg et al. (1967) and others who observed two peaks in distributions for boundary layers subjected to large adverse pressure gradients. The Simpson et al. data indicate that as detachment is approached, the peak near the wall becomes weaker until it vanishes near detachment ($\gamma_p = 0.5$). In the backflow zone of the detached flow there is relatively little shear production as indicated by Figure 37 and advection is also insignificant. Hence the only mode by which turbulence energy can reach the backflow zone is by turbulent diffusion. The dissipation rate in the near wall region upstream and downstream of detachment was established by Shiloh et al. (1981) to be $\varepsilon\delta/U_e^3 = 4 \times 10^{-3}$ and is balanced by the turbulent diffusion. As pointed out by Simpson et al. (1981b) diffusion plays a major role in transporting the turbulent kinetic energy in separated flows from the middle part of the layer, where it is mainly produced, to the outer region and the region near the wall. The absence of significant production near the wall in separated flow also leads one to conclude that the backflow near the wall is controlled by the large-scaled outer region flow, rather than by some wall-shear-stress-related "law-of-the-wall".

IV. B.3.e Effects of Separation on Flatness and Skewness Factors

The skewness $S_u = \overline{u^3}/(\overline{u^2})^{3/2}$ and flatness $F_u = (\overline{u^4})/(\overline{u^2})^2$ factors describe the deviation of the u

velocity probability distribution from a gaussian one. $S_u = 0$ and $F_u = 3$ for a gaussian distribution. A negative skewness indicates that relatively larger negative fluctuations occur more frequently than positive fluctuations and vice versa. $F_u > 3$ indicates that relatively wider "skirts" are present on the edges of the velocity probability distribution as compared to a gaussian distribution. These factors are influenced by separation phenomena.

Upstream of detachment the outer region laser anemometer data of Simpson et al. (1981b) for F_u agrees with the zero pressure gradient boundary layer data of Antonia (1973). The good agreement observed between the two sets of data in the logarithmic region and the outer region indicates that the pressure gradient does not have much effect on F_u and F_v in those regions. Comparison with Figure 35 for the flow downstream of detachment indicates that separation phenomena also do not have much effect on F_u over the shear layer. The same comments also apply for F_v and F_w. One difference shown in Figure 35 is that a local maximum in F_u occurs between the location of the two inflexion points C and D in the $\overline{w^2}$ profile or near the maximum mean backflow velocity.

However, when plotted against y^+ (Simpson et al., 1981b), the data for F_u upstream of detachment indicate an apparent effect of pressure gradient in the region close to the wall, mainly in the buffer layer $8 < y^+ < 20$. In the viscous sublayer for both zero and adverse pressure gradient flows, the flatness factor attains values much higher than the value for a gaussian probability distribution, which is equal to 3. This is possible because the inrush of high velocity fluid from the outer region results in large amplitude positive u fluctuations and consequently produces a large skirt in the velocity probability distribution. Similarly, near the outer edge of the boundary layer, intermittent large amplitude negative u fluctuations occur as a result of the large eddies driving the fluid from the low velocity regions outwards, which tends to increase the flatness factor. In the buffer layer near a y^+ of 13, zero pressure gradient flows all show a dip in the F_u flatness factor distributions and a change in sign in the skewness factor S_u distributions for u (Simpson, et al., 1981b). This location is where u' attains the maximum value. The Simpson et al. data neither show any such predominant dip in F_u nor sign change of S_u in the buffer layer. Sandborn's (1959) data for F_u in an adverse pressure gradient boundary layer flow show a behavior similar to these data.

Simpson et al. data for S_u upstream of detachment indicate a change in sign at a location farther away from the wall ($y/\delta \simeq 0.4$). This location corresponds to the region where the Reynolds shear stress and the turbulent intensities reach their maximum values. The intense momentum exchange in this region results in the lack of occasionally very high or very low fluctuations and as a consequence the probability distribution does not have much skewness. As one moves closer to the wall, the intermittent large amplitude positive u fluctuations tend to make the probability distributions more positively skewed and vice-versa when one moves away from the wall.

The location corresponding to zero skewness for u occurs very close to the wall in zero-pressure-gradient flows because the Reynolds shear stress attains a maximum value in that region. Furthermore, the intense mixing in that region suppresses large amplitude u fluctuations, thus removing the skirt in the positively skewed velocity probability distribution and changing it to a more nearly top-hat shape with a low flatness factor. The same does not happen in adverse pressure gradient flows in the region of maximum shear because the probability distribution in that region is more nearly gaussian with only a slight skewness and with no significant large amplitude fluctuations to be suppressed.

Downstream of detachment the skewness S_u is reduced to negative values in the backflow region as shown in Figure 38. A maximum is observed in the vicinity of the minimum mean velocity. As shown in Figure 35, F_u also has a local maximum near this location. The second zero-skewness point is slightly closer to the wall than the location of the maximum shear stress.

There is a significant variation of S_v along the flow. Only downstream of intermittent transitory detachment is there profile similarity in the outer region. S_v downstream of detachment exhibits a shape approximately opposite in sign to that of S_u, with a large positive skewness factor near the outer edge of the boundary layer, gradually decreasing to negative values towards the wall. This results in the appearance of two zero-skewness points in the distributions of S_v both upstream and downstream of detachment. The zero-skewness point which is farther from the wall occurs in the region of maximum shear both upstream and downstream of detachment, which indicates that the backflow has no influence on the location of this point as in the case of S_u. Downstream of detachment the flatness and skewness factors away from the wall are in qualitative agreement with those of Wygnanski and Fiedler (1970) for a plane mixing layer. This is not surprising since the mean velocity profiles resemble those in mixing layers. S_w is approximately zero, as it should be for a mean two-dimensional flow.

Data from the Buckles et al. (1983) flow (Figure 25) also support these results. Typical velocity time histories measured at selected points in that flow are shown in Figure 39 (a) - (f) and are particularly informative. The data at $x/\lambda = 0.15$ in Figure 39 (a) represent flow very near the point of detachment and very close to the wall. The flow is equally positive and negative, and the skewness is small and positive, indicating a slight tendency towards dominant positive fluctuations. The flatness value of approximately 7.5 implies an intermittent process with equally strong positive and negative fluctuations. The amplitudes of these strong fluctuations are roughly twice the background amplitude.

Data obtained at $x/\lambda = 0.3$, presented in Figures 39 (b) - (d), are representative of flow in the middle of the stalled zone. Close to the wall the velocity exhibits substantial periods of inactivity when it remains close to zero, followed by large negative fluctuations (Figure 39 (b)). The mean velocity is slightly negative at this point, and the flow is reversed almost 70% of the time. When positive

fluctuations occur, they are usually in the form of rapid spikes separated by a mean period T of about 0.6 sec. In non-dimensional terms and using outer variables, $U_bT/\delta \approx 9$. At the location of maximum reversed mean flow (Figure 39 (c)) the periods of zero velocity are shorter, and the periods of reversed flow are correspondingly longer. Reversed flow occurs approximately 80 per cent of the time. At $y - y_s$ = 5.84 mm (Figure 39 (d)) the y-profile of the fluctuation intensity shows a local maximum. As we shall see, this maximum is associated with the centerline of a shear layer that originates close to the point of detachment. The mean velocity is $0.445U_b$ but, instantaneously, the velocity almost reaches U_b = 50.7 cm/s and occasionally drops below zero.

At x/λ = 0.3, large values of the flatness close to the wall reflect the intermittency of the velocity signals in the detached flow region. Maximum values of around 4 occur at the location of minimum mean velocity (maximum reversed flow), exactly the same location observed by Simpson et al. (1981b) in Figure 35. The most important feature of the skewness profile are the two zero crossings. The skewness changes sign in the free shear layer, roughly at the maximum in the turbulent intensity or the inflection point of the average velocity profile. The positive skewness close to the wall reflects the intermittent bursts of positive velocity indicated in the signals displayed in Figure 39. The maximum value of the skewness occurs roughly at the location where the average velocity is zero.

In the immediate vicinity of the wall the skewness again changes sign, as has previously been found by Simpson et al. (1981b). This behavior is similar to what is found at $y^+ \approx 10$ for turbulent flow over a flat plate. However, in this case the point closest to the wall has a skewness of opposite sign to what is observed for a flat plate because the fluid close to the wall is moving in the upstream direction.

The flow close to the wall in the vicinity of reattachment is represented in Figure 39 (e). The mean velocity and the root mean square of the velocity fluctuations are both small, but the root mean square is approximately four times the mean. The flow is forward about 60 per cent of the time, and it is characterized by generally small fluctuations interspersed with large positive spikes and significantly less frequent negative spikes. Directly above this point, at $y - y_s$ = 7.62 mm (Figure 39 (f)), the flow is similar to the shear layer behavior observed in Figure 39 (d).

IV. B. 3.f Effects of Separation on Eddy Structure

Turbulent boundary layers without separation and adverse-pressure gradients are quite complicated themselves and much theoretical and experimental research has been devoted to this subject without complete satisfaction. In this type of flow large-scaled (1/2 δ) transverse vortex coherent structures (Simpson et al., 1977) are present which govern the bulges in the outer edge of the boundary layer, the entrainment of inviscid freestream fluid into the boundary layer, the transport of momentum and kinetic energy within the boundary layer, and the quasi-periodicity of the viscous sublayer "bursting" phenomenon. The transverse vortex motions are formed as a result of interactions between low-speed and high-speed fluid elements in the outer region. These vortices grow in size while traveling downstream at a small angle away from the wall.

The bursting behavior occurs when low speed fluid lifts off the near wall region into the logarithmic region of the boundary layer. The frequency of occurrence of the bursting phenomenon scales on the mainstream velocity and the shear layer thickness. The beginning of a sequence of ejection of low speed fluid from and sweep of higher speed fluid toward the wall region closely correlates with the passage of a transverse vortex (Nychas et al., 1973). Since the streamwise convection velocity of disturbances in the sublayer is of the order of 12-16 U_τ, these disturbances must emanate from the outer region transverse vortex. This convection velocity is greater than the local mean velocity in the sublayer, while it is less than the mean velocity further away. The wall region ejections do not move to the outer region and give rise to the contorted edge of the boundary layers (Praturi and Brodkey, 1978).

These results suggest a simple flow model for the near wall region upstream of separation. A large-scaled outer region structure throws some higher velocity fluid toward the wall as a sweep. This fluid has some wall-ward momentum, so it displaces low velocity fluid that is nearest the wall. The low velocity fluid has lost its streamwise momentum because of viscous stress near the wall. The displaced fluid forms the ejection which moves up and around the sides of the sweep. A fold between the sweep and ejection fluid results which forms the streamwise rotational motion that has been observed. Because both the low velocity fluid and the high velocity sweep fluid contribute to the average wall shearing stress, then the wall shear velocity U_τ is a normalizing parameter for the spanwise spacing and the time duration for an ejection to occur. This time is short compared with the lifetime of outer-region transverse vortex motions. The time between sweeps is governed by the large scale outer region structure.

The characteristic large eddy passage frequency is shown in Figure 40 (Simpson et al., 1977) to decrease as detachment is approached. This frequency f_b scales on the freestream velocity U_e and the boundary thickness δ, with $U_e/\delta f_b = 10 \pm 3$ for the upstream flow and the outer region of the separated flow. The parameter $U_e/\delta f_b$ has this value and not 5 as in the zero pressure gradient case because of lag produced by the pressure gradient. In the backflow region $10 \pm 3 < U_e/\delta f_b < 50 \pm 10$ (Simpson et al., 1981b). In the Buckles et al. flow, $U_bT/\delta \approx 9$ for the non-dimensional period between rapid inrushes of fluid in toward the wall.

The spanwise spacing λ between streamwise rotational wall structures scales on the maximum turbulent shearing stress and the viscosity upstream of detachment, i.e., $\lambda_z(-\overline{uv})^{1/2}/\nu \approx 100$. Downstream of detachment λ_z is an order of magnitude greater than upstream of intermittent transitory detachment (Simpson et al., 1977). Beginning just upstream of detachment the spanwise integral length scale of the turbulence near the wall increases like δ^2. Since δ also grows rapidly along the flow, this means that the near wall detaching flow is increasingly dominated by the large-scale outer flow. Chehroudi and Simpson (1983) used a rapidly scanning laser anemometer to obtain space-time data that shows the backflow to be closely related to the local outer region flow.

The wave speed of celerity of the eddies near the wall is about 14 U_τ upstream of detachment (Simpson et al., 1977). This is a small fraction of the wave speed of the outer region eddies as separation is approached. Simpson et al. (1981b) speculate that as large scale structures pass through the outer flow at a frequency of about $U_e/10\delta$, these same structures move at a much lower celerity in the backflow region, producing a much lower frequency spectrum.

The length of the zone between ID and D in Figure 1 is likely to be related to the ratio of scales of turbulent motion in the outer and reversed flow regions. In terms of the flow geometry, the length of the detachment zone should decrease for increasing divergence of the surface from the mainstream flow direction.

As measured by Buckles et al. (1983) the rms surface pressure fluctuations increase at detachment to a maximum just downstream of reattachment ($\gamma_{pu} = 1/2$). These fluctuations are large, being of the same order as the local mean pressure difference. This behavior is consistent with that of other detached and reattaching flows, as reviewed by Mabey (1972). The maximum rms value near reattachment is too large to be explained entirely by wandering of the reattachment location. Rather, it appears to be influenced by wide variations of the velocity of the fluid impinging on the wall of reattachment. These unsteady motions may be a combination of the unsteadiness caused by the passage of large scale structures and by unsteadiness associated with the location of the reattachment point fluctuating upstream and downstream as discussed in section IV. C below.

IV. B.3.g Effects of Surface Curvature on Detaching Turbulent Boundary Layers

Convex or concave surface curvature without streamwise pressure gradients clearly influence the behavior of a turbulent boundary layer. Bradshaw (1973), Gillis et al. (1980), and Baskaran (1983) reviewed the results from a number of experimental investigations in which δ/R was as large as 0.1. For surface co-ordinates (s,n) with velocity components U, u, V and v, the governing equations are

$$U\frac{\partial U}{\partial s} + V\frac{\partial U}{\partial n} + \frac{\partial \overline{u^2}}{\partial s} + \frac{\partial(\overline{uv})}{\partial n} + \left(\frac{UV+2\overline{uv}}{R}\right) = \frac{-1}{\rho}\frac{\partial P}{\partial s} \qquad \text{(IV.22)}$$

$$U\frac{\partial V}{\partial s} + V\frac{\partial V}{\partial n} + \frac{\partial \overline{uv}}{\partial s} + \frac{\partial \overline{v^2}}{\partial n} - \frac{(U^2+\overline{u^2}-\overline{v^2})}{R} = \frac{-1}{\rho}\frac{\partial P}{\partial n} \qquad \text{(IV.23)}$$

for along and normal to the surface. Equations (IV.17) and (IV.18) in a Cartesian co-ordinate system also apply. As pointed out by Wadcock (1980), the highly-directional nature of the structure of a turbulent shear flow probably suggests that a mean streamline coordinate system be used so that familiar turbulence descriptions for low curvature flows will apply approximately. In other words, since the turbulence structure is not invariant with co-ordinate system rotation, the co-ordinate system following the flow should be used.

From these experiments emerges an explanation of the effects of surface curvature on a flow. If the streamlines of the flow near the freestream in the turbulent-non-turbulent region are convex curved, then $\partial P/\partial n > 0$ and there is a reduction in entrainment downstream. This occurs because the tongues of large-eddy fluid that erupt into the freestream to engulf high momentum fluid encounter an opposing pressure gradient that reduces their movement into the freestream. With a reduction in entrainment, there is less mixing, lower Reynolds shearing stresses, lower triple-velocity correlations, and lower turbulence diffusion in the outer region. For concave curvature, $\partial P/\partial n < 0$ and greater entrainment, mixing, and turbulent shearing stresses result.

In the above experiments, the measurements were made in ducts where the streamwise pressure gradient was adjusted to zero. For flows over airfoils and blades, both convex surface curvature and adverse pressure gradients influence the detachment of a turbulent boundary layer. When an adverse pressure gradient is present, the outer region streamlines are not curved as much as the convex surface, so there is less influence of curvature on entrainment than for a zero pressure gradient case. Smits, Baskaran, and Joubert (1981) showed that convex curvature ($\delta/R = 0.03$) reduces the momentum transport through a strong adverse pressure gradient turbulent boundary layer and causes detachment to occur farther upstream than for a comparable pressure gradient flow without curvature.

For example, the data of Schubauer and Klebanoff (1951) showed little effect of surface curvature on the mean velocity profile upstream of detachment, though δ/R was 0.01 at the beginning of curvature and 0.024 near detachment. In fact, Perry and Schofield (1973) showed that these data fall within the scatter of data from flat surface experiments and that they obey their strong-adverse-pressure-gradient velocity profile correlations. The "zero skin friction" experiments of Stratford (1959) for flow over a short length of convex wall and a longer length of concave wall produced results also in close agreement with the Perry and Schofield correlations. Wadcock (1980) investigated with a flying hot-wire anemometer a separating turbulent boundary layer on the convex-curved surface of an NACA 4412 airfoil with $\delta/R \approx 0.01$ upstream of detachment and $\delta/R \approx 0.05$ near the trailing edge. These sets of data also agree with the flat surface h vs. δ^*/δ detachment criteria of Sandborn and Kline (1961)(Figure 26).

Wadcock's data showed no reduction in turbulence activity in the outer region, although in surface co-ordinates the shear stress $-\overline{uv}$ and turbulence energy production $-\overline{uv}\,\partial U/\partial n$ were negative there. Because $-\overline{uv}$ in those co-ordinates was low, $-\overline{uv}/q^2$, $-\overline{uv}/u'v'$, $\varepsilon_M/U_E\delta^*$, and ℓ/δ are about half those values for the Simpson et al. (1981) flow. The curvature term in equation (IV.22) was relatively negligible, while the curvature term in the normal equation (IV.23) was significant.

When the curvature of the surface quickly changes, the outer region streamlines do not curve as rapidly. Near such a convex surface the flow direction and magnitude change quickly due to a local increase in flow cross-sectional area and to an increase in surface pressure. As observed by Baskaran (1983), an "internal" boundary layer near the surface occurs in such cases, as shown in Figure 25 for the channel flow data of Buckles et al. (1983). Note the distinct knee in the velocity profile or discontinuity in $\partial U/\partial y$ as the flow proceeds downstream of the wave crest. As in the Sandborn and Liu (1968) and Chou and Sandborn (1973) flows, velocities near the wall decrease rapidly, thus changing the velocity profile shape and the h vs. δ^*/δ path of the flow in Figure 26 and causing detachment to occur at lower values of h.

The data of Thompson and Whitelaw (1982) and Adair et al. (1983) and the data of Gersten et al. (1983) in Figure 41 appear to show this effect of rapidly changing surface curvature. In the outer region of these cases, there is lower curvature of the streamlines than the wall and lower turbulence and velocity gradients. Thompson and Whitelaw indicate that the backflow mean velocity profile described by equation (IV.11) appears to hold downstream of detachment, indicating that the flow next to a diverging surface is little different from that on a flat surface.

IV. B.3.h Summary - The Nature of a Separating Turbulent Boundary Layer

As a turbulent boundary layer undergoes an adverse pressure gradient, the flow near the wall decelerates until some backflow first occurs at incipient detachment. Large eddies, which bring outer region momentum toward the wall, supply some downstream flow. These large eddies grow rapidly in all directions and agglomerate with one another to decrease the average frequency of passage as detachment is approached. Substantial pressure gradient relief begins near intermittent transitory detachment as the detaching shear layer grows at a rate proportional to δ^2.

These large-scale structures supply the turbulence energy to the near wall detaching flow. The velocity fluctuations in the backflow region are greater than or at least comparable to the mean backflow velocities. Since the freestream flow is observed to be rather steady, this means that the near wall fluctuations are not mainly due to a flapping of the entire shear layer, but due to turbulence within the detached flow. Even though the outer region mean velocity profiles look like those for a free mixing layer, the inner third is substantially different.

The mean backflow appears to be just large enough to satisfy continuity requirements. The backflow mean velocity profile scales on the maximum negative velocity and its distance from the wall, which is nearly proportional to the shear layer thickness δ. Downstream of detachment the mean backflow can be divided into three layers: a viscous layer nearest the wall that is dominated by the turbulent flow unsteadiness but with little Reynolds shearing stress effects; a rather flat intermediate layer that seems to act as an overlap region between the viscous wall and outer regions; and the outer backflow region that is really part of the large-scaled outer region flow. No "law-of-the-wall" type of velocity profile based on a wall shearing stress is valid for the backflow.

The intermittently forward flow ($\gamma_{pu} > 0$) in the mean backflow region can be due to only two effects. Either high momentum forward flow moves toward the wall or high momentum turbulent motions away from the wall set-up instantaneous streamwise pressure gradients that are impressed onto the low momentum wall region to produce instants of forward flow. Both of these effects contribute to the turbulent diffusion of energy, which is consistent with the conclusion given in section IV. B.3.d that turbulent diffusion and dissipation are the main terms in the backflow turbulence energy balance.

As detachment is approached the large eddies produce $\overline{w^2} = \overline{v^2}$ away from the wall. As a large structure the order of δ in height and width supplies fluid toward the wall in the separated region, v fluctuations decrease and are exactly zero on the wall. Because of continuity requirements the fluid must be deflected and contribute to u and w fluctuations. Thus u' and w' are a little greater due to this wall effect than they would be with large scale structure effects alone. This explains why u' and w' distributions have the inflexion points near the wall. No plausible explanation of these data appears possible when the mean backflow is required to come from far downstream.

The Reynolds shearing stresses in this region must be modeled by relating them to the turbulence structure and not to local mean velocity gradients. The mean velocity profiles in the backflow are a result of time-averaging the large turbulent fluctuations and are not related to the cause of the turbulence. In contrast, in flows for which the eddy viscosity and mixing length models appear to be useful, the instantaneous velocity gradients are not extremely different from the local mean velocity gradient, i.e., the Reynolds shearing stress can be physically related to the mean velocity gradient.

Normal stresses effects contribute significantly to the momentum and turbulence energy equations. Negligible turbulence energy production occurs in the backflow. Normal and shear stresses production in the outer region supply turbulence energy to the backflow by turbulent diffusion. These turbulence energy results lead to the conclusion that the backflow is controlled by the large-scale outer region flow. Movies of laser-illuminated smoke also have clearly revealed that the large eddy structure supplies most of near wall backflow. The small mean backflow does not come from far downstream as suggested in Figure 42 (a), but appears to be supplied intermittently by large-scale structures as they pass through the separated flow as suggested by Figure 42 (b). Thus as pointed out by Simpson et al. (1981a), the Reynolds shearing stresses in this region must be modeled by relating them to the turbulence structure and not to local mean velocity gradients. The mean velocity profiles in the backflow are a result of time-averaging the large turbulent fluctuations and are not related to the cause of the turbulence. Blockage of the backflow region far downstream of detachment does not seem to affect the detachment location (Simpson et al., 1981b).

The flow of Buckles et al. also support this view. Visualization of separated flow over a wave using surface injected dye streaks (Zilker and Hanratty, 1979) showed the separated shear layer rolling up into vortices which fill the entire wave trough. In contrast, if this region behaved as a free shear layer, we would expect instead, to see more isolated eddy structures with a passive fluid in the reversed flow zone separating the shear layer from the wave surface (Buckles et al., 1983).

The photographs of Zilker showed columnar motions carrying dye between the wave surface and the shear layer. The directions of these flows cannot be ascertained, but the wall 'splat' effect discussed in conjunction with the Buckles intermittency data indicates at least some of the dye columns correspond to strong, intermittent downward motions.

The data of Buckles et al. suggest a qualitative picture of the flow in which shear layer vortices send fluid downward toward the wall and entrain fluid from the reversed flow region upwards into the shear layer. Large, positive skewness values and large flatness values in the reversed flow region near the wall imply intermittent pulses of forward moving fluid, possibly associated with the passage of shear layer vortices overhead. These observations led Buckles et al. to suggest that the detached shear flow was driven by a mechanism other than just the external pressure gradient.

Of course, this mechanism for supplying the backflow may be dominant only when the thickness of the backflow region is small as compared with the turbulent shear layer thickness, as in the Simpson et al.(1981a)

flow. Experiments (Fox and Kline, 1962) on separation in wide-angle diffusers indicate that the mean backflow can come from far downstream when the thickness of the backflow region is comparable to the thickness of the forward flow. However, the measurements of Ashjaee et al. (1980) indicate that for large transitory stall, γ_{pu} is never zero! Thus, some forward flow is supplied to the near wall region by the large eddies.

IV. C. Separation from Two-Dimensional Sharp-Edged Bluff Bodies and Reattachment

The main obstacle to understanding this class of flows comes from the fact that the major detachment occurs near the sharp edges of the body, with accompanying large variations in velocity and pressure around the detachment location. Here intermittent detachment is located very near detachment. The flow downstream of detachment is strongly dependent upon the upstream velocity distribution and the local geometry of the surface around the detachment location. Downstream of detachment the thickness of the energetic outer region flow is comparable in size to that of the backflow region. The zone of recirculating fluid is a substantial portion of the entire detached shear layer. At some distance downstream the turbulent shear layer reattaches to the surface or mixes with an adjacent stream in the near wake.

Bluff body, fence, rib, and forward-facing step data will be discussed together because the mean flow streamline at detachment from a sharp edge is at some large angle to the freestream direction. For backward-facing step flows, the mean streamlines at detachment are almost parallel to the on-coming freestream velocity direction. This flow will be discussed separately for this reason and the fact that it has been studied by many researchers. Flows with self-induced oscillations will be discussed in section IV. E.3 below. No review of the large amount of base pressure data will be given.

Data for cases with a thick initial boundary layer, $\delta/H >> 1$, will not be discussed. For these latter flows, the on-coming turbulent boundary layer structure is dominant and a bluff body on the surface acts as a roughness element. For such roughness elements the inner layer parameters $U_\tau H/\nu$ appears to correlate data. Castro (1979) indicates that the rapid distortion theory of Counihan et al. (1974) is qualitatively correct for the downstream flow, but fails to give good quantitative results downstream of reattachment. Castro (1981) also indicated that when $\delta/H >> 1$, no periodic behavior of the turbulent structure was apparent. Young and Paterson (1981) recently reviewed drag data for such surface excrescences.

IV. C.1 Backward-Facing Step Reattachment Flow

IV. C.1.a Nature of the Flow

Although the backward-facing step is the simplest reattaching flow, the flow field is still very complex. Figure 43 illustrates some of the complexities. The upstream boundary layer detaches at the sharp corner forming a free-shear layer. If the boundary layer is laminar, transition begins soon after detachment, unless the Reynolds number is very low (Armaly et al., 1981, 1983).

The separated shear layer appears to be much like an ordinary plane-mixing layer through the first half of the separated flow region. The dividing mean flow streamline is only slightly curved, and the shear layer is thin enough that it is not affected by the presence of the wall (Figure 43). However, the reattaching shear layer differs from the plane-mixing layer in one important aspect; the flow on the low-speed side of the shear layer is highly turbulent, as opposed to the low-turbulence-level stream in a typical plane-mixing layer experiment. Some authors, including Chandrsuda et al. (1978) have suggested that the turbulent recirculating flow causes the reattaching shear layer to be substantially different from a plane-mixing layer.

The separated shear layer curves sharply downwards in the reattachment zone and impinges on the wall. Part of the shear-layer fluid is deflected upstream into the recirculating flow by a strong adverse pressure gradient. The shear layer is subjected to the effects of adverse pressure gradient and strong interaction with the wall in the reattachment zone. A rapid decay of Reynolds normal and shear stresses occur within the reattachment zone.

The recirculating flow region below the shear layer cannot be characterized as a dead air zone. The maximum measured backflow velocity is usually over 20% of the free stream velocity, and negative skin-friction coefficients as large as $C_f = -.0012$ (based on the free-stream velocity) have been measured (Eaton and Johnston, 1980).

Downstream of reattachment, the Reynolds stresses continue to decay rapidly for a distance of several step heights. Simultaneously, a new sub-boundary layer begins to grow up through the reattached shear layer. The measurements of Bradshaw and Wong (1972) and more recent measurements by Smyth (1979) and Troutt et al. (1984) have shown that the outer part of the reattached shear layer still has the most of the characteristics of a free-shear layer as much as 50 step heights downstream of reattachment. This observation demonstrates the persistence of the large-scale eddies which are developed in the separated free-shear layer.

This flow is very unsteady. Very large turbulent structures with length scales at least as large as the step height pass through the reattachment region. In addition, flow visualization by Abbott and Kline (1962) showed that the length of the separation region fluctuated so that the instantaneous impingement location of the shear layer moved up and downstream. Quantitative measurements by Eaton and Johnston (1980, 1981a) confirmed this conclusion and showed that the short time-averaged reattachment location deviated from the long-time-averaged reattachment location by as much as $\pm$ 2 step heights. Their data indicate that the non-dimensional frequency of this motion $fX_R/U_o \approx 0.6$ to 0.8, which agrees with the results of Driver et al. (1983). Here X_R is the distance from the step to the location of reattachment and U_o is the inviscid flow velocity upstream of the step.

The period between flow reversals in the reattachment region appears to be random with no apparent correlation between the near wall flow upstream and downstream of reattachment. Although the time T between flow reversals $X_R/TU_\infty \approx 0.09$, these flow reversals are short-lived during time t with $X_R/tU_\infty \approx 0.6$. (Driver et al., 1983).

The largest structure in the flow originates from the roll-up and multiple pairing of spanwise vortices (Pronchick, 1983). This roll-up is similar to the vortex roll-up and pairing process seen in the plane

free shear layer. Troutt et al. indicate that the convective speed of these structures is about 0.6 U_o. Pronchick observed that the spanwise coherence or organization of these vortical structures starts to breakdown 3 step-heights downstream of detachment. Kasagi et al.(1977) used flow visualization to observe that the turbulence structure becomes fully three-dimensional upstream of reattachment.

From their flow visualization studies, Müller and Gyr (1982) explained this breakdown behavior conceptually. As soon as a vortex tube is bent or distorted, it starts to induce velocities on itself (Biot-Savart law). A vortex loop bent in the downstream direction moves away from the adjacent wall while a vortex loop bent in the upstream direction moves closer toward the wall. The velocity induced on the near wall vortex loop by its image vortex can cause it to move upstream relative to the surrounding flow, thus supplying some backflow and forming a very large streamwise length scale and a long time scale. The vortex tubes that are stretched in the streamwise direction lead to more intense mixing, greater Reynolds shearing stresses and turbulence intensities. This is another way of stating McGuinness' (1978) hypothesis: some of the eddies are swept upstream with the backflow while others move downstream.

Pronchick did not observe large-scale structures in the backflow zone. He observed that the backflow consists of small-scale turbulent fluid created by eddy impingements on the wall and directed upstream by the adverse pressure gradient. This is not inconsistent with the conceptual description of Müller and Gyr which deals with the outer region upstream of reattachment.

The turbulence intensity level of the detached flow is 5 - 10% higher than for the plane-mixing layers, which is believed to be due to a very low frequency ($fX_R/U_o < 0.1$) vertical or "flapping" motion of the reattaching shear layer (Eaton and Johnston, 1981b; Driver et al., 1983). Streamlines of the flow field at various times in a flapping sequence show that the amplitude of flapping is less than 20% of the shear layer thickness and that the flapping correlates with strong flow reversals in the vicinity of reattachment. There is a reduction in the reverse flow rate with abnormally short instantaneous reattachment lengths. The shear stress in the flow increases dramatically with longer instantaneous reattachment lengths. Driver et al. suggest that the flapping is produced when a particularly high momentum structure moves far downstream before reattaching. This would create a somewhat greater pressure gradient that would cause greater backflow at some time later. The flapping motion produces negligible contributions to the Reynolds shearing stress.

IV. C.1.b Reattachment Length

The distance from the step to the reattachment location X_R, where $\gamma_{pu} = 0.5$ and $C_f = 0$, is an important length scale for normalizing data. Eaton and Johnston (1981a), Durst and Tropea (1982), Wauschkuhn (1982), and Gersten et al. (1983) have reviewed much of the available data and present tables of parameters and conditions for those experiments. The data in Figures 44 and 45 indicate that the turbulent flow reattachment length to step height ratio X_R/H is mainly a function of the expansion ratio (h_2/h_1) for step height Reynolds numbers Re_h above 10^4. Armaly et al. (1981, 1983) also found a strong Reynolds number dependence for $Re_H < 6000$. For $h_2/h_1 > 2$, there is little expansion ratio dependence (Durst and Tropea, 1981, 1982).

A survey of these data indicate that the momentum thickness Reynolds number at the step was under 2000 for most cases. Cheun et al. (1981) and Westphal and Johnston (1983) indicate that X_R/H seems to increase with increasing initial momentum thickness Reynolds number.

Driver and Seegmiller (1982) found that adverse pressure gradients increase X_R/H, as did LeBalleur and Mirande (1975), who produced an adverse pressure gradient by diverging the reattachment surface away from the flow. Westphal and Johnston (1983) also found an increased X_R/H when the reattachment surface was divergent from the flow with a zero pressure gradient. This is plausible since the large-scale structures of the shear layer must travel farther in order to interact with the reattachment surface. Nice et al. (1966) found that the X_R/H could be reduced 20% or so by using a curved edge on the backward-facing step.

Eaton and Johnston (1981a) summarize other flow effects on reattachment length. High freestream turbulence levels reduce the reattachment length. Low aspect ratio test channels (width/step height < 10) produce lower reattachment lengths. Rotation of the channel about a spanwise axis in the stabilizing direction reduces the three-dimensional turbulence and increases the reattachment length about 8% over the no rotation case. Rotation in the opposite direction enhances the three-dimensional motions and decreases the reattachment length by 50% (Rothe and Johnston, 1979).

IV. C.1.c Structure of the Mean Flow

Figure 46 shows typical mean velocity profiles downstream of a moderately low expansion ratio step. The reattachment length to step height ratio X_R/H for the data is about 6.0, which agrees with Figure 44 for a 1.16 expansion ratio. The h vs. δ^*/δ path of the reattachment data of Kim et al. (1978) ($1.3 < h_2/h_1 < 2.0$), Pronchick (1983) ($h_2/h_1 = 1.43$), and Wauschkuhn (1982) ($h_2/h_1 = 1.2$) are about 0.02 to 0.05 above the correlation line given by Kline et al. (1981) in Figure 26.

Near the step ($x/H < 2$), the mean backflow has a relatively flat profile over about a third of the inner shear layer. Downstream where a rather peaked mean backflow profile exists, available data closely obey the $|U_N|/U_e$ vs. 1/H behavior given by the dashed line in Figure 24. This location is also closer to the beginning of the reattachment zone which occurs downstream of the minimum in near wall γ_{pu} (Figure 43). Although there are few data available for the very near wall backflow, the data of Westphal and Johnston (1983) support equations (IV.11) and (IV.12). The LDA data of Wauschkuhn, Pronchick, and Gersten et al. (1983) show similar backflow behavior.

Figure 27 shows that the reattachment data of Pronchick closely agree with the γ_{pumin} vs. h data for detaching flows, while those of Driver and Seegmiller and Eaton and Johnston ($h_2/h_1 = 1.66$) differ significantly. The Eaton and Johnston γ_{pumin} values were determined by a thermal tuft and are somewhat higher than values obtained by an LDA (Figure 5).

Using the reattachment length as a normalizing length, Westphal and Johnston (1983) (h_2/h_1 = 1.66, Re_H = 4.2 x 10^4) showed that γ_{pumin} vs. $X^* = (X-X_R)/X_R$ was independent of flow conditions at the step and the divergence angle α of the reattachment wall (Figure 47). Eaton and Johnston's data (Figure 43) agree with this correlation, while the data of Driver and Seegmiller and Pronchick deviate slightly. Pronchick's profiles of γ_{pu} vs. y agree with the detaching flow data shown in Figure 28; M/δ^* vs. γ_{pumin} data also agree with detaching flow data in Figure 29.

The non-dimensional reattachment length X* is also a good scale to correlate the shape of C_f and surface static pressure distributions (Narayanan et al., 1974)(Figures 48 and 49). Note that C_f achieves its most negative value at X* = -0.4, near where the reattachment zone begins and the surface static pressure begins to rise.

In Figure 49, C_p^* uses 1 - $C_{p\ min}$ as a normalizing scale. A better correlation is obtained if (C_{pR} - C_{pi}) is used, where $C_{pR} = C_p$ at X_R and $C_{pi} = C_p$ at the step. LeBalleur and Mirande (1975) showed that the shape of this non-dimensional pressure rise distribution was independent of δ/H at the step. The ideal maximum pressure recovery for the expansion ratio (h_2/h_1) is given by the Borda-Carnot relation

$$C_{pc} = \frac{2}{(h_2/h_1)} \left[1 - \frac{h_1}{h_2}\right] \qquad \text{(IV.24)}$$

If (C_{pc} - C_{pi}) is used as the normalizing scale, pressure recoveries for various expansion ratios can be correlated with C_{pc} and C_{pi} known a priori (Tropea, 1982).

IV. C.1.d Turbulence Structure

Figure 46 shows that the maximum Reynolds shearing stress occurs near the maximum $\partial U/\partial y$ value, as in detaching flows, and moves toward the wall as reattachment is approached. According to Pronchick's data, the shear correlation coefficient $-\overline{uv}/u'v'$ is about 0.5 in the middle of the detached shear layer, decreasing toward the wall and the freestream. The data of Simpson et al. (1981a) for a detaching flow in Figure 33 show a much lower value.

The mixing length and eddy viscosity ($\varepsilon_m/U_e\delta^*$) distributions for the detached flows of Driver and Seegmiller and Pronchick have maximum values of about half those for an attached flow. This is in agreement with the results of Simpson et al. (1981a). The Reynolds normal stresses terms of the momentum equations (IV.17) and (IV.18) appear to be important in these flows.

The normal stresses term of the turbulent kinetic energy equation (IV.19) were found to be important in the flows of Durst and Tropea (1982), Driver and Seegmiller (1982), and Pronchick (1983). Measurements of $\overline{u^2v}$ and $\overline{v^3}$ were obtained by Driver and Seegmiller and Pronchick. The y derivative of $\frac{\overline{vq^2}}{2}$ in equation (IV.19) is the velocity turbulence diffusion term. Figure 46 shows that little diffusion of turbulence energy occurs in the backflow before the reattachment region is reached ($\partial\gamma_{pu}/\partial x > 0$). In the backflow as reattachment is approached, the turbulence energy is supplied by diffusion and is balanced by dissipation, since the production and advection terms are negligible. This behavior is consistent with that for detaching flows.

Mabey (1972), in his review of surface pressure fluctuation data, found that the maximum energy content of wall pressure fluctuations near reattachment occurred at $fX_R/U_o \approx 0.6$ to 0.8, which is the same non-dimensional frequency as for the velocity fluctuations discussed above. Driver et al.(1983) showed similar results (Figure 50). The parameter $p_w'/\frac{1}{2}\rho U_o^2$ in a backward facing step flow increases from detachment to a maximum of about 0.05 at reattachment, as shown in Figure 51. The data of Driver et al. indicate about the same value at reattachment and that $p_w'/(-\rho\overline{uv})_{max} \approx 10$. Mabey (1982) suggests that the maximum shearing stress is the proper stress scale on which to correlate and normalize surface pressure fluctuations.

IV. C.2 Fence, Rib, and Forward-Facing Step Flows

IV. C.2.a Nature of The Flow

Figures 52 show some recent laser anemometer results for flow over an airfoil at a large angle of attack (Young et al., 1978). While detachment from this surface does not occur at a sharp edge, this flow contains many of the features of such a flow, such as comparable thicknesses of the outer shear flow and backflow regions. Mean velocity profiles obey a similarity distribution downstream of the quarter-chord point. The shape of the profile in the outer part of the backflow region is similar to that obtained just downstream of a backward-facing step.

At a higher chord Reynolds number of 1.4 x 10^6 and M = 0.49, discrete vortices were reported to be shed from near the crest of the airfoil at regular time intervals. They initially move up and then move in the streamwise direction by the 15 percent chord location. The vortex speed accelerates from about one-half of the freestream value near the crest to nearly the freestream speed at the trailing edge. The vortex paths are less regular near the trailing edge, but the repeatability of the period of the vortex passage remains high from leading edge to trailing edge. While this vortex-shedding behavior is not yet completely explained, it emphasizes the important influence that the flow behavior near detachment has on the downstream flow and the entire flowfield.

Figure 53 shows mean flow streamlines for a uniform freestream flow normal to a plate with a long splitter plate. The splitter plate eliminates the periodic vortex shedding from the two edges of the normal plate that occurs when used alone. Figure 54 shows an instantaneous view of this flow obtained from visualization patterns. According to Smits (1982a), after an initial Kelvin-Helmholtz-like roll-up of the vortex

sheet, the vortices are seen to pair, triple and even quadruple together. This process results in lower energy-containing frequencies in the downstream direction (Hillier et al., 1983). This appears to be the mechanism for the rapid growth of the shear layer and bears many similarities to the structure of a simple mixing layer. The structure which results from a number of vortices joining together appears to behave like a single vortex. The three-dimensionality of the structures increases downstream but the essential features of the flow, even near reattachment, are still recognizable.

Only vortex pairing is shown for simplicity. Because of the high velocity gradient, small differences in the initial conditions of vortex pair A cause them to come together as in pair B. They commence to roll around each other and deform in response to strains caused by their induced velocity (pair C). Viscosity smears out the vorticity and the pair acts like a single vortex, shown as vortex D. Two pairs (C and D) begin to roll around each other forcing the saddle point closer to the splitter plate. S becomes the instantaneous reattachment point, or saddle point, N. Vortex E enters the separation bubble while F proceeds downstream. Although E becomes highly distorted, stretched and eventually entrained in the shear layer, there appears to be no vortex splitting, as suggested by Bradshaw and Wong (1972). Note that all vortices are shown as foci, that is, flow goes into the vortices which means they are three-dimensional. In the secondary separation bubble G the fluid is transported laterally and expelled into the flow at the junction of the side wall and the splitter plate and a complex eigenvalue critical point is observed at that point. Ruderich and Fernholz (1983) observed the same behavior.

As in the backward-facing step case, Hillier and Cherry (1981) reported a significant low frequency motion that was described as a flapping of the shear layer near detachment and a modulation of shedding characteristics near reattachment. For each of the geometries shown in Figure 55, low frequency fluctuations are present with a characteristic time scale in which the shear layer disturbances convect several reattachment lengths. Kiya et al.(1982) reports similar results for geometry A as did Ruderich and Fernholz (1983) for the flow shown in Figure 53. Hillier et al. (1983) found from flow visualization studies that vorticity was shed from the recirculating flow of geometry A as a series of more-or-less discrete turbulent structures with streamwise spacings of the order of 0.6 to 0.8 X_R. Between the shedding of successive structures, there was a noticeably thinner shear layer downstream of reattachment. They suggested that the low frequency motions perhaps correspond to the period between shedding phases.

When there is an incident boundary layer on a fence, rib, or forward-facing step, the first detachment occurs upstream of the bluff body due to the adverse pressure gradient induced by the bluff obstacle (Figure 56). Reattachment occurs on the front of the obstacle. For sharp-edged bodies the second detachment is located at the leading edge with the second reattachment on the obstacle if it is long enough. For short bodies the second reattachment occurs far downstream, while for long bodies a third detachment occurs with a backward-facing step type of flow. In either case, the downstream region of recirculation contains two vortices of opposite sense, as in the backward-facing step and splitter-plate flows.

The large-scale structures of the incident boundary layer are accelerated as it moves over the leading edge of an obstacle, increasing the energy-containing frequencies and possibly subdividing the large-scale structures (Crabb et al., 1981). Downstream of the flow acceleration, the energy-containing frequencies decrease because of the pairing process, described above for the splitter plate flow and for the backward-facing step flow. The data of Crabb et al. indicate for a square rib that $f_{max}X_R/U_\infty$ varies from about 7 near detachment to near 1 at reattachment, where f_{max} is the peak frequency of fF(f) vs. log|f|u' spectral data. The data of Hillier et al. (1983) also show that $f_{max}X_R/U_\infty$ decreases an order of magnitude to near unity at reattachment for geometries A, B, and E of Figure 55. For these same cases, they found that spanwise spatial correlations at reattachment were the same when normalized on the vorticity thickness and were independent of Reynolds number.

The blockage effect of the obstacle in a flow channel increases the acceleration of the flow over the obstacle, leading to increased velocity gradients and turbulent mixing and increases the entrainment of fluid in the separated zone back into the shear layer. This in turn causes reattachment to occur farther upstream than if less blockage were present (Smits, 1982b; Castro and Fackrell, 1978). As in the backward-facing step case, the reattachment length is the streamwise length scale for describing the reattaching flow.

IV. C.2.b Reattachment Length

Figure 57 shows the blockage effect for the splitter-plate in a uniform stream flow of Figure 53. The data of Smits (1982b), Ruderich and Fernholz (1983), Hillier et al. (1983) for geometry B of Figure 55, and earlier studies reviewed by Smits are in very good agreement. As shown by the data in Figure 55, and by Smits (1982b), the reattachment length is lower for lower flow angles at detachment. This is because the flow around the body at low angles is not deflected as far away from the body as at higher angles. For a given blockage ratio, the non-dimensional reattachment length $X_R/H = X'$ can be crudely approximated by

$$\frac{X'(\Theta) - X'(0°)}{X'(90°) - X'(0°)} = \sin\Theta \qquad \text{(IV.25)}$$

where X'(0°) is from the backward-facing step case and X'(90°) is from the splitter-plate flow shown in Figure 53.

The reattachment length for a blunt body in a uniform stream, such as geometry A of Figure 55, is substantially lower than for the flow in Figure 53. There is less distance normal to the freestream for the detached flow to travel before returning to the surface. There is less backflow than in Figure 53, so there is less entrainment of this backflow into the outer shear layer, thus forcing the shear layer to remain closer to the surface. The data of Kiya et al. (1982) agree with those in Figure 55, considering differences in the blockage effect.

Figure 56 shows the detachment and reattachment length data for the forward facing step as compiled by Robertson and Taulbee (1969). The data of Durst and Rastogi (1979), Cenedese et al. (1979), and Moss and Baker (1980) agree with these data.

Figure 58 shows that the reattachment length behind a fence or square rib is strongly dependent on the channel blockage caused by the rib or fence, as in the above mentioned cases. As pointed out by Crabb et al. (1981), the fence has a longer reattachment length than the rib, especially for a sharp-edged (45°)

fence. This difference is probably due to the smaller backflow on the top of the rib that is available for entrainment into the outer shear layer, which forces the shear layer to remain closer to the surface. The data of Crabb et al. (L/H = 3, δ/H = 0.55, X_R/h = 10.2) and Moss and Baker (L/H = 2, δ/H = 0.8, X_R/H = 12) show that increasing the length L of the rib decreases the reattachment length. The data of Crabb et al. (δ/H = 0.55, X_R/H = 12.3 and δ/H = 0.34, X_R/H = 12.9), Cenedese et al. (δ/H = 1, X_R/H = 10.5), Castro (1981) (δ/H = 0.8, X_R/H = 12.8), and Durst and Rastogi (1979) (δ/H = 1/2, X_R = 13.5) for square ribs with 11 < H_D/H < 13.3 show that X_R/H decreases slightly with increasing δ/H when δ/H < 1. For fence flows, Castro and Fackrell (1978) found that X_R/H increased very slightly with increasing H/H_D for δ/H > 2.3 but decreased with H/H_D for δ/H < 2.3. The earlier data that were reviewed by Frost (1973) agree approximately with these later results.

IV. C.2.c Flow Structure

The reattachment length can be used as the streamwise length scale to normalize the shapes of surface C_p, C_f, and γ_{pu} distributions, and describe the behavior of velocity profile distributions. Figure 55b shows $\tilde{C}_p$ distributions for the flows shown in that figure and that

$$\tilde{C}_p = \frac{C_p - C_{pb}}{1 - C_{pb}} = f\left(\frac{X}{X_R}\right) \qquad \text{(IV 26)}$$

where C_{pb} is the base pressure coefficient. The backward-facing step data shown are different than the data for the other geometries, but agree with the backward-facing step data discussed above. The data of Smits (1982b) and Ruderich and Fernholz (1983) for their splitter-plate flows and the data of Kiya et al. (1982) for geometry A of Figure 55 agree with these data. Smits found that there was no simple relationship between C_{pb} and X_R for various blockage ratios but at low blockage ratios C_{pb} = -0.45. The location of maximum pressure occurs downstream of reattachment, indicating that turbulent stress gradients are important (Smits, 1982b).

For all of the forward-facing step, rib, and fence experiments discussed above the $\tilde{C}_p$ data downstream of detachment from a sharp edge agree with the above equation. Figure 59 shows surface C_p distributions upstream and downstream of the step in a forward-facing step flow. The upstream portion has approximately the same shape as for a rib flow (Moss and Baker, 1980). The data of Lamb and McCotter (1984) are in good agreement with the form of equation (IV.26) for ribs with quarter-round leading and trailing edges. Castro and Fackerell (1978) reported that C_{pb} for ribs decreases with blockage for all δ/h ratios.

Ruderich and Fernholz (1983) report a C_f distribution for their splitter-plate flow (Figure 53) with the same shape and scaling on X_R as shown in Figure 48 for the backward-facing step flow. Because of the higher near wall backflow velocities (Figure 60), C_f values are over 3 times those reported for the backward-facing step. Ruderich and Fernholz also report $2 < C_f' \times 10^3 < 3$ for the rms shear stress coefficient with a maximum near where C_f has a maximum negative value; $-1 < C_f/C_f' < 1$, which reflects large near wall velocity fluctuations relative to the mean flow. Equation (IV.11) seems to agree with these mean backflow data. C_f has a gaussian probability distribution at reattachment.

Figure 60 shows also the acceleration of the outer region flow just downstream of the normal-to-flow plate. As in the fence, rib, and forward-facing step cases, the outer region velocity maximum initially moves away from the wall like the large-scaled vortices (Figure 54); only downstream of reattachment does this maximum vanish. Figure 61 shows that the maximum turbulent shearing stress reaches a peak value just upstream of reattachment, as in the backward-facing step case, with a slow decay downstream. The magnitude of the normalized maximum shearing stress $-\overline{uv}_M/U_e^2$ at reattachment is an order of magnitude higher than at detachment from a smooth surface (Simpson et al., 1981a).

Figure 62 shows mean velocity profile data for flow over a square rib. Castro and Cheun (1982b) showed that the maximum level of turbulence downstream scales on $(U_e + |U_N|)^2$ and is greater for rib flows than backward-facing step cases because of greater backflow. They showed that $\overline{u^2}$ is in all cases much greater than in the standard mixing layer, typically by a factor of 2.

Although there have not been as many detailed studies of the turbulence structure as in the backward-facing step case, there are many similarities between reattaching flows. The maximum non-dimensional mixing length and eddy viscosity values are about half those for an attached flow. Reynolds normal stresses terms of the momemtum and turbulence energy equations are important. Turbulence diffusion supplies the turbulence energy near the wall as reattachment is approached.

Figure 51 shows Mabey's (1972) $p_w'/\frac{1}{2}\rho U_e^2$ results for flows with detachment from fences, leading edges, and forward-facing steps, as well as the backward-facing step data discussed above. Again the streamwise length of the stalled zone is the length scale that seems to correlate the maximum $p_w'/\frac{1}{2}\rho U_e^2$ that occurs at reattachment. As in the backward-facing step flows, the maximum energy content of wall pressure fluctuations occurs near $fX_R/U_o \approx 0.6$ to 0.8 in a fF(f) vs. log(f) plot as shown in Figure 50.

The data of Hillier and Cherry (1981) for geometry A of Figure 55 indicates that $p_w'/\frac{1}{2}\rho U_e^2$ is about 0.04 near detachment with large contributions at low frequencies ($fX_R/U_o \leq 0.1$) due to the low frequency flapping. Downstream of X/X_R = 0.1 this part of the spectrum becomes relatively unimportant because the higher frequency

contributions become the major part of the spectrum. At reattachment $p'_w/\frac{1}{2}\rho U_e^2 \approx 0.14$, which is not much larger than values shown in Figure 51 for forward step and leading edge bubble cases. The data of Kiya et al. (1982) for geometry A of Figure 55 are in close agreement. From this rare experiment in which both turbulent shearing stresses and surfaces pressure fluctuations were measured, their data indicate that $p'_w/(-\rho\overline{uv})_{max} \approx 10$ for $X/X_R > 0.4$ upstream of reattachment. This result agrees with the Driver et al. (1983) data for the backward-facing step. Although there is not an abundance of data available, a relationship between the surface pressure fluctuation and the maximum shearing stress seems to have more physical basis than $p'_w/\frac{1}{2}\rho U_e^2$, since $-\overline{uv}_m$ scales the mean velocity gradient and turbulence structure, which in turn determine the surface pressure fluctuation in a Poisson integral.

IV. D. Compressibility Effects on Separation

Aside from the variable density effects, the main effect of compressibility on separation is produced by the presence of shock waves. Shock waves are produced in supersonic and transonic flows and can induce separation by a large pressure rise over a very short streamwise distance. For example, transonic compressors have subsonic relative approach velocities near the hub and supersonic velocities near the tip. This leads to incident shocks on the leading edges near the tip that impinge on other blades and are reflected to other surfaces. Even though the approach Mach number is subsonic in many transonic cases, the flow within a blade passage can be accelerated to locally supersonic values in the midchord region. This locally supersonic flow can produce a shock at higher blade loadings, leading to separation and large losses.

Green (1970) reviewed the possible shock wave-turbulent boundary layer interactions encountered at speeds from transonic to high supersonic. Holden (Hankey and Holden, 1975) reviewed experimental studies of shock wave-boundary layer interactions in supersonic and hypersonic flow. At the time of those reviews, the shock patterns could be explained and valid surface pressure, skin friction, and heat transfer data could be obtained. However, no valid measurements describing the detached and reversed flow regions had been obtained. Here no further discussion of surface data presented in those reviews or of compressible inviscid flow will be made. The emphasis here will be on the turbulent flow behavior near and in the detached and reversed flow region. Compressible flow self-induced unsteadiness is discussed in section IV.E.3.

IV. D.1 Transonic Separated Flows

Delery (1983) presented measurements of three transonic flows with different degrees of shock-induced detachment. In each case the transonic flow was produced by a bump on the wall of the wind tunnel test section. For the third case, Flow C, which has a large detached flow zone, Figure 63 shows Mach number contour plots obtained from a finite fringe interferogram. An infinite fringe interferogram is also shown, which gives a more vivid visualization of the entire flowfield around the shock pattern.

The "lambda" shock structure for this flow is typical. The compression waves coalesce into the oblique shock C_1 which produces a rapid pressure rise that induces detachment of the turbulent boundary layer. This oblique shock is "weak" (McDevitt, 1979) near the turbulent shear layer because supersonic flow continues downstream. This supersonic flow downstream of C_1 is terminated by another oblique shock C_2, which appears in Figure 63 to be a normal shock. Shocks C_1 and C_2 meet at the bifurcation point I, from which a strong oblique shock C_3 begins. A vortex sheet shear layer must originate at the bifurcation point if the entropy production of the strong shock is much greater than the combined entropy production of the weaker shocks.

Across a shock wave the pressure rise causes a rapid deceleration of the fluid with an accompanying thickening of the turbulent boundary layer and an increase in δ^*. Kooi (1975) showed that the initial pressure rise distribution across a shock could be modeled approximately by using Prandtl-Meyer compression wave theory and a ramp produced by the rapidly increasing δ^*. Yoshihara (1981) gave a simple correlation for the pressure P_2 downstream of a shock when the incident $M < 1.35$: $P_2/P_t = 0.54 \pm 20\%$ for airfoils with $2 \times 10^5 < Re_c < 3 \times 10^7$, where P_t is the total pressure.

Although $\bar{\rho}_e/\bar{\rho}_w = 0.83$ in Delery's flows, the change in ρ across the outer part of the turbulent flow is very small. Thus, there should be many direct similarities between shock-induced and incompressible adverse-pressure-gradient induced detaching flows. Childs et al. (1981) showed that the Kooi (1975) flow ($M = 1.4$) with incipient detachment and downstream reattachment obeyed the η vs. δ^*/δ relationship derived from the compressible Van Driest velocity profiles. The Kooi and Délery flows fall among the reattachment data shown in Figure 26 for incompressible flow.

For $\gamma_{pu} > 0.8$, the Perry and Schofield (1973) velocity defect profile appears to hold (Figure 64). For Delery flows B and C, detachment and regions of mean backflow occur (Figure 65). As shown on Figure 24, the $|U_n|/U_e$ vs. $1/H$ relationship for incompressible detaching flows holds for Délery flows B and C. Thus, for a given H, the Delery mean velocity profiles compare approximately with those of Simpson et al. For the reattachment portion of these flows, the $|U_n|/U_e$ vs. $1/H$ path for these flows lies a little above the detachment line, indicating a slightly different velocity profile shape. Clearly, the initial conditions, i.e., the upstream boundary layers, of these detached flows are not extremely important in defining the flow structure since detaching flows with and without shock waves have closely the same features. Flows A, B, and C have δ/R shear layer to surface radius of curvature ratios of 0.006, 0.012, and 0.012. Curvature effects appear to be unimportant for these cases. Note that the x-y coordinates are parallel and perpendicular to the flat downstream test section wall.

Figure 66 shows that at no position in any of the Delery flows is there always a reversed flow. This feature is also like that for the incompressible adverse-pressure-gradient induced detaching flows. These data are evidence that the outer region of compressible flows locally supplies some of the near wall flow at least a portion of the time.

The turbulence structure has many features similar to the incompressible separating flow structure.

As shown in Figure 64 for Flow A, the maximum shearing stress at a given streamwise location occurs in the middle of the shear layer. The maximum shear stress coincides practically with the reattachment location As shown in Figure 67 the maximum shear stress at reattachment is 10 times the maximum value at detachment. Hysteresis loops in Figure 67 show the similarity between different detached and reattaching flows, but that the mean velocity profile and maximum shear stress have a different relationship for detachment and reattachment.

Since detached flow mean velocity profiles depend so strongly on local conditions, the production of turbulence continues in proportion to the growth of the large-scaled structure until reattachment occurs (Seegmiller et al., 1978; Délery, 1983). The production of turbulence energy due to normal stresses is as high as production due to shear stresses over a streamwise distance of $5\,\delta_o$ in the detaching flow region of steepest streamwise pressure gradient. Normal stresses terms are also important in the momentum equation. Farther downstream the contributions of these terms become less important. In the detached flow zone, the mixing length to shear layer thickness ℓ/δ is about half of the flat plate model values. The Bachalo and Johnson (1979) axisymmetric bump flow has a similar structure.

Figure 68 shows the mean streamwise velocity, turbulent shear stress, and turbulent kinetic energy for the detached region of a steady transonic shock-induced separation on a bi-circular arc airfoil with a thickness to chord ratio of 0.18 at zero angle of attack (Seegmiller et al., 1978). The presence of the trailing edge has a negligible effect on the upstream detached flow structure. Like the Simpson et al. (1981a) and Délery flows, the maximum values of the shear stress and turbulence kinetic energy are located above the dividing streamline and close to the location of the maximum normal velocity gradient. Low shear stresses occur in the backflow. The recirculation region is supplied continually by the higher turbulent portion of the shear layer, like for the Simpson et al. flow. The non-dimensional eddy viscosity and mixing length distributions do not change much along the separated flow above the airfoil. Downstream of the trailing edge they increase by 50% as the separated shear layers merge to form the wake. The velocity and turbulence profile shapes in the streamwise direction are comparable with similar data taken downstream of separation in a transonic flow over a bump on a wind-tunnel wall.

Although no shocks were present, the M = 0.7, $Re_c = 40 \times 10^6$ trailing edge separating flow of Viswanath and Brown (1980, 1983) had many qualitative features similar to other adverse-pressure-gradient-induced detaching flows. Figure 69 and 70 show the flow configuration and the mean velocity profiles in the detached and near wake regions. Detachment occurs near X = -2cm. Curvature effects seem to be important since $\delta/R \approx 0.05$ for this flow and the mean velocity profile has a significantly different shape than for low curvature flows. Like the low curvature cases the normal stresses terms are important, the eddy viscosity and mixing length values are half of those for flat plate correlations, and $\gamma_{pu} > 0$ everywhere. The maximum shearing stress, maximum $\partial U/\partial y$, and maximum turbulence energy production occur at about the same locations.

IV. D.2 Supersonic Separated Flows

Figure 71 shows schematically the geometry of a supersonic compression corner shock-wave boundary-layer interaction with detached flow and the presence of reversed flow. The oncoming turbulent boundary layer passes through an initial rise in pressure near the upstream foot of the shock wave system. The upstream distance of this pressure rise location from the corner is the "interaction length" or "upstream influence length", L_M. Shortly downstream of this location, detachment of this highly retarded flow occurs with flow reversal near the wall, if α is sufficiently large.

The location of L_M in experiments is unambiguous since the mean pressure rise is steep (Figure 72a). Dolling and Murphy (1982) point out that the shock wave structure near detachment conditions is highly unsteady, having streamwise excursions of the order of the boundary layer thickness and producing large amplitude pressure fluctuations. This shock wave motion is apparently driven by the large-scale structures whose streamwise length is several times δ_o, since the disturbance frequency is an order of magnitude smaller than U_∞/δ_o. This shock structure results in a large rms pressure fluctuation at the mean position of the upstream part of this shock system as shown in Figure 72b. The initial pressure rise is due to the occasional presence of the oscillating shock wave at that position.

Roshko and Thomke (1976) found that L_M could be correlated by:

$$\frac{L_M}{\delta_o} = \sigma(\alpha)(C_{f_o} - C_{f_o}^*(\alpha)), \quad \sigma(\alpha) = 10^3\left(\frac{\alpha}{18.29}\right)^{2.81}$$

$$C_{f_o}^* = 10^{-3}\,(1 - 0.001189\alpha^2) \qquad \text{(IV.27)}$$

for $10^5 < Re_{\delta_o} < 10^7$, $2.9 < M < 4.9$ and $9° < \alpha < 40°$. Settles and Bogdanoff (1982) suggest that

$$\frac{L_M}{\delta} Re_{\delta_o}^{1/3} = 0.9 \exp(0.23\alpha) \qquad \text{(IV.28)}$$

fits the data better. Note that these relations are formally independent of the Mach number. These authors, Sirieix (1975), and Stollery (1975) surveyed a number of experiments on supersonic shock-boundary layer interactions and summarized the results from much surface heat transfer and pressure data for detached compression corner flows with $10^4 < Re_{\delta_o} < 10^7$, $M < 10$.

Appels and Richards (1975) reviewed "incipient separation" detection methods and observed from their surface oil flow data that two types of detached flows were possible. The "small separation" only had flow reversal in the viscous sublayer region. The "large separation", such as shown in Figure 71, occurs at larger α values where the outer portions of the boundary layer become involved. The length of the

detached flow zone increases with increasing α at a rate several times larger than the growth rate for the "small separation" region.

To obtain a correlation when detached flow was first observed, Roshko and Thomke (1976) selected data on the occurrence of "incipient separation" that were obtained by surface techniques, not by the relatively insensitive location of a kink in the streamwise mean pressure distribution as used by some researchers. As noted in section III.B, the oil flow technique only gives an approximate idea of the location of detachment. No known experiment for this type of flow has located detachment using the fraction of time that the flow moves downstream, γ_{pu}. Roshko and Thomke found that a "small separation" was present when $L_M/\delta_o \approx 0.1$ and a "large separation" occurred when $L_M/\delta_o \approx 0.55$. They showed that using these values in equation (IV.27) one can calculate the ramp angles at which these types of detached flows occur. These results apply only to adiabatic wall cases and have a limiting value of $\alpha = 31°$ as $Re_{\delta_o} \to \infty$.

The initial rise in mean surface pressure to the detachment location for the "large separation" case can be given by

$$\frac{p_D}{p_o} - 1 = 62.5\, M_o^3\, C_{f_o} \qquad \text{(IV.29)}$$

as shown by Appels and Richards. As shown in Figure 72a, between detachment and reattachment the pressure rises more slowly. Farther downstream it resumes a more rapid rise. The static pressures upstream of the shock and well downstream of reattachment are relatively constant. Settles, Vas, and Bogdanoff (1976) found that the decay in the normal to wall pressure gradient in the boundary layer persisted for $5\delta_o$ downstream of the corner. The surface pressure fluctuations downstream of detachment increase to reattachment, in the same way that is observed for subsonic flows (Figure 51).

Standard low-pressure-gradient compressible flow "laws of the wall and wake" closely describe the oncoming boundary layer mean velocity profiles (Hayakawa and Squire, 1982). Downstream of the beginning of the shock-wave boundary layer interaction, the boundary layer thickens and the mean velocity profiles resemble strongly retarded incompressible profiles. Havener and Radley (1974) inferred velocity profiles from density profiles, as discussed in section III.I. Settles et al. (1976) used a reversed pitot tube for the mean backflow region which produced mean velocity profile results similar to those for incompressible flows. Thick mean backflows with maximum values of about 0.1 to 0.15 of the velocity outside of the boundary layer were observed. There are not adequate velocity profile data available for regions with intermittent backflow; measurements near the wall using a LDA are needed.

Recently, two studies of the turbulence structure of compression corner flows have revealed much about their nature. Ardonceau (1984) observed that a quasi-periodic vortex sheet emanated from the foot of the shock wave for an 18°, Re = 1.1 x 10^7/m, M = 2.25 ramp. A low frequency component of the frequency spectrum was observed in the vicinity of the reversed flow zone. This possibly inviscid unsteadiness doesn't affect other parts of the flow. Large amounts of turbulence energy are contained in large-scale structures that are 2δ in streamwise extent and δ in the spanwise and normal to wall directions.

As in other detaching flows, the maxima for the Reynolds stresses profiles occur in the middle of the shear layer. The correlation coefficient $-\overline{uv}/u'v'$ is 0.4 upstream of the shock structure, near unity at the shock, and decays to about 0.6 downstream. Apparently the vortex sheet contributes strongly to the coherence of the flow structure near the shock, which decays downstream. Near the wall there are very low values of $-\overline{uv}/u'v'$, as observed by Simpson et al. (1981) for the backflow of incompressible flows. As in incompressible detaching flows, the Reynolds normal stress term $\partial\overline{u^2}/\partial x$ contributes significantly to the streamwise momentum balance.

Muck and Smits (1984) found that shock oscillation in their $\alpha = 20°$, Re = 6.3 x 10^7/m, M = 2.87 ramp flow appears to cause $-\overline{uv}/\overline{u^2}$ to decrease from 0.27 to 0.2 across the shock, whereas this parameter increases across shocks for 8° and 16° cases due to dilational and concave curvature effects. Among the many common features in the Ardonceau and Muck and Smits experiments is that inviscid unsteadiness causes $\overline{u^2}$ to increase while not increasing $-\overline{uv}$. The dramatic growth in $-\overline{uv}$ and $\overline{u^2}$ is proportional to the imposed pressure gradients. The turbulence structure does not appear to have much lag in its response to destabilizing influences, although these flows are not in equilibrium.

Modarress and Johnson (1976) presented laser velocimeter measurements for the oblique supersonic shock-induced separation shown in Figures 73-76. Marvin et al. (1975) presented forward flow measurements and surface data for a similar flow while Voisinet (1975) presented such data for a detaching flow on a nozzle wall produced by a continuous compression. Because of the sudden imposition of the adverse pressure gradient by the incident shock, the velocity quickly decelerates, producing relatively high near wall turbulence intensities and intermittent backflow. The location of the maximum streamwise turbulence intensity begins to move away from the wall as the mean velocity profiles change shape. Large positive and negative velocities ($\sim 0.1U_\infty$) occur within the shear layer. Dramatic changes in U and u' occur as the flow passes from intermittent transitory detachment ($\gamma_{pu} \approx 0.8$) near $\xi = -3.44$ through detachment ($\gamma_{pu} \approx 0.5$) upstream of $\xi = -2.70$. Bachalo et al. (1977) point out that $\partial\overline{u^2}/\partial x$ is as large as the streamwise pressure gradient, so neglect of this term in the momentum equation is not justified.

After the induced shock the near wall region reaccelerates with reattachment and negative V everywhere within the boundary layer. As shown in Figure 75, the maximum turbulence intensity continues to occur in the middle of the boundary layer downstream of reattachment, which occurs near $\xi = 0.2$. Note from Figure 74 and 76 that while there is mean backflow near the wall, γ_{pu} is never close to zero. This indicates that the local outer region flow influences the backflow as was observed for incompressible flows.

IV. D.3 Compressible Reattachment Flows

Sirieix (1975) presented a survey of empirical correlations for reattaching compressible shear layers. Figure 77 shows a reattachment test flow that will be used to illustrate the flow features. The classical Chapman-Korst flow model describes this situation except that it proposes that reattachment occurs at the end of the pressure gradient. Settles et al. (1982) showed that reattachment occurred where 0.35 of the pressure rise was realized. In a review of earlier work contained in their paper, Settles et al. showed that the streamwise distribution of the pressure rise in Figure 77 could be scaled on the incoming shear layer thickness at reattachment. This "free interaction scaling" (Chapman et al., 1958) is consistent with the lack of downstream influence on the reattachment process.

The mean velocity profiles downstream of reattachment look qualitatively like those shown in Figure 46 for incompressible flow. The reattaching boundary layer associated with Figure 77 appeared to be in local equilibrium when the Clauser pressure gradient parameter was defined in terms of the kinematic thickness rather than the compressible displacement thickness.

The maximum turbulent fluctuations occurred downstream of reattachment at about the downstream end of the shock system. As in the incompressible case, a fairly rapid decay of this fluctuation level occurs downstream. Hayakawa et al. (1983) showed the same effect for the same flow situation. They demonstrated that mean dilatation significantly contributes to the amplification of the turbulence intensities near reattachment. They also suggest that the turbulence length scale is reduced by the division or bifurcation of eddies near reattachment and amplified by the action of extra rates of strain due to dilatation and longitudinal curvature. As for supersonic detaching flows, further LDA measurements of intermittently reversed flow regions are needed to reveal details of the flow nature and structure.

IV. E. Unsteady Effects on Separation

While all turbulent flows are inherently unsteady, the term "unsteady" will mean here an organized time dependent motion in contrast to the relatively aperiodic motion of turbulence. Periodic flow is by far the most common organized time-dependent motion. Two types are possible: one where a periodic flow condition is imposed on a turbulent boundary layer; and the other where the turbulent flow interacts with adjacent flow regions to set up a quasi-periodic motion.

Telionis (1977) reviewed unsteady boundary layer work, although little experimental data on the structure of unsteady separating turbulent boundary layers were available at that time. McCroskey (1977) presented a broader review of unsteady flow cases, including unsteady inviscid transonic and subsonic flow, vortex shedding from bluff bodies, and dynamic stall. Recent symposia have been held on these topics (Michel et al., 1981; Francis and Luttges, 1984).

Section IV.E.1 deals with experiments on unsteady separating turbulent flows with imposed periodic inviscid freestream velocity and pressure oscillations. Dynamic stall on helicopter and compressor blades is an example of the first type of periodic condition imposed on the boundary layer and is described in section IV.E.2. Self-induced quasi-periodic motion has been observed under some conditions in diffuser, airfoil and duct flows including shock-induced separation and is discussed in section IV.E.3 below. The transitory stall in a subsonic diffuser, which was discussed in section IV.B.2 above, is also an example of a flow with self-induced oscillations.

IV. E.1 Unsteady Separating Turbulent Boundary Layers

Unsteady turbulent boundary layers are governed by the same equations as for the steady case, except that time-dependent effects must be included. The continuity and streamwise momentum equations for incompressible unsteady turbulent boundary layers are respectively

$$\frac{\partial \hat{U}}{\partial x} + \frac{\partial \hat{V}}{\partial y} = 0, \tag{IV.30}$$

$$\frac{\partial \hat{U}}{\partial t} + \hat{U}\frac{\partial \hat{U}}{\partial x} + \hat{V}\frac{\partial \hat{U}}{\partial y} = \frac{\partial \hat{U}_e}{\partial t} + \hat{U}_e\frac{\partial \hat{U}_e}{\partial x} + \frac{\partial}{\partial y}\left[\nu\frac{\partial \hat{U}}{\partial y} - \hat{uv}\right]. \tag{IV.31}$$

Here $\hat{U}$ and $\hat{V}$ are ensemble-averaged or phase averaged streamwise and normal-to-wall velocity components and $-\hat{uv}$ is the ensemble-averaged Reynolds shear stress. For periodic unsteady turbulent flow, the ensemble-averaged F of instantaneous values of a quantity F for a specific phase $2\pi t/T$ of the outer-flow oscillation is given by

$$\hat{F} = \lim_{N\to\infty} \frac{1}{N} \sum_{n=1}^{N} F(t + nT), \tag{IV.32a}$$

where T is the period of the imposed oscillation and N is the number of cycles that are averaged. This ensemble average is also called a 'periodic sample' or a 'phase average'. F can also be represented as

$$F = \overline{F} + \tilde{F} + f, \tag{IV.32b}$$

where $\overline{F}$ is the time-averaged or mean value, $\tilde{F}$ is the periodic oscillation and f is the turbulent fluctuation. By comparison of these two equations

$$\hat{F} = \overline{F} + \tilde{F}. \tag{IV.32c}$$

The ensemble-averaged variance for the turbulent fluctuations is given by

$$\hat{f^2} = \lim_{N\to\infty} \frac{1}{N} \sum_{n=1}^{N} (F - \hat{F})^2, \tag{IV.32d}$$

$$\hat{f^2} = \overline{f^2} + \tilde{f^2}, \tag{IV.32e}$$

where $\overline{\delta^2}$ is the time-averaged or mean value and δ^2 is the periodic oscillation of the variance. The periodic oscillations $\tilde{F}$ and $\tilde{\delta^2}$ are presented here in terms of their Fourier components

$$\tilde{F} = \sum_{n=1}^{\infty} \tilde{F}_n \cos(n\omega t - \phi_n), \tag{IV.32f}$$

$$\tilde{\delta^2} = \sum_{n=1}^{\infty} \tilde{\delta^2_n} \cos(n\omega t - \lambda_n). \tag{IV.32g}$$

Note the sign convention used for the phase angles ϕ_n and λ_n.

The difficulty of solving these equations is the same as that for steady flows, namely describing the behavior of $-\hat{u}\hat{v}$. A number of investigators have argued that, as long as the period of the organized unsteadiness is relatively long compared with the turbulence timescales, it should be acceptable to use the approximation that the turbulence structure is unaffected by the unsteadiness. Quasi-steady flow exists when the phase-averaged flow can be described by the steady freestream flow structure. For moderate amplitude oscillations ($\tilde{U}/\overline{U} < 0.37$), Houdeville et al. (1976) and Cousteix et al. (1977, 1979) have shown that under such conditions $-\hat{u}\hat{v}/\hat{u}\hat{v}$ is independent of phase angle and has values corresponding to steady turbulent boundary layers, thus confirming this argument. All moderate amplitude measurements indicate that outside of the near-wall region the turbulence structure is basically unaffected by organized unsteadiness.

When the frequency of the organized unsteadiness is comparable to energy-containing turbulence frequencies, this approximation may not hold. Substantial interaction between the periodic unsteadiness and the aperiodic turbulence may occur in this case although the time-varying phase differences between these two kinds of motion at the same frequency suggest that there will be little effect on ensemble-averaged quantities.

Several experiments on strong adverse-pressure-gradient unsteady turbulent boundary layers with moderate amplitude oscillations indicate that the outer region of ensemble-averaged velocity profiles look like Perry and Schofield (1973) strong adverse pressure gradient steady turbulent boundary layers. A semi-logarithmic velocity-profile region exists with a constant phase angle. Kenison (1977) had traveling wave unsteadiness on a flat surface with $\tilde{U}_e/\overline{U_e} \leq 0.13$ and $k = \omega C/2U_\infty < 1.54$. Covert and Lorber (1983) used a rotating elliptic cylinder to produce a periodic blockage near a stationary airfoil for $\tilde{U}_e/\overline{U_e} < 0.05$ and $0.5 < k < 6.4$. Data of Cousteix et al. (1979), Simpson et al. (1983) and Simpson and Shivaprasad (1983) also support this description.

Competing influences of the oscillating pressure gradient, Reynolds shearing stress, and inertia determine the phase shift of oscillating profiles within the boundary layer. Kenison observed increasing phase lags as his flows approached separation. Covert and Lorber also had increasing phase lags while Cousteix et al. and Simpson et al. observed phase leads. If the flow nearest the wall is governed by viscosity and the oscillating and mean pressure gradients, then the solution to the unsteady vorticity equation

$$\frac{\partial \omega_z}{\partial t} = \nu \frac{\partial^2 \omega_z}{\partial y^2} \tag{IV.33}$$

indicates that the near-wall velocity oscillation leads the pressure gradient oscillation by 135°.

Jayaraman et al. (1982) examined unsteady turbulent boundary layers with the freestream velocity.

$$\hat{U}_e(X,t) = U_o \left[1 - \frac{a(X - X_o)}{L} (1 - \cos \omega t)\right] \tag{IV.34}$$

Upstream of X_o, the flow was essentially steady. For most of the cases that they examined ($\tilde{U}_e/\overline{U_e} < 0.22$, $\omega\delta/\overline{U}_e < 1.2$), ensemble-averaged velocity profiles at various phases are like steady attached flows. At higher frequencies and amplitudes, ensemble-averaged flow reversal next to the wall similar to Figure 23 was observed for 1/4 cycle, although the mean velocities were never negative and a semi-logarithmic region existed farther from the wall. The ensemble-averaged velocity profile shape factor $\hat{H}$ never exceeded 1.4, indicating that the outer 99% of the boundary layer behaved like an attached flow. One should not think of such a periodically reversed flow as detached since no breakaway, as discussed in section II, was observed. In these latter cases, the imposed oscillatory pressure gradient dominated the low momentum wall region and produced phase leads relative to the freestream that agreed approximately with the Stokes solution to equation (IV.33).

The experiments of Simpson et al. (1983) show that a periodic unsteady separating turbulent boundary layer with $Re_x = 4.7 \times 10^6$, $k = 0.61$, $\tilde{U}_e/\overline{U}_e = 0.3$ has both similarities and differences with a steady freestream separating turbulent boundary layer at the same free-stream conditions (Simpson et al.,1981)(Figure 17). Upstream of where intermittent backflow begins ($\hat{\gamma}_{pu} < 1$), the flow and turbulence structure behaves in a quasi-steady manner. A semi-logarithmic velocity-profile region exists with a constant phase angle.

After the beginning of detachment, large amplitude and phase variations develop through each flow and the structure is not quasi-steady. Unsteady effects produce hysteresis in relationships between flow parameters. As the free-stream velocity during a cycle begins to increase, the fraction of time that the flow moves downstream $\hat{\gamma}_{pu}$ at a given phase of the cycle increases as backflow fluid is washed downstream (Figure 78). As the free-stream velocity nears the maximum value in a cycle, the increasingly adverse pressure gradient causes progressively greater near wall backflow at downstream locations while

$\hat{\gamma}_{pu}$ remains high at the upstream part of the detached flow. After the free-stream velocity begins to decelerate, the location where flow reversal begins moves upstream. This cycle is repeated as the free-stream velocity again increases. Kenison also observed an oscillatory reversed flow region.

Near the wall in the backflow region, the ensemble-averaged velocity leads the freestream velocity by a large amount. The phase angle of the periodic backflow velocity and $\tilde{U}_1/\overline{U}$ are nearly independent of y near the wall. The mean backflow profile in terms of $\overline{U}/\overline{U}_N$ and $y/\overline{N}$ are approximately the same as for the comparable steady freestream case (Figure 23). Thus, it appears that the ensemble-averaged backflow near the wall behaves like a quasi-steady flow when normalized on $\hat{U}_N$ and $\hat{N}$. Figure 24 shows the normalized backflow velocity $|\hat{U}_N|/\hat{U}_e$ vs. $1/\hat{H}$ for this flow.

Downstream of detachment $\overline{u^2}$ and $\overline{v^2}$ are slightly higher for the unsteady flow than the steady flow, especially near the wall where mean backflow occurs. The phase angle for $\hat{u}_1^2$ in the backflow is progressively greater than the freestream velocity phase angle as the flow moves downstream. The turbulence structure progressively lags the ensemble-averaged flow oscillation with $-\tilde{uv}_1$ lagging $\tilde{U}_1$ in the backflow by about 20°. The ratio $-\tilde{uv}_1/-\overline{uv}$ increases from about 0.5 upstream of detachment, as also observed by Covert and Lorber, to about 0.7 downstream.

Near the wall $\hat{\gamma}_{pu}$ is nearly in phase with $\hat{U}_1$, but since $\overline{U}$ is <u>negative</u> the ensemble-averaged backflow is greatest when $\hat{\gamma}_{pu}$ is low and when $\tilde{u^2}$ and $\tilde{v^2}$ are near the maximum values. In other words, $\hat{U}$ in the backflow is nearly in phase with $\tilde{u^2}$ and $\tilde{v^2}$. This is consistent with the general observation from the steady flow that $\overline{u^2}$ and $\overline{v^2}$ are greater when there is more mean backflow.

The steady flow results show that $-\overline{uv}/u'v'$ decreases with decreasing $\overline{\gamma}_{pu}$. In the unsteady flow $-\hat{uv}$ is greater with less ensemble-averaged backflow or greater $\hat{\gamma}_{pu}$. In other words, $\hat{U}$ is lower and $\tilde{U}_1$ is nearly in phase with $-\tilde{uv}$. As in the steady free-stream flow, $-\hat{uv}/\hat{u}\,\hat{v}$ decreases with decreasing $\hat{\gamma}_{pu}$, although there is some hysteresis and phase lag for the unsteady flow.

Simpson and Shivaprasad (1983) reported measurements for a reduced frequency of 0.90 also with $\tilde{U}_{1e}/\overline{U}_e = 0.3$. The 0.90 reduced frequency has the same qualitative behavior as the 0.6 reduced frequency case. Downstream of detachment in both flows, the free-stream velocity and the pressure gradient are in phase. In both sinusoidally unsteady flows, the ensemble-averaged detached flow velocity profiles agree with steady freestream profiles for the same $\hat{\gamma}_{pumin}$ value near the wall when $\partial\hat{\gamma}_{pumin}/\partial t < 0$ (Figure 79). However, the higher reduced frequency flow has much larger hysteresis in ensemble-averaged velocity profile shapes when $\partial\hat{\gamma}_{pumin}/\partial t \geq 0$ than the lower reduced frequency (Figure 80). Larger and negative values of the ensemble-averaged velocity profile shape factor $\hat{H}$ occur for this flow during phases when the nondimensional backflow is greater and $\hat{\gamma}_{pumin} \rightarrow 0.01$.

Sandborn (1970) presented unsteady detachment and reattachment results for a flat plate turbulent boundary layer with the free-stream velocity varying between 2 fps to 6.5 fps. The non-sinusoidal oscillatory flow at 81 Hz was produced by a siren. When the velocity was decreasing with time, the h vs. δ^*/δ path was the same as for a steady separating turbulent boundary layer. After the velocity began to increase, the flow reattached along the "unrelaxed" attachment line although at a much lower δ^*/δ than for the detaching flow. Until after the flow velocity began to decrease, the h vs. δ^*/δ path in the coordinates of Figure 26 was almost at a constant δ^*/δ. This hysteresis is similar to that observed by Simpson <u>et al.</u> and Simpson and Shivaprasad.

Sajben <u>et al.</u> (1984) subjected transonic diffuser flows to downstream periodic pressure fluctuations that were generally less than 2% of the local static pressure. The results showed that neither the mean flow nor the time-mean value of the naturally present fluctuation intensities is altered appreciably by the imposed perturbations. No resonance effect was observed when the excitation frequency was near any of the well-defined natural frequencies determined from shock-displacement spectra. For $M < 1.27$ a weak shock occurs with no detachment and with one-dimensional acoustic waves. For $M > 1.28$, shock-induced detachment results with the boundary layer and inviscid core flows strongly interacting.

The amplitude and waveform of the oscillation strongly influence the behavior of the detached flow. Simpson (1983) presented some results for an axial-compressor-type waveform and a large amplitude oscillation. The parameter $(\hat{U}_{e_{max}} - \hat{U}_{e_{min}})/2\overline{U_e}$ was 0.238 and 0.752 for these cases. In each case the mean free-stream velocity U_e near the throat (Figure 16) was the same as for the steady case (Figure 17). Although the compressor-type waveform had a moderate amplitude, the higher harmonic effects changed the intermittent backflow behavior.

Figure 81 shows $\hat{\gamma}_{pumin}$ vs. X at various ωt for the large amplitude oscillatory flow. During $20° < \omega t < 120°$, the backflow is completely washed out with $\hat{\gamma}_{pumin}$ becoming unity. As the free-stream velocity reaches the maximum velocity, $\hat{\gamma}_{pumin}$ decreases in the downstream zone. Some second harmonic effects are evident for $120° < \omega t < 240°$. At larger ωt, $\hat{\gamma}_{pumin}$ drops to very low values in the downstream zone and backflow occurs as far upstream as the test-section throat (1.62m). The quantitative differences between

Figures 78 and 81 indicate that the oscillation amplitude influences the detached flow behavior.

Mean velocity profiles for the large amplitude flow are much different in shape than those of the lower amplitude sinusoidal cases since large variations of the detached shear flow occur and the shapes of the ensemble-averaged profiles for each phase of the cycle are much different than those of the lower amplitude flows. Unlike the lower amplitude sinusoidal waveform flows, there is little variation of this phase angle through the detached shear layer. This does not mean that this detached flow is quasi-steady because higher harmonics and non-linear effects are important. The waveform and amplitude of the unsteadiness strongly influence the detached flow behavior. In order to improve understanding of unsteady detached flows, measurements of Reynolds stresses and the turbulence structure are being made for these cases.

For backward-facing step flows, Mullin et al. (1980) reported that Lebouché and Martin pulsated the mean velocity of flow in a duct which had symmetric enlargements on both sides. Symmetric separation zones were observed. When $fH/\overline{U} < 0.07$, the recirculation zone appeared to wash out periodically while for $fH/\overline{U} > 0.7$, the recirculation zone appeared stable but was smaller than for steady freestream flow. The reattachment location X_R was found to fluctuate $\pm 1.3H$ about the mean value of 7H. In terms of X_R this means that for $fX_R/\overline{U} < 0.5$ washout occurs and $fX_R/\overline{U} > 0.5$ produces the stable stall zone. This dimensionless frequency is close to the $0.6 < fX_R/U_o < 0.8$ values observed by Eaton and Johnston (1980, 1981a) and Driver et al. (1983) for the large turbulent structures that pass over the steady freestream recirculation zone (section IV.C.1.a).

In their own experiment Mullin et al. used $fX_R/\overline{U} \simeq 0.04$ and $\tilde{U}/\overline{U} = 0.12$ for a 1Hz sinusoidal velocity oscillation. The stall zone was washed out periodically. Figure 82 shows isovels of the ensemble-averaged velocities that occur 5/8 of a cycle after the occurrence of the maximum favorable pressure gradient. Note that at $X/H \simeq 3.5$ or about halfway between detachment and reattachment, velocities throughout the detached shear layer are greater than time-averaged velocities. Although the amplitude of the oscillating pressure gradient can be a substantial fraction of the dynamic pressure distributed over the reattachment length, large-scale turbulent structures encounter both favorable (negative) and adverse (positive) unsteady gradients whose effects tend to cancel. It is unlikely that oscillating pressure gradients can explain the low frequency washout behavior. Unfortunately, no Reynolds shear stress or other structural measurements were made to lead to a conclusive explanation of the washout process.

IV. E.2 Dynamic Stall

Dynamic stall on helicopter and compressor blades is associated with unsteady gusts and rapid changes in the angle of attack (Crimi, 1975). If the angle of attack of an airfoil or other lifting surface oscillates about the static stall angle, large hysteresis develops in the fluid dynamic forces and moments (McCroskey, 1977, 1981, 1982). The unsteady turbulent boundary layers cannot be ignored because there is considerable interaction between the boundary layer and the inviscid flow during high lift operating conditions of these devices. In such cases the relatively thick boundary layer on the suction side of the lifting body is near separation.

For the practical range of reduced frequencies $0.1 < k = \omega C/2U_\infty < 1$ (ω is the angular frequency, C is the chord length, and U_∞ is the free-stream velocity), the smoke study motion pictures of McCroskey et al. (1976) clearly reveal the many features of dynamic stall. Figure 83, taken from their paper, illustrates these features. First, for an increasing angle of attack, the fluid near the leading edge of the upper surface is accelerated and, as shown in the upper left photo of Figure 83, the boundary layer is rather thin and remains attached further along the chord than in the static case at the same angle of attack. As shown in the accompanying normal force diagram, the normal force continues to increase with increasing incidence well above the static values until a catastrophic drop occurs.

During the last stages of the increasing normal force, the boundary layer near the trailing edge has thickened and the region of this thickened layer has gradually moved forward to the 30% chord position, as shown in the upper righthand photograph. At the maximum normal force angle of attack, the boundary-layer flow on the front 30% of the chord abruptly separates causing the catastrophic drop in the normal force. The magnitude of the reversed flow near the surface increases as the large separation vortex forms and moves downstream.

As the angle of incidence begins to decrease the flow along the leading surface reattaches. Because the leading surface is moving downward, the boundary layer is rather thick and not energetic enough to resist detachment so the situation is like that of the lower left photo. Not until the airfoil begins to increase its incidence angle again is the separated vortex completely washed out and the normal force increases again. At freestream Mach numbers above 0.3, shock/boundary layer interaction effects must be included (Ericsson and Reding, 1984).

Much effort has been made to describe the forces and moments associated with dynamic stall by using empirical correlations for the coefficients in damped oscillator model equations. McCroskey (1977, 1981, 1982) discusses work on this approach in some detail. No review of this is given here.

Many investigators have used flow visualization to study this sequence of motions (McCroskey et al., 1981, Francis and Luttges, 1983). Lee et al. (1984) have used laser holographic interferometry to determine density distributions and under certain conditions velocity distributions. De Ruyck and Hirsch (1984) have made hot-wire anemometer measurements on an oscillating airfoil. Figure 84 shows $\hat{U}$, $\hat{u}$, and $-\hat{uv}$ profiles at various phases of oscillation. Well away from the surface the measurements are valid, but in regions with intermittent backflow the results are suspect. The turbulence structure appears to be quasi-steady. At any instant, the detached flow pattern does not look exactly like the corresponding steady detached flow at the same angle of attack (Figure 52) because of the time lag required for the flow to move over the surface.

Although the results in Figure 84 have not been completely analyzed by the authors, the turbulence structure is similar to that observed by Simpson et al., (1983). Large Reynolds shear stresses occur at about the same locations as large u and $\partial U/\partial y$ values. Local $\hat{u}/|\hat{U}|$ values in the backflow exceed 1/3, indicating substantial flow reversal. Hysteresis of the flow behavior is also observed.

IV. E.3 Self-induced Unsteadiness in Separating Turbulent Flows

In many detaching turbulent boundary layers, there are conditions when unsteadiness is induced throughout much of the flowfield by the interacting inviscid and turbulent flow regions, even when the approaching flow is extremely steady. Several cases have already been discussed. In section IV.B.2 and Figures 14 and 15, large transitory stall in a two-dimensional diffuser was discussed. This type of self-induced unsteadiness is discussed more below. In section IV.C.1.a self-induced low frequency flapping of the detached shear layer for a backward-facing step was discussed. As discussed below, flows with shock waves can induce unsteadiness.

In transitory stall, the maximum unsteadiness occurs for angles 2θ in the range 20° to 24°. Large amplitude fluctuations can occur more or less periodically as detached flow washes in and out of the downstream end of the diffuser or as the stalled region grows and collapses in the lateral direction. Lyrio et al. (1981) summarized the experiments on the period between washouts of part of the stalled fluid. A periodic inlet disturbance induces only moderate changes in the exit unsteadiness and a substantial change in the size of the exit blockage. Smith and Kline (1974) obtained an almost log-normal histogram of the stall period for undisturbed inlet conditions with the mean period $\overline{T}_N$ given by the dimensionless grouping

$$\tau = \frac{\overline{T}_N \overline{U}_1}{L \sin 2\theta} = 180 \pm 60$$

where L is the length, U_1 is the average entrance velocity and 2θ is the total included angle of the diffuser. Since 2θ is between 15° and 30°, the reduced frequency $2\pi L/T_N U_1 \sim 0.1$. McCroskey (1977) pointed out that this reduced frequency is approximately the boundary between quasi-steady and unsteady behavior for large-ampitude oscillating airfoils. The amplitude of the natural unsteadiness velocity was about 6% of the inlet velocity.

Layne and Smith (1976) concluded from their experiments that transitory stall induces inlet-flow unsteadiness on an otherwise disturbance free flow, withthe greatest unsteadiness occurring for 2θ between 16° and 22°. Smith (1978) obtained τ values of about 4000. He suggested a Reynolds number dependence to correlate the limited available data. Although Ashjaee et al. (1980) obtained a τ value of 28, their experiments indicated that the stall frequency was independent of 2θ between 10° and 24°, as reported by Layne and Smith. These widely-varying values for τ and the almost log-normal distribution for T_N suggest that the turbulent boundary layers in a diffuser with this range of 2θ strongly interact with the inviscid flow and are susceptable to self-induced disturbances. There are insufficient data of entire flowfields to confidently explain what determines the period of transitory unsteadiness.

In section IV.D.1 steady transonic flow over a bi-circular arc airfoil was discussed (Figure 68). The flow over this airfoil at zero incidence is unsteady for a narrow range of free-stream Mach numbers shown in Figure 85 (Seegmiller et al., 1978; Marvin et al., 1979). Figure 86 is a shadowgraph sequence of the unsteady shock location in this shock-separation-induced oscillatory flow with a reduced frequency of 0.49. This reduced frequency compares with that observed by Finke (1975) in another circular arc airfoil investigation. Highly periodic pressure and velocity oscillations occur in the separated region. Profiles of conditionally-sampled ensemble-averaged streamwise velocity, turbulent shear stress, and turbulent kinetic energy profiles were observed for the same conditions shown in Figure 86.

During the initial portion of the cycle, the flow on the upper surface of the airfoil is attached and accelerating. As the speed increases, a series of compression waves strengthen and coalesce into a single shock wave that moves upstream. A thick shear layer develops downstream of the shock wave and detachment occurs. As the shock wave approaches midchord, it weakens and the shear layer collapses and is convected downstream. On the other side of the airfoil, a similar sequence occurs 180° out of phase.

Time histories of the data show that the turbulent kinetic energy and shear stress downstream of the shock wave increase dramatically. The time required for each to reach its maximum level depend on the shock-wave strength and the position in the boundary layer. Downstream dissipation and diffusion of turbulence exceed production and the turbulent kinetic energy and shear stress decrease. The shear appears to be in phase with the turbulent kinetic energy away from the wall because the times to achieve maxima and minima are about the same.

Sajben et al. (1977, 1981, 1982) report similar self-induced shock position oscillations for transonic diffuser flow. If the Mach number before the shock was less than about 1.28 for their case, flow separation occurred well downstream of the shock and was induced by the adverse pressure gradient. For stronger shocks the separation occurred earlier and downstream reattachment occurred later. The energy-containing turbulence frequencies decreased from 5kHz near the shock to about 300 Hz near the end of the divergent section, while the rather coherent shock oscillation and associated pressure fluctuations were near 100 Hz. Thus, significant interaction between the periodic and large-scale turbulent motions occurred, which is believed to be the reason for the shock oscillation. Both pressure and shock displacement amplitudes are greater, and only one natural frequency was observed. The natural frequency of this oscillation mode is independent of duct length and is not predicted by acoustic theory. The frequency appears to scale with the length of the inviscid core flow and is related to convective effects in the shear flow (Salmon et al., 1981). Note the qualitative similarity between this turbulence-shock-induced oscillation and large transitory stall in subsonic diffusers. In fact, the reduced frequency for this oscillation is $\omega L/U_o \sim 0.1$, which is the same order of magnitude as for large transitory stall discussed above.

Meier (1975) discussed shock-separation-induced oscillations for transonic flow in a curved channel, over a symmetric airfoil at an angle of attack, and in a Laval nozzle with the same mechanism as discussed here for airfoil and diffuser flows. Data for a mixed supersonic and subsonic flow in a duct with sudden enlargement of the cross section were reported by Anderson et al. (1977), Meier et al. (1978), and Albers et al. (1980). For a certain domain of base pressure, large base pressure and shock oscillations occur. The mechanism of the flow oscillation is a shock wave / detached flow interaction. The frequency of this oscillation is mainly determined by the length of the receiver duct. Albers et al. present data that show $\omega X_R/C \sim O(0.1)$, which is similar to that observed for backward-facing step flows (section IV.C.1.a).

Rockwell (1983) offered several hypotheses on why self-induced oscillations of turbulent flows occur. An imbalance between fluid entrained by the detached flow and that returned to the recirculation zone at reattachment can occur, setting up oscillations that scale on the reattachment length. The large-scale structures of the turbulence can interact with the surface to produce low frequency oscillations. Thirdly, in supersonic cases, the resonant organ pipe modes of the downstream ducting can produce oscillations.

V. CALCULATION METHODS FOR SEPARATING AND REATTACHING FLOWS

The features of several different types of separated flow were presented in section IV. Here we will discuss the physical concepts and approaches that are contained in a representative sample of turbulent-shear-flow calculation methods for adverse-pressure-gradient induced and bluff body detachment and reattachment cases. Compressibility and unsteady effects are discussed.

The weaknesses and limitations of modeling turbulent separation largely reflect the same weaknesses and limitations of any other turbulent flow case. All methods that are used are "post-dictive", to use Saffman's word, rather than predictive because so much experimental information has been used to develop them. Few, if any, of these methods apply to a wide class of flows (Kline et al., 1978). Non-dimensional correlations, zonal models, and numerical solutions for the Reynolds-averaged equations appear to be the useful engineering approaches for the next 10 years. Large-eddy simulation with subgrid closure and complete solution of the Navier-Stokes equations will remain research methods until significant advances in computation speed and cost reduction occur (Kline et al., 1982).

The objective of zonal modeling is to divide the flowfield into several regions, each dominated by a particular type of flow, and to analyze each region by the computationally optimum numerical technique for that region. No single turbulence closure model is the best for all regions, so one needs to use the best available for that region. In order to make the best use of available computer capability for large flowfields of interest, it is important that the following approaches be followed:

1. Locally asymptotic solutions should be used in regions where the flow detail is known, e.g., the law of the wall should be used when applicable.

2. Locally-fine computing meshes should be used in regions where large changes of terms in the governing equations occur.

3. Curvilinear flow-oriented co-ordinates should be used so that relatively large grids can be used without sacrificing flow detail.

4. The simplest form of the governing equations that contain all important terms should be used; the simplest turbulence models that will work should be used.

For separated flows the approach in all of the inviscid/turbulent shear flow interaction models is to simultaneously or iteratively calculate the inviscid potential flow and the detached turbulent shear flow. Various numerical methods have been used for the inviscid flow and various turbulence models in integral or finite-difference formulations have been used for the shear flow. Rather than review all procedures that are known at this writing, a representative sample of the physical models that are used will be discussed.

V. A Inviscid Simulation Methods

Several inviscid models have been used to calculate the approximate time-mean behavior of some detached flows. In section IV.B.1, several inviscid models were discussed that describe massive detached flow zones around airfoils. Taulbee and Robertson (1972) used a frozen vorticity analysis to describe the mean flow over a forward-facing step. This analysis used the rotational inviscid equation for the streamfunction and Bernoulli's equation for each streamline. Calculations were begun 16 step heights upstream of the step using experimental data. In a comparison with data a fairly good surface pressure distribution was computed. Perry and Fairlie (1975) used the Perry and Schofield (1973) mean velocity profile as the initial profile in a frozen vorticity analysis of a detaching and reattaching flow on a flat surface. Good agreement was obtained with experimental mean streamlines. An advantage of such analyses is that the irrotational free-stream and the rotational flow can be computed simultaneously. However, since the entrainment of non-turbulent free-stream fluid and the diffusion of vorticity are neglected in these analyses, some errors are present.

Several simulations of the instantaneous behavior of high Reynolds number two-dimensional separated flows have been performed using discrete-vortex models. Ashurst et al. (1980) performed simulations for the backward-facing step, while Spalart and Leonard (1981) studied flow over a square body and an oscillating airfoil and Kiya et al. (1982) examined a blunt flat plate. A number of discrete vortices are born at the body surfaces and are tracked through the flow in a Lagrangian description using essentially inviscid equations of motion. Viscous effects spread away from these vortices at a distance approximately $(\nu t)^{1/2}$ where t is the age of the vorticity since its birth. A viscous analysis next to the surface supplies vorticity to the outer region flow.

The simulated flow patterns look very much like those observed in flow visualization experiments. When detachment occurs from a sharp edge, the flow remains fairly two-dimensional until near reattachment. Mean velocity and turbulence profiles for two-dimensional vortices look qualitatively like experimental data, but there are still large differences. Kiya et al. also obtained reasonable calculations of the time-mean and rms values of the velocity and the surface-pressure fluctuations. When three-dimensional effects are included there is a significant improvement, especially near reattachment.

V. B Incompressible Flow Adverse-Pressure-Gradient-Induced Separation Models.

All of the known models make use of the established ideas for attached turbulent boundary layers. Eddy viscosity, mixing length, turbulence kinetic energy, and entrainment models are used as well as empirical correlations. Here we will discuss integral and differential methods and present some of their results and deficiencies. Integral methods are possible, even though there are large regions of backflow, because the displacement of streamlines from the surface, the backflow, and the pressure distribution can be computed simultaneously or iteratively with a given velocity profile model. On physical grounds, the local large-eddy structure strongly influences the local backflow, as discussed in section IV.B.3.h so a downstream marching calculation method for the velocity field is possible. Unfortunately, many of the calculation methods have drawn too heavily from attached flow concepts without making use of available

experimental knowledge about these flows. For example, most methods do not incorporate the correct physics for the backflow region: namely, that turbulence diffusion and dissipation control the backflow behavior and that the backflow mean velocity profile is determined by the large-scale fluctuations. Hopefully, future calculation methods will build on this experimental information.

Whether an integral or differential method is used, it is often informative to calculate the location of detachment. In fact, the calculation of detachment and reattachment locations appears to be very important as an indicator of the accuracy of a flow model. The mean velocity profile changes drastically around detachment and reattachment. As noted in section IV. C_p, C_f, γ_{pu}, and surface pressure fluctuation distributions scale on the length of the detached flow.

Hahn et al. (1973) reviewed several simple calculation methods for the position of detachment, including those by Stratford (1959a), Townsend (1962), Sandborn and Liu (1968) and others. The Townsend method, as slightly modified by Hahn et al., agreed the best with data. All of these methods require the free-stream velocity distribution as input information. Townsend's method assumes that the total pressure and the Reynolds shearing stress are unchanged along streamlines of the mean flow outside of an internal boundary layer and that the semi-logarithmic mean velocity distribution holds within the internal layer. This approach, first used by Stratford (1959a), leads explicitly to the detachment location. Hahn et al. also demonstrated that a boundary layer integral method well calculated the location of detachment.

Sanders (1969) showed that when pressure and inertia forces are dominant, as near detachment where τ_w and the entrainment momentum are relatively small, then

$$\left(\frac{1}{H^2} - 1\right) / \left(\frac{1}{H_i^2} - 1\right) = \left(\frac{U_e}{U_{ei}}\right)^2 \tag{V.1}$$

where the subscript i denotes initial conditions at the beginning of the strong adverse pressure gradients and $U_e(x)$ is the local velocity just outside the boundary layer. By using H criteria for intermittent transitory detachment and detachment from section IV.B.3.b, the streamwise positions of these conditions can be determined.

V. B.1 Integral Methods

Cousteix (Kline et al., Vol. II, 1982) presented a review of integral method techniques. The set of global equations consists of an integral momentum equation, e.g., the von Kármán equation (V.2),

$$\frac{d\theta}{dx} + (H + 2)\frac{\theta}{U_e}\frac{dU_e}{dx} = \frac{C_f}{2} + \frac{1}{U_e^2}\frac{d}{dx}\int_0^\infty (\overline{u^2} - \overline{v^2})dy \tag{V.2}$$

and a secondary equation, either an entrainment equation, a moment of momentum or a mean kinetic energy integral equation. The second term on the right side of equation (V.2) is the normal stresses term. For each set of two integral ordinary differential equations, there are more unknowns than equations, so closure relationships are needed. Three types of relationships are usually considered: (1) relationships among integral thicknesses or shape parameters; (2) a skin-friction relation; and (3) entrainment equations, dissipation integrals or some other shear-stress integral. In general, the large-eddy-dominated outer region flow away from the wall lags the behavior of an equilibrium flow under the same boundary conditions, so a model ordinary differential equation for the lag effect is used for calculating the entrainment coefficient or dissipation integral.

Strickland (Simpson et al., 1973) developed a simple calculation method for the flow upstream of detachment. The momentum integral equation with normal stresses terms, equation (V.2), the Ludwieg-Tillmann skin friction equation (IV.2), and equation (V.1) were used to obtain good agreement with the Simpson et al. (1973, 1977) flow.

Most integral methods use Coles' law-of-the-wall and law-of-the-wake velocity profile, equation (V.2) to determine the relationships among integral thicknesses, the skin friction relation, or at least the forms of the relationships. Here

$$\frac{U}{U_\tau} = \frac{1}{\kappa}\ln\left|y\frac{U_\tau}{\nu}\right| + C + \frac{\Pi}{\kappa}(1 - \cos\frac{\pi y}{\delta}) \tag{V.3}$$

where $\kappa = 0.41$, $C = 5.0$, and Π is the wake amplitude. This profile does not fit closely the mean velocity profiles of detached turbulent boundary layers, even when the sign of U_τ is changed to account for mean backflows. Thus, earlier researchers, such as Kuhn and Nielsen (1973, 1975), who used equation (V.3) with attached flow constants did not obtain very good results. As more experimental data have become available, better fits of data to the forms of the relationships among parameters have been obtained.

Woolley and Kline (1973, 1978) presented a method for calculating fully-stalled diffuser flows that used the ad hoc assumption that the pressure is constant downstream of detachment, as is observed from experiments. The attached boundary layer is calculated using the Nash and Hicks (Kline et al., 1968) integral method. This method uses the momentum and moment-of-momentum boundary layer integral equations and equation (V.3). The shear-stress integral is determined from an empirical first-order ordinary differential equation that allows the shear stress to lag behind the equilibrium value for a given value of H. The Sandborn criterion (equation IV.3) for intermittent transitory detachment ITD is used to stop the attached flow calculation. The displacement thickness line and the potential flow core downstream of this location is determined so that the resulting pressure is constant. This procedure is successful in calculating pressure distributions and patterns to the accuracy of the data. No calculation of the separated turbulent shear flow was made.

Ghose and Kline (1976), Ghose (1979), and Ashjaee et al. (1980) developed an integral method for diffusers with a small amount of intermittent backflow ($\gamma_p > 0.5$ everywhere). The Coles law-of-the-wall and law-of-the-wake velocity profile, the momentum integral equation, an outer shear layer edge matching

equation, and an entrainment equation are used. The shear velocity U_τ in the law of the wall is defined as $(\tau_w/\rho)(|\tau_w|/\rho)^{-1/2}$ to account for the negative sign downstream of detachment. The maximum turbulent shearing stress is used in the Bradshaw et al. (1967) entrainment relation

$$E = \frac{1}{U_e}\frac{d}{dx}[U_e(\delta - \delta^*)] \text{ where } E = 10\frac{\tau_{max}}{\rho U_e^2} \tag{V.4}$$

An eddy viscosity model is used to determine the equilibrium shear layer maximum shear stress, τ_{max}, equation. The shear stress lag equation of the form

$$\frac{d\tau_{max}}{dx} = \frac{\lambda}{\delta}(\tau_{max,\,eq} - \tau_{max}) \tag{V.5}$$

is used to account for departure from equilibrium. The lag parameter λ was obtained from numerical experiments.

Ghose (1979) used this integral boundary layer method to provide boundary conditions for a finite difference representation of the inviscid core. The boundary layer equations are applied at the floating boundary line, resulting in a simultaneous set of nonlinear block tridiagonal equations which are solved iteratively using a successive-line-relaxation technique first applied by Moses et al. (1978). Calculations by this method were made for the Simpson et al. (1977) flow. The pressure recovery coefficient C_p, skin friction coefficient C_f, δ^*, and H are well predicted up to ITD. Downstream δ^*, H, and the entrainment parameter $10\,\tau_{max}/\rho U_e^2$ are not as well predicted. Ashjaee et al. (1980) also obtained good pressure recovery predictions for asymmetric diffusers. Cousteix et al. (Kline et al., Vol. III, 1982) used the entrainment relations and method developed by Michel et al. (Kline et al., 1968) from self-similar solutions to calculate the Simpson et al. (1981) flow. Good agreement with experimental data was obtained upstream of detachment but progressively poorer velocity profiles were obtained downstream.

Moses et al. (1979) also solved their boundary layer method simultaneously with a finite difference potential core formulation by successive line relaxation. Their boundary layer method used the momentum equation (V.2) and kinetic energy integral equation

$$\frac{d}{dx}(U_e^3\theta^*) = \int_0^\infty \frac{2\tau}{\rho}\frac{\partial U}{\partial y}\,dy \tag{V.6}$$

with approximations for the integral parameters derived from the law-of-the-wall and the law-of-the-wake velocity profile. To limit the magnitude of the backflow, the wake function was started at a varying distance from the wall. Moses et al. (Kline et al., 1982) obtained good agreement with the outer region velocity profile of the Simpson et al. (1981) detached flow. Gersten et al. (1980, 1983) and Wauschkuhn (1982) also used the energy integral equation and correlations among integral parameters and C_f. Only qualitative agreement with data was obtained (Figure 41).

Assassa and Papailiou (1979) also used the integral momentum and energy equations but included the normal stresses terms that have been found experimentally to be important near separation. The law-of-the-wall and the law-of-the-wake velocity profile is used with a skin friction law, an empirical relation between the Clauser form factor $G = (H - 1)/H\sqrt{C_f/2}$ and the pressure gradient parameter $(\delta^*/\tau_w)(dP/dx)$, and two other empirical functions. Calculations upstream of separation are good. No potential flow calculation method was solved simultaneously, however, so no interaction with the inviscid core can be calculated.

It should be pointed out again that the practical problem is one with inviscid/turbulent shear flow interaction where the displacement thickness effect is not negligible and the potential flow and shear layer calculations are not independent. The normal approach for attached flows, i.e., specifying P(x) or $U_e(x)$ for calculations using the boundary layer equation (V.2), prevents convergence of the solution at detachment. This is due to the fact that the differential boundary layer equation has a weak singularity when $\tau_w = 0$.

Ghose (1979), Bradshaw (1978), Cebeci and Bradshaw (1977) pointed out that an inverse boundary layer technique can be used to eliminate this computational problem. A matching parameter such as δ^*, C_f, or streamline angle at the outer edge of the boundary layer is used for the separate computations in the inviscid and shear regions instead of P or U_e. P and U_e are free to vary so that a smooth variation of δ^* or the matching parameter always occurs. If the resulting pressure gradient does not match the desired distribution, the matching parameter is adjusted and the process repeated to convergence. The successive-line-relaxation method of Moses et al. (1978) used by Moses et al. (1979, 1982) and Ghose (1979) also avoids the weak singularity because the flow in both inviscid and shear flow regions is computed simultaneously. East et al. (1977) formulated an inverse calculation procedure using the lag-entrainment method that avoids this singularity. Smith et al. (1981) used this to calculate an equilibrium detached flow.

Recent improvements to some of these methods and ideas have been made, largely as a result of the availability of additional experimental data. Lyrio et al. (1981) used the form of the law-of-the-wall and the law-of-the-wake velocity profile to obtain the relationships among h (Figure 26), δ^*/δ, Re_{δ^*}, and $C_f/2$. Numerical values in these relations were determined by fitting experimental data. Different entrainment correlations were used for different conditions. Good estimates of the overall detached flow behavior can be made since the correlations make use of data from many different experiments.

Thomas (1984) examined several of these different ingredients to integral methods. Whitfield et al. (1981) used a mean kinetic energy equation and correlations of all shape factors and C_f in terms of H, as developed by Swafford (1983). LeBalleur's (1981) modified law-of-the-wall/wake model also was examined.

LeBalleur shifted the wake function away from the wall to permit a constant region of reversed flow next to the wall. The East et al. (1977) lag-entrainment method was also examined. In non-interactive calcualations with the freestream, Thomas obtained fair agreement with experimental results from which the correlations were derived.

One idea that needs to be pursued in an integral method is the use of $\tau_{max}/\rho U_e^2$ as the descriptive shearing stress. As discussed in section IV.B, this is the controlling shear stress for the shear layer upstream and downstream of detachment. The wall shear stress is very small in detaching flows and influences only the near wall region. Schofield (1981) presented a method that incorporates the maximum shear stress that is based on the Perry and Schofield (1973) correlation for strong-adverse-pressure-gradient equilibrium attached boundary layer. This method has not yet been extended to detached flows.

V. B.2 Differential Methods

Simpson and Collins (1978) and Collins and Simpson (1978) modified the Bradshaw et al. (1967) calculation method to account for normal stresses and calculate the backflow behavior. The Bradshaw et al. method uses a model for the large-eddy diffusion of turbulence kinetic energy, which produces a set of hyperbolic differential equations whose solution marches downstream. In view of the large-eddy structure of detached flows, streamwise marching solutions for these flows can be obtained.

Collins and Simpson used the assumption that a minimum free-stream pressure gradient is achieved downstream of detachment. This degenerates to the constant pressure assumption in the case of fully-stalled diffuser flows but also handles cases such as the SMU flows where a small residual positive pressure gradient remains after detachment. In this method an attached turbulent boundary layer procedure is used until intermittent transitory detachment. The displacement thickness and displacement thickness gradient calculated at this location are used as initial conditions for the detached flow displacement thickness. A far downstream condition of δ^* is used that is physically realistic, e.g., that the direction of the displacement thickness approaches the direction of the far downstream potential flow. With these conditions, the potential flow is solved iteratively with possible displacement thickness distributions until one is found that satisfies the minimum pressure gradient condition. Notice that this method does not require any interaction with the shear layer to calculate the potential flow. Collins and Simpson used the resulting U and V velocity distributions at the boundary layer edge and calculated inward toward the wall. Only a continuity requirement was used in the backflow, but fairly good estimates of the mean backflow resulted. In general, this approach is unsatisfactory because of the requirement that the freestream pressure distribution be determined before calculating the shear flow. Had a good model for the backflow, such as shown in Figure 23, been available at that time, it could have been used instead of the minimum free-stream pressure gradient assumption. An inviscid/turbulent shear flow interaction calculation could have been made.

Cebeci, Khalil and Whitelaw (1979) presented the results from two different models that show the limitations and characteristic features of parabolic momentum equation and elliptic momentum equation methods. The elliptic method used the continuity and momentum equations:

$$\frac{\partial U}{\partial x} + \frac{\partial V}{\partial y} = 0 \tag{V.7}$$

$$\rho U\frac{\partial U}{\partial x} + \rho V\frac{\partial U}{\partial y} = \frac{-\partial P}{\partial x} + \frac{\partial}{\partial x}\left(\mu_t \frac{\partial U}{\partial x}\right) + \frac{\partial}{\partial y}\left(\mu_t \frac{\partial u}{\partial y}\right) \tag{V.8}$$

$$\rho U\frac{\partial V}{\partial x} + \rho V\frac{\partial V}{\partial y} = -\frac{\partial P}{\partial y} + \frac{\partial}{\partial x}\left(\mu_t \frac{\partial V}{\partial x}\right) + \frac{\partial}{\partial y}\left(\mu_t \frac{\partial V}{\partial y}\right) \tag{V.9}$$

The TEACH procedure of Gosman and Pun (1974) was used to solve these equations.

With the solution of the elliptic equations, the turbulence was characterized by further elliptic equations representing the turbulence kinetic energy and dissipation rate. These equations form the Boussinesq k-ε model (Launder and Spalding, 1974). They may be written as:

$$\frac{\partial}{\partial x_i}(\rho U_i k) - \frac{\partial}{\partial x_i}\left(\frac{\mu_t}{\sigma_k}\frac{\partial k}{\partial x_i}\right) = P_1 - \rho\varepsilon \tag{V.10}$$

and

$$\frac{\partial}{\partial x_i}(\rho U_i \varepsilon) - \frac{\partial}{\partial x_i}\left(\frac{\mu_t}{\sigma_\varepsilon}\frac{\partial \varepsilon}{\partial x_i}\right) = C_{\varepsilon 1}\frac{\varepsilon P_1}{k} - C_{\varepsilon 2}\frac{\rho\varepsilon^2}{k} \tag{V.11}$$

with

$$\mu_t = C_\mu \rho k^2/\varepsilon, \quad k = \frac{1}{2}\overline{u_i u_i}, \quad P_1 = -\rho\overline{u_i u_j}\partial U_i/\partial x_j$$

and

$$-\rho\overline{u_i u_j} = \mu_t\left(\frac{\partial U_i}{\partial x_j} + \frac{\partial U_j}{\partial x_i}\right) - \frac{2}{3}\rho k\delta_{ij}$$

The five parameters were assigned the following values in accordance with Pope and Whitelaw (1976):

C_μ	σ_k	σ_ε	$C_{\varepsilon 1}$	$C_{\varepsilon 2}$
0.09	1.0	1.3	1.44	1.92

The boundary layer calculation used

$$U\frac{\partial U}{\partial x} + V\frac{\partial U}{\partial y} = -\frac{1}{\rho}\frac{dP}{dx} + \frac{\partial}{\partial y}\left(\frac{\mu_t}{\rho}\frac{\partial U}{\partial y}\right) \tag{V.12}$$

instead of equations (V.8-9) and was solved by the procedure described in detail by Cebeci and Bradshaw (1977). The effective viscosity formulation by Cebeci and Smith (1974) was used. In the inner region

$$\mu_t = \rho \ell^2 \frac{\partial U}{\partial y} \tag{V.13}$$

with

$$\ell = 0.4y[1 - \exp(y^+/A^+)] \tag{V.14}$$

$$A^+ = \frac{26}{N},\ N = (1-11.8p^+)^{1/2},\ p^+ = \frac{\nu U_e}{U_\tau^3}\frac{dU_e}{dx}$$

and, in the outer region,

$$\mu_t = 0.0168\ U_e \delta^*$$

Both models have been extensively tested and discussed in the literature. The two-equation model is considered to be the simplest approach compatible with elliptic equations and the recirculating flows which they represent. The algebraic eddy-viscosity formulation used with the boundary-layer equations has proved to be successful in representing attached boundary-layer flows. The node point adjacent to a wall was linked to the wall by law-of-the-wall functions for the velocity, shear, and dissipation.

Rodi and Scheuerer (1983) showed that the k-ε model gives consistently too high C_f values in attached adverse-pressure-gradient flows. This originates from too steep an increase of turbulent kinetic energy and $-\overline{uv}$ near wall. This is due to too small ε values relative to the production rate of k. An increase in ε production is necessary in adverse-pressure-gradient flows to correct this feature. Rodi and Scheuerer used a modified ε equation and an algebraic stress model to obtain good results for mild adverse pressure gradients. The normal stresses production term

$$P_2 = \rho(\overline{u^2} - \overline{v^2})\partial U/\partial x \tag{V.15}$$

shown in equation (IV.19), was included in the right side of equation (V.10) and a modified normal stresses term $C_{\varepsilon 3}P_2$ was used in equation (V.11). They had to adjust $C_{\varepsilon_3} = 2.5$ to produce good results for strong adverse pressure gradient flows.

Figure 87 shows some of the elliptic k-ε procedure results of Cebeci et al. for the Simpson (1977) flow. The mean backflow is greatly overpredicted while Re_θ is well predicted. H and C_f are slightly underpredicted. Although Figure 87b shows that mean backflow begins within the same two streamwise positions as suggested by the measurements, the calculated location of intermittent transitory detachment and detachment were not presented. Adair et al. (1983) used the k-ε model for the curved wall flow of Thompson and Whitelaw (1982). Upstream of detachment, C_f was too high while the outer region mean velocity profiles were approximately correct. Downstream of detachment the computed shear layer was too thick. The mean backflow region was about the correct thickness, but computed mean velocities in the middle and outer regions were too low.

Figure 88 shows the results from the boundary layer method using the Cebeci-Smith model. The sharp peaked backflow profile shown in Figure 88 is characteristic of too large a mixing length in the near wall region (Simpson, 1979b). Murphy (Kline et al., Vol. II, 1982) obtained similar results with this model for the Simpson et al. (1981) flow. Detachment was calculated too far upstream.

Pletcher (1978) performed boundary layer calculations for the Simpson et al. (1977) flow using several different models. An inverse computational technique was used to compute δ^* downstream of detachment iteratively until the potential flow and boundary layer results were consistent. All models used the law-of-the-wall velocity profile nearest the wall in the form of a mixing length distribution.

Model A used a constant L/δ for the outer region while Model B used Cebeci and Smith's (1974) outer region eddy viscosity model. Model C used a turbulence kinetic energy equation and the Prandtl-Kolmogorov relation between turbulent viscosity and turbulent kinetic energy (Launder and Spalding, 1974). Model D used Model A and a "lag" equation for the mixing length

$$U_e \frac{dL}{dx} = 1.2\sqrt{\frac{|\tau_w|}{\rho}}\left(\frac{L}{\delta} - 0.12\left(\frac{L}{\delta}\right)^2\right) \tag{V.16}$$

Model E used Model C and equation (V.16). Models A and C produced coincident results as did Models D and E. The justification for the lag equation is that the large eddy structure lags the local conditions of the shear flow.

Model D best calculates C_f, U_e, and the mean velocity profiles (Figure 89). Figure 90 shows how the outer region mixing length must vary in order to produce this result. In effect the mixing length is almost frozen after separation. The thickness of the "law-of-the-wall" region is a smaller fraction of the boundary layer than in Model A since the inner and outer region mixing lengths are equal at the switch point. Much lower shearing stress and turbulence kinetic energy profile values are predicted than were experimentally observed.

Note that Models A and B produced backflow mean velocity profiles that strongly resemble those produced by Cebeci et al. in Figure 88. Collins and Simpson (1978) report that lower mixing length values produce mean velocity profiles like those for Model D and produce too low shearing stresses.

While Model D appears to work to some degree, it does not contain entirely correct fluid physics. Equation (V.16) implies that the small wall shear stress strongly controls the separated flow behavior. As noted in section IV.B.3,h, the large structures produce most of the turbulence kinetic energy and shear stress well away from the wall and diffusion and dissipation are the main phenomena near the wall. Little momentum and energy are in the near wall region. In reality, ℓ/δ in the outer region does decrease slowly along the separated flow as discussed in section IV.B.3.c, but not as much as Pletcher requires.

Mellor and Celenligil (Kline et al., Vol. III, 1980) used a 5 equation model of turbulence to compute the Simpson et al. (1981) flow. Five transport equations for $\overline{u^2}$, $\overline{v^2}$, $\overline{w^2}$, and $-\overline{uv}$, and a master length scale

were used with a law-of-the-wall velocity profile for the near wall region. Good results were obtained upstream of detachment, but downstream of detachment velocity and shear stress profiles were progressively poorer. Low shear stresses and too large backflows were computed.

Johnson and King (1984) proposed a hybrid Reynolds stress/eddy viscosity model for separating flows to account for experimentally-observed lower eddy viscosities than given by the Cebeci and Smith model. They proposed that the Cebeci-Smith model is adequate when turbulence energy production and dissipation rates are in balance or "equilibrium", but needs to be modified to account for strong non-equilibrium cases. Taking a cue from the experimentally-observed fact that the maximum turbulent shearing stress $-\rho\overline{uv}_{max}$ is the proper shearing stress scale for strong adverse pressure gradient and separating flows, they proposed an ordinary differential equation for $-\overline{uv}_{max} = g^{-2}$ that was derived from the turbulence energy equation:

$$\frac{dg}{dx} = \frac{a_1}{2U_M L_M}\left[1 - \left(\frac{g}{g_{eq}}\right)^{1/2}\right] + \frac{C_{dif}}{2\delta U_M[0.7-y/\delta/_M]}\left[1 - \left(\frac{\nu_{to}}{\nu_{to,\,eq}}\right)^{1/2}\right] \qquad (V.17)$$

Here, equilibrium values are given by

$$\nu_{t,\,eq} = \nu_{t,o\,eq}\,[1-\exp(-\nu_{ti,\,eq}/\nu_{to,\,eq})] \qquad (V.18a)$$

$$\nu_{ti,\,eq} = \ell^2\,(-\overline{uv}_{max})^{1/2}/0.4y \qquad (V.18b)$$

with ℓ from equation (V.14) and $A^+ = 15$

$$\nu_{to,\,eq} = 0.0168\,U_e\delta^*/(1+5.5(y/\delta)^6) \qquad (V.18c)$$

$$\ell_M = 0.4\,y_M \text{ for } y_M/\delta \leq 0.225 \qquad (V.18d)$$

and

$$\ell_M = 0.09\delta \text{ for } y_M/\delta > 0.225.$$

C_{dif} is a modeling constant and U_M is the mean velocity at the maximum shearing stress location. These equations reduce to the form of the Cebeci-Smith model for the equilibrium case.

Because the eddy viscosity is lower in the detached flow zone, the Johnson and King model produces outer region mean velocity profiles, surface pressure and skin friction distributions, shape factor H distributions, and maximum shearing stresses that are in much better agreement with experimental values than the unmodified Cebeci-Smith model (Figure 91).

As was the case for integral methods, an inverse computational scheme should be used for differential methods to eliminate the weak singularity at $\tau_w = 0$. Arieli and Murphy (1980) and Murphy and King (1982) discuss a pseudo-direct procedure, starting from a given pressure distribution, for the automatic iteration of an inverse boundary layer calculation method coupled with a potential flow procedure. Murphy and King point out that the system of differential equations, rather than the numerical technique, can produce non-unique solutions. Iterations must be carefully done to avoid jumping from one solution to the other. Ardonceau et al. (1980) note a similar behavior when $(dP/dx)/(d\delta^*/dx) < 0$ is calculated. Johnson et al. (1980) noted that for some skin friction distributions, no unique solution to the inverse boundary layer equations was possible; for a given pressure distribution two distinct solutions were possible.

V. B.3 Incompressible Flow over Airfoils

Several of the methods discussed in sections V.B.1-2 with interaction with the inviscid flow have been applied to incompressible flow over stalled airfoils. The Wadcock (1980) NACA 4412 stalled airfoil experiment (Figure 12) was used as a test case at the 1981 Conference on Complex Turbulent Flows (Kline et al., 1982). In this author's opinion, the methods of LeBalleur (also LeBalleur and Neron, 1980) Chow, McDonald, Moses et al. (1982) and Dvorak, in the order of performance, were able to calculate the C_p distribution. Chow used a Boussinesq two-equation k-ε model with the law-of-the-wall profile in the Reynolds-averaged Navier-Stokes equations. McDonald used a one-equation model with a damped eddy viscosity in the Reynolds-averaged Navier-Stokes equations. The other methods have been discussed above in sections V.B.1 and IV.B.1.

McCroskey (Kline et al., Vol. II, 1982) discussed the performance of these methods. None of these methods correctly calculated the near wake and the correct drag. The drag is probably a useful and sensitive criterion for assessing the calculation of the interaction of the shear flow and the inviscid flow. Some methods achieved good agreement for C_p in the leading-edge region but not near the trailing edge, whereas the ones that computed the correct trailing-edge region failed to get the correct leading-edge suction peak. Smith et al. (1981) used the East et al., (1977) inverse lag-entrainment method to compute C_p distributions for this flow. The H and θ on the suction side were underestimated while C_p on the pressure side and C_L were overestimated.

Leading edge laminar-turbulent transitional detachment and reattachment bubble flows on airfoils are not presented here since only turbulent flows are discussed. Briley and McDonald (1975), Cebeci et al. (1980), and Kwon and Pletcher (1983) are sources of additional references.

V. B.4 Diffuser Flows

The purpose of diffusers is to decelerate the incoming flow to obtain the maximum pressure rise. Ashjaee et al. (1980) and Strawn and Kline (1981) point out that this optimum performance does not occur with $C_f = 0$ all along diffuser as suggested by Stratford (1959b) and Fernholz (1966), but only with small amounts of backflow. Strawn and Kline show that $\delta^*/\delta = 0.42$ produces this condition. For larger δ^*/δ values, δ^* rises rapidly and performance declines. Stratford's original experiment also showed a small positive C_f, indicating that the flow was not detached.

The numerous methods for diffuser flows without separation will not be discussed here. Moses and Chappell (1967) were among the first to calculate diffusers with some stall. The integral boundary layer method and inviscid core flow analysis has been further refined by Moses and his colleagues, as discussed in section V.B.1.

Kline and his colleagues have applied the Lyrio et al. (1981) method to the calculation of diffusers. For incompressible flow, Bardina et al. (1982) present a boundary integral method for the inviscid irrotational core that is derived from the Plemelj integral formula. Strawn et al. (1983) present an inverse design method for internal flow passages that gives the designer control over stall margin, or the operating range up to detachment. They also presented a new technique for coupling the integral boundary layer equations to a fully-elliptic potential flow core. More rapid convergence for flows with large regions of stall was obtained than the interaction schemes of Carter (1978) and LeBalleur (1981). Good calculations of pressure recovery were obtained.

Childs et al. (1981) extended the incompressible methods of Ghose and Kline (1976), Bardina et al. (1981), and Lyrio et al. (1981) to subsonic compressible flows. The major new element was a compressible shear flow method, which extended the incompressible correlations. Good calculations were obtained for the Ashjaee et al. (1980) 10° diffuser and the Sajben et al. (1977) planar diffuser with an inlet Mach number of 0.65. Calculations for unsteady inlet conditions are discussed in section V.E.

V. C. Calculation Methods for Bluff Body Flows

The k-ε model has been widely tested by a number of researchers for two-dimensional bluff body flows, e.g., cavity, rib, and sudden expansion flows, where detachment occurs at a well-defined location. A number of slightly different versions were used at the 1981 Stanford Conference (Kline et al., 1982) to compute the Kim et al. (1978) backward-facing step flow. Equations (V.7-11) and variations of these equations and parameters were used by Mansour, Pollard, Rodi et al., Launder et al., and Ha Minh et al. (Kline et al., Vol. III, 1982).

Rodi (Kline et al., 1982) pointed out that all of the standard k-ε models produce results for recirculating flows that are in much poorer agreement with experiment than results for simple shear layers (Vasilic-Melling, 1976; Gosman et al., 1977). All versions of the standard k-ε model tested at the Stanford Conference produced reattachment lengths that were at least 20% too short for the Kim et al. flow. Since we know from section IV.C that the flow behavior in the streamwise direction scales on the reattachment length X_R, it is no surprise that the computed C_p rises too rapidly and mean velocity profiles are in much error. Reynolds shearing stresses remain too high until about one X_R downstream of reattachment.

Launder et al. discuss the use of a Reynolds-stress transport model (RSTM) or an algebraic stress model (ASM) instead of the Boussinesq viscosity model used in the standard k-ε model. Rodi suggested that the RSTM and ASM are not significantly better for recirculating flows than the k-ε model. The ASM produces a greater X_R, in closer agreement with data, because the dissipation ε is increased and $-\overline{uv}$ is reduced in the detached flow zone.

Just as Rodi and Scheuerer (1983) observed for strong adverse-pressure-gradient flows (section V.B.2), many other investigators have concluded that the dissipation ε must be higher than computed by a standard k-ε model to get good results. Marvin (1983) noted this for the results of Sindir (1982), some of which are shown in Figure 92 for the experiments of Driver and Seegmiller (1982). Clearly, the best results occur for computations carried out with the ASM and the ε equation modified to increase dissipation. Although the faint dashed lines are difficult to see in Figures 46 (a) and (b), calculations of U and $-\overline{uv}$ profiles are in fair agreement with experiment. None of these models agree well with the turbulence kinetic energy balances shown by Driver and Seegmiller for detached flow. Mansour et al. (1983) used a rotation of turbulence term in the dissipation equation that reduced the dissipation and produced good X_R and C_p results, although k and $-\overline{uv}$ values were 30% and 10% low, respectively.

Others have used a correction similar to those employed for longitudinally curved flows, reasoning that the mean streamlines are curved. The algebraic stress model with curvature correction did fairly well at the Stanford Conference. Leschziner and Rodi (1981) suggest the use of the curvature modification to improve recirculating flow results. Gooray et al. (1983) used a functional C_μ similar to Leschziner and Rodi that accounts for streamline curvature. They obtained fairly good X_R, U, and C_p results for the Eaton and Johnston (1980) and Moss and Baker (1980) backward-facing step flows. Benodekar et al. (1983) used the curvature corrections of Launder et al. (1977) and obtained fairly good comparisons of U/U_e profiles for the Crabb et al. (1981) flow over a square rib shown in Figure 62.

Castro et al. (1979, 1981) have examined numerical schemes for bluff-body flows. Launder et al. (Kline et al., Vol. II, 1982) summarized the effect of numerics on k-ε computations. For the backward-facing step flow, Launder believed that initial conditions were more responsible for the results than slight differences in numerical schemes. Benodekar et al. (1983) used a "bounded skew hybrid differencing scheme" which they conclude is better than the hybrid difference scheme used by Durst and Rastogi (1979) for the rib type of flow and requires about half of the CPU time.

Ilegbusi and Spalding (1983) used a k-$\overline{\omega^2}$ model to compute the Kim et al. flow, with apparently better computations than the standard k-ε model. The reattachment length and maximum shear stress were well computed for one Tropea backward-facing step flow. The authors state that this method also works well for simple turbulent flows. More examination of this method for detached flows is needed.

For the Kim et al. backward-facing step flow the method of Celenligil and Mellor, discussed in section V.B.2, produces a too large X_R, as does the integral method of Moses et al. Computed C_p distributions are no worse than those by various k-ε versions. Kwon and Pletcher (1981) used 5 different turbulence models that are related to models A-E discussed in section V.B.2. Considerable adjustment of these models was done to specially fit them to backward-facing step flows. Celenligil and Mellor, like other investigators found that they did not need conditions downstream of reattachment to compute this type of flow.

V. D Compressible Flow Calculation Methods

Because of the interest in calculating transonic airfoil flows with some separation, there is much current activity in developing methods that include significant compressibility effects. Several recent review papers discuss a wider scope of references on this subject than will be presented here. Marvin (1983) reviewed some results of turbulence modeling studies, many of which were discussed at the 1981 Stanford Conference (Kline et al., Vol. II and III, 1982). LeBalleur (1981) and Melnik (1981) reviewed developments in theoretical concepts for the analysis of viscid-inviscid interactions on airfoils at transonic speeds under conditions where the boundary layer was attached, turbulent over most of the surface, and of significant thickness over some of the surface.

In a number of methods, detached flow models for the turbulent flow have not been included, but the ideas for handling the viscid-inviscid interaction are largely applicable to detached flow cases. Otto and Thiede (1973), Adamson and Messiter (1980), Bohning and Zierep (1980), Gordon and Rom (1981) employed attached flow physics in their models. Jou and Murman (1980) modeled the thickened turbulent boundary layer downstream of a transonic flow shock wave ($M < 1.3$) as a bump which was used to calculate the inviscid flow more correctly and better estimate the shock location. Yoshihara (1981) used a correlation for the pressure rise across a shock (see section IV. D.1) and a Prandtl-Meyer ramp to obtain $d\delta^*/dx$ at the shock. Downstream he used the Green lag-entrainment method for the attached boundary layer and a successive line over-relaxation method for the inviscid flow in a viscid-inviscid interaction. Melnik (Kline et al., Vol. II, 1982) noted that the Whitfield, LeBalleur, and Melnik integral methods did a credible job for thick attached boundary layers on transonic airfoils while the Cebeci-Smith eddy-viscosity model produced poorer results.

Marvin (1983) pointed out that the Cebeci-Smith model had difficulty calculating the pressure and skin friction satisfactorily for shock-induced separated flows. As was the case for incompressible flows, the mean backflow was too thin because the eddy viscosity was too large. Naturally, when some relaxation length is used, better results are obtained, as in the incompressible case. Of course, the results are a function of the relaxation length, which will differ from flow to flow. Marvin et al. (1975), Shang and Hankey (1975) and Rubesin et al. (1976) presented algebraic eddy-viscosity model results for supersonic and transonic flows with shock waves that support this observation.

Mixing length models fare no better. Murphy et al. (1975) had to employ an exponential lag model to obtain good surface pressure and skin-friction results for a $M = 3$, $Re = 5.7 \times 10^7/m$ flow. Figure 64 shows that Michel's mixing length model as well as an unmodified k-ε model fail to calculate accurately both velocity and shearing stress profiles for a transonic reattachment flow downstream of a shock system (Délery, 1983). They lead to an overprediction of the shear stress level at the interaction beginning. Farther downstream they fail to represent the slow relaxation of the turbulent flow. This is due partly because the models were derived for boundary layers with relatively weak pressure gradients, not for strongly non-equilibrium conditions typical of shock-induced separation. Special attention must be given to correctly model the very first stage of the shock interaction, where a precise calculation of all Reynolds stresses is essential for correct modeling of the downstream flow.

This result suggests that only turbulence models using one or more transport equations are able to correctly represent the shear layer behavior. Coakley and Viegas (1977) found that the unmodified Glushko-Rubesin turbulent kinetic energy equation model was better than a zero transport equation model for calculation of C_f and velocity profiles for transonic flow. A modified length scale model also was required to accurately calculate C_f and heat transfer for hypersonic flow.

Figure 70 shows some results from Horstman's (1982) calculations of the Viswanath and Brown (1982) shockless transonic trailing edge flow. Results from the k-ε model of Jones and Launder (1972), the k-ε model with curvature effects, the Cebeci-Smith eddy viscosity model, and the $k-\omega^2$ Wilcox-Rubesin model are shown. Viscous-inviscid interaction was important in the flow and in these calculations. The best results were obtained with the Reynolds-averaged Navier-Stokes equation and the k-ε model with the Cousteix curvature effect model, which agrees with incompressible flow results discussed in sections V.B.2 and V.C. The $k-\omega^2$ model produced almost as good surface pressures, δ^*, and mean velocity and shear stress profiles. Normal stresses were important in this flow and were included in both calculations. The $k-\omega^2$ model seemed to represent the normal stresses better. The Cebeci-Smith model yielded low δ^* and a too thin backflow region, which is typical of this model as discussed above. None of the models produced proper U profiles in the near wall region. Horstman states that the Reynolds-averaged Navier-Stokes equations, rather than boundary layer equations, are required to get the best results.

Marvin (1983) showed the Stanford Conference (Kline et al., 1982) results of Viegas, Horstman and Hung obtained with the two-equation Wilcox-Rubesin model for the Settles et al. (1976) $M = 2.85$ compression corner flow. Good surface pressure and mean velocity distributions were obtained. In other Stanford Conference results for this flow, the Cebeci-Smith method used by Hung and the LeBalleur lag-entrainment integral method produced good surface pressure distributions, but low mean velocity profiles. This latter result is consistent with the extremely low skin-friction calculations produced by the latter two methods. Ardonceau et al. (1980) used algebraic eddy viscosity and mixing length models to obtain better surface pressure results for a compression corner than reported by Shang and Hankey, but poorer than for a two equation model. The earlier eddy viscosity, relaxation length and turbulent kinetic energy modeling of Horstman et al. (1977) for this flow generally support these observations.

For the Bachalo and Johnson (1979) $M = 0.875$ transonic shock-induced separating and reattaching flow, Viegas, Horstman, and Hung used the Wilcox-Rubesin model to obtain mean velocity and turbulent shear stress profiles in good agreement with experimental data and better than Cebeci-Smith model results. Johnson and King (1984) point out that the eddy viscosity is too large in the Cebeci-Smith model for this flow and in the Johnson and Spaid (1983) DSMA 671 supercritical airfoil flow ($M = 0.72$), which has adverse-pressure-gradient induced detachment near the trailing edge. Johnson and King note that while two-equation (k-ε and $k-\omega^2$) eddy viscosity models calculate the skin friction downstream of reattachment better than the Cebeci-Smith model, they are more complex and produce unsatisfactory results for surface pressures in transonic flows with large detached flow zones.

Liou et al. (1981) used the Wilcox-Rubesin model to compute the Sajben et al. (1977) steady transonic diffuser flows. Good agreement with the experimental results was obtained for the inviscid flow pattern even for one flow with massive separation induced by a strong shock. The distinct lambda shock pattern observed in the experiment was closely duplicated by the calculations. However, near reattachment and downstream the calculated velocity profiles were not in good agreement with data. Liou and Coakley (1981) applied this model in calculations of the Sajben et al. (1977, 1981) forced and self-induced oscillatory unsteady flows. Lower eddy viscosity values were required to obtain fairly good agreement with forced oscillation results. For the naturally present, self-sustaining oscillations, some success was obtained in calculating the shock pattern and time-mean quantities. The calculated shock oscillation frequency was too large for a strong shock wave case but was well estimated for two weaker shock cases.

The Johnson and King (1984) model discussed above in section V.B.2 scales the eddy viscosity on the maximum shearing stress and does a good job calculating the surface pressures. Calculated and experimental mean velocity profiles for the Bachalo and Johnson flow look very much like those shown in Figure 91.

Marvin (1983) concludes that neither zero nor two transport equation eddy-viscosity models shows the proper upstream influence of the viscous-inviscid interaction when a large stall zone is present. Consequently, the detachment and shock wave locations are not usually correctly calculated. The compressible form of the turbulent kinetic energy and shear-stress equations contains additional correlations that arise because of compressibility, but are usually ignored (Coakley and Viegas, 1977). Marvin suggests that these terms may be needed for flows with shock waves and for hypersonic flows, so further investigation of these effects is warranted.

Several integral methods do a fair job of calculating important parameters of detached compressible flows. Most of their difficulties stem from weaknesses in their correlations that are present for low speed flows too. The results of East et al. (1977), LeBalleur (1981), and Whitfield et al. (1981) and the results of Thomas (1984) using the models of these methods show fairly good agreement with experimental results for flows with relatively slow variations. Some type of lag model must be used in these methods across shock waves and in highly non-equilibrium conditions.

Childs et al. (1981) extended the Lyrio et al. (1981) incompressible flow integral method to handle subsonic diffuser flows. Correlations were extended to include compressible flow data. A lag-entrainment model based on the Bradshaw entrainment correlation was used. An inviscid-viscid interaction scheme was employed that suppresses the boundary layer equation singularity at detachment. Good calculations of surface pressure were obtained for the Sajben et al. (1977) steady separating diffuser flow with inlet $M = 0.65$.

V.E Unsteady Flow Methods

Steady flow calculation models and methods have been extended to unsteady turbulent flows. Prior to the late 1970's, there were very few sets of experimental unsteady turbulent boundary layer data. The validity of calculations that were made with various initial and boundary conditions to explore possible unsteady flow patterns was uncertain because of this lack of test data with which to make comparisons. McCroskey (1977) and Telionis (1977) have reviewed many of these earlier efforts. As discussed in section IV.E, only recently have reliable experimental velocity field data in oscillating detached flow zones become available.

In view of our discussion of experimental data in section IV.E, it is clear that unsteadiness does not alter the turbulence structure much from that for steady flows, except perhaps in large amplitude oscillation cases where non-linear effects within the flow become stronger. Bradshaw (1978) pointed out that substantial derivative of $-\hat{u}\hat{v}$, $D(-\hat{u}\hat{v})/Dt$, for the ensemble-averaged movement of a fluid element cannot exceed values for which the turbulence model is satisfactory in steady flow and still be valid in unsteady flow. Separate bounds on the streamwise wavelength and on frequency in a spatially dependent unsteady flow are not required; the upper limit on the frequency seen by a moving fluid element can be derived from steady-flow considerations. If a steady flow turbulence model cannot respond to spatial changes with a wavelength less than L, then the moving-axis frequency of the unsteady flow cannot exceed $\overline{U}_e/L$. Cebeci (1981) concurred that the ability of a turbulence model to calculate unsteady flows can be gaged by its ability to calculate steady flows. Unsteadiness relieves none of the numerical and turbulence model difficulties encountered with steady freestream separation.

The linear unsteady velocity terms in equation (IV.31) must be included in all calculations except for very slowly varying conditions, when these terms are negligible. Since calculations must proceed in time as well as in two spatial dimensions, care is needed to avoid numerical instability and to minimize computation time, especially when flow reversal occurs. Nash and Scruggs (1977), Shamroth (1981), Tassa and Shankar (1981), Orlandi (1981), and Cebeci and Carr (1981), for example, use implicit procedures, Cebeci and Carr used the "characteristic box" method to compute the first profile on a given time-line, which permits velocity profiles with partial flow reversal to be computed. An alternating-direction implicit (ADI) method was used by Nash and Scruggs. Shamroth and Tassa and Shankar used forms of the Briley-McDonald ADI procedure.

The turbulence models used in these investigations have not produced very good results for steady freestream separating flows. Algebraic eddy viscosity models used by Cebeci and Tassa and Shankar, and turbulence kinetic energy models used by Nash and Scruggs, Orlandi, and Shamroth with length scale equations have not done particularly well for either steady or unsteady separating cases. Figure 93 shows that the five equation k-ε-u^2-v^2-uv model used by Cousteix, Houdeville, and Javelle (1981) produces results in better agreement with data than mixing length or k-ε models for an adverse pressure gradient flow without detachment. Fairly good qualitative agreement results for oscillating airfoil flows (Shamroth, Tassa and Shankar) as long as there are some turbulent layer effects that produce hysteresis in the size of the oscillating stall zone.

Such was the case for calculations of the transonic self-induced oscillatory biconvex airfoil flow shown in Figures 85 and 86 and discussed in section IV.E.3. A mixing-length model (Levy, 1978; Seegmiller et al., 1978; Marvin, 1980) was used in the Reynolds-averaged Navier-Stokes equations with the mixing length frozen at its value at detachment. The computed frequency of oscillation of detachment from one side of the airfoil to the other was about 20% lower than experimentally observed. The calculations failed to reproduce the correct shock obliqueness and correct pressure distribution downstream of the shock wave,

deficiencies that were also present in steady freestream computations. The unsteady transonic diffuser calculations of Liou and Coakley (1981) were discussed in section V.D.

Levy and Bailey (1981) showed that the time-dependent Reynolds-averaged Navier-Stokes equations provide the essential features of transonic, turbulent, unsteady flows about airfoils even when a steady flow algebraic eddy-viscosity turbulence model is used. Agreement between the computed and available experimental buffet boundaries is good at higher freestream Mach numbers and lower lift coefficients where the onset of unsteady flow is associated with shock-wave induced boundary-layer separation. At lower Mach numbers and higher angles of attack where the onset of unsteady flows is associated with an upper surface leading-edge separation bubble, the computed boundaries are not in good agreement, but perhaps can be improved by accounting for transition.

Cousteix, Houdeville, and Javelle (Michel et al., 1981) and Cousteix and Houdeville (1980) used the unsteady momentum integral equation

$$\frac{C_f}{2} = \frac{1}{U_e^2}\frac{\partial}{\partial t}(U_e\delta^*) + \frac{\partial\theta}{\partial x} + \frac{\theta(H+2)}{U_e}\frac{\partial U_e}{\partial x} \qquad (V.19)$$

and an entrainment equation, equation (V.4) but with

$$H^* = (\delta-\delta^*)/\theta = \frac{\beta H^2 + H}{H-1} \qquad \beta = 0.631 \qquad (V.20)$$

for the entrainment model. These equations form a hyperbolic set of first order partial differential equations in δ^* and θ. For $H > 1$, there are always two distinct real characteristic directions in the x, t plane. One direction is always positive while the second is positive for $H < H_c$ and negative for $H > H_c$, where $H_c \approx 2.6$. This value of H_c is the shape factor near the steady free-stream detachment location. The location where $H = H_c$ is a limit between regions with upstream influence and downstream influence.

Lyrio and Ferziger (1983) used the steady free-stream flow lag entrainment model mentioned in section V.B.1. Although their set of equations is also hyperbolic, they chose to compute the conditions for all times at each x location before moving to the next location. Computed results for a Houdeville and Cousteix adverse pressure gradient flow and a conical diffuser unsteady flow were in good agreement with experimental results as far downstream as the time-averaged detachment location. The computed results for these low amplitude oscillatory flows support the observation made in section IV.E that the mean flow parameters of attached boundary layers are almost unaffected by oscillations. Farther downstream δ^* and H are overpredicted. As suggested by Lyrio and Ferziger, the shortcomings of the method in the presence of flow reversal may be that the Coles velocity profile and/or the entrainment correlation may not hold in the unsteady reversed-flow region. Simpson et al. (1983) and Simpson and Shivaprasad (1983) observed from their data that the ensemble-averaged or phase-averaged velocity profiles look like steady free-stream profiles for the same γ_{pumin} when $\partial\gamma_{pumin}/\partial t < 0$. For $\partial\gamma_{pumin}/\partial t > 0$, the profiles differed significantly from the steady free-stream results, but looked much like the Coles velocity profile. Since the Coles velocity profile model does not fit the steady free-stream velocity profile data well nor model the velocity profile hysteresis, the profile model used in this method needs to be modified.

Strickland, Oler, and Im (Francis and Luttges, 1984) used the Lyrio and Ferziger method to compute some unsteady airfoil flows. Qualitative agreement with data was obtained. Good quantitative agreement was observed for small angles of attack.

Nearly all of the investigators mentioned above point out that inverse calculation procedures must be used in unsteady inviscid-viscous calculations in order to avoid numerical difficulties. As discussed in section V.B, in an inverse computation δ^* or some other matching parameter is used for separate computations in the inviscid and shear regions instead of P or U_e, which are free to vary so that a smooth variation of δ^* or the matching parameter occurs.

VI. CONCLUDING REMARKS

From this brief review, it is clear that many modern advances in measurements technology have been made for separated flows. A personal view is that laser anemometry should be exploited further to provide needed information on the structure of turbulent separated flows. While traditional hot-wire anemometry has a less useful future, the thermal tuft and pulsed-wire anemometry appear to be quite useful, especially so for variable density and dirty flows. Holography has been shown to be quite useful for research in compressible separated flows. Pitot tubes should be totally abandoned for velocity measurements in flow regions with intermittent backflow since reliable data interpretation is not possible. Surface film gages appear to have been considerably improved, as have the static pressure probe and pressure transducers. Modern digital data acquisition and processing equipment and techniques are now more readily available to deduce much about the flow structure of separating boundary layers.

There are several common features for all types of separating and reattaching flows that were discussed here. In the vicinity of detachment the turbulence intensities become the largest in the middle of the shear layer. Lower $-\overline{uv}/u'v'$ correlation coefficients occur than for attached flows. Substantial pressure gradient relief begins near intermittent transitory detachment. Large-scale structures pair to form larger structures which pass downstream at lower frequencies. Mean velocity profiles look much like those for mixing layers, except near the wall where backflow occurs. The mean backflow profile scales on the maximum mean backflow velocity and its distance from the wall. The backflow is strongly controlled by the maximum shear stress within the flow. The traditional semi-logarithmic law-of-the-wall velocity profile does not describe the backflow.

For thick regions of mean backflow, such as occur for the detached flow just downstream of a bluff body, there are relatively few instants of forward flow. For thinner regions of mean backflow, the backflow is more intermittent. The large-scale structures which dominate detached flows, supply the turbulence energy to the near wall backflow, either by inrushes of outer region fluid toward the wall or by turbulence energy diffusion by pressure fluctuations. Velocity fluctuations in the backflow are greater than or at least comparable to the mean backflow velocities. For highly intermittent backflow zones, the mean backflow does not appear to come from far downstream.

In the vicinities of detachment and reattachment, the normal stresses terms in the momentum and turbulence energy equations become important. Large streamwise variations in the mean velocity and turbulence profiles occur. The reattachment length, which is measured from detachment to reattachment, is the most important streamwise length on which to scale the streamwise variations of skin friction, upstream-downstream flow direction intermittency, static pressure recovery, and mean square surface pressure fluctuations.

Reattaching flows have significantly higher Reynolds stresses than detaching flows for the same mean velocity profile shape factor. Some distance downstream of reattachment these stresses decay to levels for attached boundary layers. This lag and hysteresis of the turbulence structure carries over to unsteady detaching flows. When the unsteady flow is increasingly detached, ($\partial\gamma_{pumin}/\partial t < 0$), the ensemble-averaged or phase-averaged velocity profile looks like a steady freestream profile for the same γ_{pumin}. The phase-averaged profile looks more like a reattaching steady flow when $\partial\gamma_{pumin}/\partial t > 0$. Organized unsteadiness strongly affects detached flows but low amplitude flow oscillations have a negligible effect on mean velocities of attached turbulent flows.

Under some conditions very low frequency self-induced unsteadiness is present in flows that are unconstrained and can flap. Little turbulence shearing stress is associated with these large-scale motions. Imbalances between fluid entrained by the detached flow and that returned in the recirculation or stalled fluid zone or interactions of large-scale structures with the surface can produce these low frequency motions. Interactions between the inviscid and turbulent flow regions can also be responsible for such oscillations.

Shock-induced detachment produces a flow structure similar to that for detached incompressible flows. Mean velocity profiles and the turbulence structure downstream of reattachment look qualitatively like that for incompressible reattaching flows.

All of the experiments discussed here suffer from some mean flow three-dimensional effects. All turbulent flows are three dimensional at any instant, but truly two-dimensional mean flows have the same time-averaged structure spanwise across the flow. No discussion of three-dimensional effects has been given because none of the qualitative flow features is believed to be significantly affected by mean flow three-dimensionality. Side wall boundary layers cause most three-dimensional effects. Relatively low momentum fluid in side wall corners is easily drawn into the backflow region causing crossflow (Ruderich and Fernholz, 1983). In such cases, the higher momentum outer region of the detached flow can move farther away from the wall than in a purely two-dimensional mean flow, increasing the reattachment length.

Even when side wall boundary layers are completely removed other three-dimensional effects can be present. For example, when a detached shear layer grows to a thickness greater than 1/10 to 1/3 of the spanwise channel width, the large-scale structures will not pair together or move in the spanwise direction like they would in a wider two-dimensional apparatus. Slight spanwise mean pressure gradients due to a slightly three-dimensional geometry also can induce crossflows in the backflow region. Swirl in the apparatus will lead to significant crossflows in the backflow zone.

Clearly, more experiments are needed to firmly establish the nature and structure of separating and reattaching flows. The laser and pulsed-wire anemometers should be used in these needed studies. Experiments like those done by Praturi and Brodkey (1978) for a zero-pressure-gradient boundary layer are needed. In those experiments, the three-dimensional motions marked by particles were followed by a motion picture camera moving at the average speed of the large-scale structures. The ejections of low speed fluid and the inrushes of higher momentum fluid were observed, as well as the influence of these motions on the turbulent-non-turbulent interface. Speckle velocimetry and scanning laser anemometers can be used to determine instantaneous velocity profiles, which will lead to information about large-scale motions. A great deal more information is needed on the structure of the backflow for various flows.

More measurements of the flow structure under conditions with intermittent backflow are needed. Although static pressure fluctuations can only be accurately measured on the surface, a large number of simultaneous surface pressure fluctuation measurements over the detaching flow zone can yield information on the time-dependent pressure gradients that can influence the backflow behavior. Unknown features about the structure of separating and reattaching flows with curved walls and compressible flows requires further experiments. The quantitative study of unsteady separating flows is still in its infancy. Data are needed to extend correlations discussed here.

There is still some information about the structure of detached flows that can be gleaned from available data. Although this author dug deeply into some data available to him, he had neither the time or manpower to thoroughly examine all data for additional structural details. In some cases, experiments were performed mainly to provide test cases for calculation methods. Such data need to be reexamined for new information on the flow physics.

Calculation methods need substantial improvement before they can be used confidently to compute flows for which we do not already know the answers from experiments. The shortcomings of various existing models have been discussed in section V. Based on the important experimentally-observed physical features of detached flows, better integral methods will result if velocity profile correlations based on data are used instead of forcing the law-of-the-wall/wake model to fit data. The maximum shear stress and the large-scale structures dominate detached flows. Further work using large-eddy models for the diffusion of turbulence energy is needed since this represents the correct fluid physics for supplying energy to the backflow.

Several general comments are in order about the way calculations are often presented. In many instances, calculations are made for a small number of test cases with comparisons with experimental mean velocity and turbulence profiles at a few locations. No effort is made currently to quantify the agreement with data, as suggested in the Appendix. In the future, such objective and quantitative comparisons need to be made. Calculation methods also should be able to reproduce the experimentally-observed functional dependence of flow parameters, e.g., C_p, X_R, C_f, detachment and reattachment locations and shock locations, on the Reynolds number and geometry of the flow. For example, a robust calculation method for bluff body flows should be able to reproduce the effect of blockage on the reattachment length (Figure 57).

APPENDIX A PROPOSED METHOD FOR QUANTIFYING CALCULATION METHOD PERFORMANCE

Currently only subjective judgment is used in describing the performance of calculation methods. For example, Figure 91 shows the calculations by the Johnson and King and Cebeci and Smith turbulence models that are described in section V.B.2. The Johnson and King model results are clearly in good agreement with the experimental data. Here it is proposed that several parameters be computed that will quantify the performance of calculation methods relative to experimental data.

If $Q_c(r)$ is a calculated value of some quantity at the same point r in a domain as an experimental value $Q_e(r)$, then the mean deviation d of the calculated result over D data points in the domain is given by

$$\sum_D \frac{|Q_c(r) - Q_e(r)|}{D} = d \tag{A.1}$$

An alternate measure of deviation can be given by the standard deviation σ of calculated results over D data points given by

$$\sum_D \frac{(Q_c(r) - Q_e(r))^2}{D} = \sigma^2 \tag{A.2}$$

In either of these equations, it is assumed that the uncertainties $\Delta Q_e(r)$ of the experimental values are negligible compared to the deviations by the calculation method. If the experimental uncertainties are not negligible, then we can compute the adjusted standard deviation σ_a given by

$$\sum_D \frac{(|Q_c(r) - Q_e(r)| - \Delta Q_e(r))^2}{D} = \sigma_a^2 \tag{A.3}$$

or the adjusted mean deviation d_a

$$\sum_D \frac{(|Q_c(r) - Q_e(r)| - \Delta Q_e(r))}{D} = d_a \tag{A.4}$$

where only positive values of $|Q_c(r) - Q_e(r)| - \Delta Q_e(r)$ are retained and used. These equations reflect the fact that the experimental uncertainties and the deviations of the calculated results are totally unrelated and uncorrelated. An adjusted standard deviation σ_a or adjusted mean deviation d_a that is zero indicates that the experimental uncertainties are as large or larger than differences between calculated and experimental values. In other words, the data are insufficiently certain to judge the calculated results.

Sometimes the shape of a calculated curve in a domain looks much like that of the experimental data. The product moment correlation coefficient R_c is a measure of how well a calculation method reproduces changes in a given experimentally-measured parameter over a domain. It is given by

$$R_c = \frac{\sum_D (Q_c(r) - \bar{Q}_c)(Q_e(r) - \bar{Q}_e)}{\left(\left(\sum_D (Q_c(r) - \bar{Q}_c)^2\right)\left(\sum_D (Q_e(r) - \bar{Q}_e)^2\right)\right)^{1/2}} \tag{A.5}$$

where

$$\bar{Q}_c = \sum_D \frac{Q_c(r)}{D} \quad \text{and} \quad \bar{Q}_e = \sum_D \frac{Q_e(r)}{D}$$

R_c is near unity when the experimental and calculated curves in the domain look alike. Suppose that $Q_c(r) = A\, Q_e(r)$, where A is a constant. Then the experimental and calculated curves look alike except for a constant factor which produces $R_c = 1$. In this case, $d = (A - 1)\bar{Q}_e$ and

$$\sigma = (A - 1)\left(\sum_D \frac{(Q_e(r))^2}{D}\right)^{1/2}$$

indicating some deviation between calculated and experimental values. Values of R_c much below 0.99 indicate poor agreement of the shapes of calculated and experimental curves.

As an example, the data in Figure 91(c) were used to compute d and R_c with $Q_e(r) = U(y)/U_e$ for each experimental data point and $Q_c(r) = U/U_e$ for each corresponding y position. The Johnson and King model results produce a lower mean deviation of $d = 0.025$ and a higher correlation coefficient $R_c = 0.999$ than the Cebeci and Smith model results of $d = 0.105$ and $R_c = 0.961$.

By quantifying calculation method performance, computors will be able to see quantitatively whether modifications to numerics and/or turbulence models improve agreement with data. Users of such methods can also have numerical estimates of how uncertain computed results can be.

REFERENCES

Abbott, D.E. and Kline, S.J. (1962), "Experimental Investigation of Subsonic Turbulent Flow over Single and Double Backward-Facing Steps," Trans. ASME, J. Basic Engrg., 84D, Series D, pp. 317-325.

Adair, D., Thompson, B.E. and Whitelaw, J.H. (1983), "Measurements and Calculations of a Separating Boundary Layer and the Downstream Wake," Numerical and Physical Aspects of Aerodynamic Flows, T. Cebeci, ed., Springer-Verlag, pp. 97f.

Adamson, T.C. and Messiter, A.F. (1980), "Simple Approximations for the Asymptotic Description of the Interaction Between a Normal Shock Wave and a Turbulent Boundary Layer at Transonic Speeds," AGARD-CP-291, Paper 16.

Ajagu, C.O., Libby, P.A., and LaRue, J.C. (1982), "Modified Gauge for Time-Resolved Skin-Friction Measurements," Rev. Sci. Instrum., 53, pp. 1920-1926.

Alber, I.E., Bacon, J.W., Masson, B.S., and Collins, D.J. (1973), "An Experimental Investigation of Turbulent Transonic Viscid-Inviscid Interactions," AIAA Journal, 11, pp. 620-627.

Albers, M., (1980), "Untersuchung einer transsonischen Strömungsschwingung mittels Echtzeit-Laser-Doppler--Anemometrie," DFVLR-FB 80-04, Gottingen.

Albers, M., Grabitz, G., and Meier, G.E.A. (1980), "Ein Schwingungsmechanismus einer transsonischer Strömung," DAGA '80, VDE-Verlag, pp. 543-546.

Anderson, J.S., Jungowski, W.M., Hiller, W.J., and Meier, G.E.A. (1977), "Flow Oscillations in a Duct with a Rectangular Cross-Section," J. Fluid Mech., 79, Part 4, pp. 769-784.

Appels, C. and Richards, B.E. (1975), "Incipient Separation of a Compressible Turbulent Boundary-Layer," AGARD-CP-168, Paper 21.

Ardonceau, P.L. (1984), "The Structure of Turbulence in a Supersonic Shock-Wave/Boundary Layer Interaction," AIAA J., 22, pp. 1254-1262.

Ardonceau, P., Alziary, Th., and Aymer, D. (1980), "Calcul de l'interaction onde de choc/couche limite avex decollement," AGARD-CP-291, Paper 28.

Arieli, R. and Murphy, J.D. (1980), "Pseudo-Direct Solution to the Boundary-Layer Equations for Separated Flow," AIAA Journal, 18, pp. 883-891.

Armaly, B.F., Durst, F. and Kottke, V. (1981), "Momentum, Heat, and Mass Transfer in Backward-Facing Step Flows," Third Symposium on Turbulent Shear Flows, pp. 16.1-16.4.

Armaly, B.F., Durst, F., Pereira, J.C.F., and Schonung, B. (1983), "Experimental and Theoretical Investigation of Backward-Facing Step Flow," J. Fluid Mech., 127, pp. 473-496.

Ashjaee, J. and Johnston, J.P. (1980), "Straight Walled Two-Dimensional Diffusers - Transitory Stall and Peak Pressure Recovery," J. Fluids Engineering, 102, pp. 275-282.

Ashjaee, J., Johnston, J.P., and Kline, S.J. (1980), "Subsonic Turbulent Flow in Plane-Wall Diffusers: Peak Pressure Recovery and Transitory Stall," Report PD-21, Thermosciences Div., Dept. Mech. Engrg. Stanford Univ.

Ashurst, W.T., Durst, F., and Tropea, C. (1980), "Two-Dimensional Separated Flow: Experiment and Discrete Vortex Dynamics Simulation," AGARD-CP-291, Paper 24.

Assassa, G.M. and Papailiou, K.D. (1979), "An Integral Method for Calculating Turbulent Boundary Layers with Separation," J. Fluids Engineering, 101, pp. 110-116.

Bachalo, W.D. and Johnson, D.A. (1979), "An Investigation of Transonic Turbulent Boundary Layer Separation Generated on an Axisymmetric Flow Model," AIAA-79-1429.

Bachalo, W.D., Modarress, D. and Johnson, D.A. (1977), "Experiments on Transonic and Supersonic Turbulent Boundary Layer Separation," AIAA-77-47, 15th Aerospace Sciences Meeting.

Baldwin, B.S. and Lomax, H. (1978), "Thin Layer Approximation and Algebraic Model for Separated Turbulent Flows," AIAA Paper 78-257.

Barbi, C., Favier, D., and Maresca, C. (1981), "Vortex Shedding from a Circular Cylinder in Oscillatory Flow," Unsteady Turbulent Shear Flows, (Ed: Michel, R., Cousteix, J., and Houdeville, R.), pp. 248-261, Springer-Verlag.

Bardina, J., Kline, S.J., and Ferziger, J.H., (1982), "Computation of Straight Diffusers at Low Mach Number Incorporating an Improved Correlation for Turbulent Detachment and Reattachment," Report PD-22, Thermosciences Div., Dept. Mech. Engrg., Stanford University.

Baskaran, V. (1983), "Turbulent Flow Over a Curved Hill," Ph.D. Thesis, Univ. of Melbourne, Australia.

Bellhouse, B.J. and Schultz, D.L. (1966), "Determination of Mean and Dynamic Skin Friction, Separation and Transition in Low-Speed Flow with a Thin-Film Heated Element," J. Fluid Mech., 24, pp. 379-400.

Benodekar, R.W., Goddard, A.J.H., Gosman, A.D., and Issa, R.I. (1983), "Numerical Prediction of Turbulent Flow Over Surface-Mounted Ribs," ASME paper 83-FE-13, AIAA J., 23, pp. 359-366, 1985.

Bergh, H. (1978), "Technical Evaluation Report on the Fluid Dynamics Panel Symposium on Unsteady Aerodynamics," AGARD-AR-128.

Bhateley, I.C. and Bradley, R.G. (1972), "A Simplified Mathematic Model for the Analysis of Multi-Element Airfoils near Stall," Paper 12, AGARD-AG-102.

Blackwelder, R.F. and Kaplan, R.E. (1976), "On the Wall Structure of the Turbulent Boundary Layer," J. Fluid Mech., 76, pp. 89-112.

Blinco, P.H. and Sandborn, V.A. (1973), "Use of the Split-Film Sensor to Measure Turbulence in Water Near a Wall," pp. 403-413, Proc. of Third Symposium on Turbulence in Liquids, G.K. Patterson and J.L. Zakin, editors, Dept. Chem. Engrg., Univ. Miss.-Rolla.

Bogar, T.J., Sajben, M., and Kroutil , J.C. (1981), "Characteristic Frequencies of Transonic Diffuser Flow Oscillations," AIAA-81-1291; AIAA Journal, 21, pp. 1232-1240 (1983).

Boisson, H.C., Chassaing, P., Ha Minh, H., Sevrain, A. (1981), "Some Characteristics of the Unsteady Wake Flow Past a Circular Cylinder," Unsteady Turbulent Shear Flows, (Ed: Michel, R., Cousteix, J., and Houdeville, R.), pp. 262-272, Springer-Verlag.

Bohning, R. and Zierep, J. (1980), "Normal Shock-Turbulent Boundary Layer Interaction at a Curved Wall," AGARD-CP-291, Paper 17.

Bradbury, L.J.S. (1976), "Measurements with a Pulsed-Wire and a Hot-Wire Anemometer in the Highly Turbulent Wake of a Normal Flat Plate," J. Fluid Mech., 77, pp. 473-497.

Bradbury, L.J.S.,and Castro, I.P. (1971), "A Pulsed-Wire Technique for Velocity Measurement in Highly Turbulent Flow," J. Fluid Mech., 49, pp. 657-691.

Bradshaw, P. (1967), "The Turbulence Structure of Equilibrium Boundary Layers," J. Fluid Mech., 29, pp. 625-645.

Bradshaw, P. (1970), Experimental Fluid Mechanics, Second Edition, Pergamon Press, Oxford.

Bradshaw, P. (1973), "Effects of Streamline Curvature on Turbulent Flow," AGARDograph 169.

Bradshaw, P. (1978), "Prediction of Separation Using Boundary Layer Theory," Paper 11, AGARD-LS-94.

Bradshaw, P. (1978), "Structure of Turbulence in Complex Flows," Paper 10, AGARD-LS-94.

Bradshaw, P. and Wong, F.Y.F. (1972), "The Reattachment and Relaxation of a Turbulent Shear Layer," J. Fluid Mech., 52, Part 1, pp. 113-135.

Briley, W.R. and McDonald, H. (1975), "Numerical Prediction of Incompressible Separation Bubbles," J. Fluid Mech., 69, pp. 631-656.

Buchhave, P. (1975), "Laser Doppler Velocimeter with Variable Frequency Shift," Optics and Laser Tech., pp. 11-16, February 1975.

Buchhave, P., George, W.K., and Lumley, J.L. (1979), "The Measurement of Turbulence with the Laser-Doppler Anemometer," Annual Review of Fluid Mechanics, 11, pp. 443-503.

Buckles, J., Hanratty, T.J., and Adrian, R.J. (1983), "Turbulent Flow Over Large-Amplitude Wavy Surfaces," to appear in J. Fluid Mech.; also Buckles, H. (1983), Ph.D. Dissertation, Univ. Illinois.

Butter, D.J. and Williams, B.R. (1980), "The Development and Application of a Method for Calculating the Viscous Flow About High-Lift Aerofoils," AGARD-CP-291, pp. 25.1-25.20.

Carlson, L.A. (1980), "A Direct-Inverse Technique for Low Speed High Lift Airfoil Flowfield Analysis," AGARD-CP-291, Paper 26.

Carter, J.E. (1978a), "Inverse Boundary Layer Theory and Comparison with Experiment," NASA TP 1208.

Carter, J.E. (1978b), "A New Boundary-Layer Interaction Technique for Separated Flows," NASA TM 78 690.

Carter, J.E. and Wornom, S.F. (1975), "Solutions of Incompressible Separated Boundary-Layers Including Viscous-Inviscid Interaction," NASA SP-347, pp. 125-150.

Castro, I.P. (1971), "Wake Characteristics of Two-Dimensional Perforated Plates Normal to an Airstream," J. Fluid Mech., 46, pp. 599-609.

Castro, I.P. (1979), "Numerical Difficulties in the Calculation of Complex Turbulent Flows," Turbulent Shear Flows I, pp. 220-236, Springer-Verlag.

Castro, I.P. (1979),"Relaxing Wakes Behind Surface- Mounted Obstacles in Rough Wall Boundary Layers," J. Fluid Mech., 93, Part 4, pp. 631-659.

Castro, I.P. (1981), "Measurements in Shear Layers Separating from Surface-Mounted Bluff Bodies," Journal of Wind Engineering and Industrial Aerodynamics, 7, pp. 253-272.

Castro, I.P. and Cheun, B.S. (1982a), "The Measurement of Reynolds Stresses with a Pulsed-Wire Anemometer," J. Fluid Mech., 118, pp. 41-58.

Castro, I.P. and Dianat, M. (1982), "Surface Shear Stresses on Bluff Bodies," Euromech Colloq., Lisbon.

Castro, I.P. and Dianat, M. (1983), "Surface Flow Patterns on Rectangular Bodies in Thick Boundary Layers," to appear in J. Wind Engrg. and Ind. Aero.

Castro, I.P., Cliffe, K.A., and Norgett, M.J. (1981), "Prediction of the Low Reynolds Number Laminar Flow over a Normal Flat Plate, and its Application to Turbulent Flow Calculations," Third Symposium on Turbulent Shear Flows, pp. 18.7-18.14.

Castro, I.P. and Fackrell, J.E. (1978), "A Note on Two-Dimensional Fence Flows with Emphasis on Wall Constraint," Journal of Industrial Aerodynamics, 3, pp. 1-20.

Cebeci, T. (1981), "Unsteady Separation," Symposium on Numerical and Physical Aspects of Aerodynamics Flows, Cal. State Univ., Springer-Verlag.

Cebeci, T. and Bradshaw, P. (1977), Momentum Transfer in Boundary Layers, McGraw-Hill/Hemisphere.

Cebeci, T. and Carr, L. W. (1981), "Prediction of Boundary Layer Characteristics of an Oscillating Airfoil," Unsteady Turbulent Shear Flows, (Ed: Michel, R., Cousteix, J., and Houdeville, R.), pp. 145-158, Springer-Verlag.

Cebeci, T. and Smith, A.M.O. (1974), Analysis of Turbulent Boundary Layers, Academic Press.

Cebeci, T., Khalil, E.E., and Whitelaw, J.H. (1979), "Calculation of Separated Boundary Layer Flows," AIAA Journal, 17, pp. 1291-1292,

Cebeci, T., Mosinskis, G.J. and Smith, A.M.O. (1972), "Calculation of Separation Points in Incompressible Flows," J. Aircraft, 9, pp. 618-624.

Cebeci, T., Stewartson, K., and Williams, P.G. (1980), "Separation and Reattachment Near the Leading Edge of a Thin Airfoil at Incidence," AGARD-CP-291, Paper 20.

Cenedese, A., Iannetta, S., Mele, P., and Pietrogiacomi, D. (1979), "Non-Stationary Analysis of Velocity Field Around a Square Section Blunt Body," Second Symposium on Turbulent Shear Flows, pp. 16.19-16.23.

Chandrsuda, C. and Bradshaw, P. (1981), "Turbulence Structure of a Reattaching Mixing Layer," J. Fluid Mech., 110, pp. 171-194.

Chandrsuda, C., Mehta, R.D., Weir, A.D., and Bradshaw, P. (1978), "Effect of Free-Stream Turbulence on Large Structure in Turbulent Mixing Layers," J. Fluid Mech., 85, Part 4, pp. 693-704.

Chang, P.K. (1970), Separation of Flow, Pergamon Press.

Chapman, D.R., Kuehn, D.M., and Larson, H.K. (1958), "Investigation of Separated Flows in Subsonic and Supersonic Streams with Emphasis on the Effects of Transition," NACA Rept. 1356.

Chehroudi, B. and Simpson, R.L. (1983), "Scanning Laser Doppler Anemometer and its Application in Turbulent Separated Flow," Report WT-7, Dept. Civil/Mechanical Engrg., Southern Methodist Univ., Dallas, TX 75275; DTIS Report.

Chehroudi, B. and Simpson, R.L. (1984), "A Rapidly Scanning Laser Doppler Anemometer," J. Physics E, Sci. Inst., 17, pp. 131-136.

Chen, C.P., Sajben, M., and Kroutil, J.C. (1979), "Shock-Wave Oscillations in a Transonic Diffuser Flow," AIAA Journal, 17, pp. 1076-1083.

Cheun, B.S., Toy, N., and Moss, W.D. (1981), "The Effect of Upstream Boundary Layer Thickness Upon Flow Past a Backward-Facing Step," Turbulence in Liquids Symposium, Dept. Chem. Engrg., Univ. Missouri-Rolla.

Childs, R.D., Ferziger, J.H., and Kline, S.J. (1981), "A Computational Method for Subsonic Compressible Flow in Diffusers," Report PD-24, Thermosciences Div., Dept. Mech. Engrg., Stanford Univ.

Chou, F.-K. and Sandborn, V.A. (1973), "Prediction of the Turbulent Boundary Layer Separation," Colo. State Univ. Report, NTIS AD-766845.

Chow, W.L. and Spring, D.J. (1976), "Viscid-Inviscid Interaction of Incompressible Separated Flows," J. of Applied Mech., 98, pp. 387-395.

Chu, J. and Young, A.D. (1975), "Measurements in Separating Two-Dimensional Turbulent Boundary-Layers," AGARD-CP-168, Paper 13.

Chui, G. and Kline, S.J. (1967), "Investigation of a Two-Dimensional Fully-Stalled Turbulent Flow Field," Dept. Mech. Engrg., Stanford Univ., Report MD-19.

Coakley, T.J. and Viegas, J.R. (1977), "Turbulence Modeling of Shock Separated Boundary-Layer Flows," Symposium on Turbulent Shear Flows, pp. 13.19-13.28.

Coles, D. and Hirst, E. (1969), Computation of Turbulent Boundary Layers-1968 AFOSR-IFP Stanford Conference, II, Data Compilation, Department of Mechanical Engineering, Stanford University.

Coles, D. and Wadcock, A.J. (1979), "A Flying Hotwire Study of Two-Dimensional Mean Flow Past an NACA 4412 Airfoil at Maximum Lift," AIAA Journal, 17, pp. 321-329.

Collins, M.A. and Simpson, R.L. (1978), "Flowfield Prediction for Separating Turbulent Shear Layers," AIAA Journal, 16, pp. 291-292.

Comte-Bellot, G. (1976), "Hot-Wire Anemometry," Annual Review of Fluid Mechanics, 8, pp. 209-231, M. Van Dyke, et al., editors, Annual Reviews Inc., Palo Alto, California.

Counihan, J., Hunt, J.C.R., and Jackson, P.S. (1974), "Wakes Behind Two-Dimensional Surface Obstacles in Turbulent Boundary Layers," J. Fluid Mech., 64, pp. 529-563.

Cousteix, J. and Houdeville, R. (1980), "Analogie des singularites dans les methodes directes de calcul des couches limites tridimensionnelle stationnaire et bidimensionnelle instationnaire--analyse des modes inverses," AGARD-CP-291, Paper 14.

Cousteix, J., Desopper, A. and Houdeville, R. (1977), "Structure and Development of a Turbulent Boundary Layer in an Oscillatory External Stream," Symposium on Turbulent Shear Flow, Paper 8-B, Pa. State Univ., April 18-20.

Cousteix, J., Houdeville, R., and Raynaud, M. (1979), "Oscillating Turbulent Boundary Layer with a Strong Mean Pressure Gradient," Second Symposium on Turbulent Shear Flow, Imperial College, London, July 2-4, pp. 6.12-6.17.

Covert, E.E. and Lorber, P.F. (1983), "Unsteady Turbulent Boundary Layers in Adverse Pressure Gradients," AIAA Journal, 22, pp. 22-28.

Crabb, D., Durao, D.F.G., and Whitelaw, J.H. (1981), "Velocity Characteristics in the Vicinity of a Two-Dimensional Rib," Third Symposium on Turbulent Shear Flows, pp. 16.5-16.10.

Crimi, P. (1975), "Dynamic Stall," AGARD-AG-172.

Cummins, H.Z. and Pike, E.R., editors (1977), Photon Correlation Spectroscopy and Velocimetry, Plenum Press, NY (NATO Advanced Study Institute, July 26-August 6, 1976).

Cutler, A.D. and Johnston, J. P. (1981), "The Effects of Inlet Conditions on the Performance of Straight-Walled Diffusers at Low Subsonic Mach Numbers--a Review," Dept. of M.E., Stanford Univ., Report PD-26.

Davies, P.O.A.L. and Yule, A.J. (1975), "Coherent Structures in Turbulence," J. Fluid Mech., 69, pp. 513-537.

Délery, J.M. (1983), "Experimental Investigation of Turbulence Properties in Transonic Shock/Boundary Layer Interactions," AIAA Journal, 21, pp. 180-185.

Délery, J., Chattot, J.J., and LeBalleur, J.C. (1975), "Interaction Visqueuse Avec Decollement En Ecoulement Transsonique," AGARD-CP-168, Paper 27.

Dengel, P., Fernholz, H.H., Vagt, J.-D. (1981), "Turbulence and Mean Flow Measurements in an Incompressible Axisymmetric Boundary Layer with Incipient Separation," Third Symposium on Turbulent Shear Flow, Davis, CA, September 1981.

Dengel, P. and Vagt, J.D. (1982), "A Comparison Between Hot-Wire and Pulsed-Wire Measurements in Turbulent Flows," Institutsbericht 01/82, Technische Universität Berlin; Fourth Symposium on Turbulent Shear Flows, pp. 15.12-15.16 (1983).

DePonte, S. and Baron, A. (1980), "Experiments on a Turbulent Unsteady Boundary Layer with Separation," AGARD-CP-296, Paper 12.

DeRuyck, J. and Hirsch, C. (1984), "Instantaneous Flow Field Measurements of Stalled Regions on an Oscillating Airfoil," AIAA-84-1565.

Dolling, D.S. and Murphy, M. (1982), "Unsteadiness of the Separation Shock Wave Structure in a Supersonic Compression Ramp Flowfield," AIAA-82-0986; AIAA Journal, 21, pp. 1628-1634 (1983).

Driver, D.M. and Seegmiller, H.L. (1982), "Features of a Reattaching Turbulent Shear Layer Subject to an Adverse Pressure Gradient," AIAA-82-1029.

Driver, D.M., Seegmiller, H.L., and Marvin, J. (1983), "Unsteady Behavior of a Reattaching Shear Layer," AIAA-83-1712.

Durão, D., Adrian, R., Durst, F., Mishina, H., and Whitelaw, J.H., editors (1982), International Symposium on Applications of Laser-Doppler Anemometry to Fluid Mechanics, Lisbon, July 5-7.

Durst, F. and Pereira, J.C.F. (1982), "Laser Doppler and Numerical Studies of Backward-Facing Step Flows," Int. Symp. on Appl. L.D.A. to F. Mechanics, p. 11.4.

Durst, F. and Rastogi, A.K. (1979), "Turbulent Flow Over 2-D Fences," Second Symposium on Turbulent Shear Flows, pp. 16.30-16.38.

Durst, F. and Tropea, C.D. (1981), "Turbulent Backward-Facing Step Flows in Two-Dimensional Ducts and Channels," Third Symposium on Turbulent Shear Flows, Davis, CA, USA, pp. 18.1-18.6.

Durst, F. and Tropea, C.D. (1982), "Flows Over Two-Dimensional Backward-Facing Steps," I.U.T.A.M. Symposium on Structure of Complex Turbulent Shear Flow, Marseille, 31 August - 3 September, pp. 41-52, Springer-Verlag.

Durst, F., Melling, A., and Whitelaw, J.H. (1976), Principles and Practice of Laser-Doppler Anemometry, Academic Press, NY.

East, L.F., Smith, P.D., and Merryman, P.J. (1977), "Prediction of the Development of Separated Turbulent Boundary Layers by the Lag-Entrainment Method," RAE Tech. Report 77046.

Eaton, J.K. and Johnston, J.P. (1980), "Turbulent Flow Reattachment: An Experimental Study of the Flow and Structure Behind a Backward-Facing Step," Report MD-39, Thermosciences Div., Dept. of Mechanical Engineering, Stanford University.

Eaton, J.K. and Johnston, J.P. (1981a), "A Review of Research on Subsonic Turbulent Flow Reattachment," AIAA Journal, 19, pp. 1093-1100.

Eaton, J.K. and Johnston, J.P. (1981b), "Low Frequency Unsteadiness of Reattaching Turbulent Shear Layer," Third Symposium on Turbulent Shear Flows, pp. 16.17-16.22.

Eaton, J.K., Jeans, A.H., Ashjaee, J., and Johnston, J.P. (1979), "A Wall-Flow-Direction Probe for Use in Separating and Reattaching Flows," J. Fluids Engineering, 101, pp. 364-366.

Eaton, J.K., Johnston, J.P., and Jeans, A.H. (1979), "Measurements in a Reattaching Turbulent Shear Layer," Second Symposium on Turbulent Shear Flows, pp. 16.7-16.12.

Eaton, J.K., Westphal, R.V., and Johnston, J.P. (1982), "Two New Instruments for Flow Direction and Skin-Friction Measurements in Separated Flows," ISA Trans., 21, pp. 69-78.

Ericsson, L.E. and Redding, J.P. (1984), "Unsteady Flow Concepts for Dynamic Stall Analysis," J. Aircraft, 21, pp. 601-606.

Etheridge, D.W. and Kemp, P.H. (1978), "Measurements of Turbulent Flow Downstream of a Rearward-Facing Step," J. Fluid Mech., 86, pp. 545-566.

Farcy, A., Mercier, V., and Leblanc, R. (1981), "Experimental Investigations in Transonic Highly Separated, Turbulent Flow," Third Symposium on Turbulent Shear Flows, pp. 16.30-16.34.

Fernholz, H. (1964), "Halbempirische Gesetze zur Berechnung turbulenter Grenzschichten nach der Methode der Integralbedingungen," Ing. Arch., 33, Heft 6.

Fernholz, H. (1966), "Eine grenzschichttheoretische Untersuchung optimaler Unterschalldiffusoren," Ingenieur-Archiv, 35, pp. 192-201.

Finke, K. (1975), "Unsteady Shock Wave-Boundary Layer Interaction on Profiles in Transonic Flow," Paper 28, AGARD-CP-168.

Fortunato, B. (1980), "A Second Order Accurate Numerical Method for Supersonic Interacting Boundary Layer Flow Past a Compression Corner," AGARD-CP-291, Paper 27.

Fox, M. (1980), "Effects of Oscillation Frequency and Amplitude on Separation in an Unsteady Turbulent Flow," M.S. Thesis, Naval Postgrad. School, Monterey, CA.

Fox, R.W. and Kline, S.J. (1962), "Flow Regimes for Curved Subsonic Diffusers," J. Basic Engrg., TASME, 84, pp. 303-312.

Francis, M. and Luttges, M.W., editors (1984), Workshop on Unsteady Separated Flow, USAFA, August 10-11, 1983, Univ. Colo. Aerospace Engrg. Dept., Boulder.

Frost, W. (1973), "Review of Data and Prediction Techniques for Wind Profiles Around Manmade Surface Obstructions," AGARD-CP-140, pp. 4.1-4.18.

Fuller, W.R. (1974), "Calibration of a Split-Film Sensor," M.S. Thesis, School of Engrg., Univ. Southern California.

Gaudet, L. and Winter, K.G. (1973), "Measurements of the Drag of Some Characteristic Aircraft Excrescences Immersed in Turbulent Boundary Layers," AGARD-CP-124, pp. 4.1-4.12.

Geller, W. (1976), "Calculation of the Turning Angle of Two-Dimensional Incompressible Cascade Flow," AIAA Journal, 14, pp. 297-298.

Geropp, D. and Grashof, J. (1975), "Berechnung von Strömungsfeldern mit Ablöseblasen bei großen Reynoldszahlen," Bericht G1/75, Inst. f. Strömungslehre und -Mechanik, Universität Karlsruhe.

Gersten, K., Herwig, H. and Wauschkuhn, P. (1980), "Theoretical and Experimental Investigations of Two-Dimensional Flows with Separated Regions of Finite Length," AGARD-CP-291, Paper 23.

Gersten, K., Wauschkuhn, P., and Pagendarm, H.-G. (1983), "Untersuchungen von Strömungen mit Ablösungsgebieten endlicher Länge," Bericht 100/1983, Institut für Thermo-und Fluiddynamik, Ruhr-Universität Bochum.

Ghose, S. and Kline, S.J. (1976), "Prediction of Transitory Stall in Two-Dimensional Diffusers," Report MD-36, Thermosciences Div., Dept. Mech. Engrg., Stanford University.

Ghose, S. (1979), "An Elliptic Representation of Coupled Boundary Layers and Inviscid Core for Computation of Separated Internals Flows," Turbulent Boundary Layers, H. E. Weber, ed., ASME, pp. 85-92.

Gibson, C.H. (1973), "Digital Techniques in Turbulence Research," AGARDograph 174.

Gillis, J.D., Johnston, J.P., Kays, W.M., and Moffat, R.J. (1980), "Turbulent Boundary Layer on a Convex, Curved Surface," Thermosciences Div., Stanford University Department of Mechanical Engineering Report, HMT-31; J. Fluid Mech., 135, pp. 123-153 (1983).

Ginder, R. B. and Bradbury, L.J.S. (1973), "Preliminary Investigation of a Pulsed-Gauge Technique for Skin Friction Measurements in Highly Turbulent Flows," ARC 34448.

Gogish, L.V. and Stepanov, G.Y. (1977), "Detached Flow Over a Step with the Formation of a Wake," Fluid Dynamics, 12, pp. 358-363, (English translation).

Good, M.C. and Joubert, P.N. (1968), "Form Drag of Two-Dimensional Bluff-Plates Immersed in Turbulent Boundary Layers," J. Fluid Mech., 31, pp. 547-582.

Gooray, A.M., Watkins, C.B., and Aung, W. (1983), "Improvements to the k-ε Model for Calculations of Turbulent Recirculating Flow," Fourth Symposium on Turbulent Shear Flow, Karlsruhe, F.R.G., pp. 18.25-18.31.

Gordon, R. and Rom, J. (1981), "Transonic Viscous-Inviscid Interaction Over Airfoils for Separated Laminar or Turbulent Flows," AIAA Journal, 19, pp. 545-552.

Gosman, A.D. and Ideriah, F.J.N. (1976), "A General Computer Program for Two-Dimensional Turbulent Recirculating Flows," Dept. of Mech. Engineering, Imperial College, London.

Gosman, A.D. and Pun, W.M. (1974), "Calculation of Recirculating Flows," Mech. Eng. Dept. Report HTS/74/2, Imperial College, London.

Gosman, A.D., Khalil, E.E., and Whitelaw, J.H. (1977), "The Calculation of Two-Dimensional Turbulent Recirculating Flows," Symposium on Turbulent Shear Flows, pp. 13.35-13.45.

Grant, I., Barnes, F.A. and Greated, C.A. (1975), "Velocity Measurements Using the Photon Correlation Technique in a Separated Boundary Layer," Physics Fluids, 18, pp. 504-507.

Green, J.E. (1966), "Two-Dimensional Turbulent Reattachment as a Boundary-Layer Problem," AGARD-CP-4, pp. 393-427.

Green, J.E. (1970), "Interactions Between Shock Waves and Turbulent Boundary Layers," Progress in Aerospace Sciences, 11, pp. 235-340, Pergamon Press.

Gyles, B. and Ligrani, P.M. (1981), "Hot-Wire Thermal Tuft Development for Measurement of Flow Reversal Near a Compressor Blade," preprint 1981-16/TU, VKI LS 1981-7.

Habib, M.A. and Whitelaw, J.H. (1982), "The Calculation of Turbulent Flow in Wide-Angle Diffusers," Numerical Heat Transfer, 5, pp. 145-164.

Hahn, M., Rubbert, P.E., and Mahal, A.S. (1973), "Evaluation of Separation Criteria and Their Applications to Separated Flow Analysis," AFFDL-TR-72-145; NTIS AD 757531.

Hankey, Jr., W.L. and Holden, M.S. (1975), "Two-Dimensional Shock Wave-Boundary Layer Interactions in High Speed Flows," AGARDograph 203.

Hastings, R.C. and Moreton, K.G. (1982), "An Investigation of a Separated Equilibrium Turbulent Boundary-Layer," Int. Symp. on Appl. L.D.A. to F. Mechanics, p. 11.1.

Hastings, R.C., Moreton, K.G. and Clark, R. (1984), "Mean Flow Properties Measured Around an Aerofoil Close to its Maximum Lift," Second Inter. Symp. Applications Laser Anemometry to Fluid Mech., Paper 14.1.

Havener, A.G. and Radley, R.J. (1972), "Dual Hologram Interferometry," Opto-Electronics, 4, pp. 349-357.

Havener, A.G. and Radley, R.J. (1974), "Turbulent Boundary Layer Flow Separation Measurements Using Holographic Interferometry," AIAA Journal, 12, pp. 1071-1075.

Hayakawa, K. and Squire, L.C. (1982), "The Effect of the Upstream Boundary-Layer State on the Shock Interaction of a Compression Corner," J. Fluid Mech., 122, pp. 360-394.

Hayakawa, K., Smits, A.J., and Bogdonoff, S.M. (1983), "Turbulence Measurements in Compressible Reattaching Shear Layer," AIAA-83-0299; AIAA Journal, 22, pp. 889-895.

Head, M.R. (1960), "Entrainment in the Turbulent Boundary Layer," ARC R& 3152.

Herwig, H. and Brown, S. (1982), "Two-Dimensional Separated Flow: A Report on EUROMECH 148," J. Fluid Mech., 6, pp. 202-205.

Higuchi, H. and Peake, D.J. (1978), "Bi-Directional, Buried-Wire Skin-Friction Gage," NASA TM 78531.

Hillier, R. and Cherry, N.J. (1981), "Pressure Fluctuations Under a Turbulent Shear Layer," Third Symposium on Turbulent Shear Flows, pp. 16.23-16.29.

Hillier, R., Latour, M.E.M.P., and Cherry, N.J. (1983), "Unsteady Measurements in Separated-and-Reattaching Flow," Fourth Symposium on Turbulent Shear Flows, pp. 19.19-19.24, Karlsruhe, F.R.G., Sept. 12-14.

Hinze, J.O.(1975), Turbulence, Second Edition, McGraw-Hill Book Co., NY.

Ho, C.H. and Chen, S.H. (1981), "Unsteady Kutta Condition of a Plunging Airfoil," Unsteady Turbulent Shear Flows, (Ed: Michel, R., Cousteix, J., and Houdeville, R.), pp. 197-206, Springer-Verlag.

Hoffmann, P.H. and Bradshaw, P. (1978), "Turbulent Boundary Layers on Surfaces of Mild Longitudinal Curvature," Imperial College, Aero, Report 78-04.

Horstman, C.C. (1982), "Prediction of Separated Asymmetric Trailing Edge Flows at Transonic Mach Numbers," AIAA Paper 82-1021; AIAA Journal, 21, pp. 1255-1261.

Horstman, C.C. and Hung, C.M. (1979), "Computation of Three-Dimensional Turbulent Separated Flows at Supersonic Speeds," AIAA Paper 79-0002; AIAA Journal, 17, pp. 1155-1156.

Horstman, C.C., Settles, G.S., Vas, I.E., Bogdonoff, S.M., and Hung, C.M. (1977), "Reynolds Number Effects on Shock-Wave Turbulent Boundary-Layer Interactions, AIAA Journal, 15, pp. 1152-1158.

Horstman, C.C., Settles, G.S., Williams, D.R., and Bogdonoff, S.M. (1982), "A Reattaching Free Shear Layer in Compressible Turbulent Flow," AIAA Journal, 20, pp. 79-85.

Houdeville, R., Desopper, A. and Cousteix, J. (1976), "Analyse Experimentale des Caracteristiques d'une Couche Limite Turbulente en Ecoulement Pulse. Essai de Prevision Theorique," La Recherche Aerospatiale, 1976, No. 4, pp. 183-191.

Hunt, J.C.R., Abell, C.J., Peterka, J.A. and Woo, H. (1978), "Kinematical Studies of the Flows Around Free or Surface-Mounted Obstacles; Applying Topology to Flow Visualization," J. Fluid Mech., 86, pp. 179-200.

Hussain, A.K.M.F. (1983), "Coherent Structures - Reality and Myth," Physics Fluids, 26, pp. 2816-2850.

Ilegbusi, J.O. and Spalding, D.B. (1983), "Turbulent Flow Downstream of a Backward-Facing Step," Fourth Symposium on Turbulent Shear Flow, Karlsruhe, F.R.G., pp. 18.20-18.25.

Inger, G.R. (1980), "Some Features of a Shock-Turbulent Boundary Layer Interaction Theory in Transonic Flow Fields," AGARD-CP-291, Paper 18.

Jacob, K. (1976), "Theoretische Bestimmung der Kennkurven von Tragflügelprofilen mit Klappen, Strömungsablösung und Bodeneinfluß," 9, DGLR-Jahrestagung, München.

Jacob, K. (1981), "Berechnung von Profilsystemen bei Unterschallströmung mit mehrfacher Ablösung," DFVLR-FB 81-24; English version, EUROMECH Colloquium 129, Collected Papers VMEI Lenin, Applied Math. Center, Sofia, Bulgaria, pp. 83-117 (1981).

Jacob, K. and Steinbach, D. (1974), "A Method for Prediction of Lift for Multi-Element Airfoil Systems with Separation," Paper 12, AGARD-CP-143.

Jacob, Klaus (1969),"Berechnung der abgelösten incompressiblen Strömung um Tragflügelprofile und Bestimmung des maximalen Auftriebs," Z. fur Flugwiss, 17, pp. 221-230.

Jacob, Klaus (1976), "Weiterentwicklung eines Verfahrens zur Berechnung der abgelösten Profilströmung mit besonderer Berücksichtigung des Profilwiderstandes," DLR-FB 76-36; translated as ESA-TT-377 (1977).

Johnson, D.A. (1981), "Laser Velocimetry Applied to Transonic Flow Past Airfoils," 1st Symposium Num. and Phys. Aspects of Aero. Flows, Cal. State - Long Beach, Springer-Verlag.

Johnson, D.A., Horstman, C.C. and Bachalo, W.D. (1980), "A Comprehensive Comparison Between Experiment and Prediction for a Transonic Turbulent Separated Flow," AIAA Journal, 20, pp. 737-744.

Johnson, D.A. and King, L.S. (1984), "A New Turbulence Closure Model for Boundary Layer Flows with Strong Adverse Pressure Gradients and Separation," AIAA-84-0175.

Johnson, D.A. and Spaid, F.W. (1983), "Supercritical Airfoil Boundary-Layer and Near-Wake Measurements," J. Aircraft, 20, pp. 298-305.

Jones, G.S., Barbi, C., and Telionis, D.P. (1981), "Natural and Forced Vortex Shedding, Unsteady Turbulent Shear Flows, (Ed: Michel, R., Cousteix, J., and Houdeville, R.), pp. 228-247, Springer-Verlag.

Jorgensen, F.E. (1982), "Characteristics and Calibration of a Triple-Split Probe for Reversing Flows," DISA Information, No. 27, pp. 15-22.

Jou, W.H. and Murman, E.M. (1980), "A Phenomenological Model for Displacement Thickness Effects of Transonic Shock Wave-Boundary Layer Interactions," AGARD-CP-291, Paper 15.

Kader, B.A. and Yaglom, A.M. (1978), "Similarity Treatment of Moving-Equilibrium Turbulent Boundary Layers in Adverse Pressure Gradients," J. Fluid Mech., 89, pp. 305-342.

Kasagi, N., Hirata, M. and Hiraoka, H. (1977), "Large Eddy Structures in Turbulent Separated Flows Downstream of a Rearward-Facing Step," Symposium on Turbulent Shear Flows, Penn. State Univ.

Kenison, R.C. (1977), "An Experimental Study of the Effect of Oscillatory Flow on the Separation Region in a Turbulent Boundary Layer," Paper 20, AGARD-CP-227.

Kielbasa, J. and Rysz, R. (1975), "Eine Oszillationsmethode zur Messung der Strömungsgeschwindigkeit von Gasen," contribution to the 50th Anniversary Volume of Max-Planck-Institut für Strömungsforschung, Göttingen, West Germany; also MPI Report 112 (1973).

Kiya, M., Sasaki, K., and Arie, M. (1982), "Discrete-Vortex Simulation of a Turbulent Separation Bubble," J. Fluid Mech., 120, pp. 219-244.

Kim, J.T., Kline, S.J., and Johnston, J.P. (1978), "Investigations of Separation and Reattachment of a Turbulent Shear Layer: Flow Over a Backward-Facing Step." Report MD-37, Stanford University; J. Fluids Engrg., 102, pp. 302-308 (1980).

Kline, S.J. (1980), "The 1980-81 AFOSR-HTTM-Stanford Conference on Complex Turbulent Flows: Comparison of Computation and Experiment," AGARD-CP-291, Paper 22.

Kline, S.J., Bardina, J.G., and Strawn, R.C. (1983), "Correlation of the Detachment of Two-Dimensional Turbulent Boundary Layers," AIAA Journal, 21, pp. 68-73.

Kline, S.J., Cantwell, R.J., and Lilley, G.M., The 1980-81 AFOSR-HTTM-Stanford Conference on Complex Turbulent Flows: Comparison of Computation and Experiment:
Vol. I (1981) Objectives, Evaluation of Data, Spec. Test Case, Discussion and Position Papers;
Vol. II (1982) Taxonomics, Reporters' Summaries, Evaluation, and Conclusions;
Vol. III (1982) Comparison of Computation with Exp. and Computor's Summary Reports;
Thermosciences Div., Dept. Mech. Engrg., Stanford Univ.

Kline, S.J., Ferziger, J.H. and Johnston, J.P. (1978), OPINION--"The Calculation of Turbulent Shear Flows: Status and Ten-Year Outlook," TASME, J. Fluids Engineering, 100, pp. 3-5.

Kline, S.J., Morkovian, M.V., Sovran, G. and Cockrell, D.S. (1968), Computation of Turbulent Boundary Layers - 1968 AFOSR-IFP-Stanford Conference, I, Stanford Univ. Dept. Mechanical Engineering.

Kooi, J.W. (1975), "Experiment on Transonic Shock Wave Boundary-Layer Interaction," AGARD-CP-168, Paper 30.

Kreid, D.K. and Grams, G.W. (1976), "Confocal LDV Utilizing a Decoupling Beam Splitter Combiner," Applied Optics, 15, pp. 14-16.

Kuehn, D.M. (1980), "Effects of Adverse Pressure Gradient on the Incompressible Reattaching Flow Over a Rearward-Facing Step," AIAA Journal, 18, pp. 343-344.

Kuhn, G.D. and Nielsen, J.N. (1971), "An Analytical Method for Calculating Turbulent Separated Flows Due to Adverse Pressure Gradients," Project SQUID Tech., Rept. NEAR-1-PU.

Kuhn, G.D. and Nielsen, J.N. (1973), "Prediction of Turbulent Separated Boundary Layers," AIAA Paper 73-663.

Kuhn, G.D. and Nielsen, J.N. (1975), "Prediction of Turbulent Separated Flow at Subsonic and Transonic Speeds Including Unsteady Effects," AGARD-CP-168, Paper 26.

Kwon, O.K. and Pletcher, R.H. (1979), "Prediction of Incompressible Separated Boundary Layers Including Viscous-Interaction," J. Fluids Engrg., 101, pp. 466-472.

Kwon, O.K. and Pletcher, R.H. (1981), "Prediction of the Incompressible Flow Over a Rearward-Facing Step," ISU-ERI-Ames-82019, Iowa State Univ.

Kwon, O.K. and Pletcher, R.H. (1983), "Prediction of Subsonic Separation Bubbles on Airfoils by Viscous-Inviscid Interaction," 2nd Symp. Num. and Phys. Aspects of Aero. Flows, Cal. State - Long Beach.

Lamb, J.P. and McCotter, F. (1984), "Correlation of Mean Flow Parameters for Subsonic Recirculating Flows," ASME paper 84-FE-8.

Langston, L.S. and Boyle, M.T. (1982), "A New Surface-Streamline Flow-Visualization Techniques," J. Fluid Mech., 125, pp. 53-57.

Launder, B.E. (1982), "Influence of Numerics and Computer Variance in the Computation of Complex Turbulent Flows," AFOSR-HTTM-Stanford Conf. on Complex Turb. Flows, II, pp. 843-862 (Kline, Cantwell, Lilley, ed.).

Launder, B.E., Priddin, C.H., and Sharma, B.I. (1977), "The Calculation of Turbulent Boundary Layers on Spinning and Curved Surfaces," J. Fluids Engrg., 99, pp. 231-239.

Launder, B.E. and Spalding, D.B. (1974), "The Numerical Computation of Turbulent Flows," Computer Methods Methods in Applied Mechanics and Engineering, 3, pp. 269-289.

Layne, J.L. and Smith, C.R. (1976), "An Experimental Investigation of Inlet-Flow Unsteadiness Generated by Transitory Stall in Two-Dimensional Diffusers," Report CFMTR-76-4, Purdue Univ. School of Mech. Engrg., 1976; J. Fluids Engrg., 101, pp. 181-185 (1979).

LeBalleur, J.C. (1981), "Calculation of Viscous Flows with Separations and Wakes Through Viscous-Inviscid Interaction," EUROMECH 148, RuhrUniversität Bochum.

LeBalleur, J.C. (1981), "Calcul des encoulement a forte interaction visqueuse au moyen de methode de couplage," AGARD-CP-291, pp. 1.1-1.36.

LeBalleur, J.C. and Mirande, J. (1975), "Etude Experimentale et Theorique du Recollement Bidimensionnel Turbulent Incompressible," AGARD-CP-168, pp. 17.1-17.13; also NASA-TT-F-17331.

LeBalleur, J.C. and Neron, M., (1980), "Calcul D'Encoulements Visqueus Decolles Sur Profils D'Ailes Par Une Approche De Couplage," AGARD-CP-291, Paper 11.

Lee, G., Buell, D.A., Licursi, J.P., and Craig, J.E. (1984), "Laser Holographic Interferometry for an Unsteady Airfoil Undergoing Dynamic Stall," AIAA J., 22, pp. 504-511.

Leschziner, M.A. and Rodi, W. (1981), "Calculation of Annular and Twin Parallel Jets Using Various Discretisation Schemes and Turbulence-Model Variations," J. Fluids Engrg., 103, pp. 352-360.

Levy, L.L., Jr. (1978), "Experimental and Computational Steady and Unsteady Transonic Flows about a Thick Airfoil," AIAA Journal, 16, No. 6, pp. 564-572.

Levy, L.L., Jr. (1981), "Predicted and Experimental Steady and Unsteady Transonic Flows About a Biconvex Airfoil," NASA TM 81262.

Levy, L.L., Jr. and Bailey, H.R. (1981), "Computation of Airfoil Buffet Boundaries," AIAA Journal, 19, pp. 1488-1490.

Liepmann, H.W. and Skinner, G.T. (1954), "Shearing-Stress Measurements by Use of a Heated Element," NACA TN 3268.

Lighthill, M.J. (1963), "Attachment and Separation in Three-Dimensional Flow," Laminar Boundary Layers, L. Rosenhead, ed., Oxford Univ. Press, pp. 72-82.

Ligrani, P.M., Gyles, B.R., Mathioudakis, K., and Breugelmans, F.A.E. (1983), "A Sensor for Flow Measurements Near the Surface of a Compressor Blade," J. Physics E., Sci. Inst., 16, pp. 431-437.

Liou, M.S. and Coakley, T.J. (1982), "Simulation of Unsteady Transonic Flow in Diffusers," AIAA Paper 82-1000.

Liou, M.S. and Sajben, M. (1980), "Analysis of Unsteady Viscous Transonic Flow with a Shock Wave in Two-Dimensional Channel," AIAA 80-0195.

Liou, M.S., Coakley, T.J., and Bergmann, M.Y. (1981), "Numerical Simulation of Transonic Flow in Diffusers," AIAA 81-1632.

Lorber, P.F. and Covert, E.E. (1982), "Unsteady Airfoil Pressures Produced by Periodic Aerodynamic Interference," AIAA Journal, 20, pp. 1153-1159.

Ludwieg, H. (1950), "Instrument for Measuring the Wall Shearing Stress of Turbulent Boundary Layers," NACA TM 1284.

Lumley, J.L. and Tennekes, H. (1972), A First Course in Turbulence, MIT Press, Cambridge, MA.

Lyrio, A.A., Ferziger, J.H., and Kline, S.J. (1981), "An Integral Methods for the Computation of Steady and Unsteady Turbulent Boundary Layer Flows, Including the Transitory Stall Regime in Diffusers: Report PD-23, Thermosciences Div., Dept. Mech. Engrg., Stanford Univ.

Lyrio, A.A. and Ferziger, J.H. (1983), "A Method of Predicting Unsteady Turbulent Flows and Its Application to Diffusers with Unsteady Inlet Conditions," AIAA Journal, 21, pp. 534-540.

Mabey, D.G. (1972), "Analysis and Correlation of Data on Pressure Fluctuations in Separated Flow," J. Aircraft, 9, pp. 642-645.

Mabey, D.G. (1982), "Comment on 'A Review of Research on Subsonic Turbulent Flow Attachment'," AIAA Journal, 20, p. 1632.

Maltby, R.L. (ed.) (1962), "Flow Visualization in Wind Tunnels Using Indicators," AGARDograph 70, NATO-AGARD.

Mansour, N.N., Kim, J., and Moin, P. (1983), "Computation of Turbulent Flows Over a Backward-Facing Step," Fourth Symposium on Turbulent Shear Flows, Karlsruhe, F.R.G., Sept. 12-14.

Marvin, J.G., (1983), "Turbulence Modeling for Computational Aerodynamics," AIAA Journal, 21, pp. 941-955.

Marvin, J.G., Horstman, C.C., Rubesin, M.W., Coakley, T.J., and Kussoy, M.I. (1975), "An Experimental and Numerical Investigation of Shock-Wave Induced Turbulent Boundary-Layer Separation at Hypersonic Speeds," AGARD-CP-168, Paper 25.

Marvin, J.G., Levy, L.L., Jr., and Seegmiller, H.L. (1980), "On Turbulence Modeling for Unsteady Transonic Flows," AIAA Journal, 18, pp. 489-496.

Maskew, B. and Dvorak, F.A. (1978), "The Prediction of $C_{l_{max}}$ Using a Separated Flow Model," J. American Helicopter Society, 23, pp. 2-8.

Maskew, B., Rao, B.M., and Dvorak, F.A. (1980), "Prediction of Aerodynamic Characteristics for Wings with Extensive Separations," AGARD-CP-291, Paper 31.

Mayo, W.T. and Smart, A.E., editors (1980), Photon Correlation Techniques in Fluid Mechanics, Proceedings from the 4th International Conference, August 25-27, 1980, Stanford Univ. Dept. of Aeronautics and Astronautics.

Mazumder, M.K. and Wankum, D.L. (1970), "SNR and Spectral Broadening in Turbulence Structure Measurements Using a CW Laser," Applied Optics, 9, pp. 633-637.

McCroskey, W.J. (1977), "Some Current Research in Unsteady Fluid Dynamics," J. Fluids Engrg., 99, pp. 8-39.

McCroskey, W.J. (1981), "The Phenomenon of Dynamic Stall," NASA Tech. Memorandum 81264.

McCroskey, W.J. (1982), "Unsteady Airfoils," Ann. Rev. Fluid Mech., 14, pp. 285-311.

McCroskey, W.J., Carr, L.W. and McAlister, K.W. (1976), "Dynamic Stall Experiments on Oscillating Airfoils," AIAA Journal, 14, pp. 57-63.

McCroskey, W.J., McAlister, K.W., Carr, L.W., Pucci, S.L., Lambert, O., and Indergrand, R.F., "Dynamic Stall on Advanced Airfoil Sections," American Helicopter Society, July 1981.

McDevitt, J.B. (1979), "Supercritical Flow About a Thick Circular-Arc Airfoil," NASA TM 78549.

McDevitt, J.B., Levy, L.L. and Deiwert, G.S. (1976), "Transonic Flow about a Thick Circular-Arc Airfoil," AIAA Journal, 14, pp. 606-613.

McGuinness, M. (1978), "Flow with a Separation Bubble - Steady and Unsteady Aspects," Ph.D. Dissertation, Cambridge University.

Meier, G.E.A. (1975), "Shock-Induced Flow Oscillations," Paper 29, AGARD-CP-168.

Meier, G.E.A., Grabitz, G., Jungowski, W.M., Witczak, K.J., and Anderson, J.S. (1978), "Oscillations of the Supersonic Flow Downstream of an Abrupt Increase in Duct Cross-section," Mitteilungen MPI and AVA, Göttingen, No. 65 (in English).

Melnik, R.E. (1980), "Turbulent Interactions on Airfoils at Transonic Speeds - Recent Developments," AGARD-CP-291, Paper 10.

Michel, R., Cousteix, J. and Houdeville, R., editors (1981), Unsteady Turbulent Shear Flows, Springer-Verlag.

Modarress, D. and Johnson, D.A. (1976), "Investigation of Shock-Induced Separation of a Turbulent Boundary Layer Using Laser Velocimetry," AIAA Paper 76-374.

Moses, H.L. and Chappell, J.R. (1967), "Turbulent Boundary Layers in Diffusers Exhibiting Partial Stall," Basic Engrg., 89, pp. 655-665.

Moses, H.L., Hill, J.M. and Thomason, S.B. (1982), "Calculation of the Flow Over a Stalled Airfoil," AIAA--82-1265.

Moses, H.L., Jones, R.R., O'Brien, W.G. and Peterson, R.S. (1978), "Simultaneous Solutions of the Boundary Layer and Freestream with Separated Flow," AIAA Journal, 16, pp. 61-66.

Moses, H.L., Jones, R.R. and Sparks, J.F. (1979), "An Integral Method for the Turbulent Boundary Layer with Separated Flow," pp. 69-73, Turbulent Boundary Layers, H.E. Weber, ed., ASME Fluids Engrg. Conference, Niagara Falls, June 18-20, 1979.

Moses, H.L., Thomason, S.B., and Jones, R.R. (1982), "Simultaneous Solution of the Inviscid Flow and Boundary Layers for Compressor Cascades," AIAA Journal, 20, pp. 1466-1468.

Moss, W.D. and Baker, S. (1980), "Recirculating Flows Associated with Two-Dimensional Steps," Aero. Quart., 31, pp. 151-172.

Moss, W.D., Baker, S., and Bradbury, L.J.S. (1977), "Measurements of Mean Velocity and Reynolds Stresses in Some Regions of Recirculating Flow," Symposium on Turbulent Shear Flows, 1, pp. 1301-1308.

Muck, K.C. and Smits, A.J. (1984), "Behavior of a Turbulent Boundary Layer Subjected to a Shock-Induced Separation," AIAA-84-0097.

Mueller, T.J., Korst, H.H., and Chow, W.L. (1964), "On the Separation, Reattachment, and Redevelopment of Incompressible Turbulent Shear Flow," TASME, 86 D, pp. 221-226.

Müller, A. and Gyr, A. (1982), "Visualization of the Mixing Layer Behind Dunes," Euromech 156, The Mechanics of Sediment-Transport, Instanbul, July 12-14.

Mullin, T., Greated, C.A., and Grant, I. (1980), "Pulsating Flow Over a Step," Phys. Fluids, 4, pp. 669-674.

Munoz, R.J., Mocker, H.W., and Koehler, L.E. (1974), "True Airspeed Measured by Airborne Laser Doppler Velocimeter," NASA Tech. Brief 73-10506 (ARC-10763).

Murphy, J.D. and King, L.S. (1983), "Airfoil Flow-Field Calculations with Coupled Boundary-Layer Potential Codes," Second Symposium on the Numerical and Physical Aspects of Aerodyn. Flows, Cal. State Univ., Jan. 1983.

Murphy, J.D., Presley, L.L., and Rose, W.C. (1975), "On the Calculation of Supersonic Separating and Reattaching Flows," AGARD-CP-168, Paper 22.

Murthy, V.S. and Rose, W.C. (1978), "Wall Shear Stress Measurements in a Shock-Wave Boundary-Layer Interaction," AIAA Journal, 16, pp. 667-672.

Nakayama, A. (1985), "Characteristics of the Flow Around Conventional and Supercritical Airfoils," J. Fluid Mech. (in press).

Narayanan, M.A.B., Khadgi, Y.N., and Viswanath, P.R. (1974), "Similarities in Pressure Distribution in Separated Flow Behind Backward-Facing Steps," Aero. Quart., 25, pp. 305-312.

Nash, J.F. and Scruggs, R.M. (1977), "Unsteady Boundary Layers with Reversal and Separation," AGARD-CP-227, p. 18.

Nice, G.R., Tseng, W.Y., and Moses, H.L. (1966), "Separation of Turbulent, Incompressible Flow From a Curved, Backward-Facing Step," MIT Gas Turbine Lab Report No. 87.

Nychas, S.G., Hershey, H.C., and Brodkey, R.S. (1973), "A Visual Study of Turbulent Shear Flow," J. Fluid Mech., 61, pp. 513-540.

Om, D., Viegas, J.R., and Childs, M.W. (1982), "An Experimental Investigation and a Numerical Prediction of Transonic Normal Shock Wave/Turbulent Boundary Layer Interaction," AIAA Paper 82-0990.

Orlandi, P. (1981), "Unsteady Adverse Pressure Gradient Turbulent Boundary Layers," Unsteady Turbulent Shear Flows (Ed: Michel, R., Cousteix, J., and Houdeville, R.) pp. 145-158, Springer-Verlag.

Oskam, B. (1980), "Computational Aspects and Results of Low Speed Viscous Flow About Multicomponent Airfoils," AGARD-CP-291, Paper 19.

Otte, F. and Thiede, P. (1973), "Berechnung ebener und rotationssymmetrischer kompressibler Grenzschichten auf der Basis von Integralbedingungen," Fortschr.-Ber VDI-Z, Reihe 7, Nr. 33.

Owen, F.K. and Johnson, D.A. (1980), "Separated Skin Friction Measurement--Source of Error, an Assessment, and Elimination," AIAA-80-1409.

Patel, V.C. (1968), "The Effects of Curvature on the Turbulent Boundary Layer," ARC R & M 3599.

Peake, D.J. and Rainbird, W.J. (1975), "Technical Evaluation Report on the Fluid Dynamics Panel Symposium on Flow Separation," AGARD Adv. Report No. 98.

Peake, D.J. and Tobak, M. (1980), "Three-Dimensional Interactions and Vortical Flows with Emphasis on High Speeds," AGARDograph 252 (AGARD-AG-252).

Perry, A.E. and Fairlie, B.D. (1975), "A Study of Turbulent Boundary-Layer Separation and Reattachment," J. Fluid Mech., 69, Part 4, pp. 657-672.

Perry, A.E. and Schofield, W.H. (1973), "Mean Velocity and Shear Stress Distributions in Turbulent Boundary Layers," Physics Fluids, 16, pp. 2068-2074.

Perry, A.E. and Watmuff, J.H. (1979), "Phase-Averaged Large-Scale Structures in Three-Dimensional Wakes," Report FM-12, Dept. of Mechanical Engineering, University of Melbourne, Australia.

Pletcher, R.H. (1978), "Prediction of Incompressible Turbulent Separating Flow," J. Fluids Engineering, 100, pp. 427-433.

Pletcher, R.H., Kwon, O.K., Chilukuri, R. (1980), "Prediction of Separating Turbulent Boundary Layers Including Regions of Reversed Flow," Report ISU-ERI-AMES-80112, Iowa State Univ.

Pope, S.B. and Whitelaw, J.H. (1976), "The Calculation of Near-Wake Flows," J. Fluid Mech., 73, p. 9.

Praturi, A.K. and Brodkey, R.S. (1978), "A Stereoscopic Visual Study of Coherent Structures in Turbulent Shear Flow," J. Fluid Mech., 89, pp. 251-272.

Pronchick, S. (1983), "Experimental Investigation of the Turbulent Flow Behind a Backward Facing Step," Ph.D. Dissertation, M.E. Dept., Stanford Univ.

Radley, R.J. and Havener, A.G. (1973), "Application of Dual Hologram Interferometry to Wind-Tunnel Testing," AIAA J., 11, pp. 1332-1333.

Ribaut, M. (1983), "A Vortex Sheet Method for Calculating Separated Two-Dimensional Flows at High Reynolds Number," AIAA Journal, 21, pp. 1079-1084.

Robertson, J.M. and Taulbee, D.B. (1969), "Turbulent Boundary Layer and Separation Flow Ahead of a Step," Developments in Mechanics, 5, pp. 171-183.

Rockwell, D. (1983), "Oscillations of Impinging Shear Layers," AIAA Journal, 21, pp. 645-664.

Rodi, W. (1982), "Examples of Turbulence-Model Applications," Proceedings of Ecole d'Ete d'Analyse Numerique-Modelisation numerique de la turbulence, Clamart, France.

Rodi, W. and Scheuerer, G. (1983), "Scrutinizing the k-ε Model Under Adverse Pressure Gradient Conditions," Fourth Symposium on Turbulent Shear Flows, Karlsruhe, F.R.G., Sept. 12-14.

Roshko, A. and Lau, J.C. (1965), "Some Observations on Transition and Reattachment of a Free Shear Layer in Incompressible Flow," Proc. 1965 Heat Transfer and Fluid Mech. Inst., A.F. Charwat, ed., Stanford Univ. Press, pp. 157-167.

Roshko, A. and Thomke, G.J. (1976), "Flare Induced Interaction Lengths in Supersonic Turbulent Boundary Layers," AIAA J., 15, pp. 873-879.

Rothe, P.H. and Johnston, J.P. (1979), "Free-Shear-Layer Behavior in Rotating Systems," J. Fluids Engrg., 101, pp. 117-119.

Rubesin, M.W., Okuno, A.F., Levy, Jr., L.L., McDevitt, J.B., and Seegmiller, H.L. (1976), "An Experimental and Computational Investigation of the Flow Field About a Transonic Airfoil in Supercritical Flow with Turbulent Boundary-Layer Separation," NASA TM X-73, 157.

Rubesin, M.W., Okuno, A.F., Mateer, G.G., and Brosh, A. (1975), "A Hot-Wire Surface Gage for Skin Friction and Separation Detection Measurements," NASA TM X-62, 465.

Ruderich, R. and Fernholz, H.H. (1983), "An Experimental Investigation of the Turbulent Shear Flow Downstream of a Normal Flat Plate with a Long Splitter Plate Modification of a Model," Fourth Symposium on Turbulent Shear Flows, pp. 19.7-19.12, Karlsruhe, F.R.G., Sept. 12-15.

Sajben, M. and Kroutil, J.C. (1981), "Effects of Initial Boundary-Layer Thickness on Transonic Diffuser Flows," AIAA Journal, 19, pp. 1386-1393.

Sajben, M., Bogar, T.J., and Kroutil, J.C. (1981), "Forced Oscillation Experiments in Supercritical Diffuser Flows with Application to Ramjet Instabilities," AIAA-81-1487; AIAA Journal, 22, pp. 465-474 (1984).

Sajben, M., Bogar, T.B., and Kroutil, J.C. (1982), "Unsteady Transonic Flows in a Two-Dimensional Diffuser," AFOSR-TR-0622.

Sajben, M., Kroutil, J.C., and Chen, C.P. (1977), "Unsteady Transonic Flow in a Two-Dimensional Diffuser," AGARD-CP-227, Paper 13.

Salmon, J.T., Bogar, T.J., and Sajben, M. (1981), "Laser Velocimeter Measurements in Unsteady, Separated, Transonic Diffuser Flows," AIAA-81-1197; AIAA Journal, 21, pp. 1690-1697 (1983).

Sandborn, V.A. (1970), "Boundary Layer Separation and Reattachment," NASA-SP-304, pp. 279-299.

Sandborn, V.A. (1972), Resistance Temperature Transducers, Metrology Press, Fort Collins, CO.

Sandborn, V.A. and Kline, S.J. (1961), "Flow Models in Boundary-Layer Stall Inception," Journal of Basic Engineering, Trans. ASME, 83, pp. 317-327.

Sandborn, V.A. and Liu, C.Y. (1968), "On Turbulent Boundary-Layer Separation," J. Fluid Mech., 32 pp. 293-304.

Sandborn, V.A. and Slogar, R.S. (1955), "Study of the Momentum Distribution of Turbulent Boundary Layers in Adverse Pressure Gradients," NACA TN 3264.

Sanders, N. (1969), "Integral Balance of Forces and Momenta in Accelerated Boundary Layers," AIAA Paper 69-666.

Schofield, W.H. (1980), "Turbulent Boundary Layers in Strong Adverse Pressure Gradients," ARL-MECH-ENG-Report-157, DSTO, Australia; J. Fluid Mech., 113, p. 91 (1981).

Schofield, W.H. (1981), "A Prediction Method for Turbulent Boundary Layers in Adverse Pressure Gradients," ARL-MECH-ENG-NOTE-385, DSTO, Australia.

Schofield, W.H. (1983), "On Separating Turbulent Boundary Layers," ARL-ME Report 162, Melbourne, Australia.

Schraub, F.A. and Kline, S.J. (1965), "A Study of the Structure of the Turbulent Boundary Layer With and Without Longitudinal Pressure Gradient," Report MD-12, Thermosciences Div., Dept. Mech. Engrg., Stanford Univ.

Schubauer, G.B. and Klebanoff, P.S. (1951), "Investigation of Separation of the Turbulent Boundary Layer," NACA Report 1030.

Sears, W.R. and Telionis, D.P. (1975), "Boundary-Layer Separation in Unsteady Flow," SIAM J. Applied Math., 28, 1.

Seegmiller, H.L. and Driver, D.M. (1982), "Description and Data Summary of Predictive Test Flow 0422 Backward-Facing Step. Variable Opposite-Wall Angle," AFORD-HTTM-Stanford Conference on Prediction of Complex Turb. Flows, Sept. 1982, Vol. II, pp. 891-893.

Seegmiller, H.L., Marvin, J.G. and Levy, L.L., Jr. (1978), "Steady and Unsteady Transonic Flows," AIAA Journal, 16, pp. 1262-1270.

Settles, G.S. and Bogdonoff, S.M. (1982), "Scaling of Two- and Three-Dimensional Shock/Turbulent Boundary Layer Interaction of Compression Corners," AIAA Journal, 20, pp. 782-789.

Settles, G.S., Bogdonoff, S.M. and Vas, I.E. (1976), "Incipient Separation of a Supersonic Turbulent Boundary Layer in High Reynolds Numbers," AIAA Journal, 14, pp. 50-56.

Settles, G.S., Fitzpatrick, T.J., and Bogdonoff, S.M. (1979), "Detailed Study of Attached and Separated Compression Corner Flowfields in High Reynolds Number Supersonic Flow," AIAA Journal, 17, pp. 579-585.

Settles, G.S., Vas, I.E., and Bogdonoff, S.M. (1976), "Details of a Shock-Separated Turbulent Boundary Layer at a Compression Corner," AIAA Journal, 14, pp. 1709-1715.

Settles, G.S., Williams, D.R., Baca, B.K., and Bogdonoff, S.M. (1980), "A Study of Reattachment of a Free Shear Layer in Compressible Turbulent Flow," AIAA Journal, 20, pp. 60-67.

Shamroth, S.J. (1981), "A Turbulent Flow Navier-Stokes Analysis for an Airfoil Oscillating in Pitch," Unsteady Turbulent Shear Flows, (Ed: Michel, R., Cousteix, J., and Houdeville, R.), pp. 185-196, Springer-Verlag.

Shang, J.S. and Hankey, W.L., Jr. (1975), "Supersonic Turublent Separated Flows Utilizing the Navier-Stokes Equations," AGARD-CP-168, Paper 23.

Shen, S.F. (1978), "Unsteady Separation According to the Boundary Layer Equation," Advances in Applied Mechanics, 18.

Shiloh, K. and Simpson, R.L. (1982), "A Laser Anemometer for Crossflow Velocities," J. Physics E., Sci. Insti., 15, pp. 428-431.

Shiloh, K., Shivaprasad, B.G. and Simpson, R.L. (1981), "The Structure of a Separating Turbulent Boundary Layer: III, Transverse Velocity Measurements," J. Fluid Mech., 113, pp. 75-90.

Shivaprasad, B.G. and Simpson, R.L. (1982), "Evaluation of an Improved Wall-Flow-Direction Probe for Measurements in Separated Flows," J. Fluids Engineering, TASME, 104, pp. 162-166.

Siddon, T.E. (1969), "Investigation of Pressure Probe Response in Unsteady Flow," pp. 455-466 in Basic Aerodynamic Noise Research, NASA SP-207.

Simmons, J.E.L. (1975), "Effect of Separation Angle on Vortex Streets," ASCE J. Engrg.-Mech. Div., 101, pp. 649-661.

Simpson, R.L. (1975), "Characteristics of a Separating Incompressible Turbulent Boundary Layer," AGARD-CP-168, pp. 14.1-14.14.

Simpson, R.L. (1976), "Interpreting Laser and Hot-film Anemometer Signals in a Separating Boundary Layer," AIAA J., 14, pp. 124-126.

Simpson, R.L. (1977), "Features of Unsteady Turbulent Boundary Layers as Revealed from Experiments," Paper 19, Symposium on Unsteady Aerodynamics, NATA-AGARD, Ottawa, Canada, Sept. 1977; AGARD-CP-227.

Simpson, R.L. (1977), "Some Important Physical Phenomena in Flows with Separated Turbulent Boundary Layers," Turbulence in Internal Flows, pp. 311-346, S.N.B. Murthy, Ed.; Hemisphere.

Simpson, R.L. (1979), "Summary Report on Colloquium on Flow Separation," Project SQUID Report SMU-3-PU.

Simpson, R.L. (1979b), Discussion of "Prediction of Incompressible Turbulent Separating Flow," by R.H. Pletcher, J. Fluids Engineering, 101, pp. 147-148.

Simpson, R.L. (1981), "A Review of Some Phenomena in Turbulent Flow Separation," J. Fluid Engrg., TASME, 103, pp. 520-533.

Simpson, R.L. (1983), "A Model for the Backflow Mean Velocity Profile," AIAA Journal, 21, pp. 142-143.

Simpson, R.L. (1984), "Some Structural Features of Unsteady Separating Turbulent Shear Flows," pp. 90-96, Francis and Luttges (1984).

Simpson, R.L. and Barr, P.W. (1974), "Velocity Measurements in a Separating Turbulent Boundary Layer Using Sampling Spectrum Analysis," pp. 15-53, II, Second Int. Workshop on Laser Velocimetry (see Thompson and Stevenson below).

Simpson, R.L. and Barr, P.W. (1975), "Laser Doppler Velocimeter Signal Processing Using Sampling Spectrum Analysis," Rev. Sci. Inst., 46, 7, pp. 835-837.

Simpson, R.L. and Chew, Y.-T. (1979), "Measurements in Highly Turbulent Flows: Steady and Unsteady Separated Turbulent Boundary Layers," pp. 179-196, Laser Velocimetry and Particle Sizing, Hemisphere, Thompson and Stevenson, ed.

Simpson, R.L. and Collins, M.A. (1978), "Prediction of Turbulent Boundary Layers in the Vicinity of Separation," AIAA Journal, 16, pp. 289-290.

Simpson, R.L. and Shackleton, C.R. (1977), "Laminariscent Turbulent Boundary Layers: Experiments on Nozzle Flows," Project SQUID Report SMU-2-PU.

Simpson, R.L. and Shivaprasad, B.G. (1983), "The Structure of a Separating Turbulent Boundary Layer: V, Frequency Effects on Periodic Unsteady Freestream Flows," J. Fluid Mechanics, 131, pp. 319-339.

Simpson, R.L. and Shivaprasad, B.G. (1984), "The Structure of a Separating Turbulent Boundary Layer: Some Amplitude and Waveform Effects on Periodic Unsteady Freestream Flows," submitted to J. Fluid Mech.

Simpson, R.L., Chehroudi, B., and Shivaprasad, B.G. (1982), "Pointwise and Scanning Laser Anemometer Measurements in Steady and Unsteady Separated Turbulent Boundary Layers," Int. Symp. on Appl. L.D.A. to F. Mech., p. 11.3.

Simpson, R.L., Chew, Y.-T., and Shivaprasad, B.G. (1980), "Measurements of a Separating Turbulent Boundary Layer," Project SQUID Report SMU 4-PU; NTIS AD-A095 252/3.

Simpson, R.L., Chew, Y.-T., and Shivaprasad, B.G. (1981), "Measurements of Unsteady Turbulent Boundary Layers with Pressure Gradients," Southern Methodist University, Dept. of Civil and Mechanical Engineering Report, WT-6; NTIS AD-A090 585/1.

Simpson, R.L., Chew, Y.-T., and Shivaprasad, B.G. (1981a), "The Structure of a Separating Turbulent Boundary Layer: I, Mean Flow and Reynolds Stresses," J. Fluid Mech., 113, pp. 23-51.

Simpson, R.L., Chew, Y.-T. and Shivaprasad, B.G. (1981b), "The Structure of a Separating Turbulent Boundary Layer: II, Higher Order Turbulence Results," J. Fluid Mech., 113, pp. 53-74.

Simpson, R.L., Shivaprasad, B.G., and Chew, Y.-T. (1981), "Some Features of Unsteady Separating Turbulent Boundary Layers," IUTAM Symposium - Toulouse, Unsteady Turbulent Shear Flows, pp. 109-119; Michel, Cousteix, Houdeville, ed.; Springer-Verlag.

Simpson, R.L., Shivaprasad, B.G. and Chew, Y.-T. (1983), "The Structure of a Separating Turbulent Boundary Layer: IV, Effects of Periodic Free-Stream Unsteadiness," J. Fluid Mech., 127, pp. 219-261.

Simpson, R.L., Strickland, J.H., and Barr, P.W. (1973), "Features of a Separating Turbulent Boundary Layer as Revealed by Laser and Hot-Film Anemometry," Third Biennial Symposium on Turbulence in Liquids, Univ. of Missouri-Rolla, Sept. 10-12, 1973, pp. 151-171; G. Patterson and J. Zakin, editors.

Simpson, R.L., Strickland, J.H. and Barr, P.W. (1974), "Laser and Hot-Film Anemometer Measurements in a Separating Turbulent Boundary Layer," Thermal and Fluid Sciences Center, Southern Methodist University, Report WT-3; NTIS, AD-A001115.

Simpson, R.L., Strickland, J.H. and Barr, P.W. (1977), "Features of a Separating Turbulent Boundary Layer in the Vicinity of Separation," J. of Fluid Mech., 79, pp. 553-594.

Sindir, M.M. (1982), "Numerical Study of Turbulent Flows in Backward-Facing Step Geometries: Comparison of Four Models of Turbulence," Ph.D. Thesis, Univ. Cal. Davis.

Sindir, M.M. (1983), "Calculation of Deflected-Wall Backward-Facing Step Flows: Effects of Angle of Deflection on the Performance of Four Models of Turbulence," ASME Paper 83-FE-16.

Sirieix, M. (1975), "Decollement Turbulent en Ecolement Bidimensionnel," AGARD-CP-168, Paper 12.

Sirieix, M., Délery, J., and Stanewsky, E. (1981), "High Reynolds Number Boundary-Layer Shock-Wave Interaction in Transonic Flow," pp. 149-214, Lecture Notes in Physics, 148, Springer-Verlag.

Skinner, G.T., Dunn, M.G. and Hiemenz, R.J. (1982), "A Low-Speed Heat-Pulse Anemometer," Rev. Sci. Inst., 53, pp. 342-348.

Smith, C.R. (1978), "Transitory Stall Time-Scales for Plane-Wall Air Diffusers," J. Fluids Engrg., 100, pp. 133-135.

Smith, C.R. and Kline, S.J. (1974), "An Experimental Investigation of the Transitory Stall Regime in Two-Dimensional Diffusers," J. Fluids Engrg., TASME, 96, pp. 11-15.

Smith, P.D., Hastings, R.C., and Williams, B.R. (1981), "Calculation and Measurement of Separated Boundary Layers," EUROMECH 148, RuhrUniversität Bochum; RAE Tech. Memo. 1955, October 1982.

Smits, A.J. (1982a), "A Visual Study of a Separation Bubble," Flow Visualization II, (Ed: Merzkirch), Hemisphere Pub.

Smits, A.J. (1982b), "Scaling Parameters for a Time-Averaged Separation Bubble," J. Fluids Engrg, 104, pp. 178-184.

Smits, A.J., Baskaran, V., and Joubert, P.N. (1981), "Measurements in a Turbulent Boundary Layer Flow Over a Two-Dimensional Hill," Third Symposium on Turbulent Shear Flow, Davis, CA, September 1981.

Smyth, R. (1979), "Turbulent Flow Over a Plane Symmetric Sudden Expansion," Trans. ASME, J. Fluids Engrg., 101, No. 3, pp. 348-353.

So, R.M.S. and Mellor, G.L. (1972), "An Experimental Investigation of Turbulent Boundary Layers Along Curved Surfaces," NASA CR 1940.

Sovran, G. (1968), "On Prediction Criteria for Turbulent Separation," Computation of Turbulent Boundary Layers, 1968 AFOSR-IFP-Stanford Conference, Vol. 1, pp. 447-450.

Spaid, F.W. and Frishett, J.C. (1972), "Incipient Separation of a Supersonic, Turbulent Boundary Layer, Including Effects of Heat Transfer," AIAA Journal, 10, pp. 915-922.

Spalart, P.R. (1982), "Numerical Simulation of Separated Flows," Ph.D. Dissertation, Dept. Aero. and Astro., Stanford Univ.

Spalart, P.R. and Leonard, A. (1981), "Computation of a Separated Flows by a Vortex Tracing Algorithm," AIAA-81-1246.

Spangenberg, W.G., Rowland, W.R. and Mease, N.E. (1976), "Measurements in a Turbulent Boundary Layer in a Nearly Separating Condition," pp. 110-151, Fluid Mechanics of Internal Flow, Edited by G. Sovran, Elsevier Publishing Co., NY.

Spencer, B.W. and Jones, B.G. (1971), "Turbulence Measurements with the Split-Film Anemometer Probe," pp. 7-15, Proc. of Second Symposium on Turbulence in Liquids, G.K. Patterson and J.L. Zakin, editors, Dept. Chem. Engrg., Univ. Miss.-Rolla.

Squire, L.C. (1960), "The Motion of a Thin Oil Sheet under the Boundary Layer on a Body," J. Fluid Mech., 11, pp. 161-179.

Stevenson, W.H. and Thompson, H.D., editors (1972), The Use of the Laser Doppler Velocimeter for Flow Measurements, Proceedings of a Workshop Co-Sponsored by Project SQUID and the U.S. Army Missile Command, March 9-10, School of Mechanical Engineering, Purdue University.

Stevenson, W.H., Thompson, H.D., Gould, R.D., and Craig, R.R. (1982), "Laser Velocimeter Measurements in Separated Flow with Combustion," Int. Symp. on Appl. L.D.A. to F. Mech., p. 11.5.

Stevenson, W.H., Thompson, H.D., and Koesler, T.C. (1982), "Direct Measurement of Laser Velocimeter Bias Errors in a Turbulent Flow," AIAA Journal, 20, pp. 1720-1723.

Stevenson, W.H., Thompson, H.D., and Luchik, T.S. (1982), "Laser Velocimeter Measurements and Analysis in Turbulent Flows with Combustion," AFWAL-TR-82-2076.

Stollery, J.L. (1975), "Laminar and Turbulent Boundary-Layer Separation at Supersonic and Hypersonic Speeds," AGARD-CP-168, Paper 20.

Stratford, B.S. (1959a), "The Prediction of Separation of the Turbulent Boundary Layer," J. Fluid Mech., 5, pp. 1-16.

Stratford, B.S. (1959b), "An Experimental Flow with Zero Skin Friction Throughout its Region of Pressure Rise, J. Fluid Mech., 5, pp. 17-35.

Strawn. R.C. and Kline, S.J. (1981), "A Stall Margin Design Method for Planar and Axisymmetric Diffusers Dept. M.E., Stanford Univ. Report PD-25, J. Fluid Engrg., TASME, 105 (1983).

Strawn, R.C., Kline, S.J., and Ferziger, J.H. (1983), "Flowfield Prediction and Design of Internal Passages with Strong Viscous-Inviscid Interaction," Report PD-27, Thermosciences Div., Dept. M.E., Stanford Univ.

Swafford, T.W. (1983), "Analytical Approximation of Two-Dimensional Separated Turbulent Boundary-Layer Velocity Profiles," AIAA Journal, 21, pp. 923-926.

Tani, I. (1958), "Experimental Investigation of Flow Separation Over a Step," Grenzschichtforschung, H. Gortler, ed., Springer, pp. 377-386.

Tani, I., Iuchi, M. and Komoda, H. (1961), "Experimental Investigation of Flow Separation Associated with a Step or Groove," Aeron. Res. Inst. University of Tokyo, Report 364.

Tassa, Y. and Sankar, N.L. (1981), "Dynamic Stall of an Oscillating Airfoil in Turbulent Flow Using Time Dependent Navier-Stokes Solver," Unsteady Turbulent Shear Flows, (Ed: Michel, R., Cousteix, J., and Houdeville, R.), pp. 207-220, Springer-Verlag.

Taulbee, D.B. and Robertson, J.M. (1972), "Turbulent Separation Analysis Ahead of a Step," J. Basic Engrg., TASME, 94, pp. 544-550.

Telionis, D.P. (1977), "Unsteady Boundary Layers, Separated and Attached," AGARD-CP-227, Paper 16.

Thomas, J.L. (1984), "Integral Boundary-Layer Models for Turbulent Separated Flows," AIAA-84-1615.

Thompson, B.E. and Whitelaw, J.H. (1982), "A Turbulent Boundary Layer Approaching Separating," Walz-Festschrift Volume, pp. 253-264, Springer-Verlag.

Thompson, B.E. and Whitelaw, J.H. (1984), "Flying Hot-Wire Anemometry," Experiments in Fluids, 2, p. 47f.

Thompson, H.D. and Stevenson, W.H., editors (1974), Proceedings of the Second International Workshop on Laser Velocimetry, March 27-29, Two Volumes, Engrg. Exp. Station Bulletin 144, Purdue University.

Thompson, H.D. and Stevenson, W.H. (1979), Laser Velocimetry and Particle Sizing, Hemisphere, NY.

Tombach, J.H. (1973), "An Evaluation of the Heat Pulse Anemometer for Velocity Measurement in Inhomogeneous Turbulent Flow," Rev. Sci. Inst., 44, pp. 141-148.

Townsend, A.A. (1962),"The Behavior of a Turbulent Boundary Layer Near Separation," J. Fluid Mech., 12, pp. 536-554.

Trolinger, J.D. (1974), "Laser Instrumentation for Flow Field Diagnostics," AGARDograph 186, NATO-AGARD.

Tropea, C. (1982), "Die turbulente Stufenströmung in Flachkanalen und offenen Gerinnen," Ph.D. Dissertation, Universität Karlsruhe.

Troutt, T.R., Scheelke, B., and Norman, T.R. (1984), "Organized Structures in a Reattaching Separated Flow Field," J. Fluid Mech., 143, pp. 413-427.

Tsahalis, D.T. and Telionis, D.P. (1975), "On the Behavior of Turbulent Boundary Layers Near Separation," AIAA Journal, 13, pp. 1261-2.

TSI (1981), Equipment Catalogs and Literature, TSI Inc., P.O. Box 43394, St. Paul, MN 55164 USA.

Tutu, N.K. and Chevray, R. (1975), "Cross-Wire Anemometry in High Intensity Turbulence," J. Fluid Mech., 71, pp. 785-100.

Van Atta, C.W. (1974), "Sampling Techniques in Turbulence Measurements," Annual Review of Fluid Mechanics, 6, pp. 75-93, M. Van Dyke, et al., editors, Annual Reviews Inc., Palo Alto, CA.

Van de Hulst, H.C. (1964), Light Scattering by Small Particles, Wiley, NY.

Vasilic-Melling, D. (1976), "Three-Dimensional Turbulent Flow Past Rectangular Bluff Bodies," University of London, Ph.D. Thesis.

Viegas, J.R. and Horstman, C.C. (1979), "Comparison of Multiequation Turbulence Models for Several Shock/Boundary-Layer Interaction Flows," AIAA J., 17, pp. 811-820.

Veldman, A.E.P. (1981), "The Calculation of Incompressible Boundary Layers with Strong Viscous-Inviscid Interaction," AGARD-CP-291, pp. 12.1-12.12.

Vest, C.M. (1979), Holographic Interferometry, Wiley and Sons, NY.

Viswanath, P.R. and Brown, J.L. (1980), "An Experimental Documentation of a Separated Trailing-Edge Flow at a Transonic Mach Number," NASA TM 84290.

Viswanath, P.R. and Brown, J.L. (1983), "Separated Trailing Edge Flow at a Transonic Mach NUmber," AIAA Journal, 21, pp. 801-807.

Voisinet, R.L.P. (1975), "An Experimental Investigation of the Compressible Turbulent Boundary-Layer Separation Induced by a Continuous Flow Compression," AGARD-CP-168, Paper 19.

Wadcock, A.J. (1980), "Simple Turbulence Models and Their Application to Boundary Layer Separation," NASA CR 3283.

Wallace, J.M., Brodkey, R.S., and Eckelmann, H. (1977), "Pattern-Recognized Structures in Bounded Turbulent Shear Flows," J. Fluid Mech., 83, pp. 673-693.

Wauschkuhn, P. (1982), "Ein Beitrag zu den ebenen turbulenten Strömungen mit begrenzten Ablösegebieten," Dr.-Ing. Dissertation, Ruhr-Universität Bochum.

Westphal, R.V. and Johnston, J.P., (1983), "Reattaching Turbulent Shear Layers With Perturbed Structure," AIAA Paper No. 83-0603; AIAA Journal, 22, pp. 1727-1732.

Westphal, R.V., Eaton, J.K., and Johnston, J.P. (1981), "A New Probe for Measurement of Velocity and Wall Shear Stress on Unsteady, Reversing Flow," J. Fluids Engrg., 103, pp. 478-482.

Whitfield, D.L., Swafford, T.W., and Jacocks, J.L. (1981), "Calculation of Turbulent Boundary Layers with Separation, Reattachment and Viscous-Inviscid Interaction," AIAA Journal, 19, pp.1315-1322.

Wilcox, D.C. and Rubesin, M.W. (1980), "Progress in Turbulent Modeling for Complex Flow Fields Including Effects of Compressibility," NASA TP 1517.

Williard, G.W. (1949), "Criteria for Normal and Abnormal Ultrasonic Light Diffraction Effects," J. Acoustical Soc. Am., 21, pp. 101-108.

Willmarth, W.W. (1971), "Unsteady Force and Pressure Measurements," Ann. Rev. Fluid Mech., 3, pp. 147-170.

Willmarth, W.W. (1975), "Pressure Fluctuations Beneath Turbulent Boundary Layers," in Annual Review of Fluid Mechanics, 7, pp. 13-28, M. Van Dyke, et al. , editors, Annual Reviews Inc., Palo Alto, CA.

Woolley, R.L. and Kline, S.J. (1973), "A Method for Calculation of a Fully-Stalled Flow," Report MD-33, Thermosciences Div., Dept. Mech. Engrg., Stanford University.

Wooley, R.L. and Kline, S.J. (1978), "A Procedure for Computation of Fully-Stalled Flows in Two-Dimensional Passages," J. Fluids Engrg., 100, pp. 180-186.

Wygnanski, I. and Fiedler, H.E. (1970), "The Two-Dimensional Mixing Region," J. Fluid Mech., 41, pp. 327-361.

Yahnik, K.S. and Gupta, R.P. (1973), "A New Probe for Measurement of Velocity and Flow Direction in Separated Flows," J. Phys. E., Sci. Instrum., 6, pp. 82-86.

Yoshihara, H. (1981), "Transonic Shock-Boundary Layer Interaction: A Case for Phenomenology," Num. and Phys. Aspects of Aero. Flows, Cal. State Long Beach, Springer-Verlag.

Young, M. (1976), "Calibration of Hot-wires and Hot-films for Velocity Fluctuations," Report TMC-3, Thermosciences Div., Dept. of Mechanical Engineering, Stanford University, Stanford CA.

Young, A.D. and Paterson, J.H. (1981), "Aircraft Excresence Drag," AGARD-AG-264.

Young, W.H., Meyers, J.F., and Hoad, Danny R. (1978), "A Laser Velocimeter Flow Survey Above a Stalled Wing," NASA TP 1266.

Zilker, D.P., Cook., G.W., and Hanratty, T.J. (1977), "Influence of the Amplitude of a Solid Wavy Wall on a Turbulent Flow. Part I. Non-Separated Flows,: J. Fluid Mech., 82, pp. 29-51.

Zilker, D.P. and Hanratty, T.J. (1979), "Influence of the Amplitude of a Solid Wavy Wall on a Turbulent Flow. Part II. Separated Flows," J. Fluid Mech., 90, pp. 257-271.

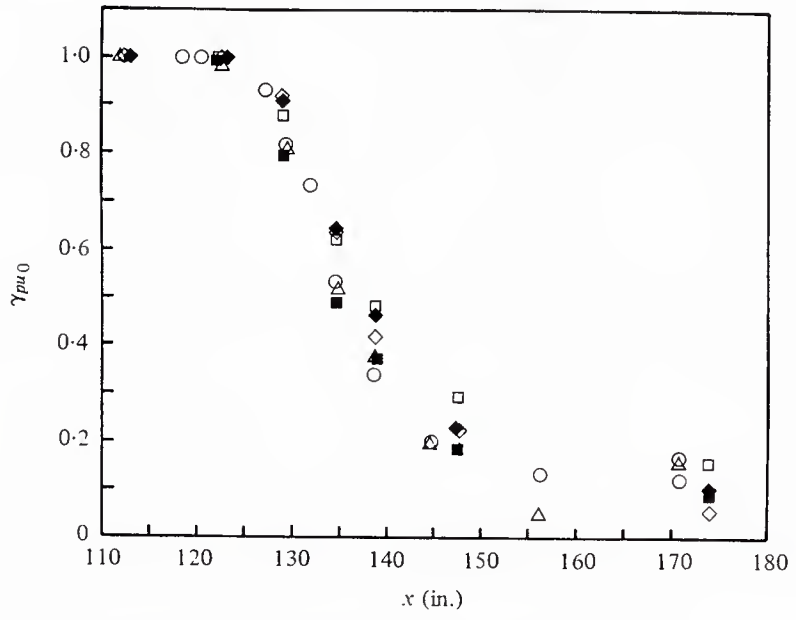

Fig. 1. Fraction of time that the flow 1.2 mm from the wall (outside viscous region) is in the downstream direction: ○, LDV direct measurement; △, LDV U and u' measurements and equation (2). Thermal tuft without side heaters: □, orientation 1; ■, reversed or orientation 2. Thermal tuft with side heaters: ◇, orientation 1; ◆, reversed or orientation 2. From Shivaprasad and Simpson (1982).

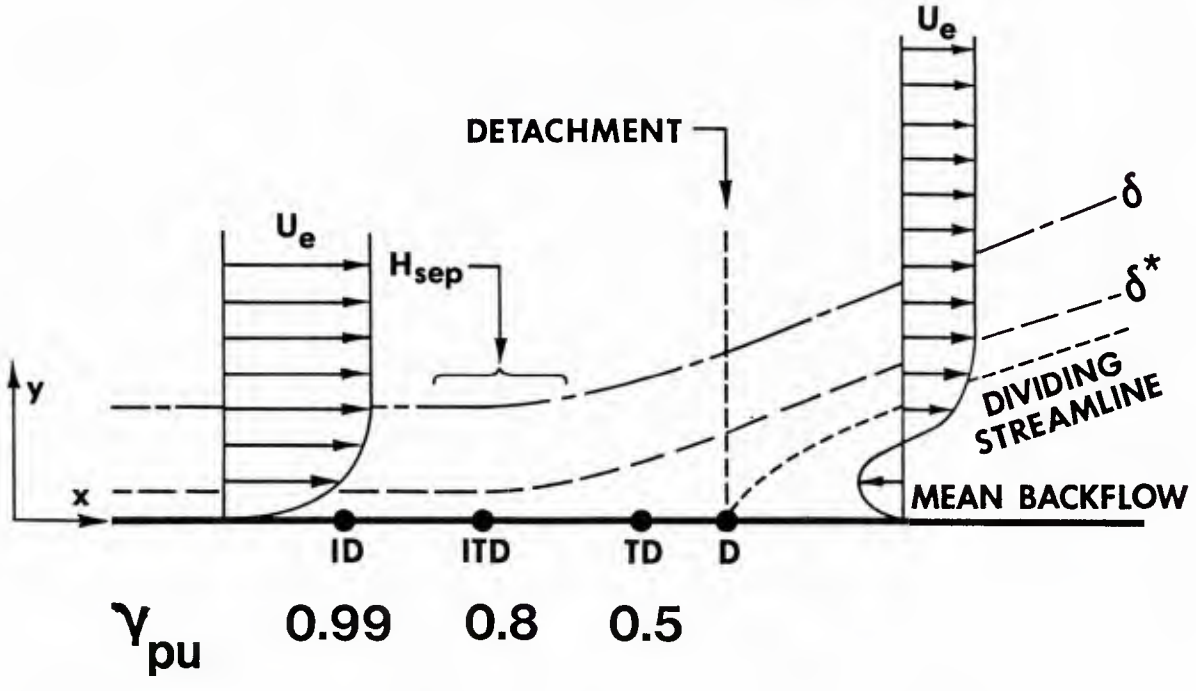

OLD TERM	SYMBOL	NEW TERM	CONDITION
none	ID	Incipient Detachment	1% Instantaneous Backflow
Intermittent Separation (Sandborn and Kline, 1961)	ITD	Intermittent Transitory Detachment	20% Instantaneous Backflow
none	TD	Transitory Detachment	50% Instantaneous Backflow
Steady or Fully-Developed Separation (Sandborn and Kline, 1961)	D	Detachment	$\overline{\tau_w} = 0$

Fig. 2. Definitions of two-dimensional turbulent detachment states. Distances not to scale. "Percent Instantaneous Backflow" means along a spanwise line at a given time, or percent of time at a point. From Simpson (1979, 1981).

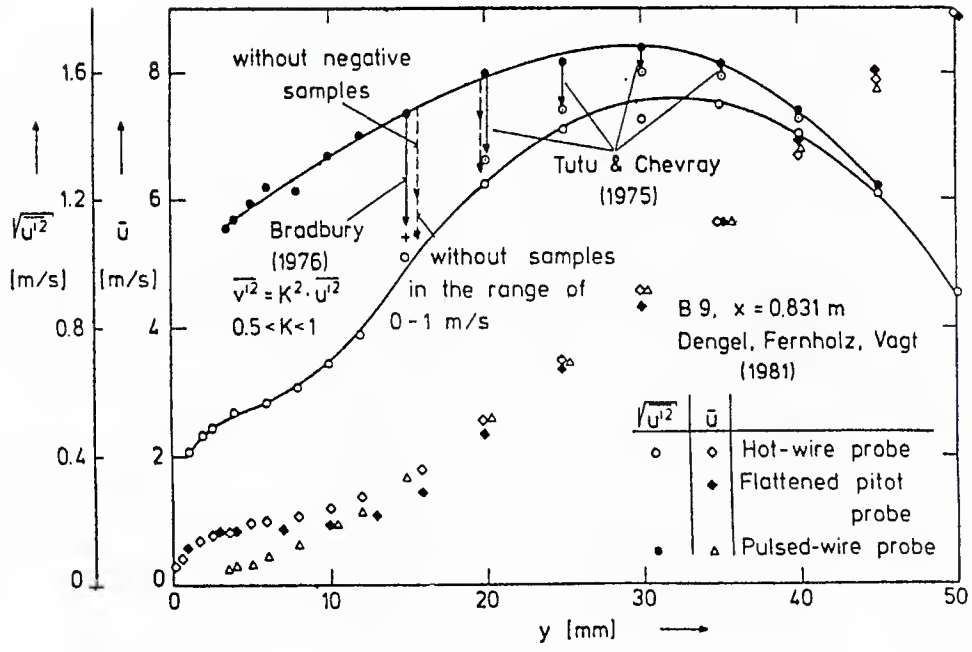

Fig. 3. A comparison between pulsed-wire and hot-wire measurements in a strong adverse pressure gradient boundary layer. Effect of hot-wire corrections. From Dengel and Vagt (1983).

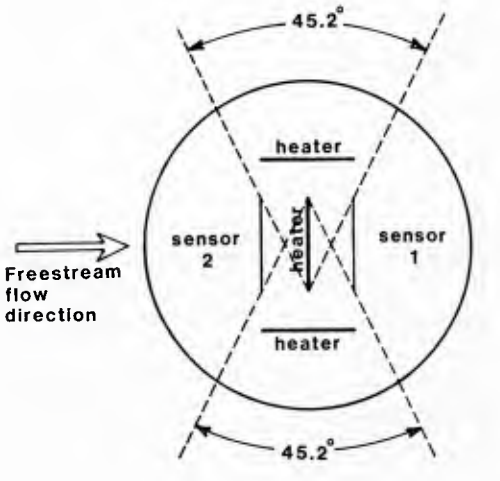

Fig. 4. Schematic planview of the modified "thermal tuft" or downstream-upstream flow direction intermittency probe. Sensors and central heater are 6 mm long 2.5 mm apart; 5 mm long side heaters are 2.5 mm from end of sensors. From Shivaprasad and Simpson (1982).

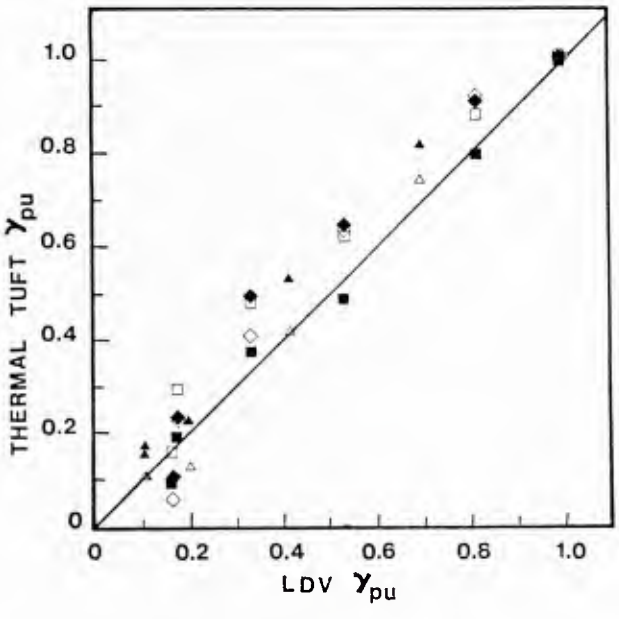

Fig. 5. Comparison of thermal tuft and LDV results for γ_{pu}. Steady flow, thermal tuft without side heaters: □, orientation 1; ■, orientation 2. Steady flow, thermal tuft with side heaters: ◇, orientation 1; ◆, orientation 2. Unsteady flow with side heaters: △, orientation 1; ▲, orientation 2. From Shivaprasad and Simpson (1982).

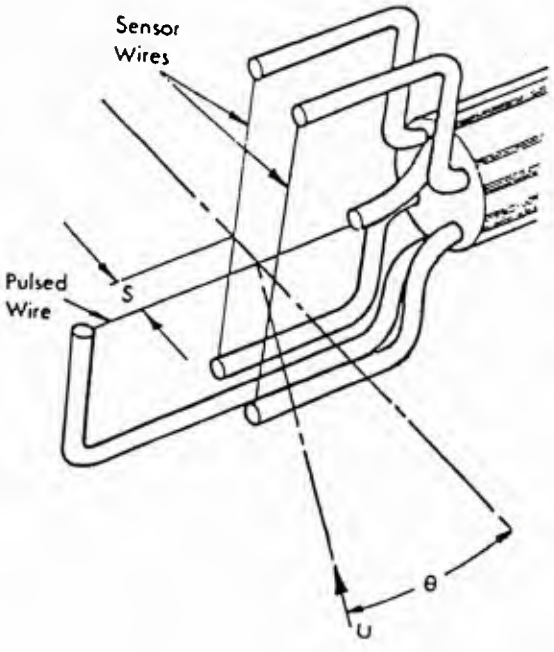

Fig. 6. Schematic of the pulsed-wire anemometer. Pela Inst. Ltd., U.K.

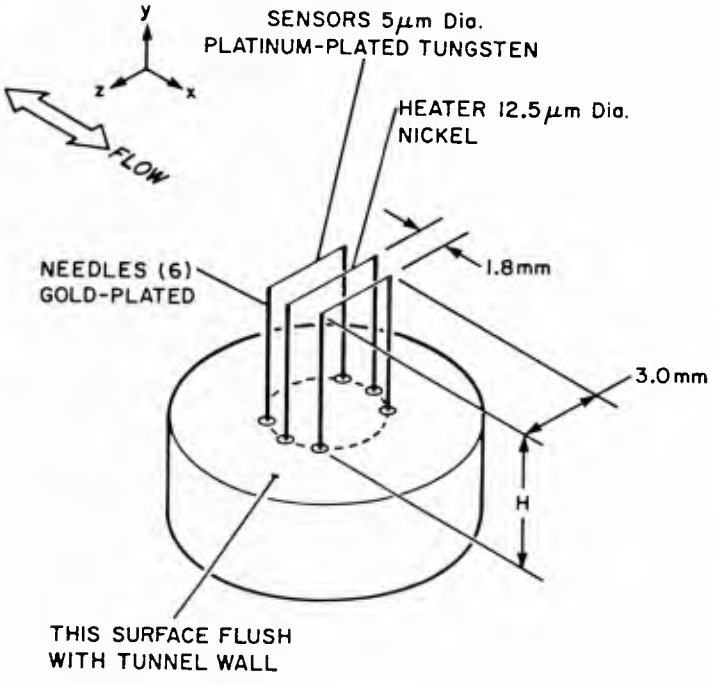

Fig. 7. Sketch of Pulsed-Wall Probe. Eaton, Westphal, Johnston (1982)

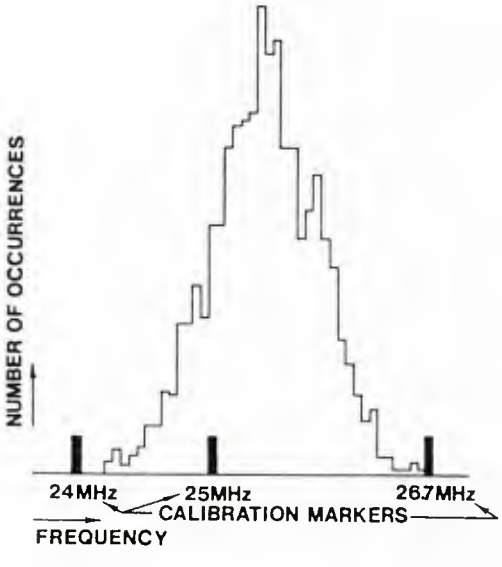

Fig. 8. Typical histogram of laser anemometer data samples in a separating flow. Zero velocity at the 25 MHz Bragg cell shifted frequency; positive velocities at higher frequencies. (Simpson, 1976)

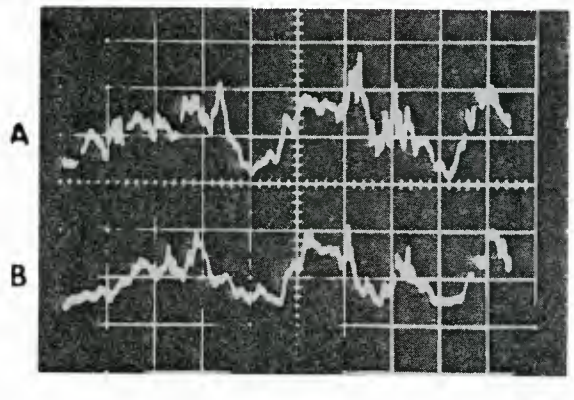

Fig. 9. Oscilloscope traces of two simultaneous surface hot film signals in the detached backflow region of the Simpson et al. (1977) flow: x of sensor A = 164.1 inches; sensor B = 0.3 inch downstream. Abscissa 50 millisec/div.

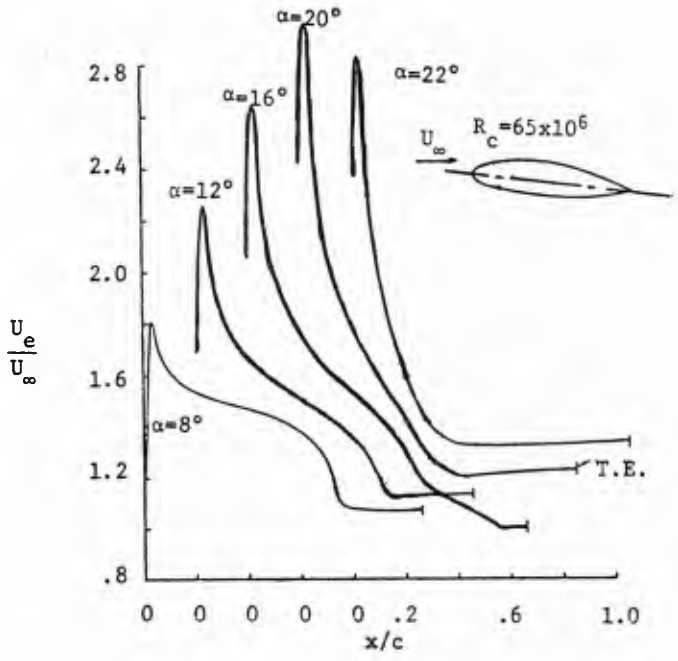

Fig. 10. U_e/U_∞ experimental distribution for the suction side of a NACA 66,2-420 airfoil. T. E. denotes trailing edge. Cebeci et al. (1972).

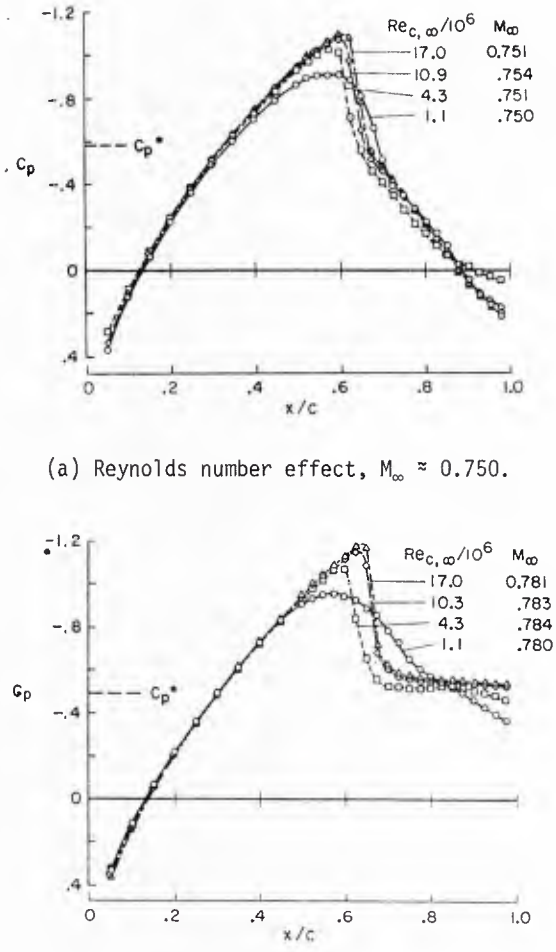

(a) Reynolds number effect, $M_\infty \approx 0.750$.

(b) Reynolds number effect, $M_\infty \approx 0.780$.

Fig. 11. C_p vs. x data for transonic flow over a biconvex circular arc airfoil. (a) detachment near x/c = 0.9 (near trailing edge detachment). (b) shock-induced detachment at higher Reynolds numbers. Note large effect at lower Reynolds numbers. At high Reynolds numbers, boundary layer displacement effect is small. From McDevitt et al. (1976).

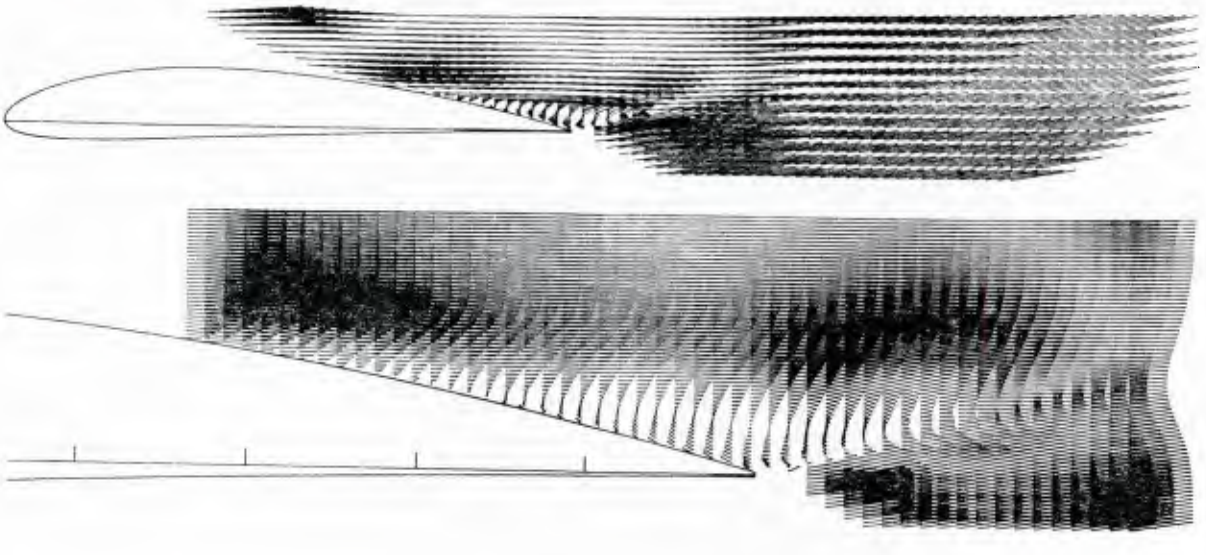

Fig. 12. Mean velocity vectors of separated flow on NACA 4412 airfoil at maximum lift and $Re_c = 1.5 \times 10^6$. Bottom figure is close-up of detached flow. Tick marks denote 0.1 of x/c intervals. Coles and Wadcock (1979).

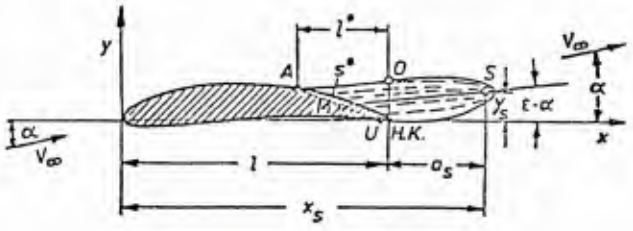

s* = Conture length between A and U

Fig. 13. Sketch of the Jacob dead air flow region model with unsymmetric separation (Jacob, 1976).

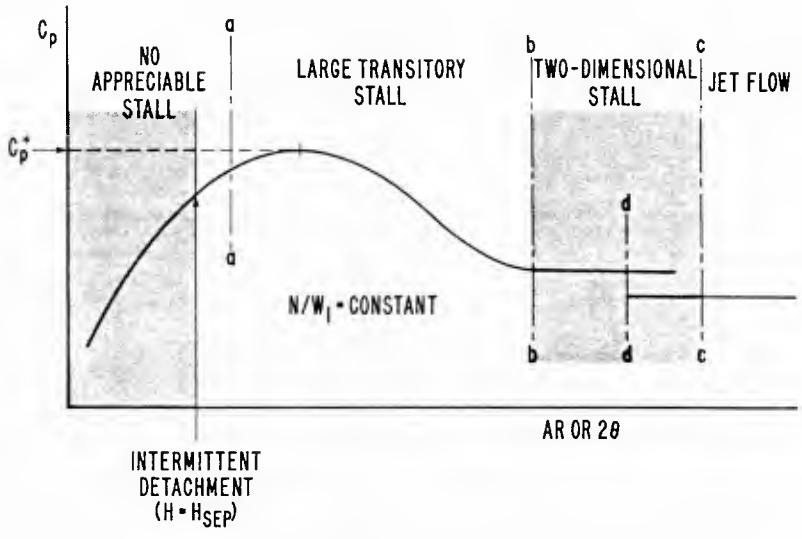

Fig. 14. Flow regimes in two-dimensional diffusers at constant N/W. Fox and Kline (1962).

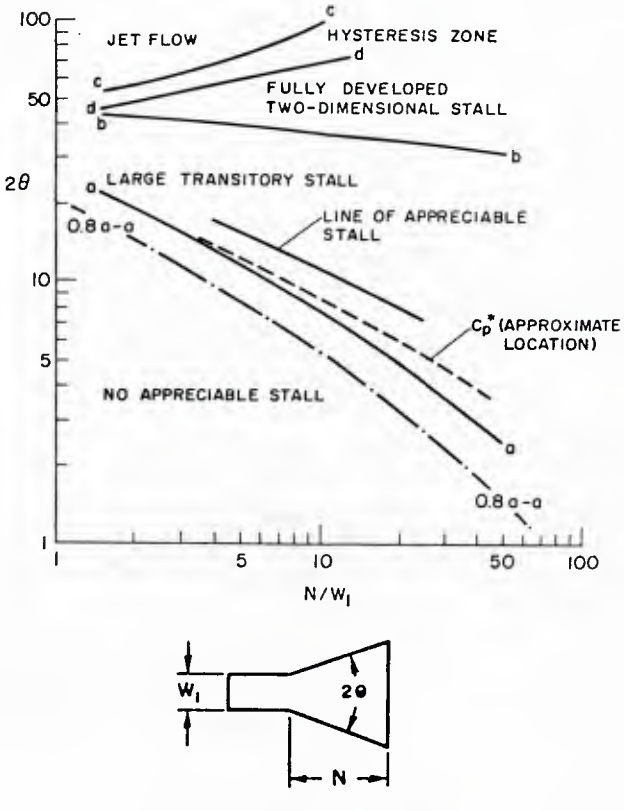

Fig. 15. Flow regimes in two-dimensional diffusers. Fox and Kline (1962).

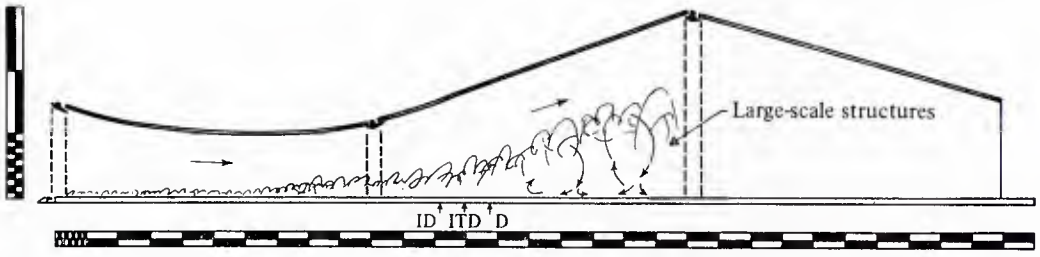

Fig. 16. Sideview schematic diagram of the test section with the steady free-stream separating turbulent boundary layer (Simpson et al. 1981a) on the bottom wall. The major divisions on the scales are 10 in. Note the baffle plate upstream from the blunt leading edge on the bottom test wall and side- and upper-wall jet boundary-layer controls.

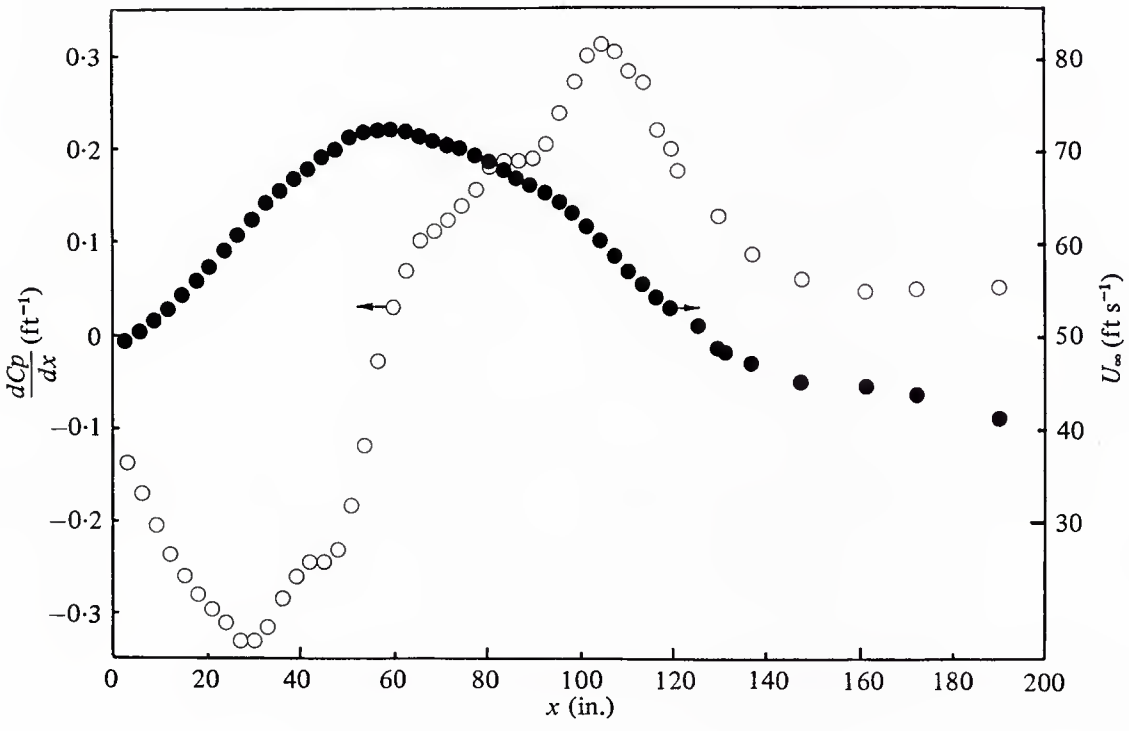

Fig. 17. Free-stream velocity and pressure gradient distributions along the tunnel centre-line.
$C_p = 2(P - P_i)/\rho U_{ei}^2 = 1 - (U_e/U_{ei})^2$, $U_{ei} = 49{\cdot}4$ ft s^{-1}.
Simpson et al. (1981a)

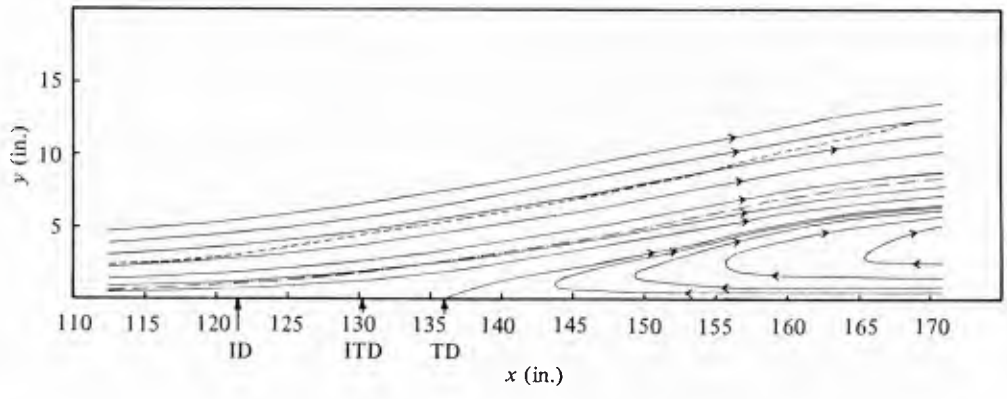

Fig. 18. Mean streamline flow pattern in the vicinity of separation. ——— streamlines, - - - - boundary layer edge, —— · —— displacement thickness distribution. ID denotes incipient detachment with 1% instantaneous backflow near the wall. ITD denotes intermittent transitory detachment with 20% instantaneous backflow near the wall. TD denotes transitory detachment with 50% instantaneous backflow near the wall. Simpson et al, (1981).

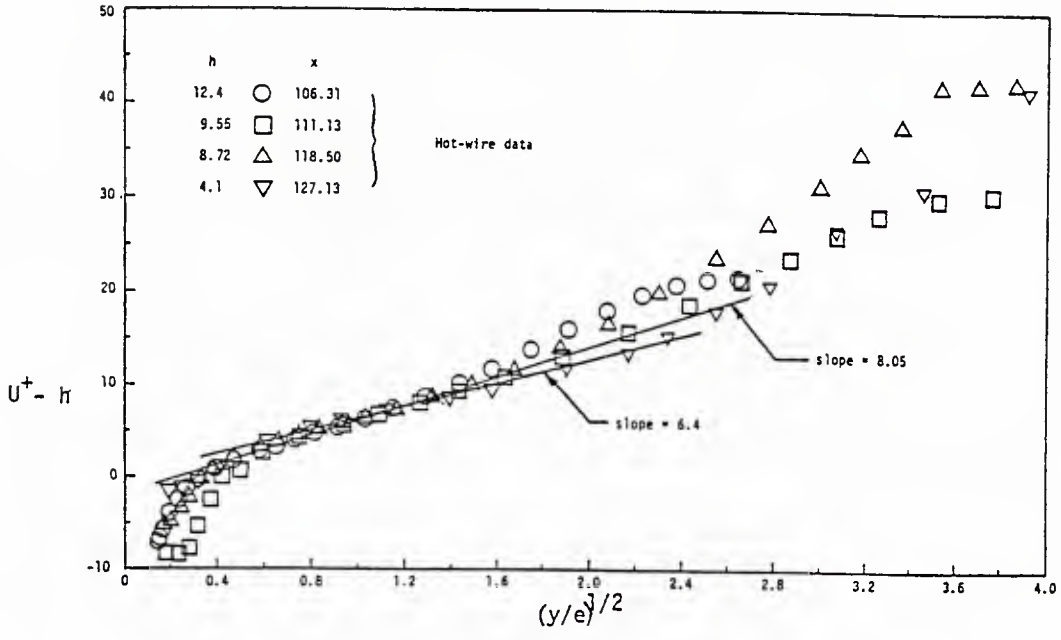

Fig. 19. Perry and Schofield inner region correlation for the Simpson et al. (1981a) data near separation, $U^+ - h$ vs. $(y/e)^{\frac{1}{2}}$, equations (IV.6) and (IV.8) given by solid lines for 6.4 and 8.05 slopes.

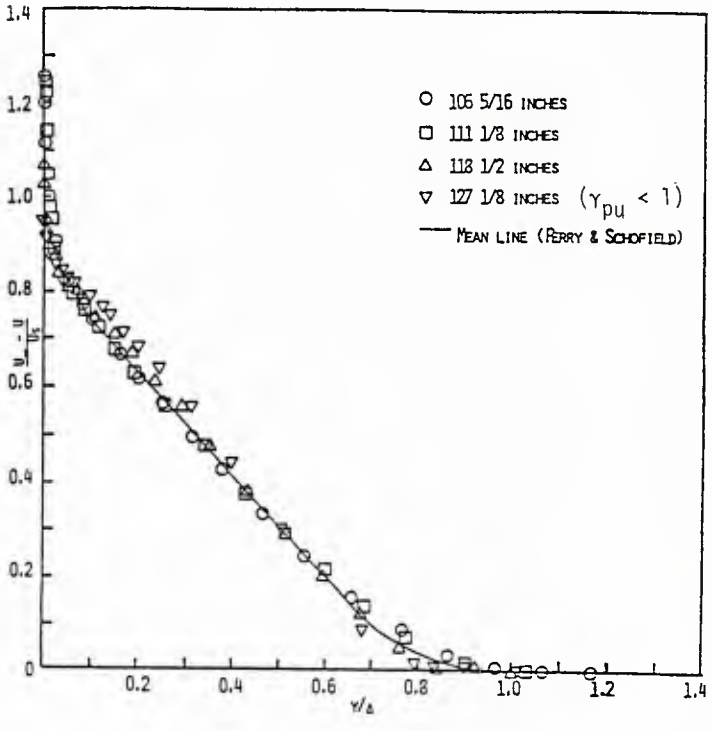

Fig. 20. Perry and Schofield outer region correlation for the Simpson et al. (1981a) data near detachment, $(U_\infty - U)/U_S$ vs. y/Δ, equation (IV.4); solid line is mean line from Perry and Schofield (1973).

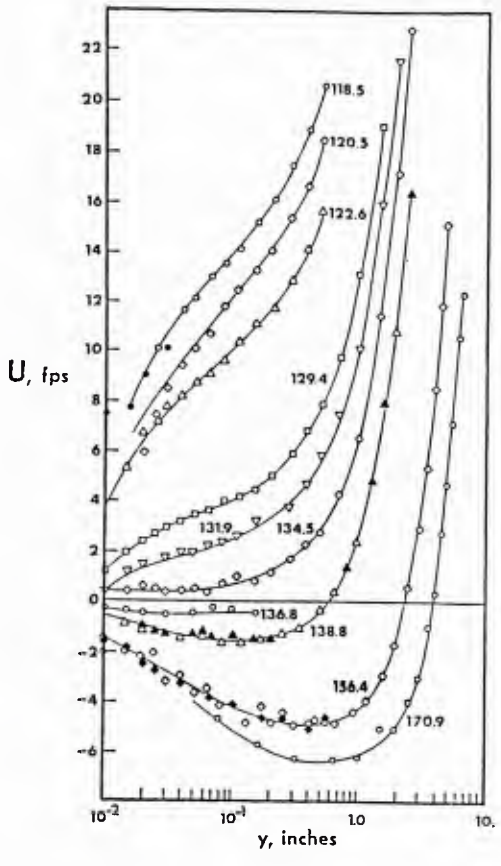

Fig. 21. Mean velocity profiles at several streamwise locations for steady freestream separating flow. Solid lines for visual aid only. (Simpson, 1981).

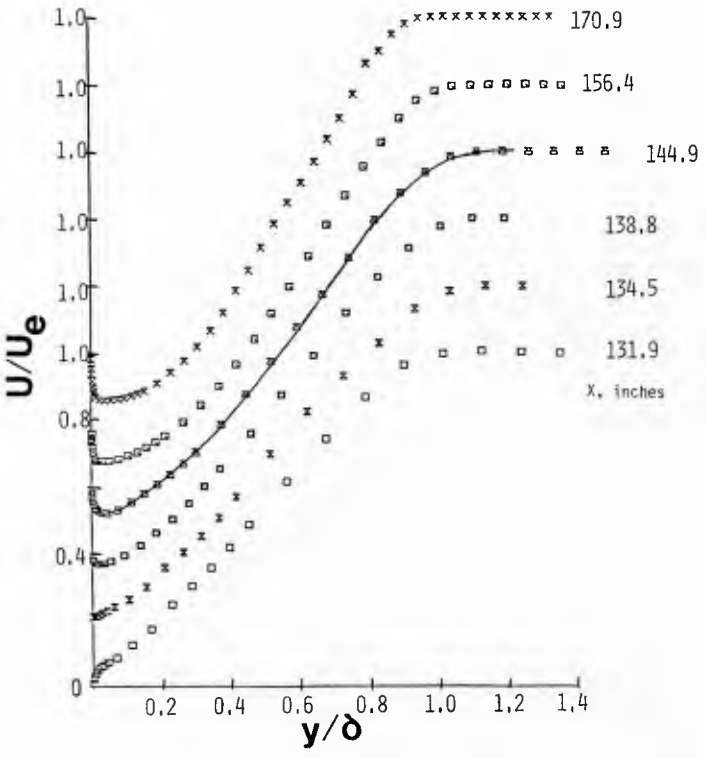

Fig. 22 Detaching flow mean velocity profiles (Simpson et al., 1981a) from laser and hot-wire anemometer data. Note displaced ordinates. Solid line denotes Re_θ = 47000, H = 5.38 data of Hastings and Moreton (1982).

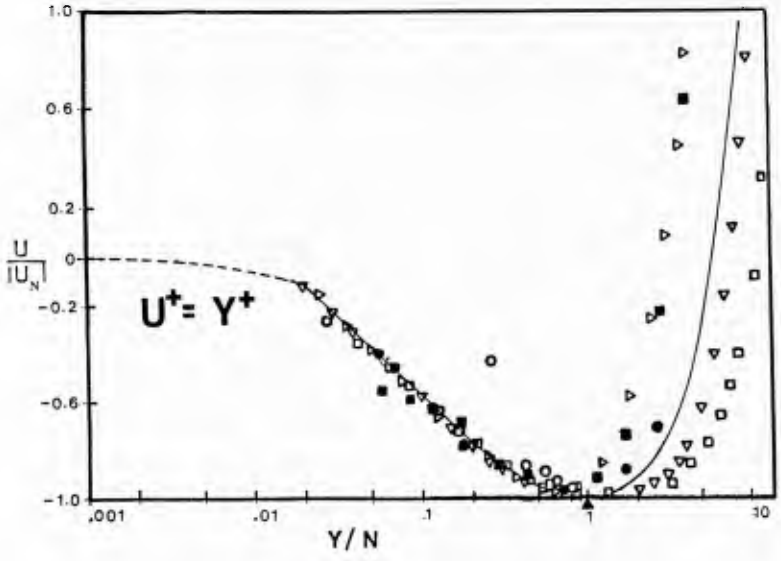

$$U/U_N = 0.3(Y/N - LN(Y/N) - 1) - 1$$

Fig. 23 Normalized backflow mean velocity profiles. Simpson et al. (1981a). LDV: ■, 3.53 m.; ▷, 3.68 m.; □, 3.97 m.; ▽, 4.34 m. Hastings and Moreton (1982): LDV ○. Westphal pulsed-wire ●. Solid line, equation (IV.11). Dashed line, equation (IV.12). From Simpson (1983).

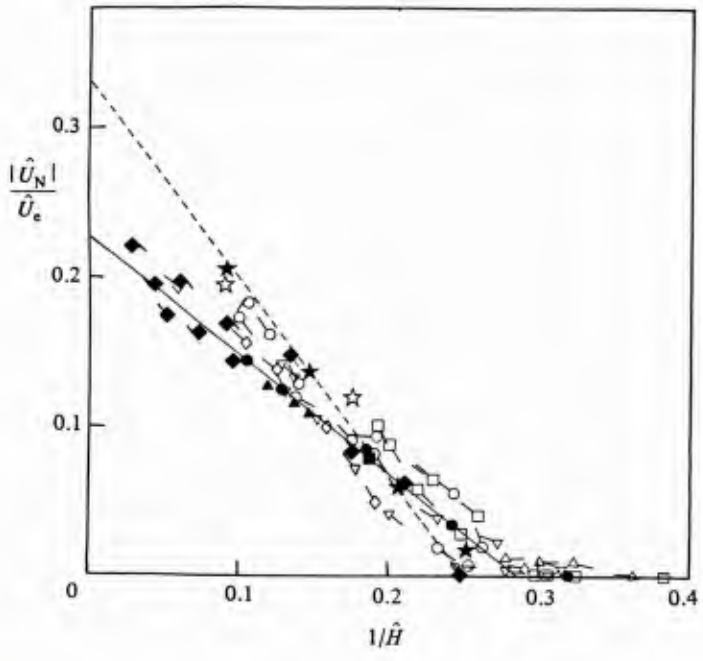

Fig. 24 $|\hat{U}_N|/\hat{U}_e$ vs. $1/\hat{H}$ for steady flows and the k = 0.61 unsteady detaching flow of Simpson et al. (1983) (denoted by open symbols). Steady detaching flows: ●, Simpson et al. (1981a); ■, Hastings and Moreton (1982); ▲, Délery (1983) flow B, M = 1.45 with some shock-induced separation; ◆, Délery (1983) flow C, M = 1.37 large shock-induced detached flow with reattachment. Steady reattaching flows: ★, Pronchick (1983); ☆, Wauschkuhn, (1982). Solid line fit to steady detachment data:

$$\frac{|\hat{U}_N|}{\hat{U}_e} = 0.807\left(1 - \frac{1}{\hat{H}}\right) - 0.577.$$

Dashed line from Simpson and Shivaprasad (1983) for reattachment:

$$\frac{|U_N|}{U_e} = \frac{4}{3}\left(1 - \frac{1}{\hat{H}}\right) - 1.$$

Leader on each symbol points in the local direction of a hysteresis loop for a given streamwise location.

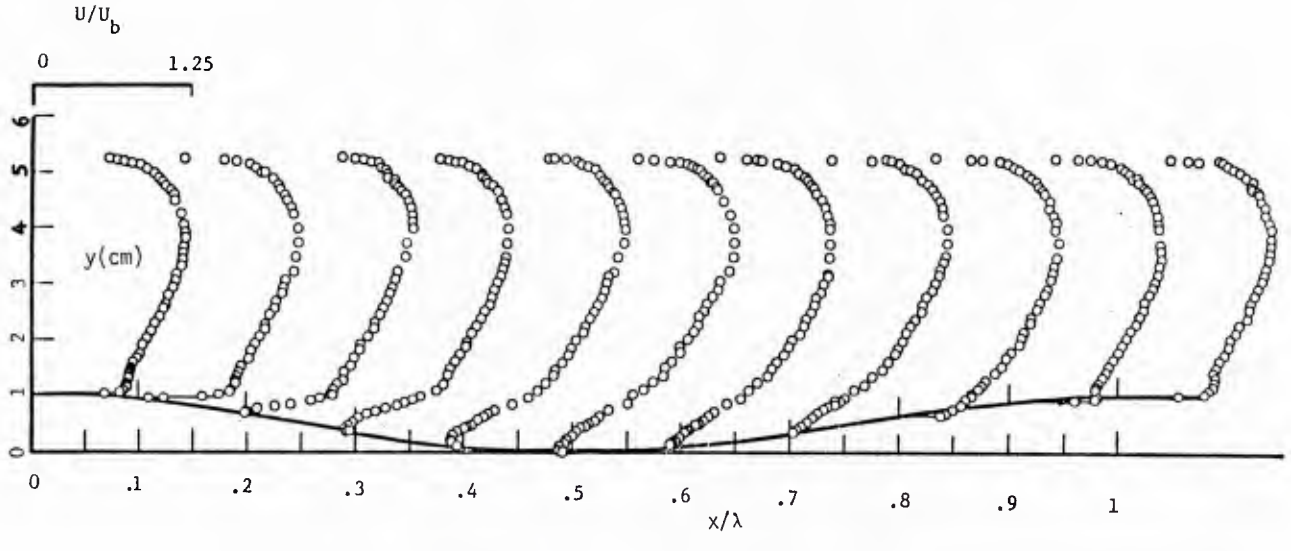

Fig. 25 Mean velocity profiles on eighth of ten waves of the Buckles et al. (1983) wavy channel flow U_b = 51 cms^{-1}; 2h = 47.4 mm; λ = 50.8 mm; $2a/\lambda$ = 1/8; $U_b(2h)/\nu$ = 12000.

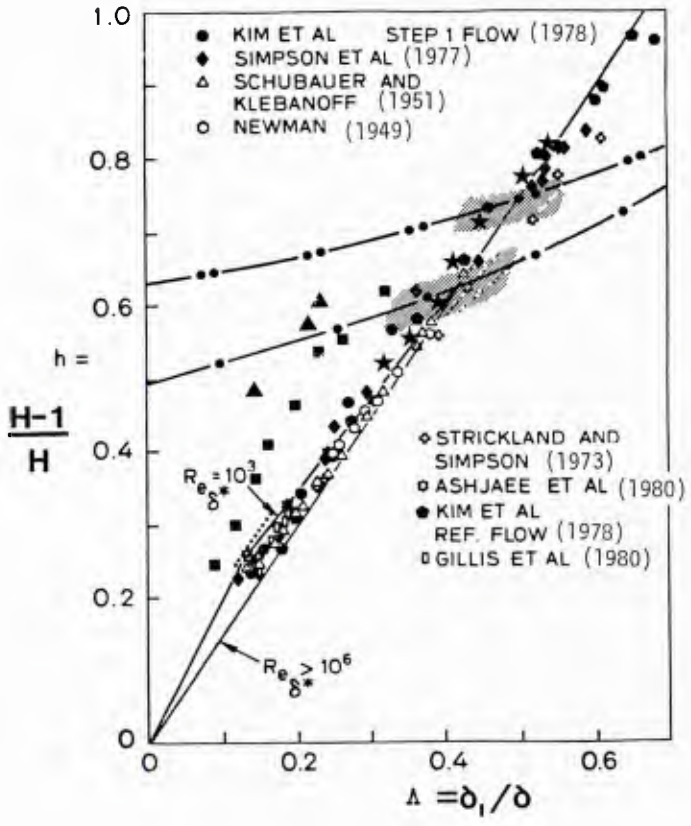

Fig. 26 h vs. δ^*/δ plot of data for detaching and reattaching flows. Shaded regions - data reviewed by Sandborn and Kline (1961). -··-, equations (6) and (7) of Kline et al. (1983); -·-, equation (IV.13); ■, data of Chou and Sandborn (1973); ▲, data of Sandborn and Liu (1968); ★, data of Wadcock (1979); ·····, data of So and Mellor (1972).

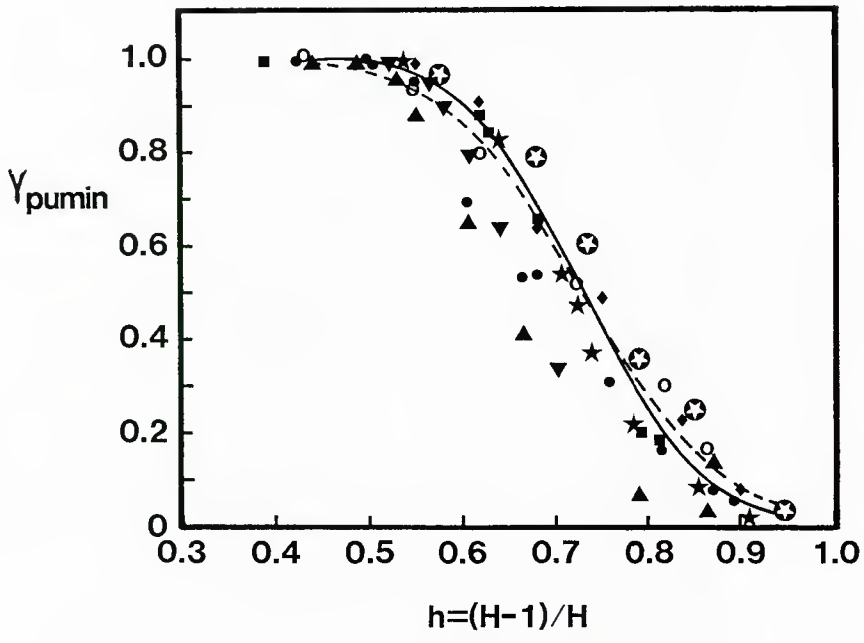

Fig. 27 $\bar{\gamma}_{pumin}$ vs. $\bar{h}$ results. Steady detaching flows: ■, LDV data (Simpson, et al., 1977); ●, LDV data; ◆ thermal tuft (Simpson et al., 1981a). Unsteady detaching flow of Simpson et al. (1983) mean values: ○, thermal tuft. Reattaching flows: ✪, Eaton and Johnston (1980), thermal tuft; ★, Pronchick and Kline (1983), LDV; ▲, α = 0 and ▼, α = 6°, LDV data of Driver and Seegmiller (1982). Equation (IV.15) with h_0 = 0.73: —, σ = 0.10; ---, σ = 0.12.

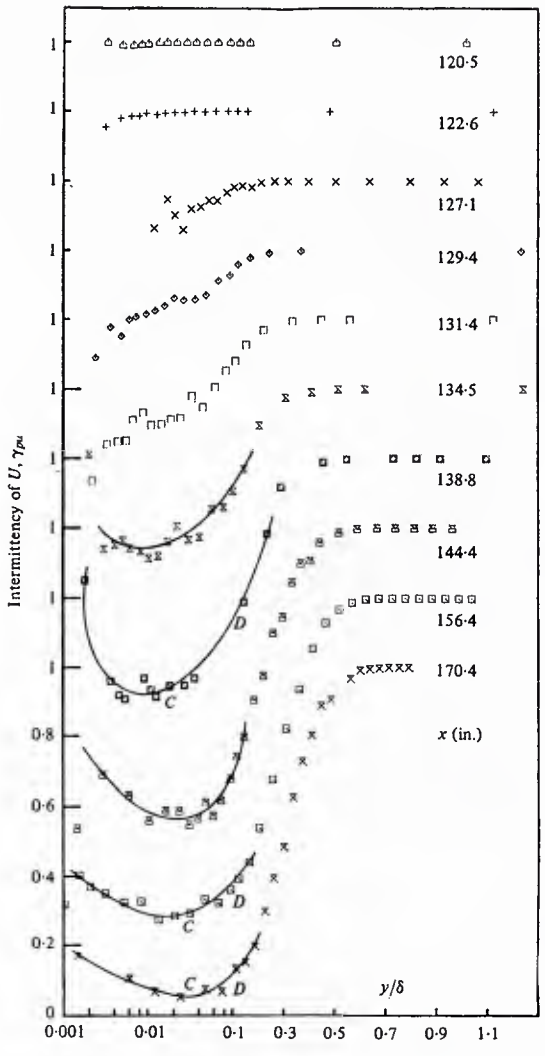

Fig. 28 Streamwise fraction of time the flow moves downstream with the locations of inflection points C and D from Shiloh et al, (1981). Solid lines are for visual aid only. Note the log-linear abscissa and displaced ordinates. From Simpson et al. (1981a).

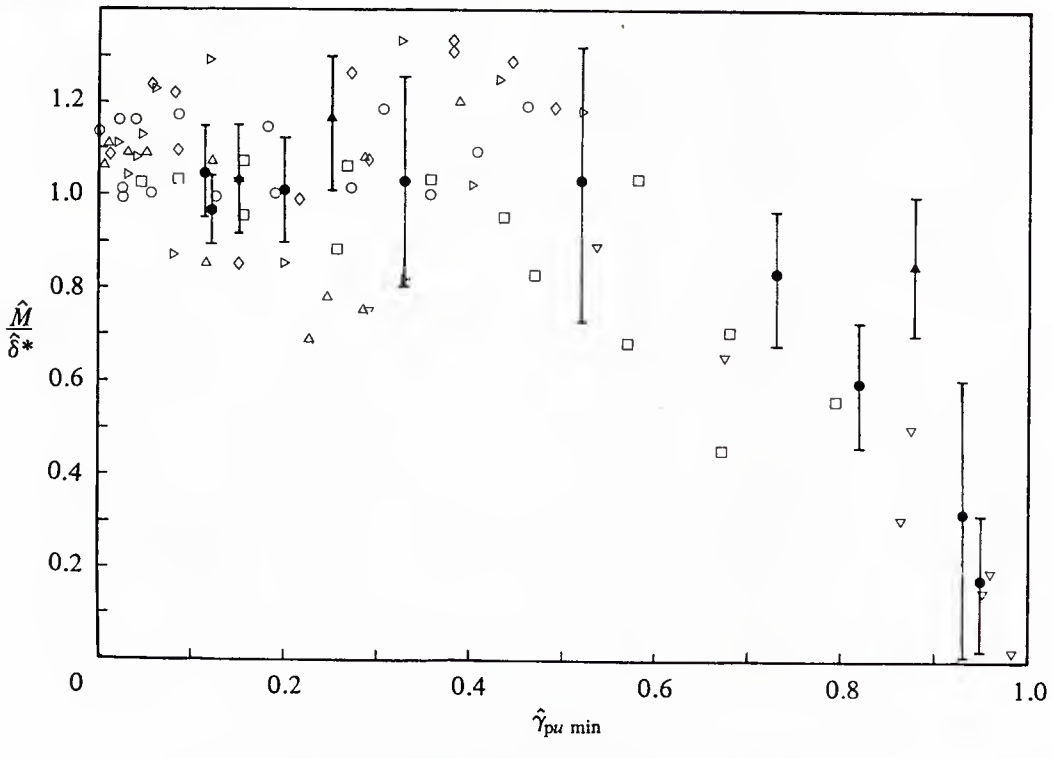

Fig. 29 Distance $\hat{M}$ from wall to where $\hat{\gamma}_{pu}$ is 0.99, normalized on δ^*. Steady-flow data: ▲, Simpson et al. (1977); ●, Simpson et al. (1981a). Note the uncertainty bands. Unsteady flow, k = 0.90; ▽, 3.00 m; □, 3.25 m; △, 3.45 m; ◇, 3.67 m; ○, 3.98 m; ▷, 4.34 m. From Simpson and Shivaprasad (1983).

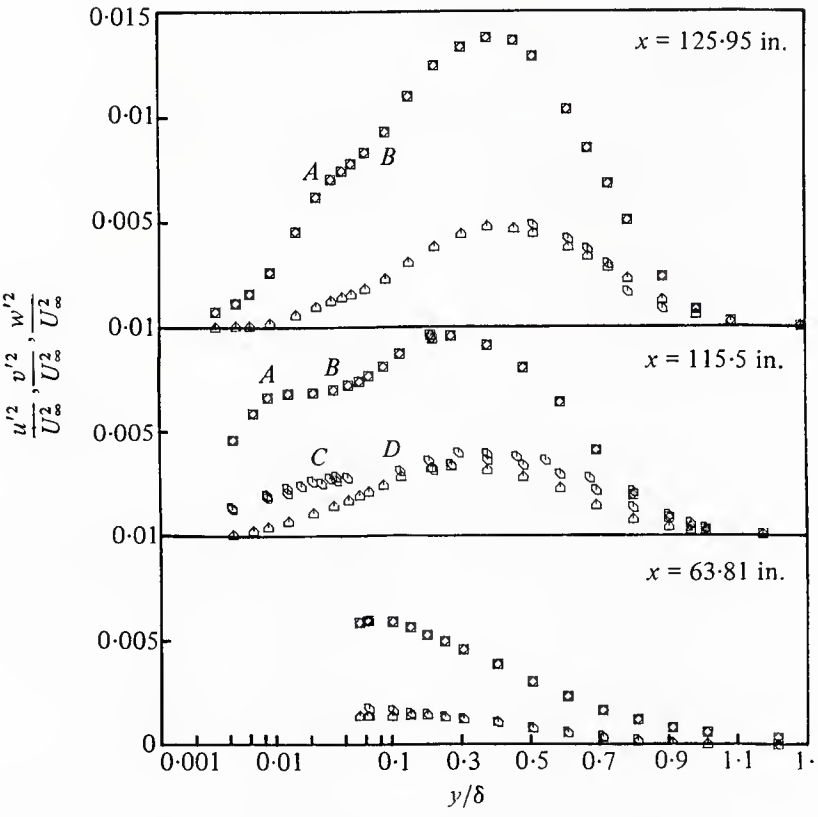

Fig. 30 Reynolds normal stresses distributions upstream of intermittent transitory detachment. Simpson et al. (1981a): ⊠, u'^2/U_∞^2; ⌂, v'^2/U_∞^2; ◊, w'^2/U_∞^2. Note the log-linear abscissa.

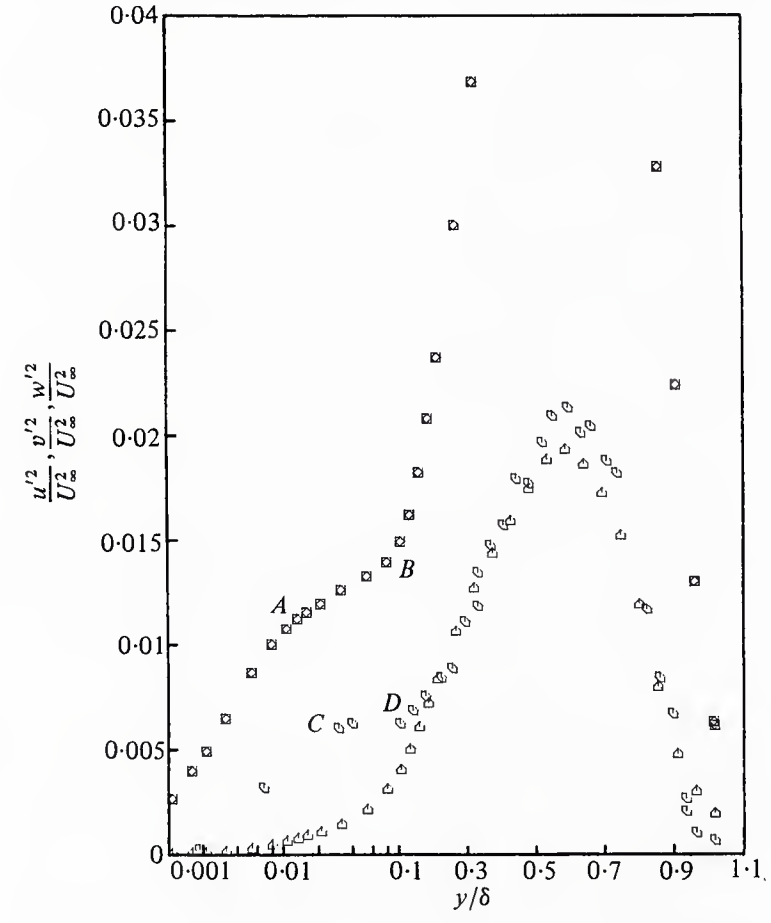

Fig. 31 Reynolds normal stresses at 173.3 inches far downstream of detachment. Legend same as Fig. 30.

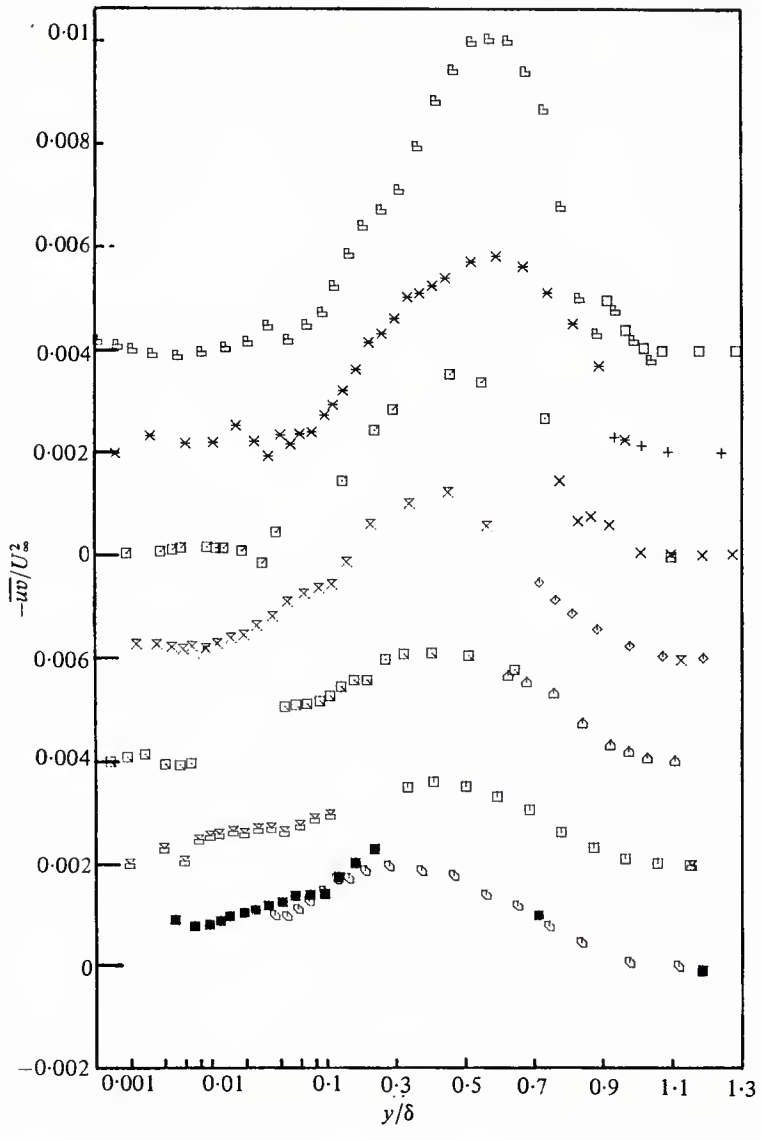

Fig. 32 Reynolds shearing stress, $-\overline{uv}/U_\infty^2$, profiles. Note the displaced ordinates and the log-linear abscissa.

x (in.)	X-wire	LDV
112	◯	■
118	□	⧖
127	⌂	◱
131	◇	×
139	×	◰
144	+	✳
156	□	⧉

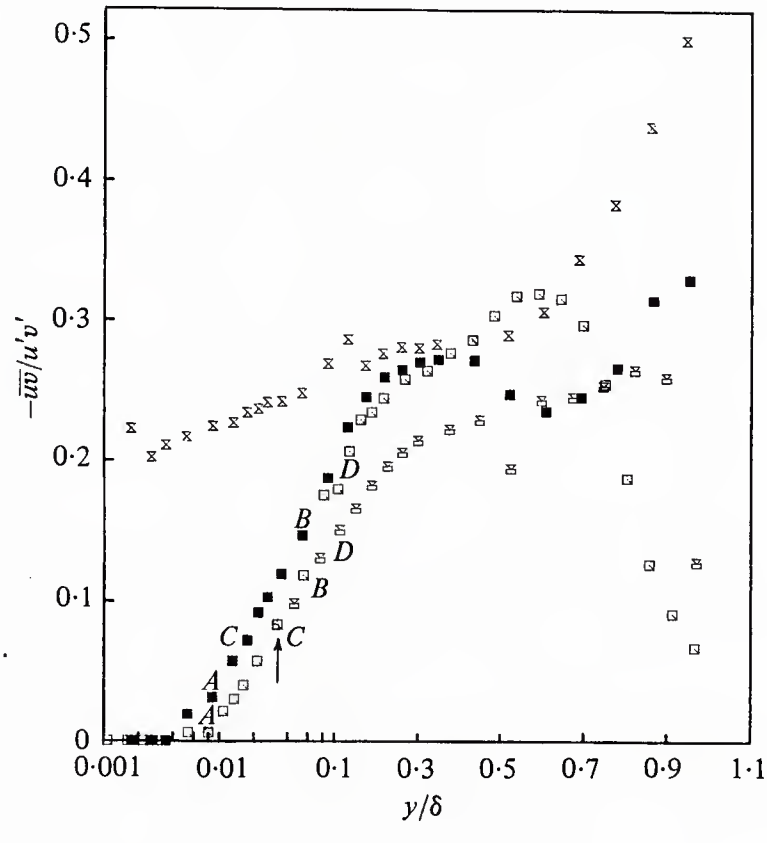

Fig. 33 Reynolds shear stress correlation coefficient profiles $-\overline{uv}/u'v'$ vs. y/δ in the detached flow region: ⧖, 134.5 in.; ■, 138.8 in.; ⧖, 144.8 in.; □, 156.4 in. Letters A-D denote turbulence profile inflection points noted by Shiloh et al. (1981). The arrow denotes the location of the minimum mean velocity. Note the log-linear abscissa. From Simpson et al. (1981a).

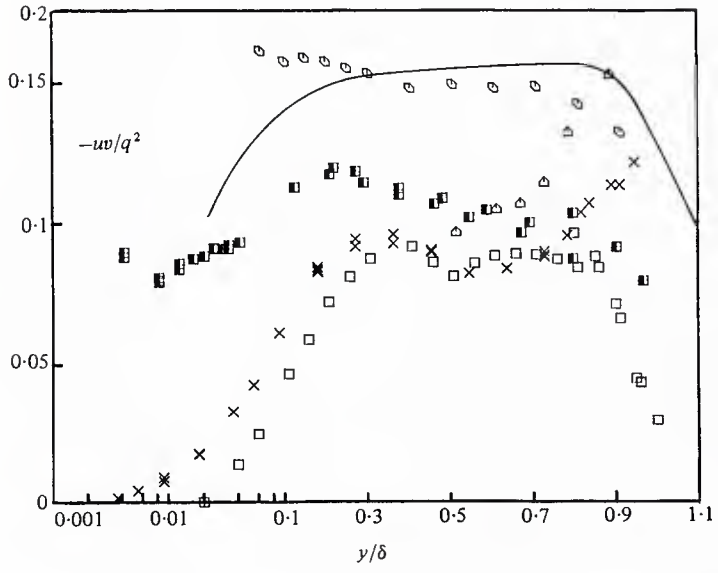

Fig. 34 Turbulence-energy correlation-coefficient $-\overline{uv}/\overline{q^2}$ distributions using the u'^2, v'^2 and $-\overline{uv}$ data of Simpson et al. (1981a) and present w'^2 data: ◇, 63·8 in.; ◧, 115·5; ⌂, 126·0; x, 138·7; □, 160·3. ——, Bradshaw (1967) zero-pressure-gradient flow. Note the log-linear abscissa. From Shiloh et al. (1981).

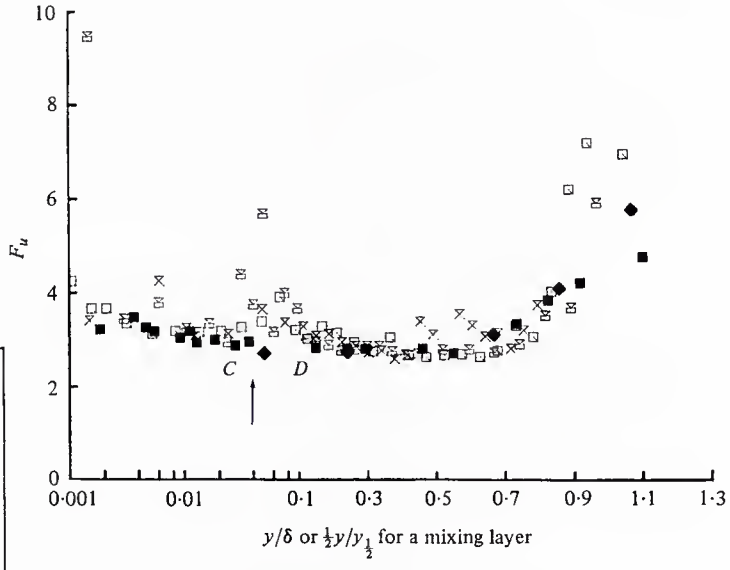

Fig. 35 Flatness-factor, F_u, profiles downstream from detachment note log-linear abscissa. C and D are the inflection points described by Shiloh et al. (1981). ■, 138·75 in.; ⧖, 144·9; □, 156·4; x, 170·9. The arrow denotes the location of minimum mean velocity U. ◆, Wygnanski & Fiedler (1970), mixing-layer data. From Simpson et al. (1981b).

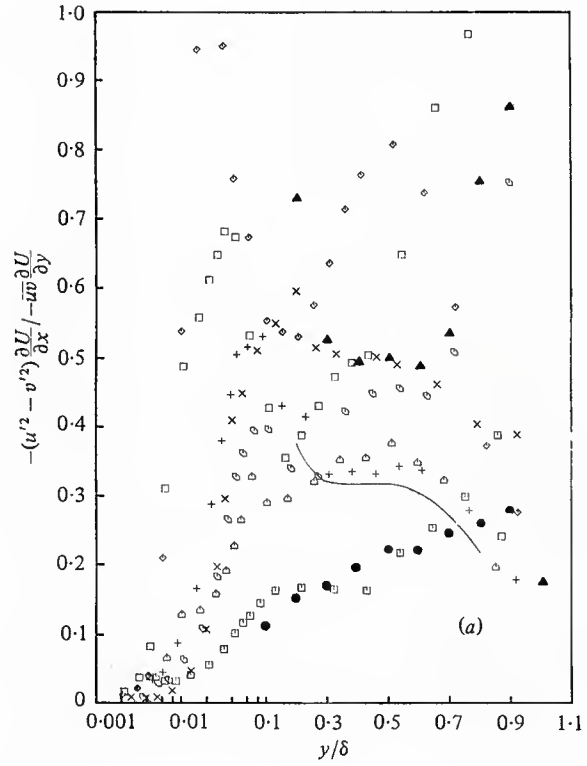

Fig. 36 Ratio of normal stresses production to shear-stress production upstream of detachment: ◫, 112·4 in.; ◇, 118·5; ⌂, 120·0; +, 122·6; X, 127·1; ◈, 129·1; □, 131·9. Schubauer & Klebanoff (1951). ——, near detachment. Simpson et al. (1977): ●, 103·8 in.; ▲, 124·3. Note the log-linear abscissa. Simpson et al. (1981a).

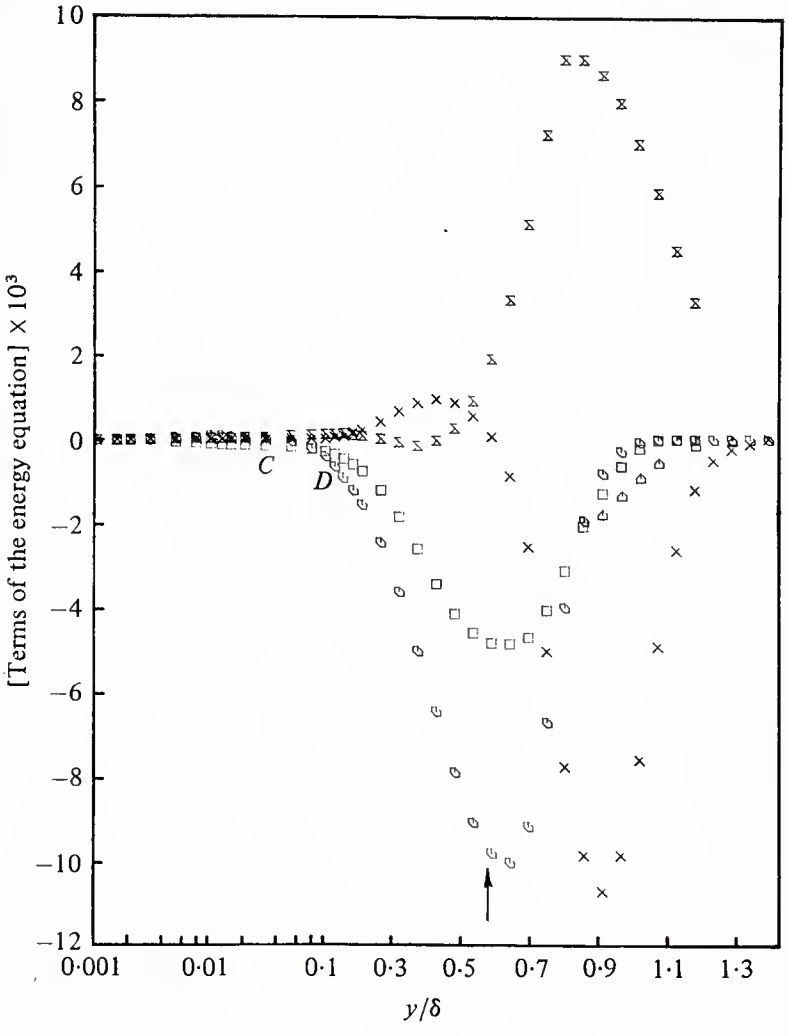

Fig. 37 Turbulence-energy balance at 156·4 in. with the location of inflection points C and D described by Shiloh et al. (1981). Note the log-linear abscissa. ⧗, $\frac{1}{2}(\delta/U_\infty^3)U\partial(\overline{u'^2+v'^2})/\partial x$; x, $\frac{1}{2}(\delta/U_\infty^3)V\partial(\overline{u'^2+v'^2})/\partial y$; ⬡, $(\delta/U_\infty^3)\overline{uv}\partial U/\partial y$; □, $(\delta/U_\infty^3)(\overline{u'^2-v'^2})\partial U/\partial x$; ⏢, $(\delta/U_\infty^3)\partial 3/4(\overline{u^2v+v^3})/\partial y$. Simpson et al. (1981b). Arrow denotes maximum shear location.

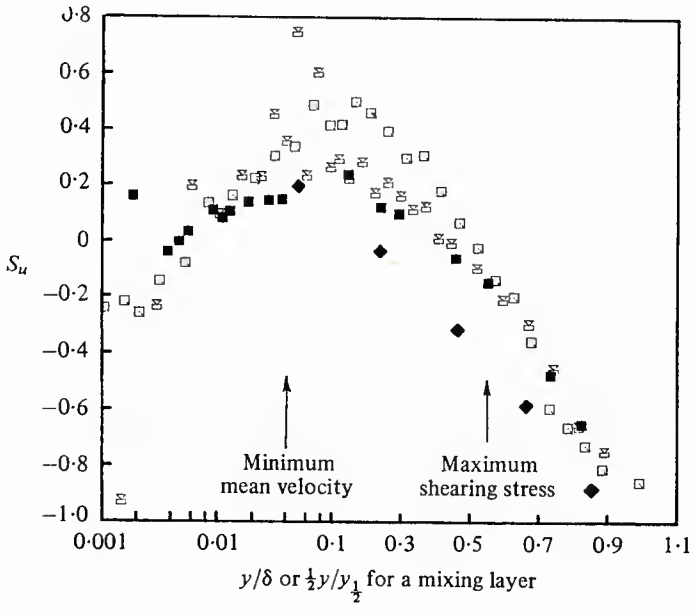

Fig. 38 Skewness-factor S_u, laser-anemometer data downstream from detachment. Note the log-linear abscissa. ■, 138·75 in.; ⧗, 144·9; □, 156·4. ◆, Wygnanski & Fiedler (1970), mixing-layer data. Simpson et al. (1981b).

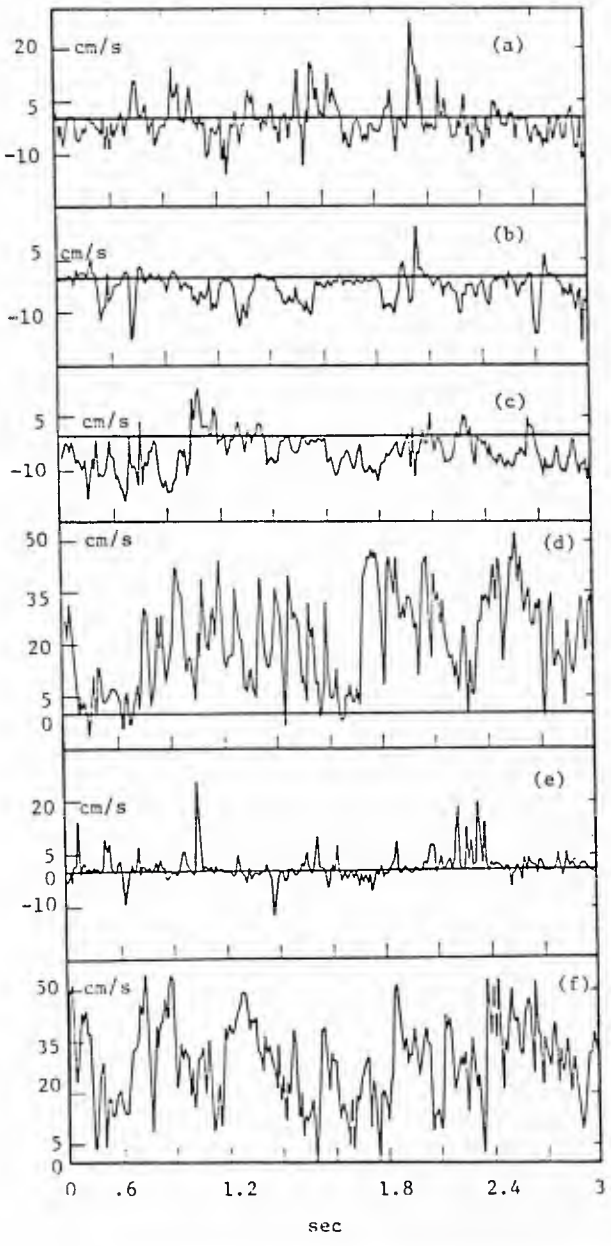

Fig. 39 Velocity-time traces for the Buckles et al. (1983) flow. See Figure 25 for other information.

	x/λ	$y-y_s$,mm	U/U_b	γ
(a)	.15	.13	-.008	.49
(b)	.30	.13	-.047	.31
(c)	.30	1.02	-.088	.21
(d)	.30	5.84	0.45	.95
(e)	.70	.13	.019	.60
(f)	.70	7.62	.49	.98

	σ_u/U_b	s	F
(a)	.11	.61	7.5
(b)	.085	-.31	5.2
(c)	.13	.79	5.0
(d)	.27	-.0048	2.5
(e)	.086	1.6	8.7
(f)	.24	-.19	2.6

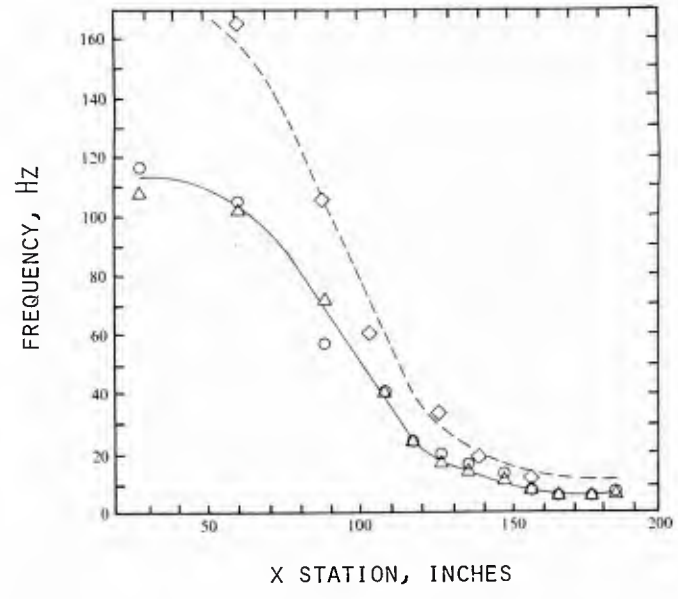

Fig. 40 Bursting and outer region turbulent-non-turbulent intermittency frequencies. ○, autocorrelation; △, spectra bursting results; ◇, intermittency results. Lines for visual aid only. From Simpson et al. (1977).

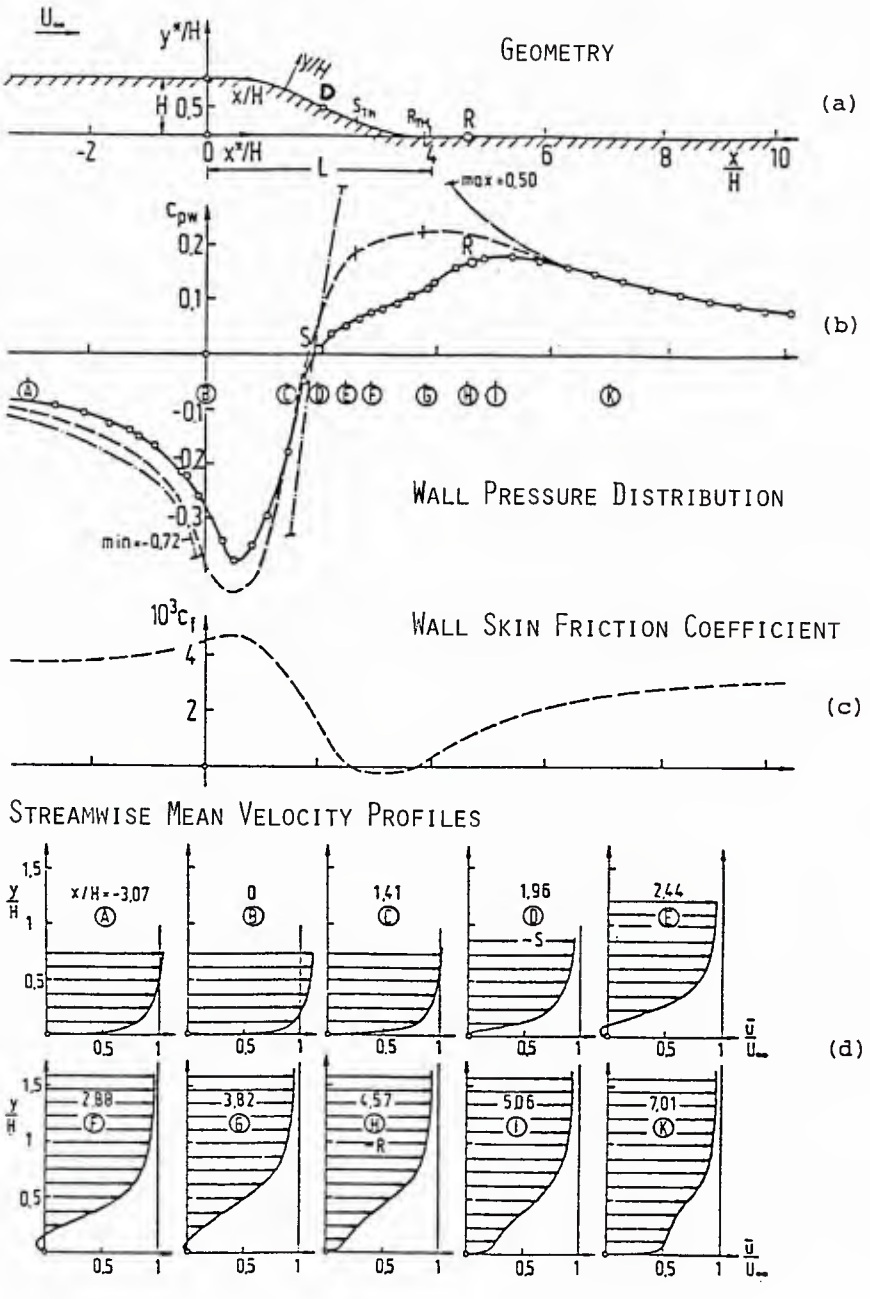

Fig. 41 Gersten, Wauschkuhn, and Pagendarm (1983) curved wall flow: (a) geometry; (b) surface pressure distribution; (c) calculated C_f from inverse method with interaction; (d) streamwise mean velocity profiles. -o-o-o-, measurements; -----, potential flow theory.

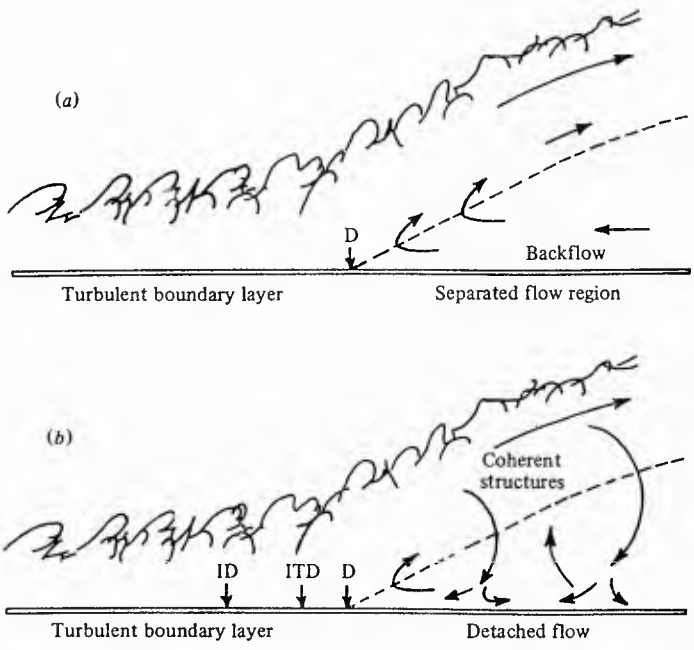

Fig. 42 (a) Traditional view of turbulent-boundary-layer separation with the mean backflow coming from far downstream. The dashed line indicates U = 0 locations. (b) A flow model with the coherent structures supplying the small mean backflow. ID denotes incipient detachment; ITD denotes intermittent transitory detachment; D denotes detachment. The dashed line denotes U = 0 locations. See Figure 18. From Simpson et al. (1981b).

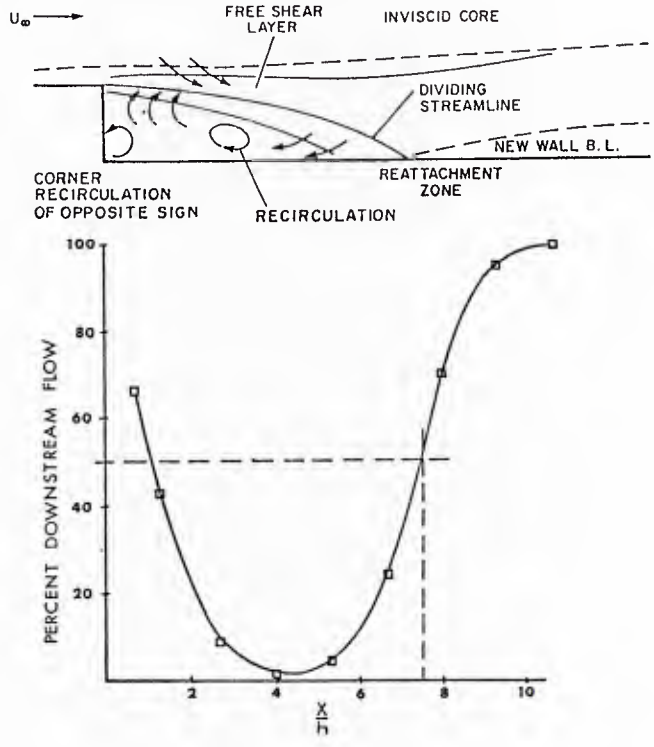

Fig. 43 Typical plot of the percent downstream flow (γ_p) for the backward-facing step flow. From Eaton and Johnston (1980).

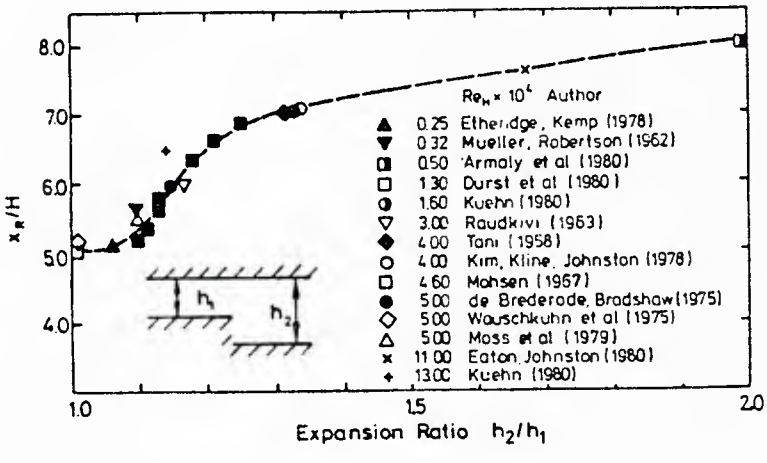

Fig. 44 Dependence of separation region length on expansion ratio. Durst and Tropea (1981).

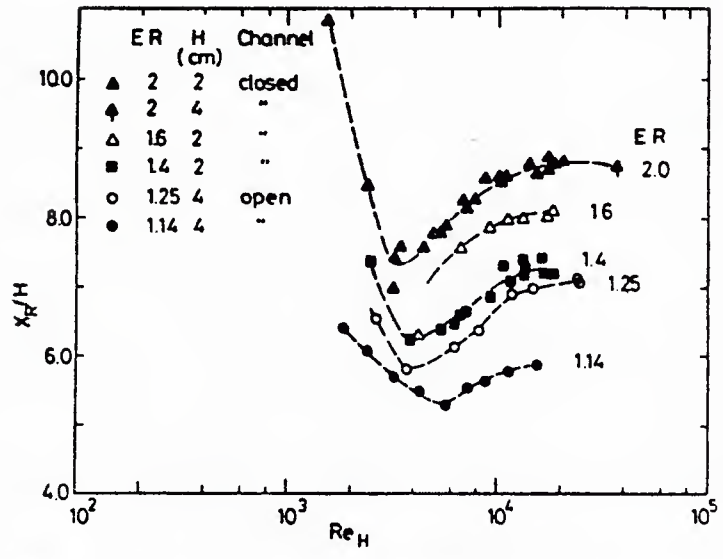

Fig. 45 Mean reattachment position as a function of Reynolds number for several expansion ratios. Durst and Tropea (1981).

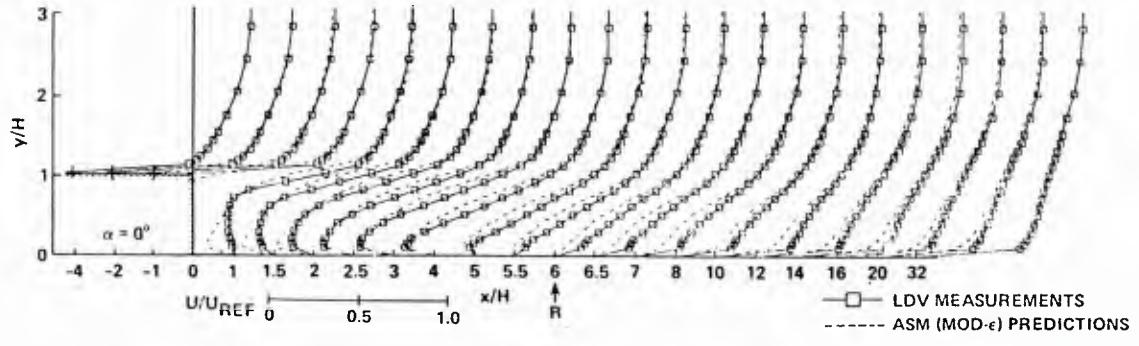

(a) Mean-velocity profiles in the separated and reattached regions.

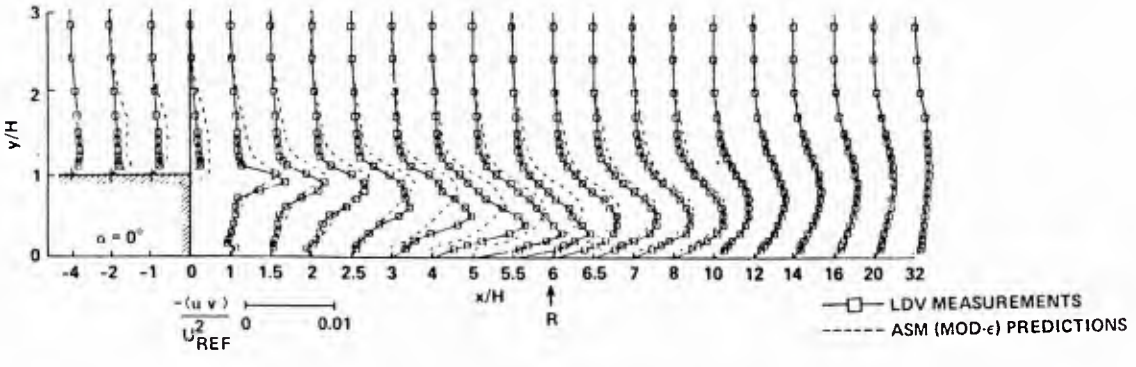

(b) Turbulent shear-stress profiles in the separated and reattached regions.

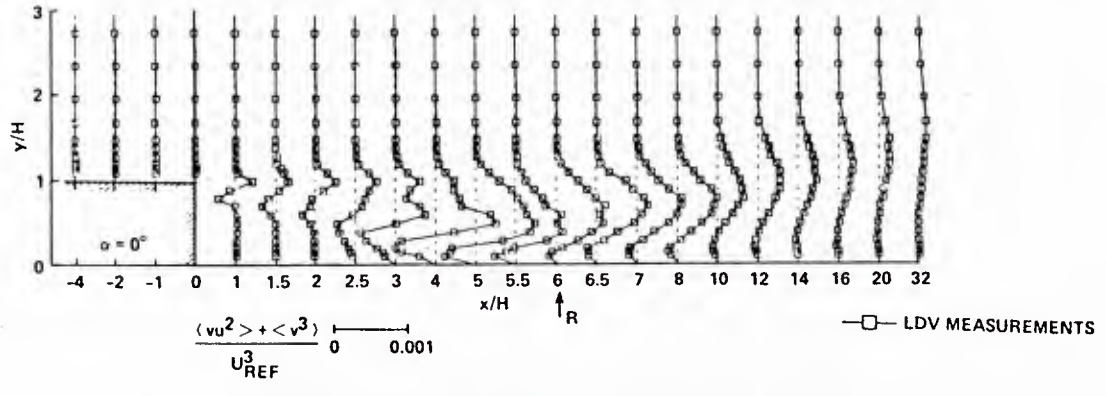

(c) Turbulent triple-product correlation profiles in the separated and reattached regions.

Fig. 46 Data of Driver and Seegmiller (1982) for the h_2/h_1 = 1.16 backward-facing step flow.

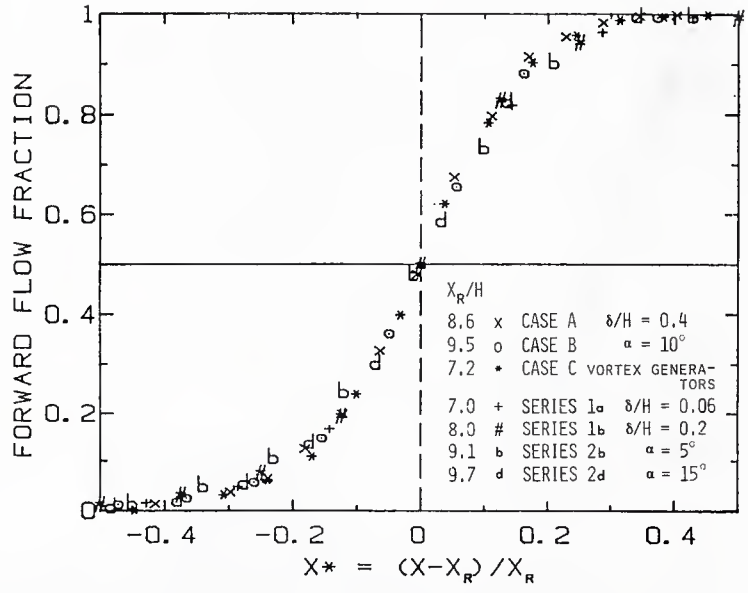

Fig. 47 Forward flow fraction near reattachment with streamwise distance normalized by the reattachment length. From Westphal and Johnston (1983). Thermal tuft data.

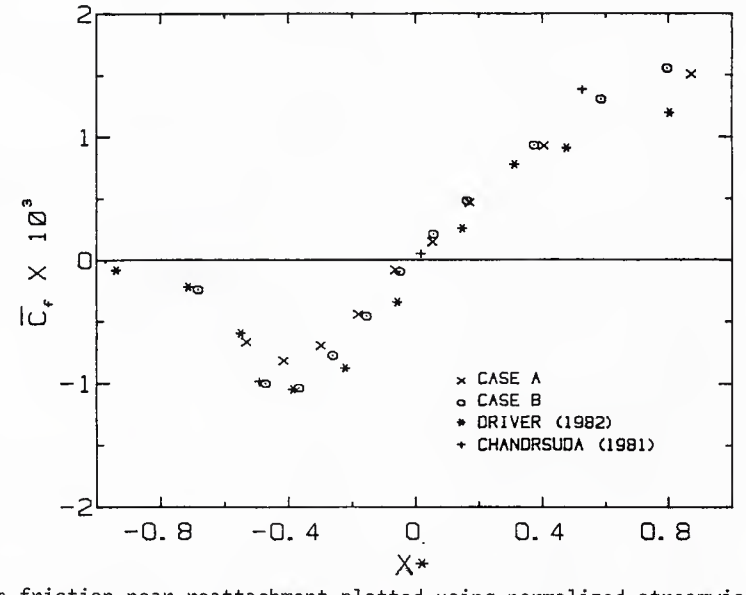

Fig. 48 Skin friction near reattachment plotted using normalized streamwise coordinate X*. From Westphal and Johnston (1983).

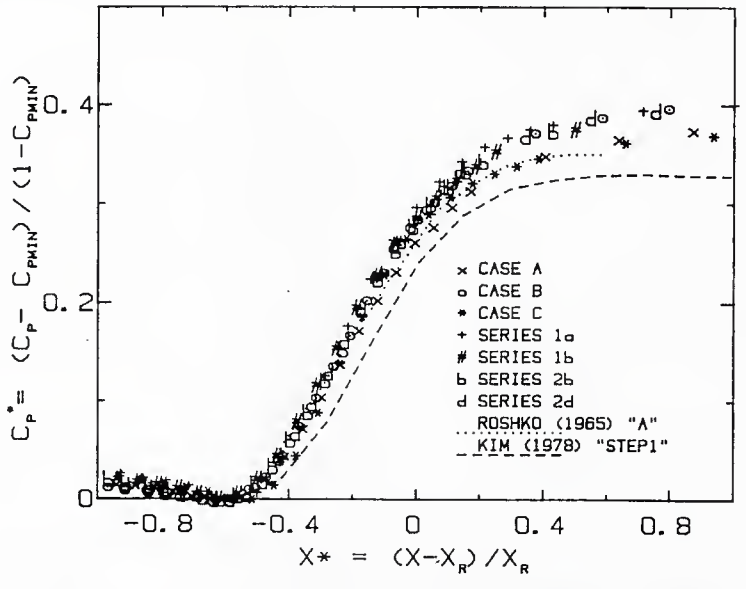

Fig. 49 Pressure distributions near reattachment, normalized as suggested by Roshko and Lau (1965). See Figure 47 for legend. From Westphal and Johnston (1983).

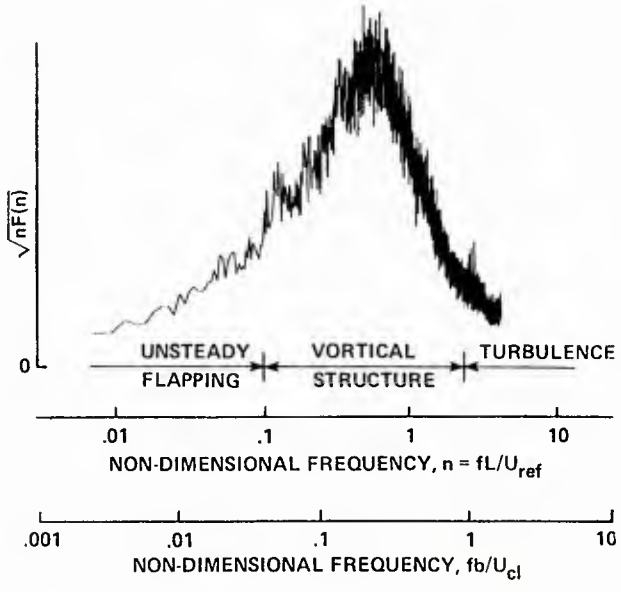

Fig. 50 Energy spectra of wall-mounted pressure sensor at X/H = 5.5. γ_{pumin} = 0.15; X_R/H = 6.1. From Driver et al. (1983).

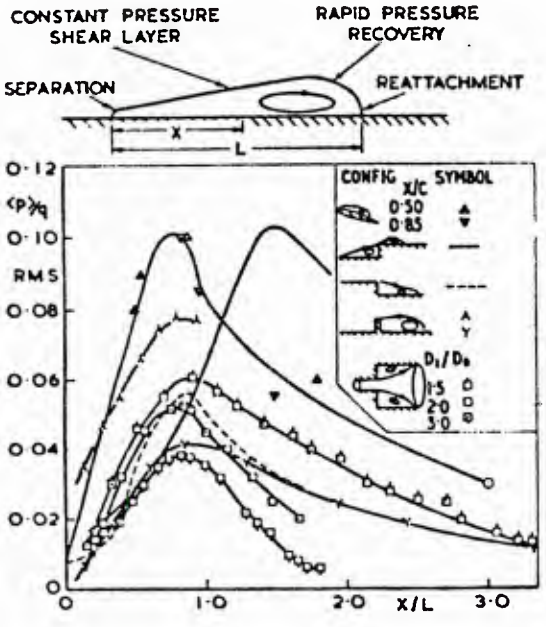

Fig. 51 RMS pressure fluctuations caused by detached flow regions. From data review by Mabey (1972).

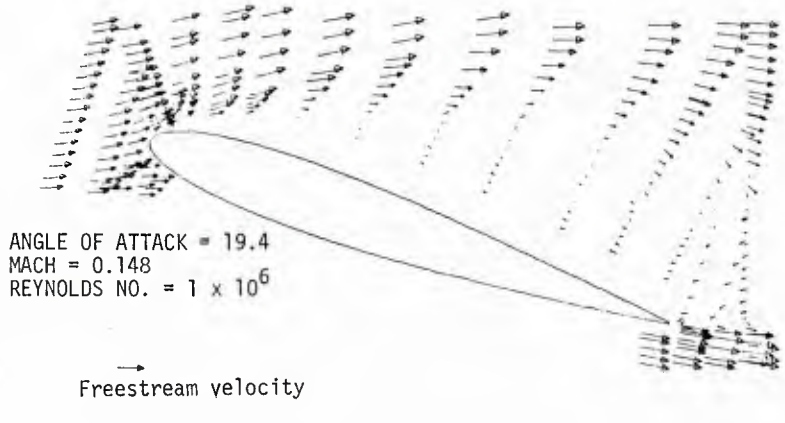

Fig. 52(a) Calculated mean velocity vectors at low Mach number. From Young et al. (1978). LDV data.

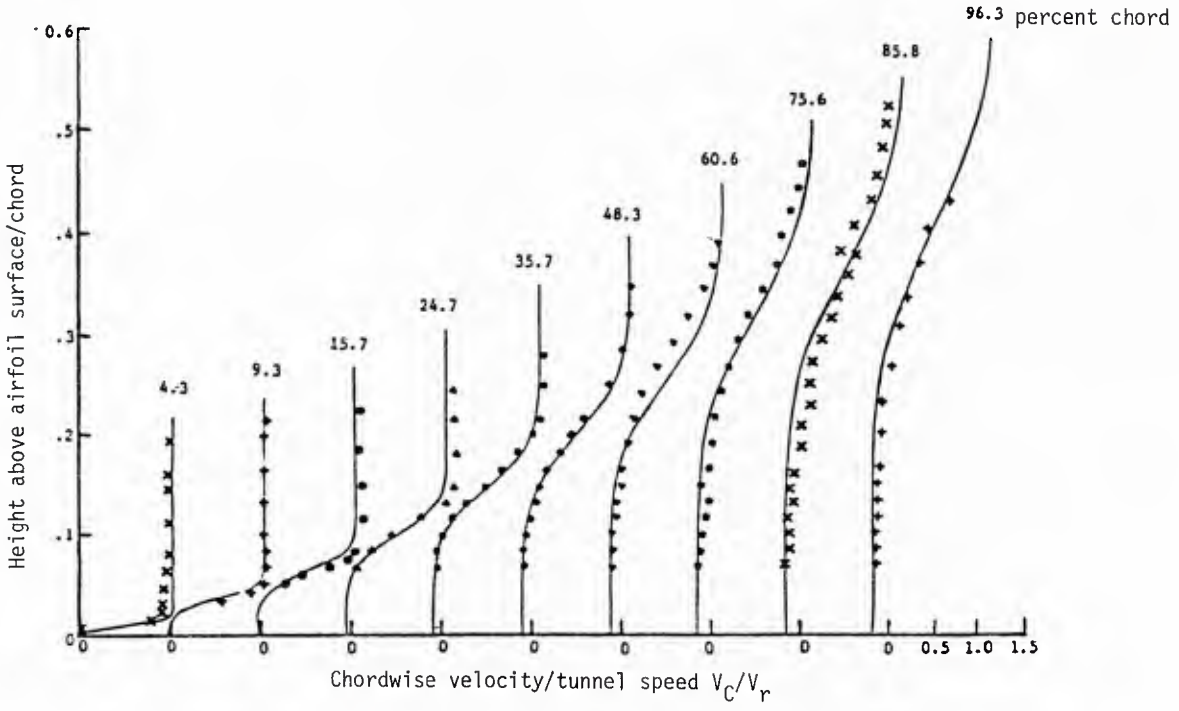

Fig. 52(b) Comparison of experimental data with calculated Görtler velocity profiles. From Young et al. (1978).

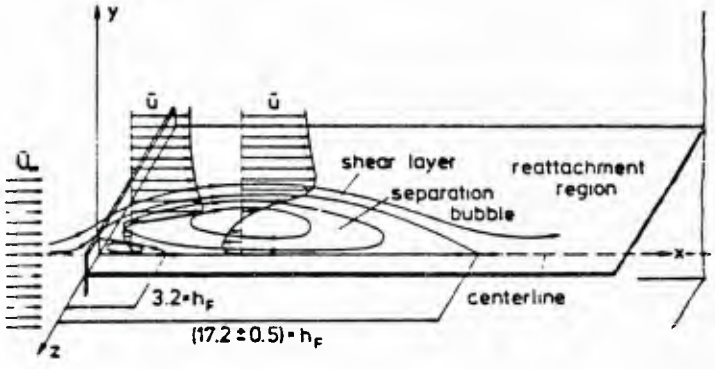

Fig. 53 Schematic diagram of the mean flow downstream of a normal plate with a long splitter plate. ($Re_{h_F} = 1.4 \times 10^4$) From Ruderich and Fernholz (1983).

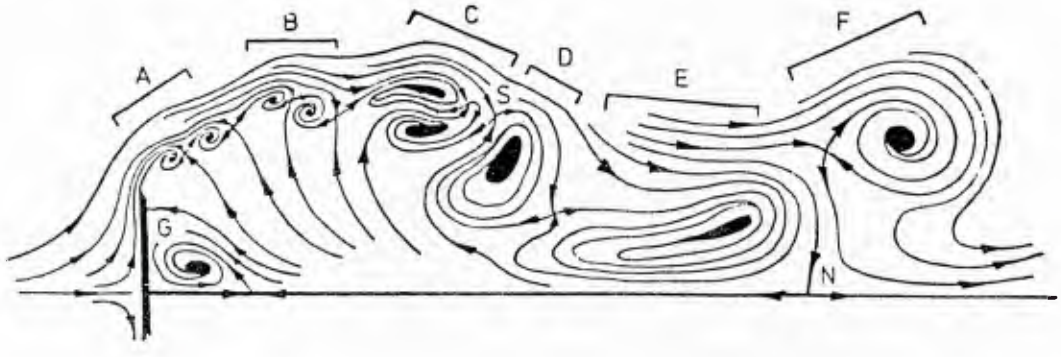

Fig. 54 Instantaneous streamlines for bluff plate with splitter plate. From Smits (1982a).

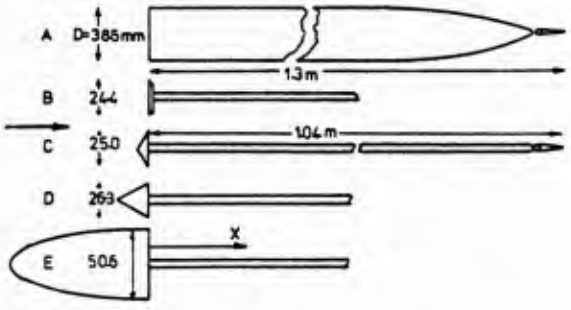

TABLE 1

Model	% solid blockage (based on D)	C_{pb}	C_{pR}	X_R/D	$\tilde{C}_{pR}$
A	3.8	-0.74	-0.18	4.89	0.32
B	2.5	-0.62	-0.1	8.84	0.32
C	2.5	-0.58	-0.07	8.00	0.32
D	2.5	-0.55	-0.05	5.26	0.32
E	5	-0.39	0.00	3.0	0.28

Fig. 55 (a) The test geometries (Hillier et al. 1983).

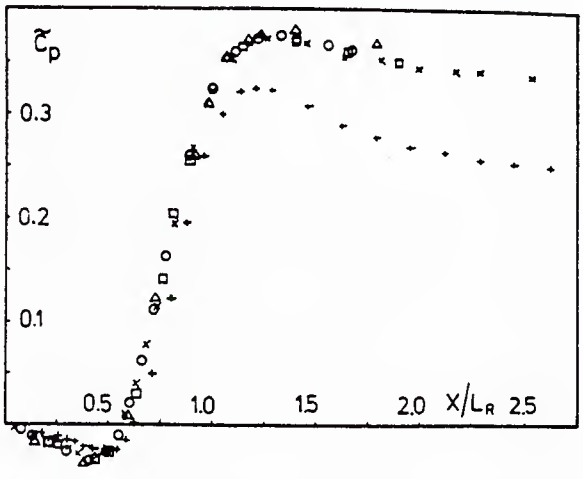

Fig. 55 (b) Distribution of reduced pressure $\tilde{C}_p$. Model A,△; B,○; C,□; D, x; E, +. From Hillier et al. (1983).

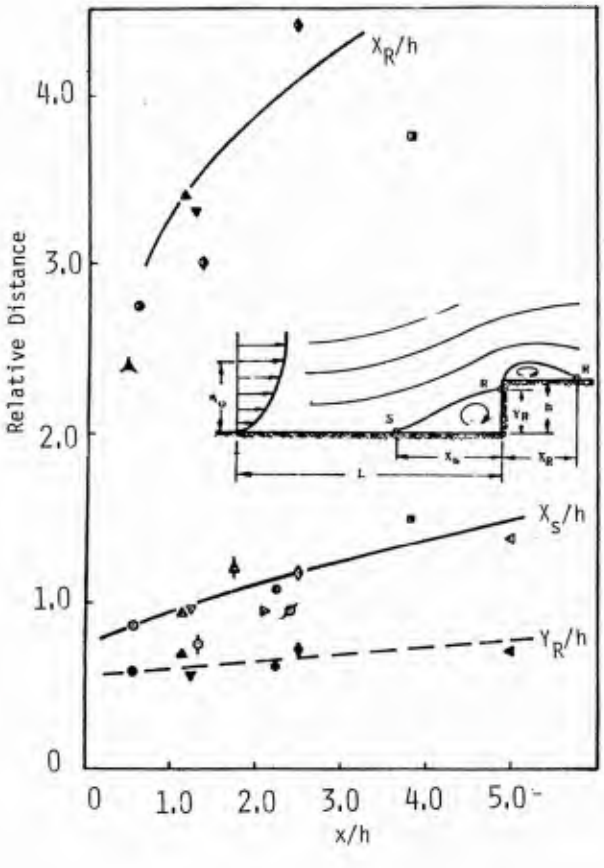

Fig. 56 Variation of detached flow dimensions with step height. Data of Robertson and Taulbee (1969); plot from Frost (1973).

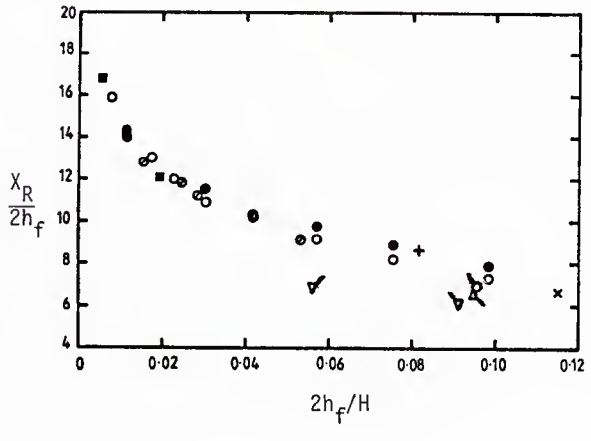

Fig. 57 Blockage ratio effect for splitter plate flow of Figure 53. From Smits (1982b). Tick marks for $\theta < 90^\circ$ data.

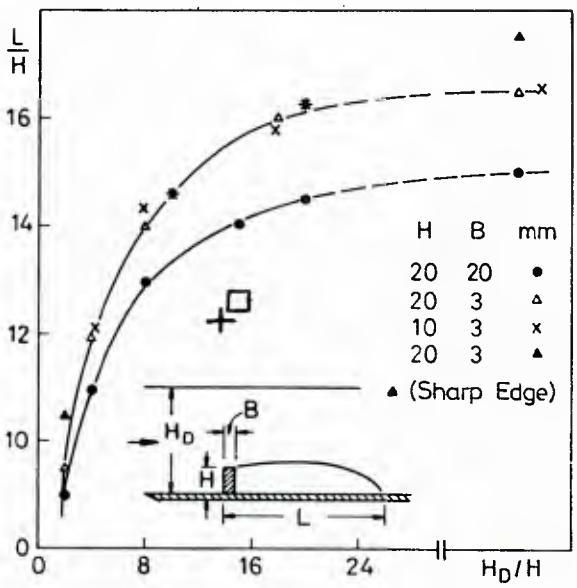

Fig. 58 Measured length of recirculation region. * Castro and Fackrell (1978). □ Castro (1981). + Crabb et al. (1981). Other data from Durst and Rastogi (1979) with δ_i = 10 mm at 150 mm upstream of fence.

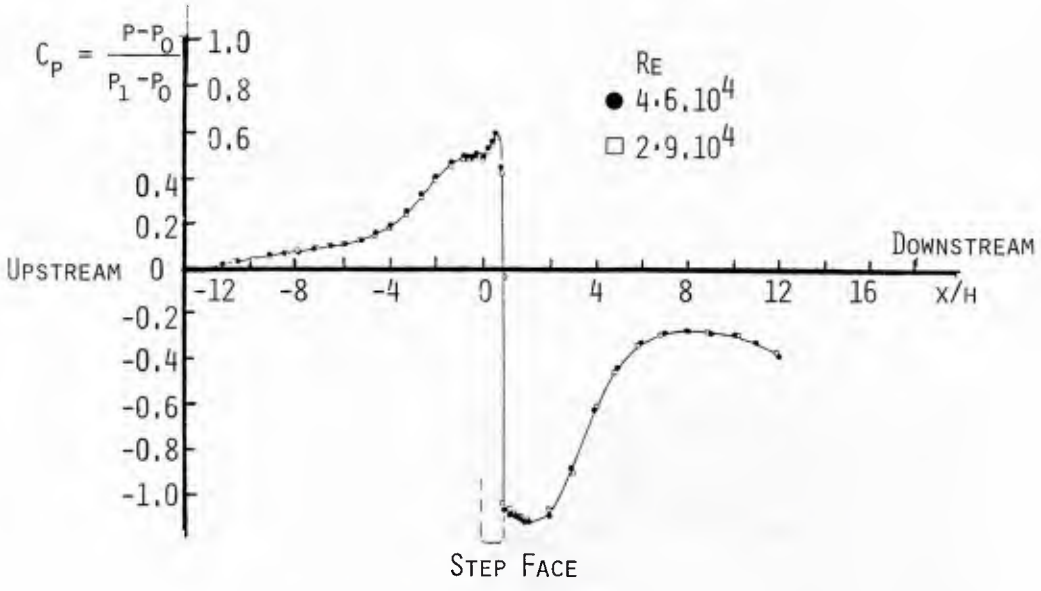

Fig. 59 Surface pressures for a front-facing step flow. From Moss and Baker (1980).

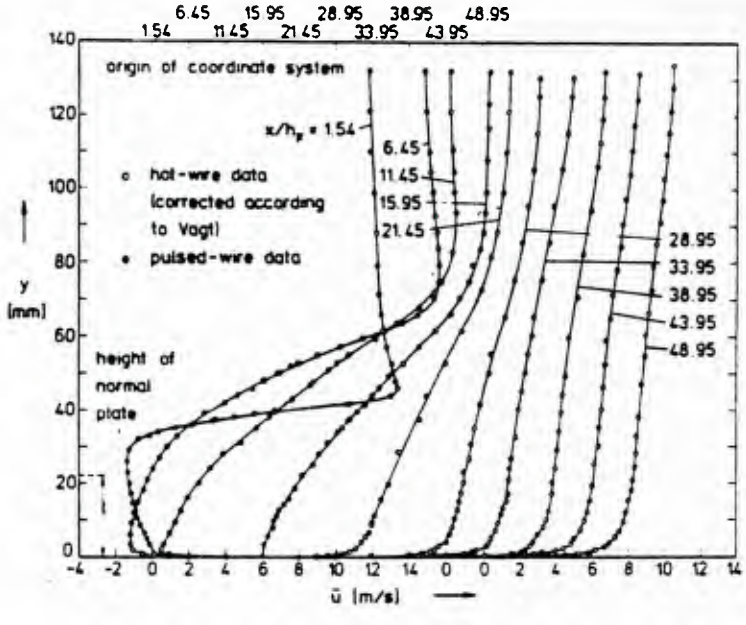

Fig. 60 Mean velocity distribution downstream of the normal plate along the centerline of the splitter plate shown in Figure 53. From Ruderich and Fernholz (1983). (Re_{h_F} = 1.4 x 10^4)

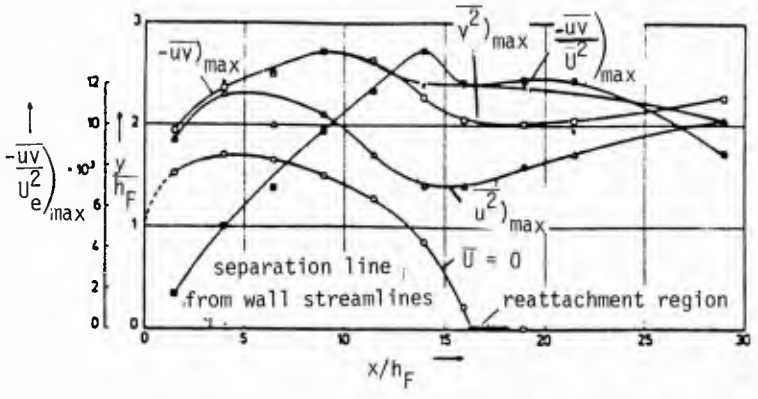

Fig. 61 Location of maximum values of Reynolds shear and normal stresses downstream of a normal plate along the centerline of a splitter plate shown in Figure 53. From Ruderich and Fernholz (1983). ($Re_{h_F} = 1.4 \times 10^4$)

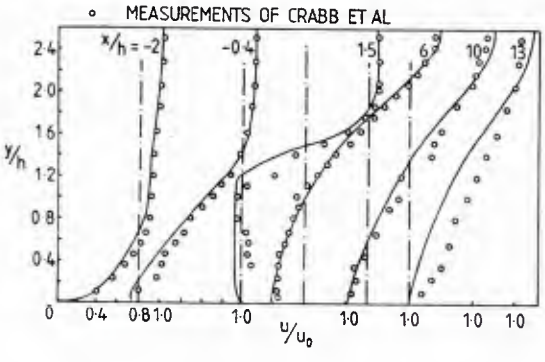

Fig. 62(a) Velocity predictions and LDA measurements for flow over square rib. ——— Calculations of Benodehar et al.(1983).

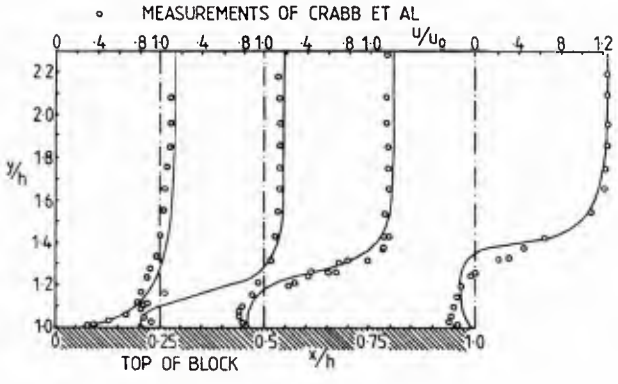

Fig. 62(b) Velocity predictions and LDA measurements for flow over square rib. ——— Calculations of Benodehar et al.(1983).

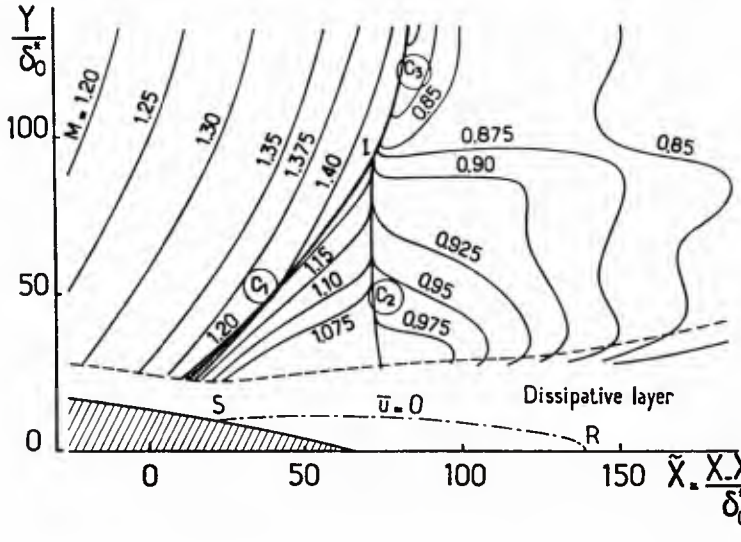

Fig. 63 Inviscid flowfield structure of flow C of Délery (1983). $M_{e_0} = 1.37$, $\delta_0^* = 0.52$ mm, $H_{i_0} = 1.27$, $Re_{\theta_0} = 3800$

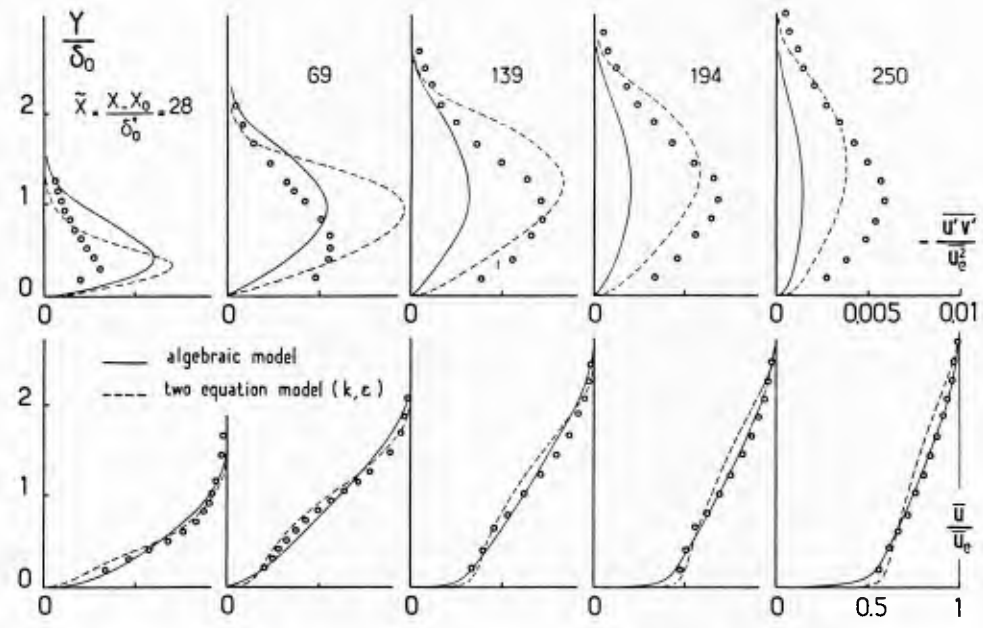

Fig. 64 Flow A boundary layer profiles of Delery (1983). Me_0 = 1.3, δ_0^* = 0.36 mm, θ_0 = 0.14 mm, H_{i0} = 1.30, Re_{θ_0} = 2400.

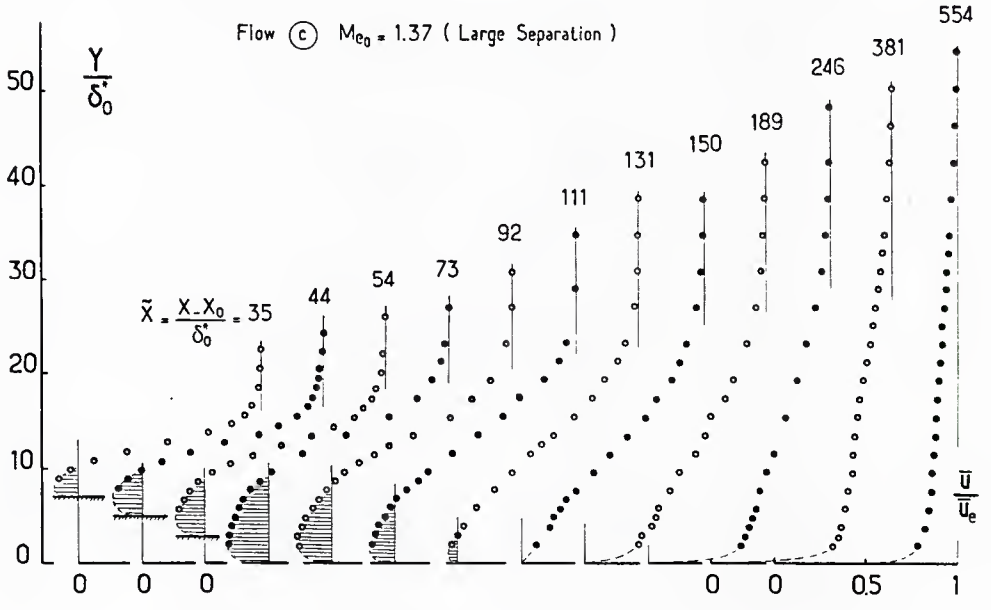

Fig. 65 Mean streamwise velocity profiles for flow C (Délery, 1983).

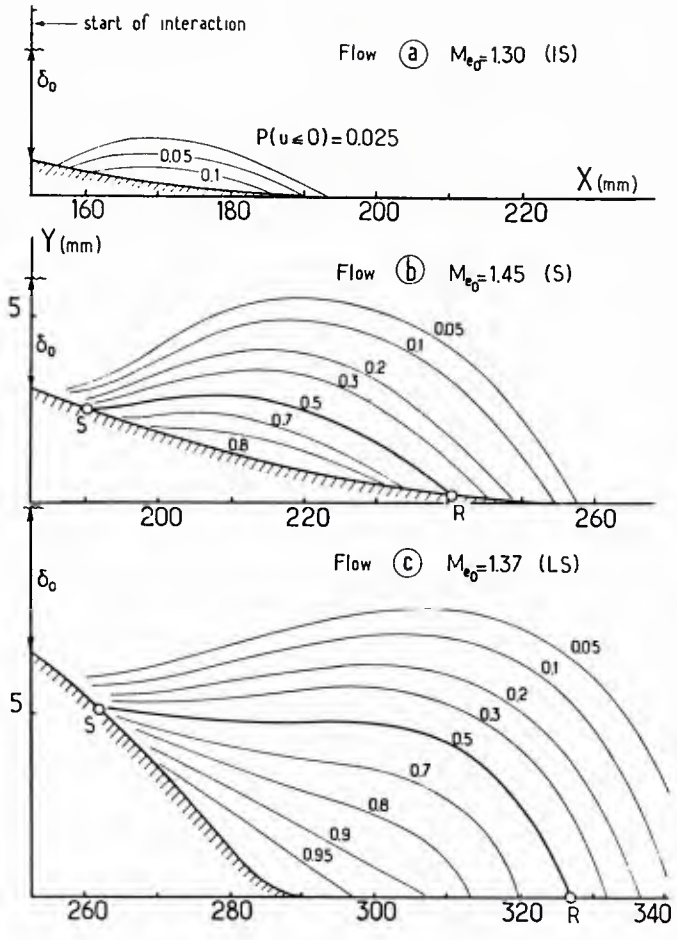

Fig. 66 Lines of constant value for the probability of backflow ($1 - \gamma_{pu}$) for the Délery flows (1983).

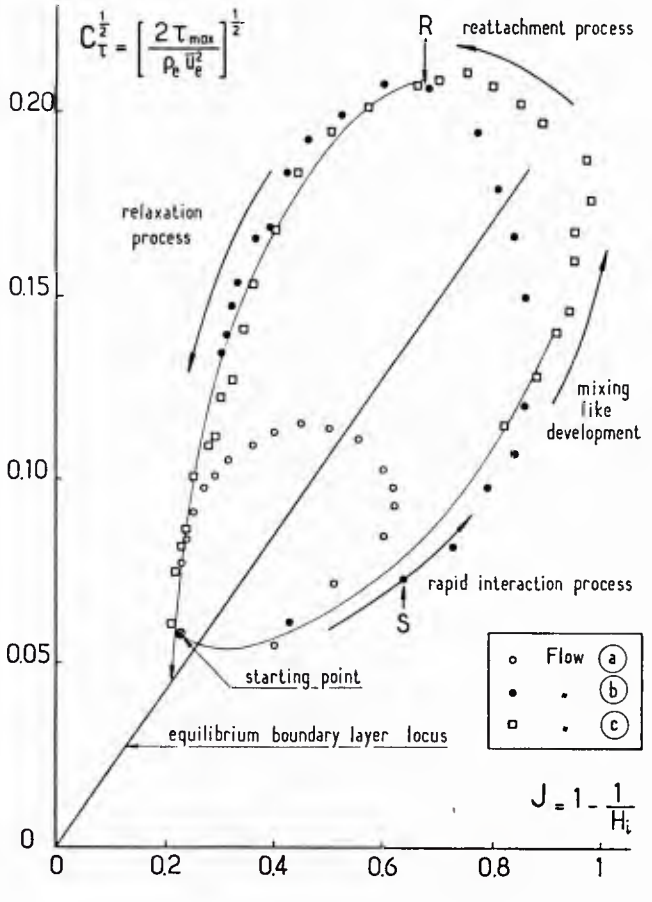

Fig. 67 Variation of the maximum shear stress with the equilibrium shape parameter for the Délery (1983) flows.

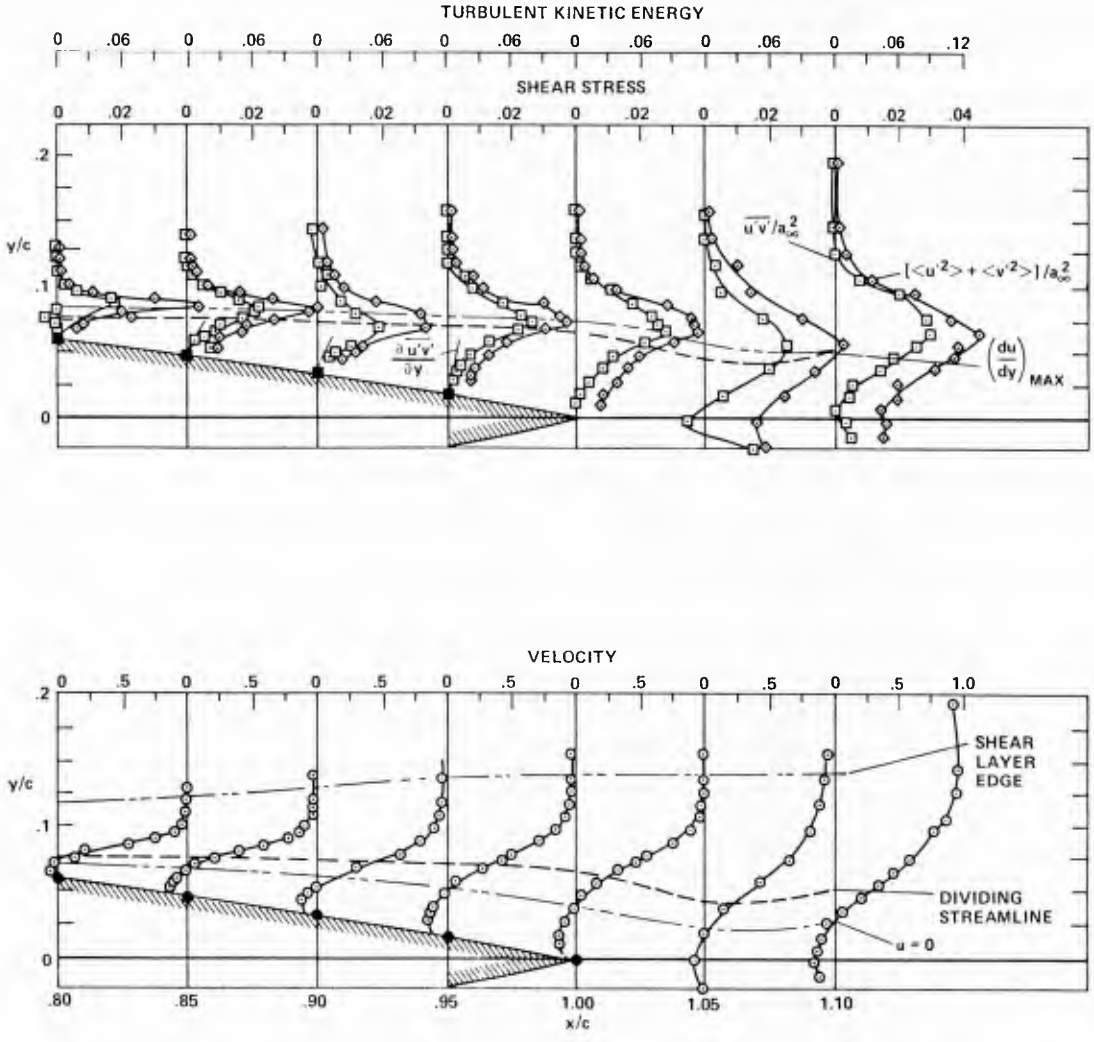

Fig. 68 Mean velocity, turbulent shear stress, and kinetic energy profiles in the shear layer downstream of detachment. $M_\infty = 0.79$ and $Re_c = 11 \times 10^6$. Seegmiller et al. (1978).

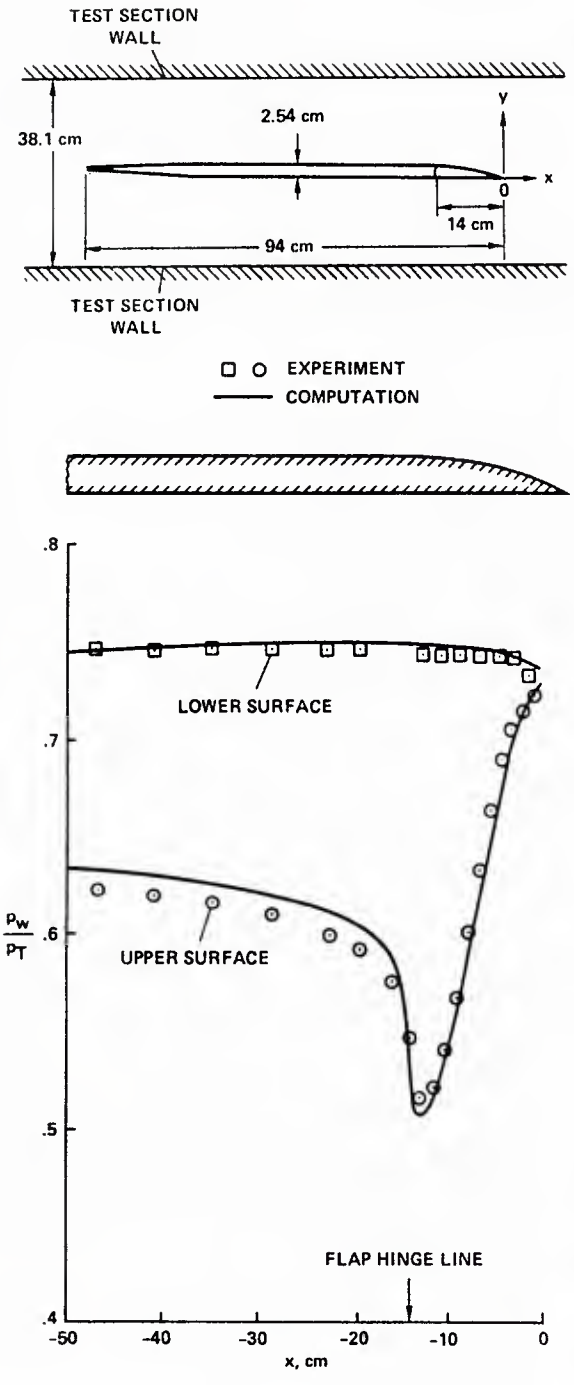

Fig. 69 Geometry and surface pressure distributions for the Viswanath and Brown (1980, 1983) trailing edge flow. Calculations by Horstman (1982) using the Jones-Launder (1972) k-ε model with Cousteix (Kline et al., 1982) curvature correction.

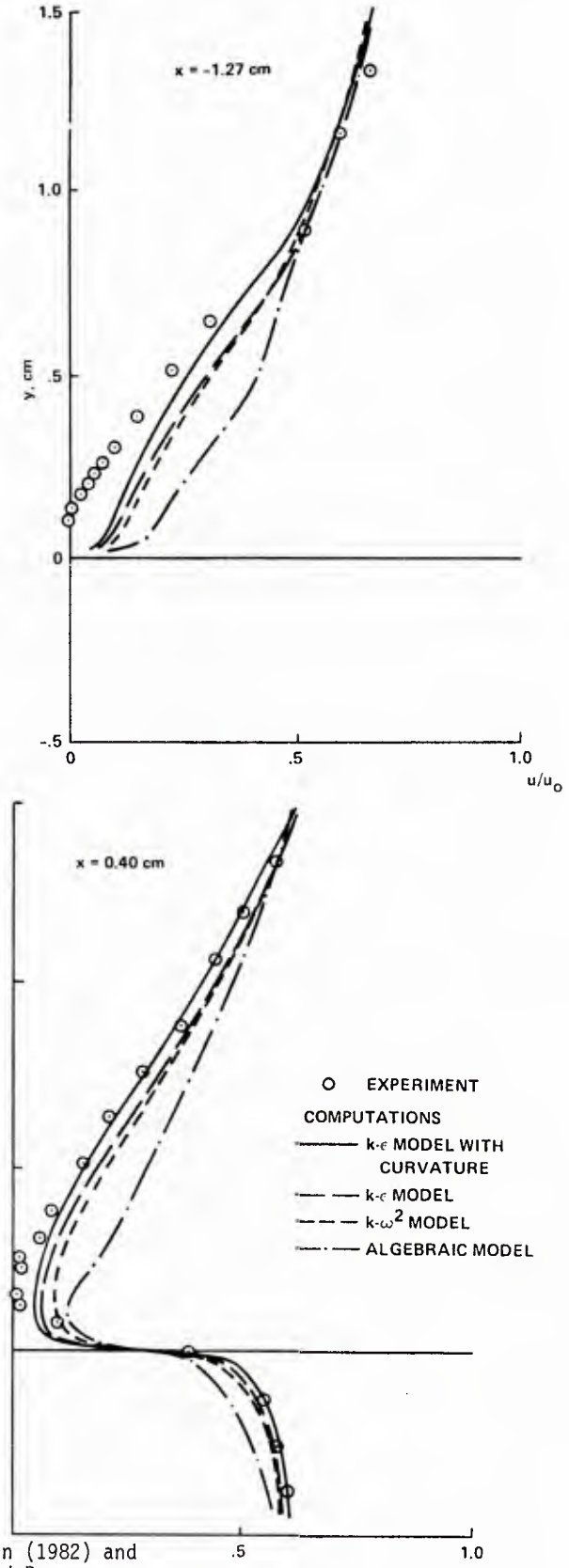

Fig. 70 Comparison between computations of Horstman (1982) and experimental mean-velocity profiles of Viswanath and Brown (1980, 1983) employing various turbulence models. M = 0.7 Freestream unit Reynolds number 4.0 x 10^7/m.

○ EXPERIMENT

COMPUTATIONS

——— k-ε MODEL WITH CURVATURE (Jones & Launder)

— — k-ε MODEL (Jones & Launder, 1972)

— — — k-ω^2 MODEL (Wilcox & Rubesin)

— · — ALGEBRAIC MODEL (Cebeci)

$M_\infty = 2.8$ $\quad Re_{\delta_o} = 0.5 - 8.0 \times 10^6$

$T_W/T_T \approx 1$ $\quad \delta_o \approx 2.5$ cm

$\alpha = 10 - 24°$

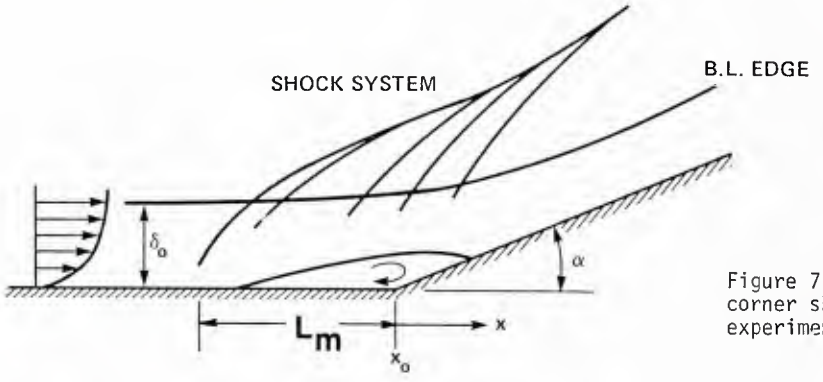

Figure 71 Geometry of supersonic compression corner shock-wave boundary-layer interaction experiment.

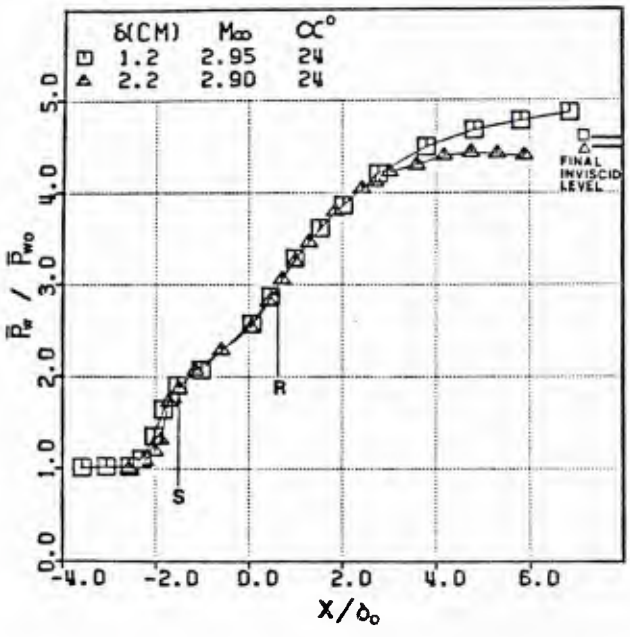

Figure 72a Mean Wall Pressure Distributions Dolling and Murphy (1982).

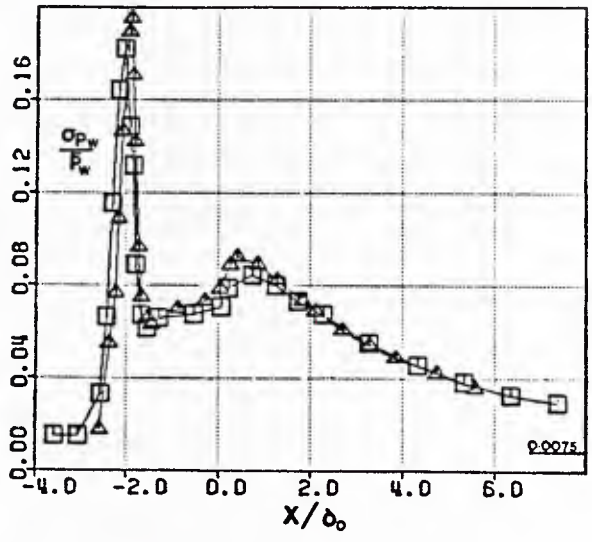

Figure 72b Wall Pressure Standard Deviation Distributions. Dolling and Murphy (1982).

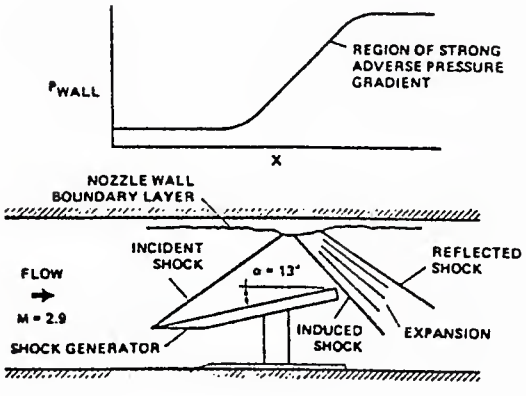

Figure 73 Flow model, shock-induced separation. $P_{final}/P_{initial} = 5$; $U_\infty/\nu = 5.7 \times 10^7$/m. Modarress and Johnson (1976).

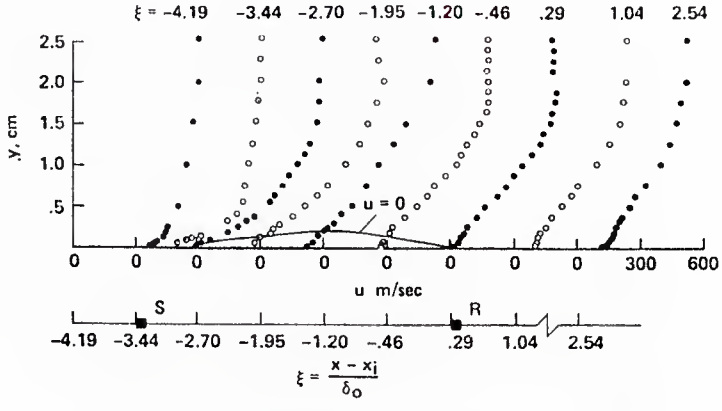

Figure 74 Mean velocity profiles of the interaction region. From Modarress and Johnson (1976). $\delta_o = 1.7$ cm.

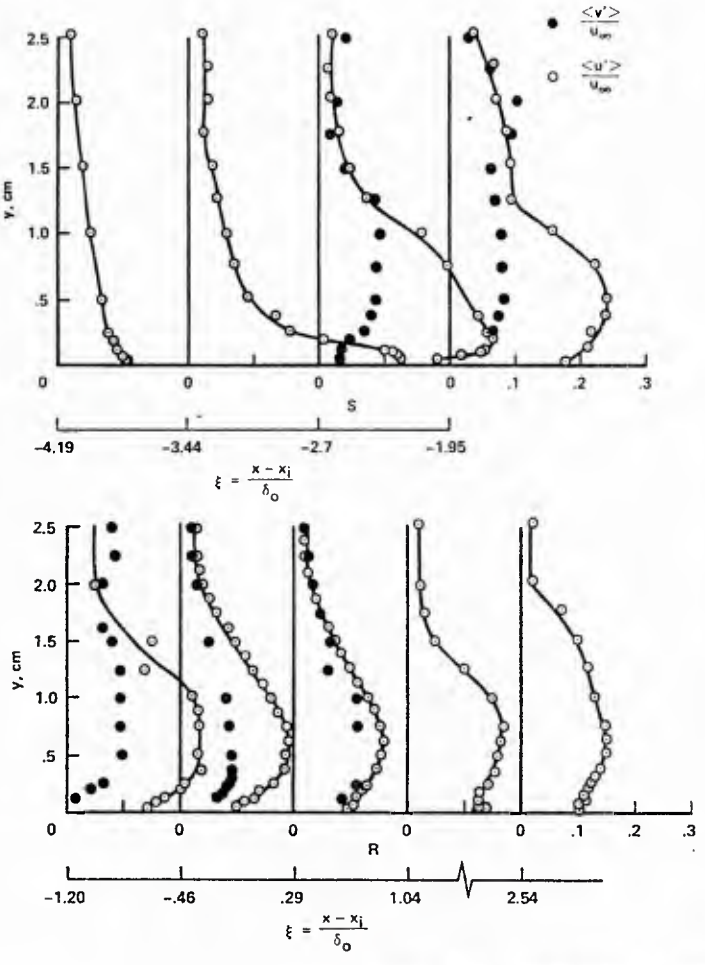

Figure 75 Turbulence intensity profiles. Modarress and Johnson (1976).

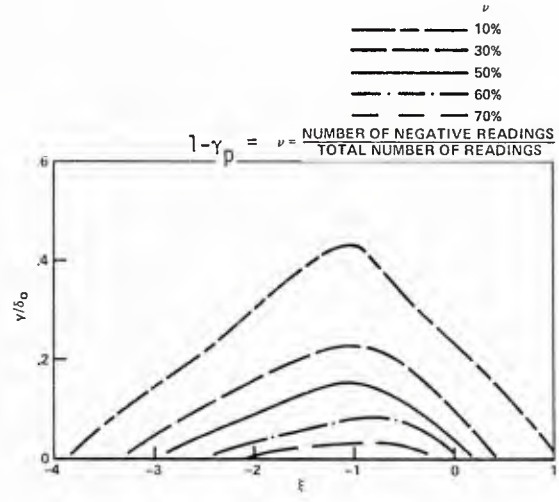

Figure 76 Lines of constant 1 - γ_p. From Modarress and Johnson (1976).

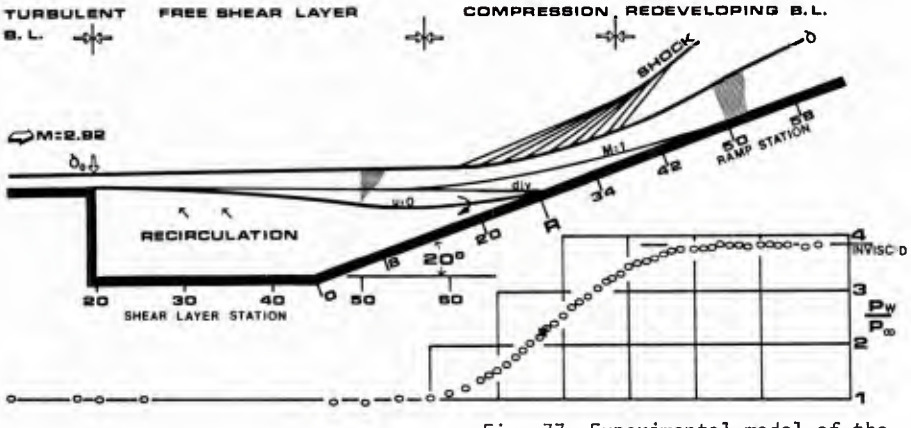

Fig. 77 Experimental model of the reattachment interaction with wall pressure distribution. $Re = 6 \times 10^7$/m and M = 2.92. Settles, et al.(1982).

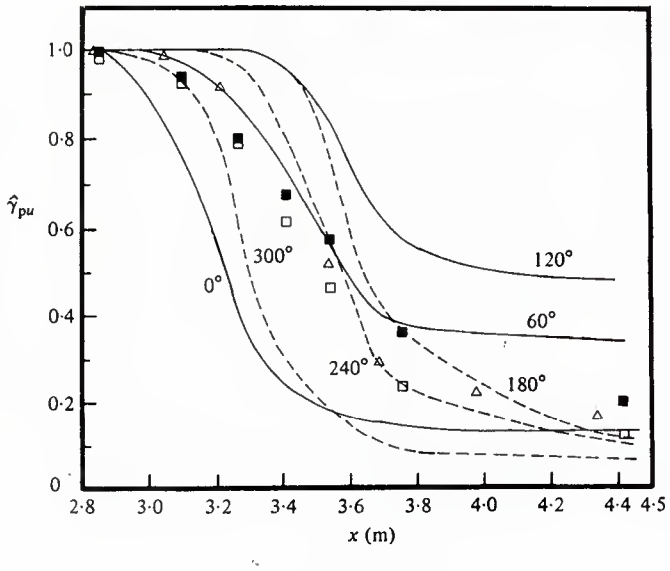

Figure 78 Phase-averaged $\hat{\gamma}_{pumin}$ vs. x for different phases of a cycle shown by lines for k = 0.61 Simpson et al.(1983) flow. Cycle-averaged $\overline{\gamma}_{pumin}$ values shown by symbols and legend from figure 1.

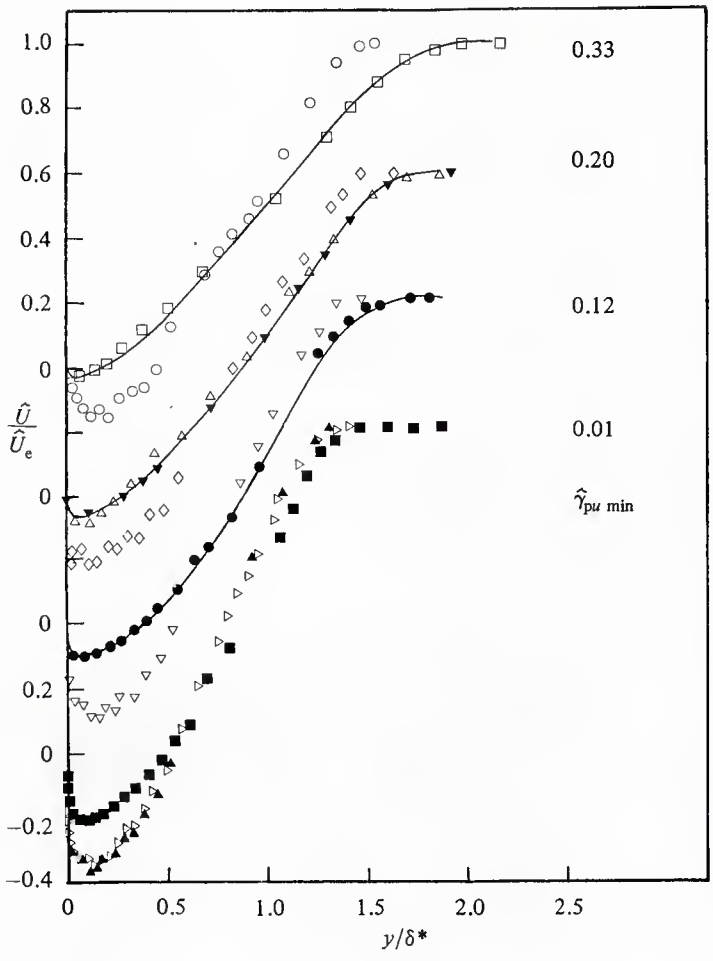

Figure 79 Phase averaged velocity profiles $\hat{U}/\hat{U}_e$ vs. y/δ^* for several values of $\hat{\gamma}_{pumin}$ for k = 0.90 Simpson and Shivaprasad flow (1983). Solid lines denote profiles from the steady flow of Simpson et al.(1981a) at the γ_{pumin} value. Note displaced ordinates. Conditions for each profile are as below.

$\hat{\gamma}_{pu\,min}$	$\partial\hat{\gamma}_{pu\,min}/\partial t$	X	Phase angle	$\hat{H}$
□ 0.33	<0	3.25 m	281°	3.78
○ 0.33	>0	3.67 m	82°	7.37
△ 0.20	<0	3.25 m	304°	4.66
▼ 0.20	<0	4.34 m	176°	5.31
◇ 0.20	≈ 0	4.34 m	79°	49.74
● 0.12	<0	3.98 m	195°	7.58
▽ $\approx$ 0.12	>0	4.34 m	60°	−21.11
■ $\approx$ 0.01	<0	3.98 m	274°	17.75
▷ $\approx$ 0.01	$\leqslant 0$	3.98 m	352°	−26.57
▲ $\approx$ 0.01	>0	4.34 m	11°	−12.18

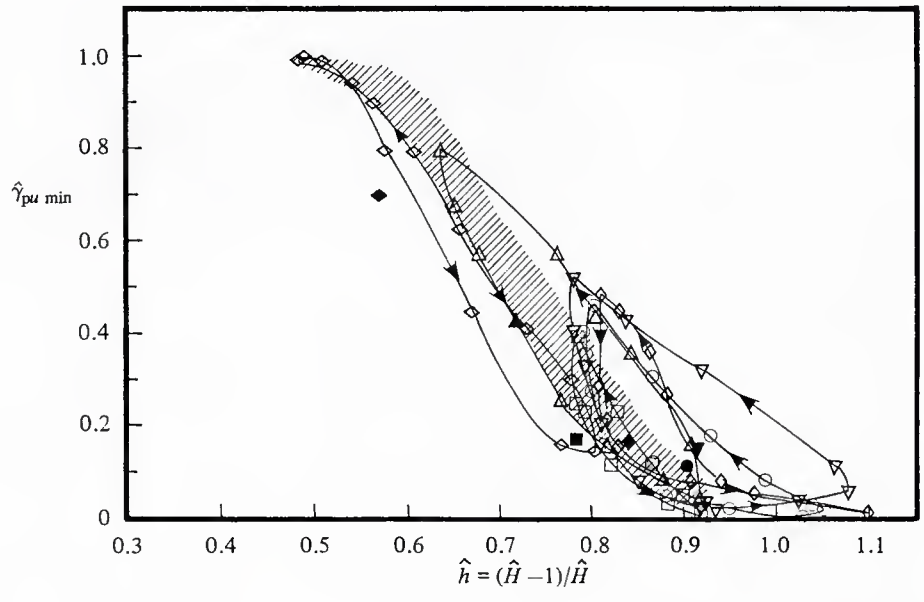

Figure 80 $\hat{\gamma}_{pumin}$ vs. $\hat{h}$ for the k = 0.90 unsteady flow of Simpson and Shivaprasad (1983) from LDV data: ◇, 3.00m; △, 3.25 m; □, 3.45 m; ◇, 3.67 m; ○, 3.98 m; ▽4.34 m. Solid lines form hysteresis loops for data at a given streamwise position. Shaded region denotes steady-flow results presented by Simpson et al.(1983). Solid symbols denote mean unsteady-flow results.

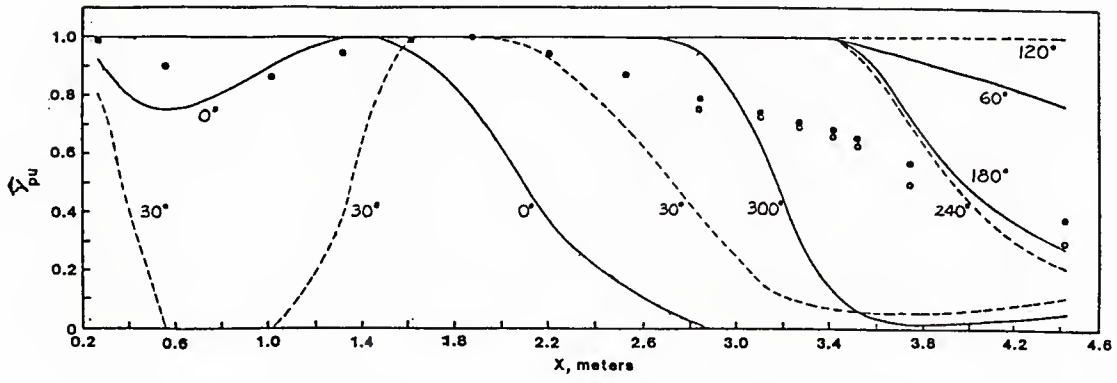

Figure 81 Phase-averaged γ_{pumin} vs. x for different ωt phases of a cycle for the large amplitude waveform. Simpson (1984).

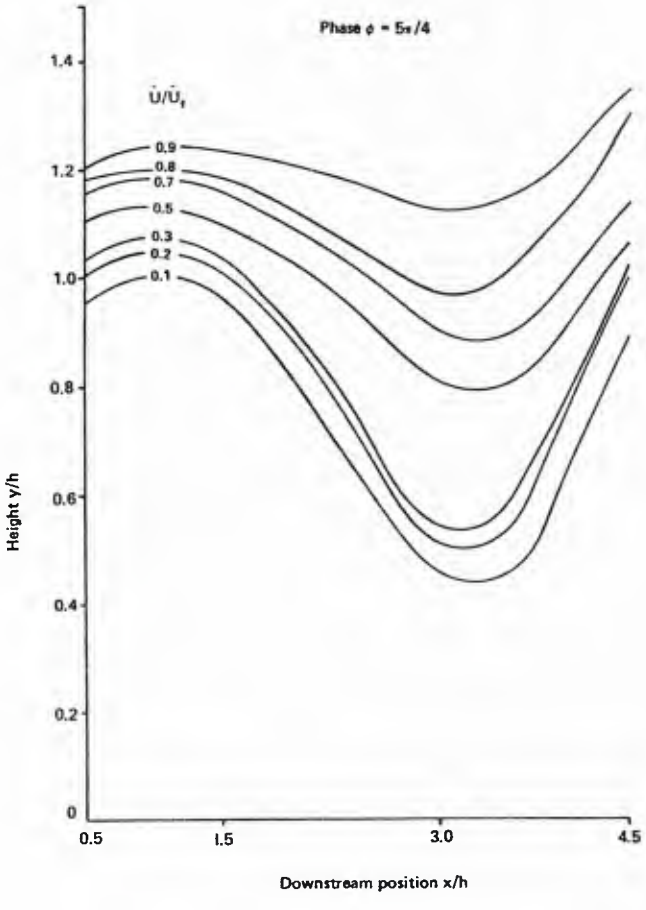

Figure 82 Isovels for phase ϕ = 225°. $\hat{U}_e$ = 1.43 + 0.173 sin(2πft) (mps). From Mullin, Greated, and Grant (1980).

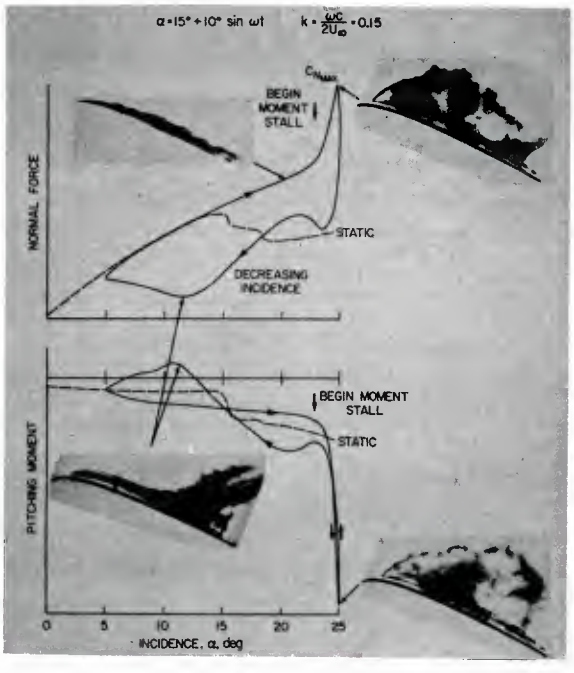

Figure 83 Normal force and pitching moment on NACA 0012 airfoil during dynamic stall. (α = 15° + 10° sin ωt, k = ωc/2U∞ = 0.15, Re = 2.5x10⁶). From McCroskey, Carr, and McAlister (1976).

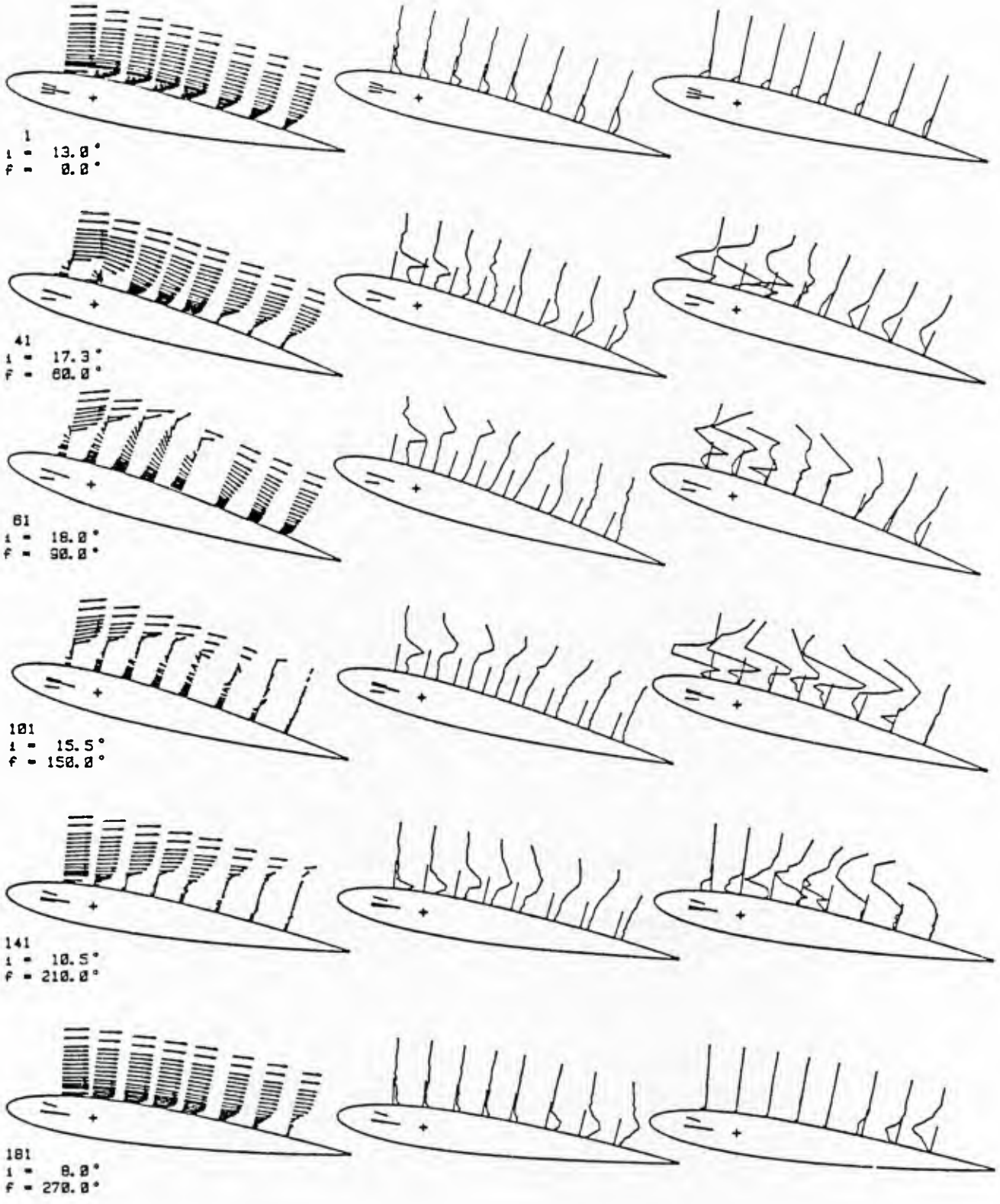

Figure 84 Slanted hot-wire anemometer measurements on a NACA 0012 airfoil oscillating sinusoidally about the quarter chord at unstalled to deeply stalled conditions. $k = 0.3$; $Re_c = 3 \times 10^5$; i denoted instantaneous angle of incidence; f is phase angle in cycle. From DeRuyck and Hirsch (1984).

leftmost figures : velocity vectors ⟼ Q
center figures : rms chordwise velocity fluctuations $\sqrt{\overline{u'^2}}$ ⟼ 30% Q
rightmost figures : Reynolds stress $\overline{u'v'}$ ⟼ 0.6% Q^2

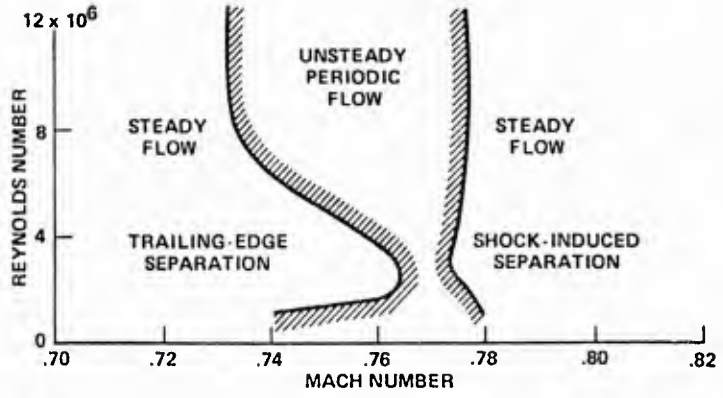

Figure 85 Experimental transonic flow domains for biconvex airfoil. From Seegmiller, Marvin, and Levy (1978).

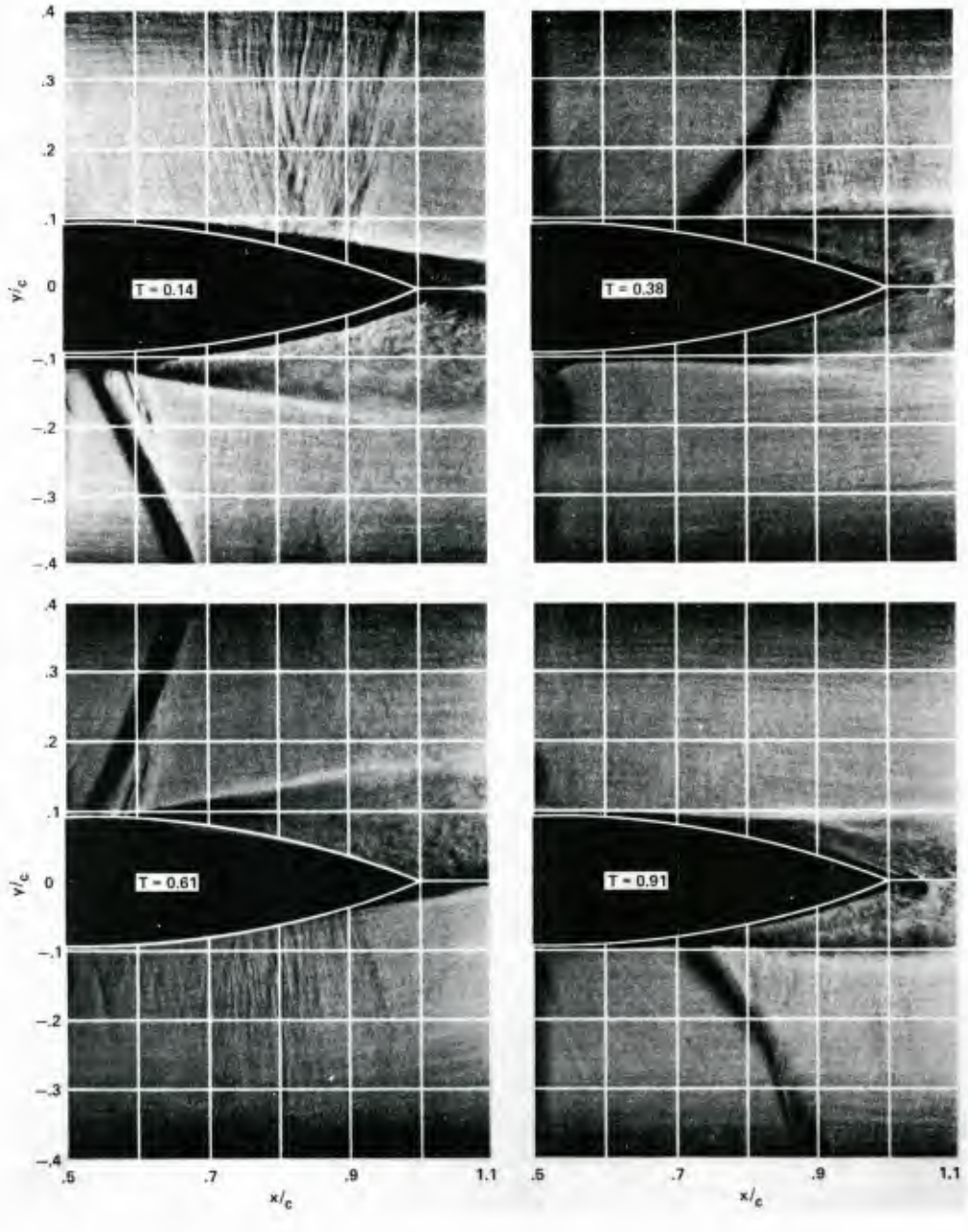

Figure 86 Composite shadowgraphs showing the unsteady flow field over the airfoil. M_∞ = 0.76, Re_c = 11x10^6. From Marvin, Levy, and Seegmiller (1979).

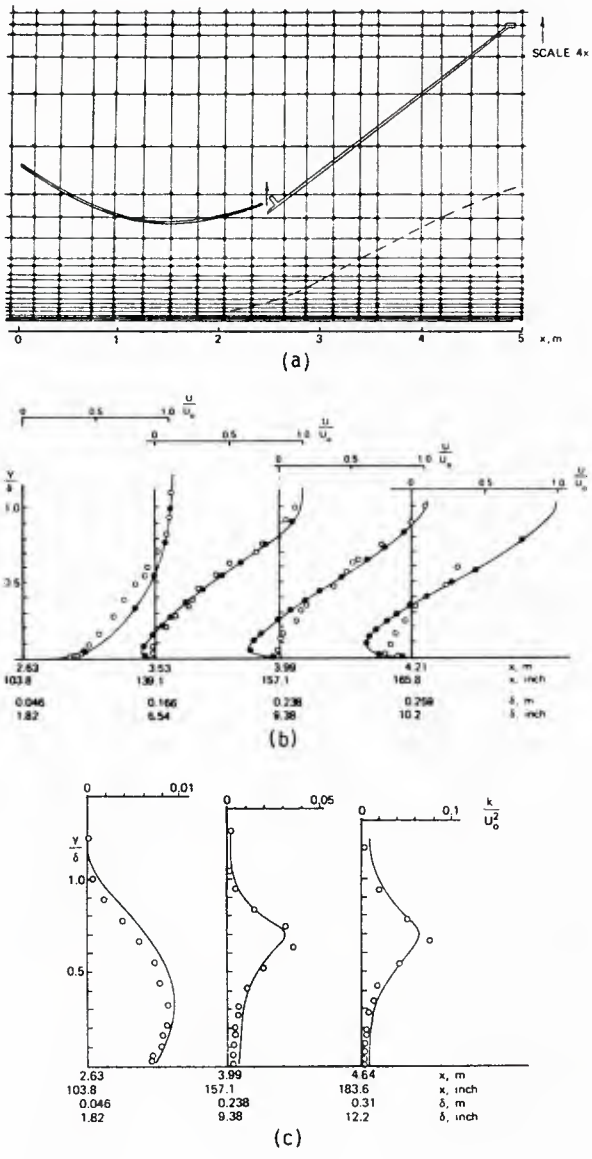

Figure 87 Comparison of elliptic equation solutions and measurements. (a) Wind tunnel arrangement, location of grid nodes and boundary-layer thickness (vertical scale amplified by a factor of 4). (b) Measured and calculated mean velocity values. o LDV results of Simpson, Strickland and Barr —●— calculations. From Cebeci, Kahlil, and Whitelaw (1979).

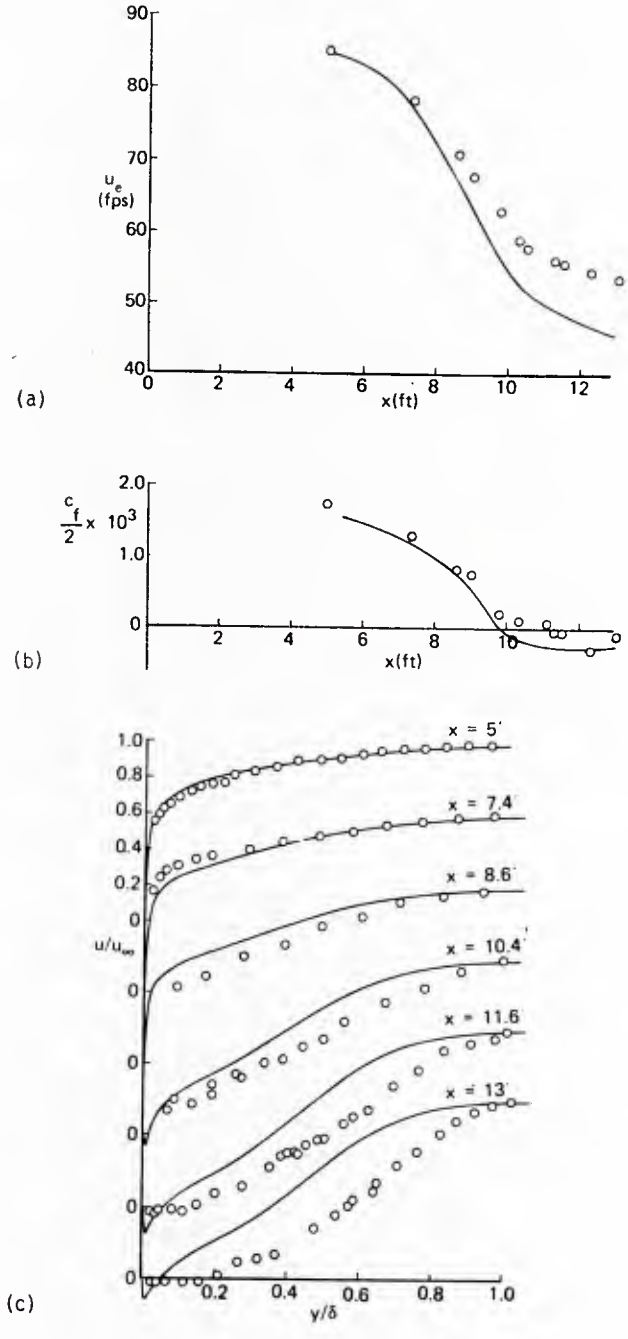

Figure 88 Comparison of boundary-layer calculations and measurements. (a) Freestream velocity distribution. o LDV results of Simpson, Strickland and Barr, ——calculated with inverse procedure and specified displacement thickness. (b) Skin-friction coefficient. (c) Mean velocity profiles normalized with experimental values of U_e. From Cebeci, Kahlil, and Whitelaw (1979).

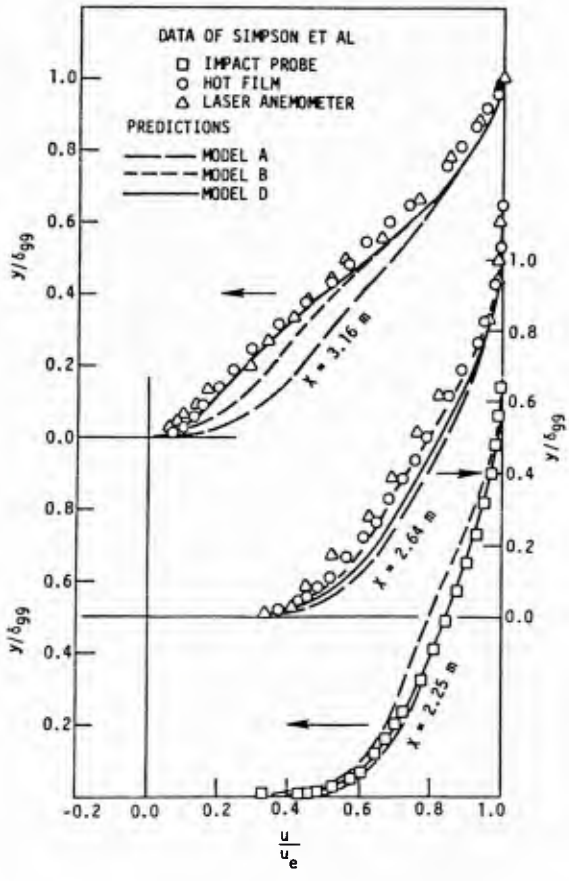

Figure 89(a) Comparison of predicted and experimental velocity profiles for the boundary layer measured by Simpson et al. (1977). From Pletcher (1978).

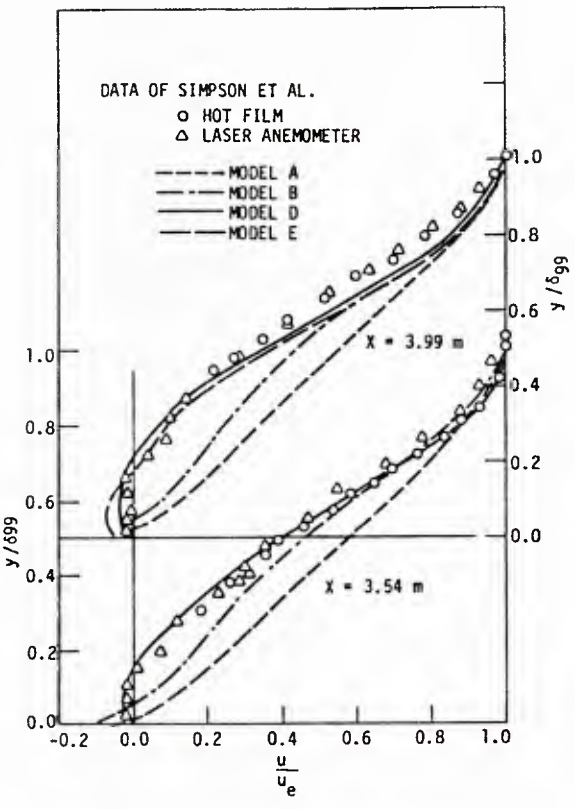

Figure 89(b) Comparison of predicted and experimental velocity profiles for the boundary layer with reversed flow measured by Simpson et al. (1977). From Pletcher (1978).

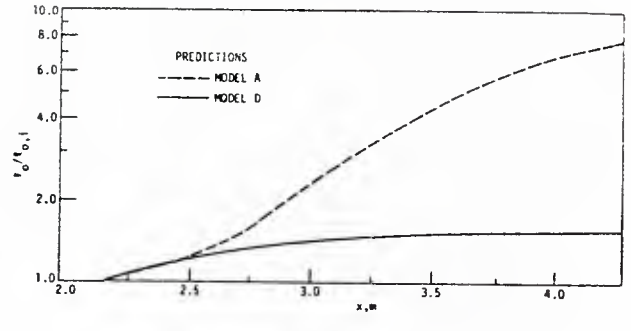

Figure 90(a) Predicted outer layer mixing length for the flow of Simpson, et al. $\ell_{o,i} = \ell_o$ at x = 2.14 m Pletcher (1979).

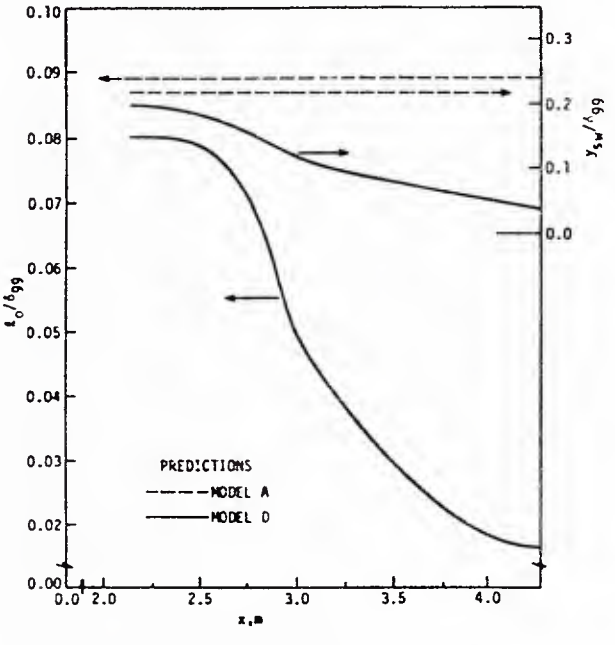

Figure 90(b) Predicted outer layer mixing length and the switch point (y_{sw}) between inner and outer region models for the flow of Simpson, et al. Pletcher (1979).

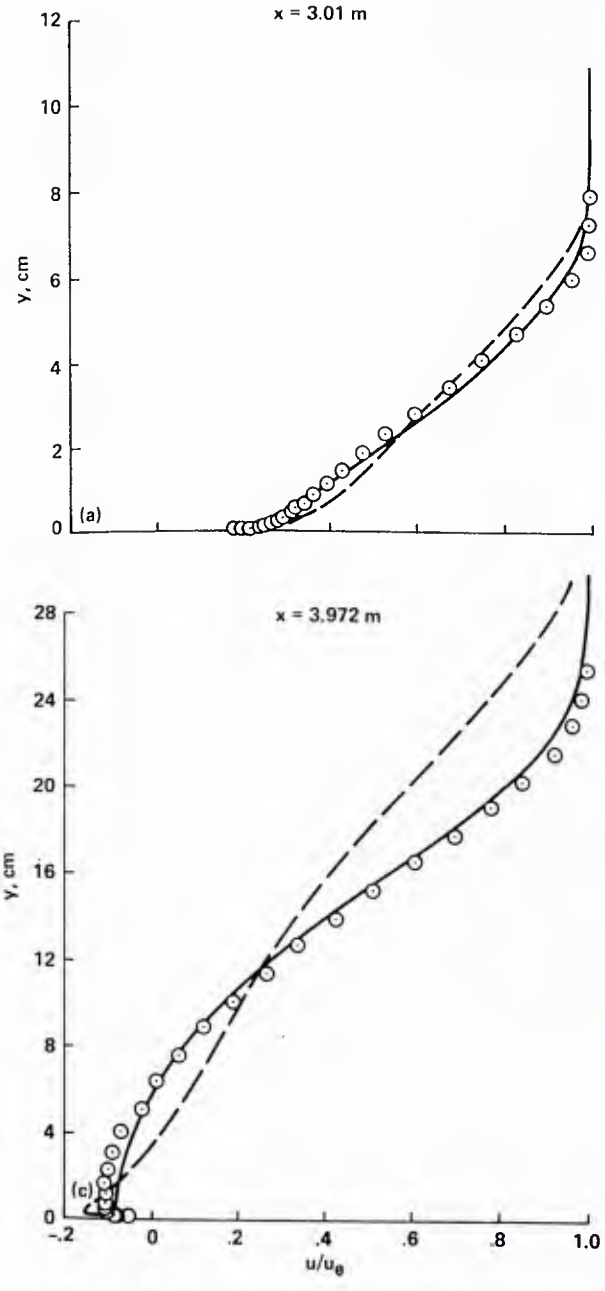

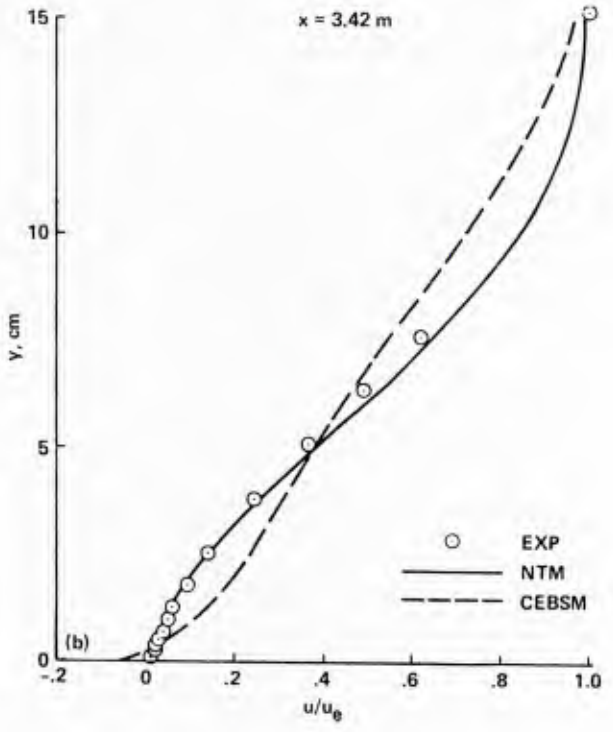

Figure 91 Low-speed diffuser flow of Simpson, et al. (1981); mean-velocity profile comparisons. a) x = 3.01 m; b) x = 3.42 m; c) x = 3.972 m. From Johnson and King (1984).

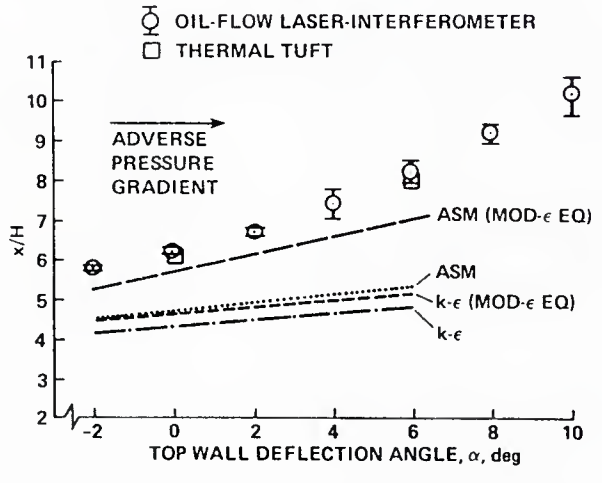

Figure 92 Reattachment location versus top-wall deflection angle. Calculations of Sindir (1982). Data of Driver and Seegmiller (1982).

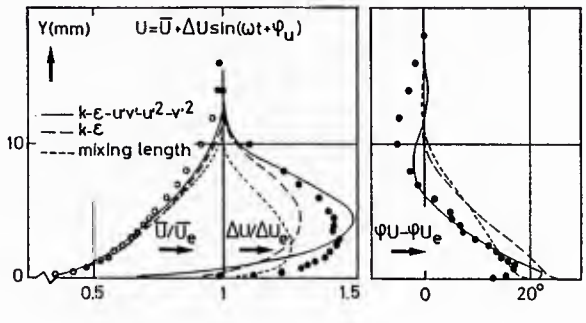

Figure 93 Unsteady turbulent boundary layer in an adverse pressure gradient. Harmonic analysis of the calculated velocity. Comparison with experiment. X = 390 mm. From Cousteix, et al. in Michel et al. (1981).

AGARDograph No.287 Volume 1
Advisory Group for Aerospace Research and Development, NATO
TWO-DIMENSIONAL TURBULENT SEPARATED FLOW
by Roger L.Simpson, edited by A.D.Young
Published June 1985
104 pages

Many different flow cases with nominally two-dimensional turbulent separated flow regimes are discussed. Because of intermittent flow reversal and backflow near the wall, directionally sensitive measurement techniques such as hot-wire, pulsed-wire and laser anemometry are discussed. Experimentally-observed structure of detached flows on streamlined surfaces and around sharp-edged corners is

P.T.O

AGARD-AG-287-Vol.1

Turbulent flow
Two dimensional flow
Velocity measurement
Aerodynamics

AGARDograph No.287 Volume 1
Advisory Group for Aerospace Research and Development, NATO
TWO-DIMENSIONAL TURBULENT SEPARATED FLOW
by Roger L.Simpson, edited by A.D.Young
Published June 1985
104 pages

Many different flow cases with nominally two-dimensional turbulent separated flow regimes are discussed. Because of intermittent flow reversal and backflow near the wall, directionally sensitive measurement techniques such as hot-wire, pulsed-wire and laser anemometry are discussed. Experimentally-observed structure of detached flows on streamlined surfaces and around sharp-edged corners is

P.T.O

AGARD-AG-287-Vol.1

Turbulent flow
Two dimensional flow
Velocity measurement
Aerodynamics

AGARDograph No.287 Volume 1
Advisory Group for Aerospace Research and Development, NATO
TWO-DIMENSIONAL TURBULENT SEPARATED FLOW
by Roger L.Simpson, edited by A.D.Young
Published June 1985
104 pages

Many different flow cases with nominally two-dimensional turbulent separated flow regimes are discussed. Because of intermittent flow reversal and backflow near the wall, directionally sensitive measurement techniques such as hot-wire, pulsed-wire and laser anemometry are discussed. Experimentally-observed structure of detached flows on streamlined surfaces and around sharp-edged corners is

P.T.O

AGARD-AG-287-Vol.1

Turbulent flow
Two dimensional flow
Velocity measurement
Aerodynamics

AGARDograph No.287 Volume 1
Advisory Group for Aerospace Research and Development, NATO
TWO-DIMENSIONAL TURBULENT SEPARATED FLOW
by Roger L.Simpson, edited by A.D.Young
Published June 1985
104 pages

Many different flow cases with nominally two-dimensional turbulent separated flow regimes are discussed. Because of intermittent flow reversal and backflow near the wall, directionally sensitive measurement techniques such as hot-wire, pulsed-wire and laser anemometry are discussed. Experimentally-observed structure of detached flows on streamlined surfaces and around sharp-edged corners is

P.T.O

AGARD-AG-287-Vol.1

Turbulent flow
Two dimensional flow
Velocity measurement
Aerodynamics

discussed for steady and unsteady incompressible and compressible cases where large-scale structures dominate the flow behaviour. A number of differential and integral calculation methods are discussed. Traditional attached flow turbulence models do not describe attached flows well and methods which include experimentally-observed features of detached flow parameters seem to perform best.

This AGARDograph was sponsored by the Fluid Dynamics Panel of AGARD. A second volume is in preparation.

ISBN 92.835-1502-1

discussed for steady and unsteady incompressible and compressible cases where large-scale structures dominate the flow behaviour. A number of differential and integral calculation methods are discussed. Traditional attached flow turbulence models do not describe attached flows well and methods which include experimentally-observed features of detached flow parameters seem to perform best.

This AGARDograph was sponsored by the Fluid Dynamics Panel of AGARD. A second volume is in preparation.

ISBN 92.835-1502-1

discussed for steady and unsteady incompressible and compressible cases where large-scale structures dominate the flow behaviour. A number of differential and integral calculation methods are discussed. Traditional attached flow turbulence models do not describe attached flows well and methods which include experimentally-observed features of detached flow parameters seem to perform best.

This AGARDograph was sponsored by the Fluid Dynamics Panel of AGARD. A second volume is in preparation.

ISBN 92.835-1502-1

discussed for steady and unsteady incompressible and compressible cases where large-scale structures dominate the flow behaviour. A number of differential and integral calculation methods are discussed. Traditional attached flow turbulence models do not describe attached flows well and methods which include experimentally-observed features of detached flow parameters seem to perform best.

This AGARDograph was sponsored by the Fluid Dynamics Panel of AGARD. A second volume is in preparation.

ISBN 92.835-1502-1

AGARD
NATO OTAN
7 RUE ANCELLE · 92200 NEUILLY-SUR-SEINE
FRANCE
Telephone 745.08.10 · Telex 610176

DISTRIBUTION OF UNCLASSIFIED AGARD PUBLICATIONS

AGARD does NOT hold stocks of AGARD publications at the above address for general distribution. Initial distribution of AGARD publications is made to AGARD Member Nations through the following National Distribution Centres.Further copies are sometimes available from these Centres, but if not may be purchased in Mircrofiche or Photocopy form from the Purchase Agencies listed below.

NATIONAL DISTRIBUTION CENTRES

BELGIUM
Coordonnateur AGARD — VSL
Etat-Major de la Force Aérienne
Quartier Reine Elisabeth
Rue d'Evere, 1140 Bruxelles

CANADA
Defence Scientific Information Services
Dept of National Defence
Ottawa, Ontario K1A 0K2

DENMARK
Danish Defence Research Board
Ved Idraetsparken 4
2100 Copenhagen Ø

FRANCE
O.N.E.R.A. (Direction)
29 Avenue de la Division Leclerc
92320 Châtillon

GERMANY
Fachinformationszentrum Energie,
Physik, Mathematik GmbH
Kernforschungszentrum
D-7514 Eggenstein-Leopoldshafen

GREECE
Hellenic Air Force General Staff
Research and Development Directorate
Holargos, Athens

ICELAND
Director of Aviation
c/o Flugrad
Reyjavik

ITALY
Aeronautica Militare
Ufficio del Delegato Nazionale all'AGARD
3 Piazzale Adenauer
00144 Roma/EUR

LUXEMBOURG
See Belgium

NETHERLANDS
Netherlands Delegation to AGARD
National Aerospace Laboratory, NLR
P.O. Box 126
2600 AC Delft

NORWAY
Norwegian Defence Research Establishment
Attn: Biblioteket
P.O. Box 25
N-2007 Kjeller

PORTUGAL
Portuguese National Coordinator to AGARD
Gabinete de Estudos e Programas
CLAFA
Base de Alfragide
Alfragide
2700 Amadora

TURKEY
Department of Research and Development (ARGE)
Ministry of National Defence, Ankara

UNITED KINGDOM
Defence Research Information Centre
Station Square House
St Mary Cray
Orpington, Kent BR5 3RE

UNITED STATES
National Aeronautics and Space Administration (NASA)
Langley Research Center
M/S 180
Hampton, Virginia 23665

THE UNITED STATES NATIONAL DISTRIBUTION CENTRE (NASA) DOES NOT HOLD STOCKS OF AGARD PUBLICATIONS, AND APPLICATIONS FOR COPIES SHOULD BE MADE DIRECT TO THE NATIONAL TECHNICAL INFORMATION SERVICE (NTIS) AT THE ADDRESS BELOW.

PURCHASE AGENCIES

Microfiche or Photocopy
National Technical
Information Service (NTIS)
5285 Port Royal Road
Springfield
Virginia 22161, USA

Microfiche
ESA/Information Retrieval Service
European Space Agency
10, rue Mario Nikis
75015 Paris, France

Microfiche or Photocopy
British Library Lending
Division
Boston Spa, Wetherby
West Yorkshire LS23 7BQ
England

Requests for microfiche or photocopies of AGARD documents should include the AGARD serial number, title, author or editor, and publication date. Requests to NTIS should include the NASA accession report number. Full bibliographical references and abstracts of AGARD publications are given in the following journals:

Scientific and Technical Aerospace Reports (STAR)
published by NASA Scientific and Technical
Information Branch
NASA Headquarters (NIT-40)
Washington D.C. 20546, USA

Government Reports Announcements (GRA)
published by the National Technical
Information Services, Springfield
Virginia 22161, USA

Printed by Specialised Printing Services Limited
40 Chigwell Lane, Loughton, Essex IG10 3TZ

ISBN 92-835-1502-1